



UNIVERSITÀ DEGLI STUDI DI ROMA
"TOR VERGATA"

FACOLTÀ DI SCIENZE MM.FF.NN.

Dottorato di ricerca in ASTRONOMIA

Ciclo XXI

**Classical Cepheids as
distance indicators and tracers of the
disk abundance gradient**

Silvia Pedicelli

A.A. 2008/2009

Docenti guida/Tutors: Prof. R. Buonanno, G. Bono and M. Romaniello
Coordinatore: Prof. P. Mazzotta

ABSTRACT

Classical Cepheids are the most popular primary distance indicator. They obey to well defined optical and near-infrared (NIR) Period-Luminosity (PL) relations and their distances can be estimated with an accuracy of a few percent. They also are, the best tracers of intermediate-mass stars. In particular, since they are distributed across the Galactic disk they can be adopted to trace the iron and heavy element radial gradients. In the past few years, significant progress has been made to understand and characterize the influence that chemical composition may have on the Cepheids Period-Luminosity relation but this issue is still unsettled. Although the existence of the Galactic abundance gradient is now widely accepted, its value still need to be established. To better understand these fundamental points, we focused our attention on two main topics:

i) the influence of the stellar iron content on the PL relation in the V and in the K band.

ii) the behavior of the Galactic iron gradient between 5 and 17 kpc, using homogeneous iron abundances for 270 Galactic Cepheids located across the disk together with accurate distance determinations.

To assess the effect of the metallicity on the PL relation, we have related the V and the K -band residuals from the standard PL relations of Freedman et al. (2001) and Persson et al. (2004), respectively, to iron abundance ($[Fe/H]$). We used iron measurements for 68 Galactic and Magellanic Cepheids based on high resolution and high signal-to-noise ratio (S/N) spectra collected with FEROS@1.5m and UVES@VLT (ESO, Telescopes). We have found a mean $[Fe/H] \sim$ solar ($\sigma = 0.10$) for our Galactic sample (32 stars), -0.33 dex ($\sigma = 0.13$) for the Large Magellanic Cloud (LMC, 22 stars) and -0.75 dex ($\sigma = 0.08$) for the Small Magellanic Cloud (SMC, 14 stars). Our abundance measurements of the Magellanic Cepheids double the number of stars studied up to now at high resolution. Our results show that the metallicity affects the Cepheid PL relation and this finding does not depend on the adopted LMC distance modulus. Results based on the canonical LMC distance ($\mu_{LMC} = 18.5$) indicate a well defined effect in the V and a mild effect in the K -band PL relations. In particular, the metal-poor and the metal-rich bins are, in the visual band, at $\sim 2\sigma$ and $\sim 9\sigma$, respectively, from the null hypothesis and the two bins differ at 3σ level. In the infrared band, the metal-poor bin is within 1σ consistent with zero while the metal-rich bin differs from the null hypothesis by $\sim 4\sigma$. Moreover, the magnitude residuals in the two metallicity bins differ by $\sim 2\sigma$. These findings support the evidence that the Cepheid PL relation is not Universal.

To investigate the Galactic abundance gradient, we provided new calibrations of two photometric metallicity indices based on Walraven photometry. The best results have been obtained by the theoretical Metallicity-Index Color (MIC) relations. They rely on a homogeneous set of scaled-solar evolutionary tracks for intermediate-mass stars and on pulsation predictions concerning the topology of the instability strip. The intrinsic accuracy of the MIC relations are ~ 0.1 dex. Using the calibrated relations we have estimated photometric metallicities for the entire Walraven sample (122 Cepheids). Among them, 51 had accurate iron abundances available in literature and 71 are new estimates. We added four metal-rich Cepheids for which we collected high resolution spectra and for which we derived accurate distances based on the Baade-Wesselink technique. Moreover, to improve the number of tracers, we have also included 116 Cepheids from Andrievsky et al. (2002), 63 from Lemasle et al. (2007), 6 from Sziládi et al. (2007) and 10 from Romaniello et al. (2008) to end up with 270 Galactic Cepheids. Our result, over the entire data set, indicates that the iron gradient in the Galactic disk presents a slope of -0.048 ± 0.004 dex kpc^{-1} which is in very good agreement with the most recent literature values. However, the hypothesis of a linear gradient is still widely debated. Several investigations suggest a bimodal distribution with a steeper slope toward the bulge and a flattening of the gradient toward the outer disk with a discontinuity at $R_G \sim 10$ kpc. Our data do not support the discontinuity hypothesis but we have found that Cepheids present an increase in the spread in iron abundance and that it may depend on the Galactocentric longitude. The occurrence of this spread indicates that linear radial gradients should be cautiously treated to

constrain the chemical evolution of the Galactic disk. Finally, with these results in hands, we decided to fit the Galactic abundance gradient with an exponential distribution, finding a good fit ($rms = 0.129$ dex).

RIASSUNTO

Le Cefeidi Classiche sono gli indicatori primari di distanza piú utilizzati. Relazioni ben definite intercorrono tra il loro periodo e la loro luminosità, sia nella banda ottica che in quella del vicino infrarosso. Grazie a queste relazioni é possibile determinare le loro distanze con grade accuratezza. Inoltre sono i migliori traccianti di stelle di massa intermedia. Infatti, poiché sono distribuite lungo tutto il disco Galattico, possono essere adottate per tracciare i gradienti radiali di abbondanza di ferro e elementi pesanti. Negli ultimi anni sono stati fatti molti progressi verso la comprensione e caratterizzazione dell'influenza che la composizione chimica potrebbe avere sulla relazione Periodo-Luminosità (PL) delle Cefeidi, ma tale problema rimane ancora irrisolto. Inoltre, nonostante l'esistenza di un gradiente di abbondanza Galattico sia oggi largamente accettata, il suo preciso valore é ancora da definire. Con lo scopo di comprendere meglio questi punti fondamentali, abbiamo rivolto la nostra attenzione su due obiettivi principali:

i) valutare l'influenza della metallicitá sulla PL nelle bande V e K .

ii) dare una stima accurata del gradiente di abbondanza Galattico tra 5 e 17 kpc, utilizzando misure omogenee di composizione chimica per un campione che comprende 270 Cefeidi situate lungo il disco e delle quali abbiamo ottenuto una buona stima delle distanze.

Per valutare l'effetto che la metallicitá ha sulla PL, abbiamo messo in relazione, per le bande V e K , i residui dalla PL standard di Freedman et al. (2001) e Persson et al. (2004), rispettivamente, all'abbondanza di ferro ($[Fe/H]$). A tale scopo, abbiamo usato misure dirette del ferro per 68 Cefeidi Galattiche e Magellaniche ricavate dall'analisi di spettri ad alta risoluzione e alto rapporto segnale rumore (S/N) ottenuti con strumenti e telescopi ESO (FEROS@1.5m e UVES@VLT). In questo studio, abbiamo trovato una metallicitá media circa solare ($\sigma = 0.10$) per il campione Galattico (32 stelle), -0.33 dex ($\sigma = 0.13$) per quello della grande Nube di Magellano (LMC, 22 stelle) e -0.75 dex ($\sigma = 0.08$) per la Piccola Nube di Magellano (SMC, 14 stelle). Il numero delle nostre misure di abbondanza per le Cefeidi Magellaniche risulta essere piú del doppio di quello totale studiato fino ad ora ad alta risoluzione. I nostri risultati mostrano che la metallicitá influisce sulla PL delle Cefeidi e questa constatazione non dipende dal modulo di distanza adottato per LMC. Risultati basati sulla distanza canonica di LMC ($\mu_{LMC} = 18.5$) indicano un ben definito effetto nella banda visuale V e un effetto piú lieve in quella nel vicino infrarosso K . In dettaglio, abbiamo visto che i due bin di metallicitá, quello povero di metalli e quello ricco, nella banda visuale, si trovano rispettivamente a $\sim 2\sigma$ e a $\sim 9\sigma$, rispetto all'ipotesi di indipendenza e i due bins hanno una differenza di 3σ . Nella banda infrarossa, il bin povero di metalli si trova entro 1σ consistente con zero mentre quello ricco di metalli differisce dall'ipotesi di indipendenza di $\sim 4\sigma$. Inoltre, i due bins differiscono tra loro $\sim 2\sigma$. Questi risultati suggeriscono che la PL delle Cefeidi non può essere considerata Universale. Per indagare il gradiente di abbondanza Galattico, abbiamo fornito due nuove calibrazioni, una empirica e una teorica, di due indici di metallicitá basati sulla fotometria di Walraven. I migliori risultati sono stati ottenuti con le relazioni teoriche tra la metallicitá e gli Indici di Colore (MIC). Queste sono basate su un insieme omogeneo di tracce evolutive solar-scaled per stelle di massa intermedia e su previsioni pulsazionali riguardanti la topologia della striscia di instabilità. Lo scatter intrinseco delle relazioni é ~ 0.1 dex. Usando le relazioni calibrate, abbiamo ottenuto metallicitá fotometriche per l'intero campione di Walraven (122 stelle). Di queste, 51 disponevano di misure accurate di abbondanza di ferro in letteratura, per le rimanenti 71 abbiamo fornito noi una nuova stima. Abbiamo, inoltre, aggiunto le 4 per cui avevamo stimato le distanze con il metodo del Baade-Wesselink. Per aumentare ulteriormente il numero dei traccianti, abbiamo incluso anche 116 Cefeidi dal set di dati di Andrievsky et al. (2002b), 63 da quello di Lemasle et al. (2007), 6 dal campione di Sziládi et al. (2007) e 10 da quello di Romaniello et al. (2008). In questo modo siamo riusciti ad ottenere un campione di 270 stelle. Il risultato ottenuto facendo un fit lineare dell'intero dataset, indica che il gradiente di abbondanza Galattico presenta una pendenza di -0.048 ± 0.004 dex kpc^{-1} , in ottimo accordo con le stime piú recenti.

In ogni modo, la variazione dell'abbondanza di ferro lungo il disco, sembra essere meglio descritta da una distribuzione bimodale con una pendenza maggiore verso il bulge e un appiattimento del gradiente in direzione del disco piú esterno con una discontinuitá attorno $R_G \sim 10$ kpc. Dall'analisi dei nostri dati non sembra emergere nessuna discontinuitá ma abbiamo trovato che le Cefeidi presentano un aumento dello spread in contenuto di ferro e che questo spread possa dipendere dalla longitudine Galattocentrica. Il verificarsi di uno spread in metallicitá in funzione della longitudine Galactocentrica indica che il gradiente radiale dovrebbe essere utilizzato con cautela nel porre dei limiti per l'evoluzione chimica in tutto il disco. Infine, con questi risultati, abbiamo deciso di fare un fit esponenziale del gradiente ottenendo uno scarto quadratico medio di 0.129 dex.

Contents

Table of Contents	III
List of Figures	VI
List of Tables	VIII
1 INTRODUCTION	1
1.1 Cepheids: a brief history	1
1.2 Cepheids: characteristics	4
1.3 Cepheids: evolution	8
1.4 The distance scale	9
1.5 The Baade-Wesselink Method	11
1.6 Period-Luminosity relation	12
1.6.1 The metallicity problem	13
1.7 The disk abundance gradient	17
1.7.1 A brief review	17
1.7.2 The Cepheid contribution	19
1.7.3 The linear gradient	20
1.8 This thesis project	21
2 Observations	23

2.1	Telescopes and instruments	23
2.1.1	The ESO-1.5m telescope and FEROS	24
2.1.2	The ESO-VLT telescope and UVES	25
2.1.3	The Dutch telescope and the Walraven photometer	28
2.1.4	The SAAO-0.75m telescope and the Mk II IR photometer	30
2.2	Data	32
2.2.1	PL-data: the Galactic sample	33
2.2.2	PL-data: the Magellanic sample	36
2.2.3	BW-data	36
2.2.4	Walraven-data	38
3	Overview of the analysis of stellar spectra	40
3.1	Line list	46
3.2	Equivalent widths	48
3.3	Stellar Parameters	48
3.4	FITLINE	49
3.5	Abundances and their uncertainties	53
4	The effect of metallicity on the PL relation	58
4.1	The adopted standard PL relations	59
4.2	Results	60
4.3	Uncertainties	64
4.4	Comparison with previous results	64
4.5	LMC distances: "short" vs "long" scale	66
4.6	Conclusions	68

5	Baade-Wesselink method	70
5.1	The model	70
5.2	Radial velocities	71
5.3	Distances	72
5.4	Conclusions	82
6	The Galactic abundance gradient	83
6.1	Interstellar reddening corrections	83
6.2	MIC Relations	84
6.3	Metallicity estimates	86
6.4	The Galactic abundance gradient	93
6.5	Conclusions	95
7	Conclusions	97
A	Light Curves	100
B	Line list	141
	Curriculum Vitae	159

List of Figures

1.1	PL Relation of Shapley 1918	3
1.2	Classification diagram for variable stars	4
1.3	Light Curve of δ Cephei	6
1.4	Light and Radial velocity Curve of δ Cephei	6
1.5	Light curve vs wavelength	7
1.6	Instability strip schema	9
1.7	PL relations in Magellanic Clouds at seven wavelengths	12
1.8	Recent results for the metallicity sensitivity of Cepheid distances	15
2.1	The FEROS complete system	25
2.2	The UVES spectrograph	27
2.3	The Dutch Telescope	28
2.4	Optical layout of the Walraven photometer	29
2.5	The 0.75m telescope	31
2.6	NIR light curves	37
2.7	Light curves in the Walraven V,B,L,U,W bands	38
3.1	The spectral sequence	41
3.2	The Hertzsprung-Russell diagram	42
3.3	Spectral range as observed in three Galactic Cepheids	43

3.4	Definition of the equivalent width W	44
3.5	The equivalent width and the profile changes with the chemical abundance	45
3.6	The distributions of the equivalent widths (EW)	47
3.7	Examples of measurements of equivalent widths with fitline	52
3.8	Histograms of the metallicity derived for the Galaxy, the LMC and the SMC	54
4.1	PL relations for our sample	59
4.2	PL relations calculated in each bin for the V band	62
4.3	PL relations calculated in each bin for the K band	63
4.4	The V -band residuals compared to Freedman et al. (2001) PL relation	65
4.5	The V -band residuals at "long" and "short" distance scale	67
5.1	Radial Velocity Curve of our BW sample	73
5.2	Optical, Infrared and radial velocity Curve for UZ Sct	74
5.3	Optical, Infrared and radial velocity Curve for AV Sgr	75
5.4	Optical, Infrared and radial velocity Curve for V340 Ara	76
5.5	Optical, Infrared and radial velocity Curve for VY Sgr	77
5.6	Baade-Wesselink method for UZ Sct	78
5.7	Baade-Wesselink method for AV Sgr	79
5.8	Baade-Wesselink method for V340 Ara	80
5.9	Baade-Wesselink method for VY Sgr	81
6.1	Comparison between theory and empirical data	85
6.2	Theoretical MIC relation (V-B)	87
6.3	Theoretical MIC relation (V-K)	88
6.4	Empirical MIC relation (V-K)	90

6.5	Theoretical MIC relation (V-B) applied to the calibrating Cepheids	91
6.6	Theoretical MIC relation (V-K) applied to the calibrating Cepheids	92
6.7	Galactic abundance gradient from the entire sample	94

List of Tables

1.1	Overview of recent results for the metallicity sensitivity of Cepheid distances	14
2.1	Main parameters and performances for FEROS	24
2.2	Main parameters and performances for UVES	26
2.3	The bandwidths and effective wavelengths of the five photometric passbands	30
2.4	Mk II System Parameters	32
2.5	Pulsation phases (ϕ) and intrinsic parameters of the Galactic Cepheids	34
2.6	Pulsation phases (ϕ) and intrinsic parameters of the Magellanic Cepheids	35
2.7	BW-data parameters	37
3.1	Stellar parameters and FeI and FeII abundances of our Galactic sample	50
3.2	Stellar parameters and FeI, FeII abundances of our Magellanic Cepheids	51
3.3	Effects on measured FeI and FeII abundances caused by changes in atmospheric parameters.	54
3.4	Comparison of the mean metallicities of the Magellanic Clouds with previous studies	56
5.1	Distances and radii from the BW-analysis	72
6.1	Coefficients of the MIC relations	86
6.2	Mean values and dispersions of the residuals of MIC relations	86
6.3	Theoretical vs empirical MIC relations	89
A.1	Physical parameters of Walraven sample	101

A.2	Physical parameters of the Walraven type II Cepheids	105
A.3	Mean <i>VBLUW</i> magnitudes	106
A.4	Mean <i>VBLUW</i> magnitudes type II Cepheids	110
A.5	NIR Photometry of Galactic Cepheids	111
A.6	NIR Photometry of type II Cepheids	115
B.1	Complete line list	142

Ad Eleonora...

*”Das anschaulichste Beispiel für die
gewaltige Anziehungskraft eines
schwarzen Loches*

*...
ist und bleibt die
Schwabinger 7”*

CHAPTER 1

INTRODUCTION

Cepheids variables have played an important role in astronomy since it was recognized that they could be used to determine distances through their Period-Luminosity relation. In the comparison between theory and observations, the physical properties of a star, such as absolute age and flux, radius size or effective temperature, depend significantly on how well one is able to determine the object distance. Therefore, measuring distances is a crucial point at the core of astrophysical research.

For over one hundred years Cepheids have served as an effective tool for studying the Universe. Cepheids provide one of the best means of determining the distances to nearby galaxies and they are used to calibrate secondary distance indicators, thus they play a crucial role to establish the extragalactic distance scale, being the first rung of the distance ladder. Furthermore the measurement of the Hubble constant (H_0), which sets the scale of the universe in space and time, depends heavily on accurate extragalactic distance measurements.

1.1 Cepheids: a brief history

The first two Cepheids were discovered by two pioneers in the systematic observation of variable stars, E. Pigott and J. Goodricke, in 1784. These were η *Aquilae* and δ *Cephei*, the latter supplied the name now used for this class of stars.

In 1894 A.A. Belopolskii detected periodic variation in the radial velocities¹ of Cepheid and, in 1899, K. Schwarzschild found the amplitude of a Cepheid luminosity variation to be considerably higher in photographic light than in visual light. This pointed to a variability of the temperature, as well as of the luminosity. These facts found their natural explanation in the hypothesis of Cepheids intrinsic variability, first proposed by Ritter in 1879 and later by Umov, Plummer and Shapley (see H. Shapley 1914).

Theoretical work of Sir Arthur Eddington put the pulsation hypothesis on a firmer basis (A. Eddington 1927, 1941, 1942). He showed that Cepheids are single stars that undergo radial pulsation hence their variability is intrinsic and does not depend on the presence of a companion. Later work by S. A. Zhevakin (1963), R. F. Christy (1966), J. P. Cox (1980, and references therein) provided a deeper understanding

¹The radial velocity of a star is the velocity in the direction of the line of sight. This can be measured from the stellar spectrum using the Doppler effect.

of the mechanism driving Cepheid pulsation, known as k, γ – mechanisms. If the star is compressed, the fraction of the Partially Ionized Regions (PIR, where $T \sim 13,000$ K) increases, raising the opacity of the material and blocking the photons trying to escape from the interior. The increased heat and pressure built up in this layer, push the outer layers of the star outward. As these outer layers fall back inward again under the force of gravity, the ionization region gets compressed again, restarting the cycle. The variation in brightness is caused by changes in temperature and in radius caused by these motions. Cepheid pulsations are therefore restricted to stars in a limited temperature range, due to the requirement that the partial ionization zone lies close to the transition from the nearly adiabatic interior to the non-adiabatic exterior of the stellar envelope.

Following the examination of hundreds of photographic plates obtained between 1893 and 1906 at the Harvard College Observatory in Peru, Henrietta Leavitt (1868 - 1921) produced a catalogue of 1777 variable stars in the Magellanic Clouds (MCs)². She classified 47 of these in one of the two clouds as Cepheid variables because of their similarities with the well documented Galactic variable δ Cephei and she noticed that those with longer periods were brighter than the shorter-period ones. She correctly inferred that as the stars were in the same distant cloud they were all at the same relative distance from us, therefore any difference in apparent magnitude³ was related to a difference in absolute magnitude⁴. When she plotted her results, she noted that they formed distinct relationships between brightness and period. Her plot showed what is now known as the period-luminosity (PL) relationship: Cepheids with longer periods are intrinsically more luminous than those with shorter ones. The Danish astronomer, Ejnar Hertzsprung (1873-1967) quickly realized the significance of this discovery: by measuring the period of a Cepheid from its light curve, the distance to that Cepheid could be determined. He realized that if the PL relation could be independently calibrated, then the distance moduli⁵ of these variable stars can be determined directly from their periods. In those days, the main topic was about the Sun's position inside our Galaxy. Hertzsprung realized the importance to calibrate the PL relation related to this problem. With his data on nearby Cepheids, he calculated the distance of the Small Magellanic Cloud (SMC) as 37,000 light years⁶ (~ 11 kpc) away.

At the beginning of the nineteenth century, Harlow Shapley using a larger number of Cepheids, recalibrated the absolute magnitude scale and revised the value of the distance to the SMC to 95,000 light years (~ 29 kpc). However, it was eventually realized that, due mainly to systematic errors and a failure to take into account extinction⁷, his zero point was approximately 1.5 magnitudes too dim. Nevertheless, an extraordinary coincidence led to this not being realized for over 30 years. He also studied Cepheids in 86 Globular Clusters⁸ (GCs), Leavitt herself had remarked upon the similarity of the bright globular cluster variables (GCv) to those in the SMC and he found that the few dozen brightest non-variable stars in each cluster was about 10 times brighter than the average Cepheid magnitude. On the basis of this evidence he could estimate the distance of a large number of globular clusters. He found that these clusters presented the same luminosity. Shapley examined the PL relation for the "long-period" variables in the GC and he found that its slope was very similar to the slope of the SMC Cepheids, accordingly he included these stars in his PL relation. In his 1918 paper, variables from seven stellar systems were combined

²Two dwarf irregular galaxies, satellites of the Milky Way.

³The logarithmic measure of the brightness of an object, measured in a specific wavelength or passband.

⁴The absolute magnitude of an astrophysical object is its magnitude at a fixed distance of 10 pc.

⁵The true distance modulus $\mu = m - M$ is the difference between the apparent magnitude m and the absolute magnitude M of an astronomical object, corrected for reddening.

⁶The light year (ly) is the distance covered by the light in one year and corresponds to $9.461 \cdot 10^{12}$ km or 3.26 pc.

⁷Absorption of light from astronomical objects by matter between them and the observer.

⁸Globular Cluster (GC) are gravitationally bound concentrations of approximately hundred thousand to more than one million of old stars (Population II).

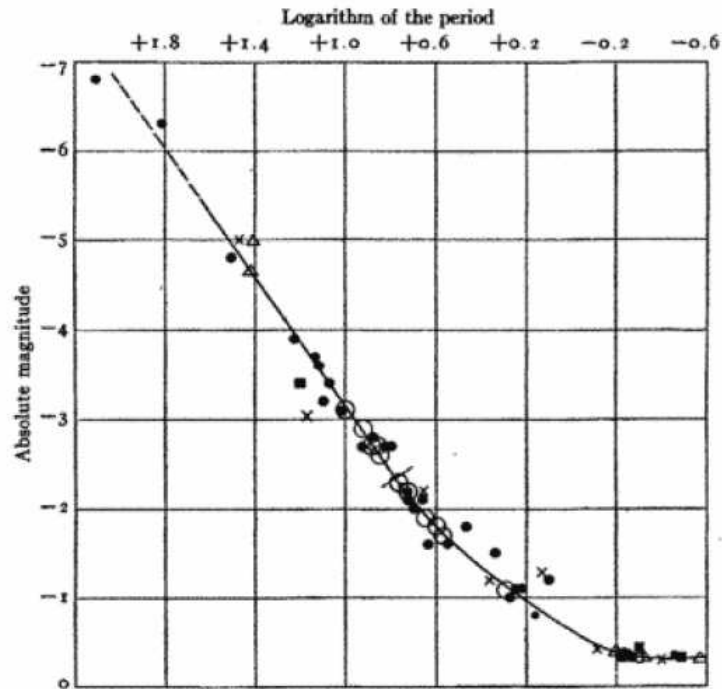


Figure 1.1: The Period-Luminosity relation found by Shapley (1918). Figure from his original paper.

into the single PL relation showed in Fig. 1.1. This figure suggests that Shapley had gone even further than this: the linear relationship breaks down at bottom right due to his inclusion of faint, short period variables. He called these stars "cluster-type Cepheids"; now known as RR-Lyrae variables, which are central He-burning low-mass stars but characterized by the same pulsating mechanism (see Fig. 1.2). By applying this PL relation, Shapley estimated for the first time the distance of the Sun from the Galactic center and found a distance of the order of ten kpc. This demonstrated that the old common belief concerning the central position of the Sun in the Milky Way was wrong. In 1924 Edwin Hubble detected Cepheids in the Andromeda nebula, M31 and the Triangulum nebula M33. Using these, he determined that their distances were 900,000 (~ 270 kpc) and 850,000 (~ 260 kpc) light years respectively. He thus established that these "spiral nebulae" were in fact other galaxies and not part of our Milky Way. This was a seminal discovery and dramatically expanded the scale of the known Universe. Hubble later went on to observe the redshift of galaxies and propose that this was due to their recession velocity, with more distant galaxies moving away at a higher speed than nearby ones. This relationship is now called Hubble's Law and it means that the Universe is expanding.

The Hubble discoveries changed completely the current view of the Universe: all the galaxies are moving away from each other.

In the next three decades several studies of the Cepheids PL relation had been carried out, in particular revisions of Shapley's zero-point for this relation. From 1944 to 1952, Baade's works revealed the existence of two kind of Cepheids with distinct PL relations, the first, known as Classical Cepheids, associated with the disk component of our Galaxy (young stellar population) and the second with the spherical component (old stellar population. These results and the studies of Cepheids in open stellar clusters⁹ (e.g. Sandage, 1958; Kraft 1961) led to the correction of zero-point of the PL relation of a value

⁹Open Clusters are physically related group of young stars (Population I) held together by mutual gravitational attraction.

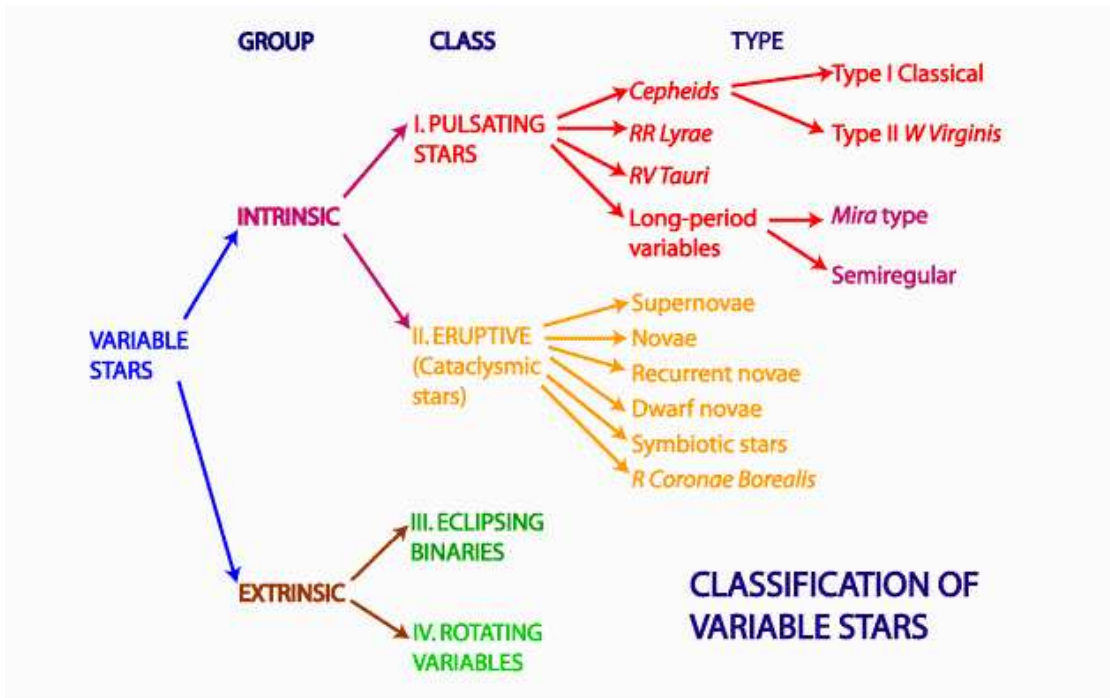


Figure 1.2: Classification diagram for variable stars.

of -1.5 magnitudes and to new estimates of galactic and extragalactic distances (nearly doubled respect to the previous estimates).

With the advent of new technologies and increased use of infrared (IR) wavelengths, the approach of modern studies to the Cepheid calibration shifted towards the empirical, rather than the speculative. Multi-wavelength observations of Cepheid magnitudes, better estimates of reddening effects (i.e. extinction, Freedman 1988), of individual distances of Galactic Cepheids (Feast & Catchpole 1997) and for the Magellanic Clouds distances (see Benedict 2002 for a review on methods and results) greatly improved the determination of the zero-point and slope of the PL relation. In particular, the calibration of the PL relation in the Large Magellanic Cloud (LMC) is essential because this galaxy is the first rung of the extragalactic ladder, since it is the closest external system to our Galaxy, it has a low extinction and little depth on the line of sight (all its Cepheids are roughly, at the same distance).

With the launch of the Hubble Space Telescope (HST) in 1990, it has also been possible to extend the Cepheid distance scale out to the Virgo and Fornax galaxies clusters (HST Key Project, Freedman et al. 2001). In this work, Cepheids play a significant role in the distance determination of galaxies and resulting cosmological implications.

1.2 Cepheids: characteristics

When we look up at the night sky it is easy to imagine that the stars are unchanging. Apart from twinkling due to the effects of our atmosphere stars appear fixed and constant to the untrained eye.

Careful observations, some even done with the naked eye, show that some stars do in fact appear to change in brightness over time. Some exhibit periodic behavior, brightening quickly then diminishing in brightness slowly only to repeat themselves. Some of these changes take place on a time scale of several days, while others occur either on a period of hours or on many months. Other stars exhibit a once-off dramatic change in brightness by orders of magnitude before fading away to obscurity. All of these are examples of what are termed variable stars. A variable star is simply one whose brightness changes over time. At a fundamental level all stars are variable as they evolve and change over time (e.g. from a main sequence to a red giant star). Furthermore, we can infer that all stars are likely to vary their light output to some extent due to variations caused by phenomena such as sunspots. In the section however, we focus our attention on stars with a measurable change in brightness. In order to understand variable stars, astronomers classified them according to observable properties. The diagram in Fig. 1.2 shows the main types of variable stars. The first criteria for classification is whether a star is an intrinsic or an extrinsic variable. Intrinsic variables are those in which the change in brightness is due to some change within the star itself such as in pulsating stars. Extrinsic variables are those in which the light output changes due to some process external to the star itself. As shown in the diagram (Fig. 1.2), Cepheids are variable stars which belong to the group of intrinsic variable and to the class of Pulsating stars. They can be divided in two categories:

1. **Type I or Classical Cepheids:** they are *intermediate-mass* stars (Population I) and we will discuss their characteristics in more details afterwards.
2. **Type II or W Virginis Cepheids :** they are *low-mass* stars (Population II), intrinsically less luminous, at given period, and older than the Classical Cepheids.

Both types of Cepheids exhibit distinct PL relations. Since the goal of this thesis project is the study of a sample of Classical Cepheids we will not discuss Type II Cepheids. For this reason the adjective "Classical" will be omitted in the following.

Cepheids are supergiant stars with luminosities 500-300,000 times greater than of the Sun ($L_{\odot} = 3.3 \cdot 10^{33} \text{ erg s}^{-1}$) and their surface temperatures are similar to the Solar temperature ($T_{\odot} \sim 6000 \text{ K}$). The masses of this type of variables are between 3 and 15 Solar Masses ($M_{\odot} = 1.99 \cdot 10^{33} \text{ g}$). They undergo regular radial pulsation (i.e. the star expands and contracts) with periods ranging from 1 to 90 days, and in the Magellanic Clouds they have been observed to have periods ranging up to 200 days. More than 400 Cepheids are known in the Milky Way, 1300 and 2000, respectively, have been found in the Large and in the Small Magellanic Clouds (thanks to the large survey of the Optical Gravitational Lensing Experiment, OGLE), as well as substantial numbers in other nearby galaxies.

Cepheids are easily recognized by their distinctive light-curves (LCs)¹⁰, which are characterized by a rapid rise to maximum brightness, followed by a slow decline to their minimum (see Fig. 1.3). This pattern of changing brightness is repeated in a very regular cycle. The light curve of a Cepheid is matched by its radial velocity curve, which is almost a mirror image of the light curve with minimum radial velocity at the light maximum. An example is shown in Fig. 1.4. We only note that in this light curve, the magnitude has been plotted as a function of phase¹¹. The positive (redshifted) half of the velocity curve corresponds to the contraction of the star from its maximum to minimum radius, which is the later part of the decreasing of the light curve to minimum brightness and the beginning of the rising to maximum brightness. The negative (blueshifted) half of the velocity curve corresponds to the expansion of the star and the brightest part of the light curve. During the same period the surface temperature reaches

¹⁰The variation of the luminosity of the stars as a function of time.

¹¹ $\phi = (t - E)/P$ where t is the date of observation in JD, E is the Epoch of maximum and P is the period.

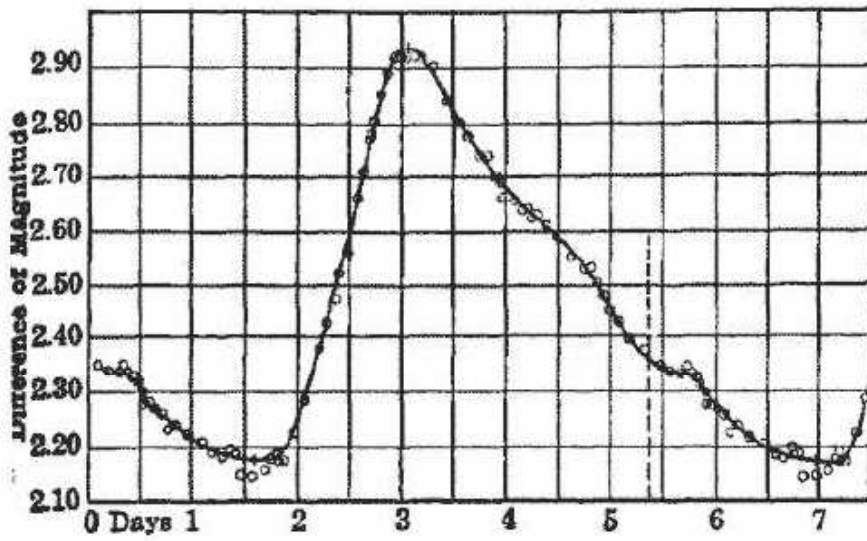


Figure 1.3: The light curve of δ Cephei, the prototype of this class (from Hoskin 1999).

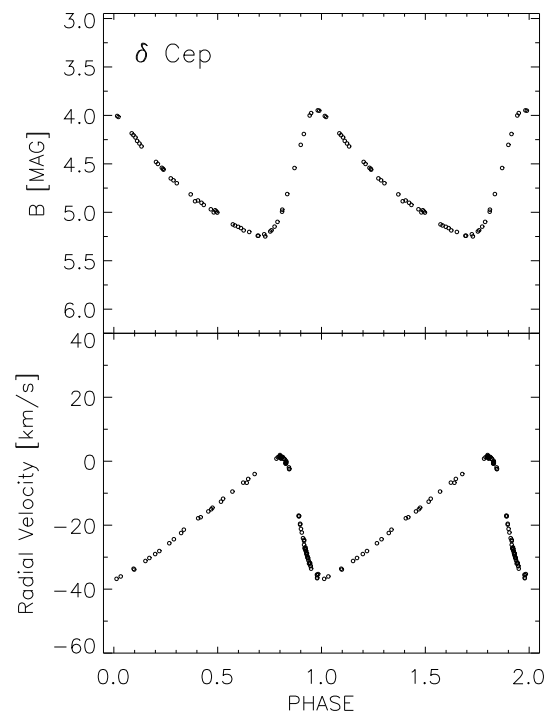


Figure 1.4: Top panel: The light curve of δ Cephei in B band (data from Moffett et al. 1984). Bottom panel: Radial Velocity Curve of δ Cephei (data from Bersier et al. 1994). In both panels we plot two periods of their cycle.

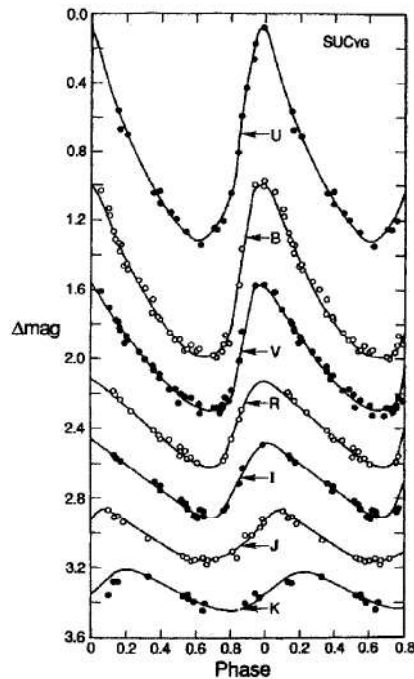


Figure 1.5: Light curves in different colors for a Galactic Cepheid, showing the change in amplitude and phase with the selected bands (from Madore & Freedman 1991).

its highest effective temperature and gradually cools as the star completes its expansion. The amplitude usually lies in the range $30 - 60 \text{ km} \cdot \text{s}^{-1}$.

Because of their characteristic light curve and intrinsic brightness, these stars can be identified at great distances and make excellent markers for determining distances through their period-luminosity relationship.

The first study of Cepheid light curves which gave useful results were those of E. Hertzsprung (1926). He selected 37 of the most reliable curves and described the main features of their variations with an increase in period. The principal result of this and other studies of the time can be summarized as follows:

- up to a period of 6 days the light curves are usually smooth, with a rapid rise in luminosity and a more gradual drop;
- at about 6 days a hump appears on the descending branch of the light curve, and then the hump grows and approaches the principle maximum;
- close to a period of 9 or 10 days the hump is so large that the light curve sometimes has two nearly identical peaks;
- with a further increase in the period, the secondary feature becomes the maximum and the true maximum becomes a hump on the ascending branch.

The changes in the shape of the light curve with the period is now known as the Hertzsprung progression.

Applying Fourier analysis to the light curve, the existence of the Cepheids that do not pulsate in the fundamental mode (as in general a Cepheid does) has been discovered. Cepheids can pulsate in the first overtone mode (Pel & Lub 1978; Böhm-Vitense 1994), the second overtone mode (Udalsky et al. 1999b; Bono et al. 2001) and also in the two modes simultaneously (Fitch 1970; King et al. 1975; Pardo & Poretti 1997). Theoretical predictions and observations suggest that first overtone periods range from $\log P \sim 0.6$ to 0.9 for the Milky Way, from $\log P \sim 0.7$ to 0.8 for LMC and from $\log P \sim 0.6$ to 0.8 for SMC (Bono et al. 2002). The double-mode Cepheids usually pulsate in the fundamental and the first overtone modes and the longer of the two is between 2 and 4 days. Appendix A includes all the LCs of our photometric sample (~ 170 Cepheids).

Photometric observations of Cepheids have shown a number of other interesting characteristics. The amplitude of variation is observed to decrease with increasing wavelength (see Fig. 1.5). The *B* and *V* band photometric variations are due primarily to changes in the surface temperature, while in the near infrared, the observed luminosity changes are primarily due to the variation in the radius of the star. From *B* to *K* band a typical Cepheid amplitude drops from 1.0 mag to 0.2 mag. As shown in Fig. 1.5 the variation of the amplitude in the infrared is relatively small, it means that a single observation in the near infrared can be enough to estimate the average luminosity and give a useful distance determination while, at bluer wavelengths, to obtain the same results would be required several dozen observations (see also section 1.6).

Another important characteristic of Cepheids has emerged from radial velocity measurements: the incidence of binaries (mainly spectroscopic¹²) among these variables exceeds 50% (Szabados 1995). The orbital periods of these binary systems are generally long (1-5 yrs) and a typical companion is a main sequence star. It means that the companion is much hotter (temperature between 20,000 K and 10,000 K) therefore its light contribution is in the ultraviolet while the Cepheid dominates at visible wavelengths (Evans 1991).

1.3 Cepheids: evolution

Cepheids are evolved intermediate-mass stars, in particular they experience central He-burning and hydrogen shell burning evolutionary phases. They are associated with the so-called *Blue Loops* and are crossing the Cepheid instability strip¹³ (Becker & Iben 1979; Bono et al. 1999) in the Hertzsprung-Russell (HR) diagram¹⁴ (see Fig. 1.6). Cepheids cross the instability strip more than once during their lifetime and the crossing times also depend on the stellar mass. The first crossing of the instability strip occurs during the hydrogen-shell burning phase as the star evolves on its way to become a red giant¹⁵. The occurrence of the blue loop causes the second and third crossing of the instability strip. The morphology of the Blue Loops depends on several mechanisms (convection, mass-loss, rotation) and on input physics (radiative opacities). We still lack a firm knowledge of the phenomena driving its temperature extension and occurrence (Bono et al. 2000b). However, current theoretical prediction indicate that Cepheids spend

¹²Two stars that are gravitationally bound to each other and that cannot be visually resolved. Their components are distinguished spectroscopically.

¹³The Cepheid instability strip define a range of luminosities and effective temperatures within which stars are pulsationally stable.

¹⁴The Hertzsprung-Russell diagram is a plot of luminosity vs temperature, except that the temperature is decreasing to the right of the horizontal axis. It is used to classify stars according to their luminosity, spectral type, color, temperature and evolutionary stage.

¹⁵Stars of Solar mass or higher which have exhausted the hydrogen in their cores and started burning hydrogen in a shell outside the core.

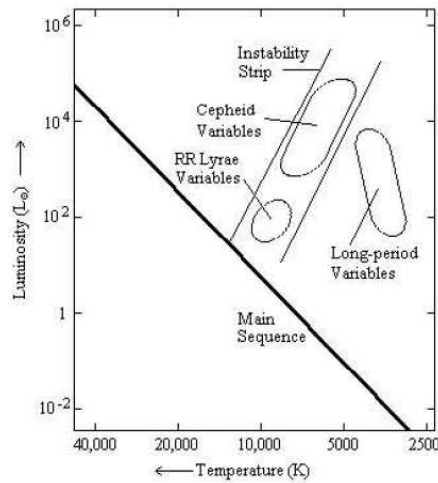


Figure 1.6: Schematic representation of the instability strip in the HR diagram.

a significant fraction of their lifetime in the second and third crossing of the instability strip.

1.4 The distance scale

Classical Cepheids are the keystone of both Galactic and extragalactic distance scale. In fact they are the best known primary distance indicators, they are used to provide the step from our Galaxy to the nearby universe and to calibrate secondary distance indicators, such as supernovae type Ia (SNeIa) and the Tully-Fisher relation¹⁶. During the last years microlensing experiments (MACHO, EROS) detected and measured a large sample of Cepheids in the Magellanic Clouds (MCs). At the same time space telescopes such as Hipparcos supplied very accurate distance determinations of Galactic Cepheids by means of trigonometric parallaxes (Feast & Catchpole 1997), while HST detected a good sample of Cepheids in galaxies in the Virgo cluster (Ferrarese et al. 1996). In spite of this unprecedented observational effort several long-standing problems concerning the properties of Cepheids and thus the determination of the distances need to be firmly assessed. In fact even though it has been suggested (Gould 1994) that the Cepheid intrinsic luminosity depends on the chemical composition both the sign and the value of the scaling factor for correcting the distance modulus obtained by Sasselov et al (1997) are at odds with theoretical predictions (Bono et al. 1998a,b).

Classical Cepheids present several advantageous features when compared with other stellar distance indicators. These are illustrated by the points below:

- they are bright giants that can be easily identified due to their intrinsic variability and for which accurate photometric and spectroscopic data can be collected;

¹⁶The Tully-Fisher relation measures the distance to rotating spiral galaxies by the width of galactic spectral lines. This empirically-derived relation states that the luminosity of a galaxy is directly proportional to the fourth power of its rotational velocity, which can be calculated from the width of the spectral line, especially the 21-cm hydrogen line.

- they obey to well defined optical and near-infrared (NIR) Period-Luminosity (PL) relations and their distances can be estimated with an accuracy of the order of a few percent (Benedict et al. 2006; Marconi et al. 2006; Natale et al. 2007; Fouque et al. 2007);
- they are distributed across the Galactic disk, and therefore, they can be adopted to trace the radial distribution of intermediate age stars (Kraft & Schmidt 1963). In particular, they provide robust constraints on the iron and heavy elements radial gradients (Lemasle et al. 2007, and references therein).
- are common enough in the spiral galaxies that large samples can be collected to beat down statistical noise.

However, Classical Cepheids also present a few drawbacks:

- the lifetime they spend inside the instability strip is approximately two orders of magnitude shorter than the central hydrogen burning (Bono et al. 2000). This together with the low spatial density and the high reddening account for the limited sample of Galactic Cepheids currently known (Ferne et al. 1995)
- they cannot be observed far enough, with current technology, to measure directly the Hubble constant H_0 , i.e. they can only be observed in galaxies among which the gravitational interactions are more important (local universe) than the relative motion of non-interacting galaxies due to the expansion of the universe.
- Accurate mean magnitudes and colors require a detailed time sampling along the pulsation cycle. The Cepheid periods range from a few days to hundred days. Therefore, well sampled multiband light curves require long observing runs.
- They are intermediate-mass objects so they are not found in the elliptical galaxies;
- In the Milky Way are barely within the reach of geometrical distance determination and tend to suffer high extinction due to dust in the disk;
- Are still difficult to model in some respects, particularly concerning the location of the red edge of the instability strip in the HR diagram (Bono et al. 1997, 1999).

On the other hand a lot of work has been accomplished using these stars as first step of the extragalactic distance scale and to calibrate several secondary distance indicators. The PL relations are calibrated locally in the Milky way and in the Magellanic Clouds. In recent years, extragalactic studies have mostly used PL relations derived in the LMC. Prior to HST, Cepheids had only been well studied in the Local Group and other galaxies within about 4 Mpc (Cepheids had been detected in more distant galaxies but only in very small numbers). At that time very few of these galaxies were useful for checking and calibrating secondary distance indicators. With HST the situation has changed dramatically so that 30 new galaxies have been observed for Cepheids reaching to 30 Mpc and more. Furthermore, these were mostly chosen specifically to be useful from the point of view of secondary indicators (Freedman et al 2001). Establishing accurate distances over cosmologically significant scales is crucial to pin down the value of the Hubble constant (see Jensen et al 2003 for a review on the extragalactic distance scale). This constant sets the correlation between the recession velocity v of a galaxy and its distance d , i.e. the Hubble law: $v = H_0 d$. The inverse of H_0 sets the age of the universe, t_0 , and the size of the observable universe,

$R_{obs} = ct_0$, given a knowledge of the total energy density of the universe. The square of the Hubble constant relates the total energy density of the universe to its geometry (Peacock 1999). The current value of H_0 is now known with an accuracy better than 10% and this is largely due to the tremendous increase in the number of galaxies in which Cepheids have been discovered that we have mentioned above (HST Key Project, Freedman et al 2001). Increasingly accurate secondary distance indicators, many calibrated using Cepheids, now provide largely concordant measurements of H_0 . The value found by Freedman et al (2001) is $H_0 = 72 \pm 8 \text{ km}^{-1} \text{ Mpc}^{-1}$. The largest sources of errors result from photometric calibration of the HST Wide Field and Planetary Camera 2, uncertainties in the distance to the LMC and the effects of the metallicity on the Cepheid PL relation.

1.5 The Baade-Wesselink Method

Obtaining accurate distances to stars is a non-trivial matter. Cepheids are considered an important standard candle as they are bright and are thus the link between the distance scale in the nearby universe and that further out via those galaxies that contain both Cepheids and SNeIa. Distances to local Cepheids may be obtained via main sequence fitting for those Cepheids in clusters (e.g. Feast 1999) or via determination of the parallax. Until recently only Polaris had an accurate parallax determination via Hipparcos (Evans et al 2008). Benedict et al. (2007) recently published absolute trigonometric parallaxes for nine Galactic Cepheids using the *Fine Guidance Sensor* on board the *Hubble Space Telescope* and revised, more accurate, Hipparcos parallaxes have also become available (van Leeuwen et al. 2007; van Leeuwen 2007). In addition, distances to Cepheids can be obtained from the Baade-Wesselink method (BW). This method relies on the availability of Infrared Surface-Brightness (IRSB) relations to link variations in color to variations in angular diameters and understanding of the projection (p-) factor that links radial velocity to pulsational velocity variations. The IRSB relations can be obtained using Cepheids that have accurate interferometrically determined angular diameters over the pulsation phase and accurate multi-wavelength light curves. This has allowed Kervella et al. (2004) and Groenewegen (2007, hereafter G07) to derive such relations, in particular using the $(V - K)$ color, which gives the highest precision in the derived angular diameter. The p-factor can also be obtained from Cepheids with interferometrically determined angular diameters over the pulsation phase when in addition accurate radial velocity (RV) curves are available (see e.g. Mérand et al. 2005). G07 assembled all currently available data to find that a constant p-factor represents the best fit to the available data. A strong dependence on period, like $p \sim -0.15 \cdot \log P$ as proposed by Gieren et al. (2005), could be ruled out. A moderate dependence of $p \sim -0.03 \cdot \log P$ as used in the Gieren et al. papers (1993, 1997, 1998; Storm et al. 2004; Barnes et al. 2003), or $p \sim -0.064 \cdot \log P$ as advocated by Nardetto et al. (2007) are also consistent with the available data. The distances to the galactic Cepheids mostly came from BW-distances available at that time from Fouqué et al. (2003). In the last few years significant progress has been made in several areas. On the one hand more Cepheids have interferometrically determined angular diameters. Combined with improved theoretical studies (Nardetto et al. 2007, and references therein) this has led to an improved understanding of the p-factor and IRSB relations, as was studied in G07. On the other hand, more basic photometric light curves and radial velocity data have become available and new studies have presented metallicity determinations for significant samples.

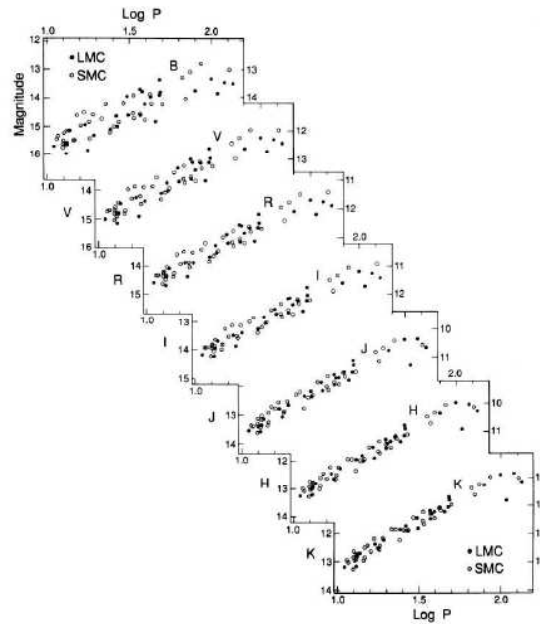


Figure 1.7: Magellanic Clouds Cepheid PL relation at seven wavelengths, from the blue to the near-infrared. The LMC Cepheids are shown as filled circles; the SMC data, shifted to the LMC distance, are shown as open circles (from Madore & Freedman 1991). Note the decreased width of the relations as longer and longer wavelengths are considered.

1.6 Period-Luminosity relation

As we have already mentioned before Cepheids are good distance indicator through their Period-Luminosity relation. Its general form is:

$$\langle M \rangle = \alpha + \beta \cdot \log P \quad (1.1)$$

where $\langle M \rangle$ is the mean absolute magnitude of the Cepheid at a given wavelength, P is the period of the variable, α is the zero point and β is the slope of the relation. The PL relation presents an intrinsic scatter in luminosity at a given period. This scatter is correlated to the finite width of the instability strip hence to a color term (see Fig 1.6). At constant period, the B-magnitude total width of the PL relation is about 1.2 mag while the V-magnitude width is measured to be about 0.9 mag. The intrinsically bluest¹⁷ Cepheids are expected to have the brightest absolute magnitudes for a given period. The PL relation is, then, a statistical relation, which provides the average of the Cepheid absolute magnitudes. In estimating distances, any individual Cepheid could deviate from the statistical ridge line by up to ± 0.6 mag in B band; such an error (if applied to one Cepheid) would translate into an equivalent error of about $\pm 30\%$ in distance. Large samples can decrease the error on the magnitude inversely with the square root of the number of stars, a formal error of only 10% being possible with a sample containing as few as a dozen Cepheids. However this is true only if the sample of Cepheids well-populated the whole PL relation, i.e. covers a wide range in period. As we have already mentioned in section 1.2, different works (e.g. Pel et al 1981; Böhm-Vitense, 1994; Bono et al 2002) pointed out the existence of two distinct PL relations

¹⁷i.e. hottest, near the left edge of the instability strip.

for Cepheids that pulsate in the fundamental (F) mode and in the first overtone (FO) mode. The range of periods for the FO PL relation and the width of their instability region is significantly smaller than for the fundamental one. Current predictions (Bono et al, 2002) suggest that, at $\log P = 0.3$, the width of the FO instability strip is 400 K, while for F Cepheids it is 900 K at $\log P = 1$. Therefore, distances based on FO PL relation are less affected by intrinsic spread when compared with F one. Regrettably complete and accurate samples of FO variables are available only for Magellanic Cepheids and the detection of this type of stars in external galaxies is more difficult than for the F Cepheids, since they are fainter and the luminosity amplitudes are smaller. Regarding double mode Cepheids, theoretical models and observations support the evidence that F and FO modes of double-mode Cepheids follow very well the PL relations of pure F and pure FO pulsators. As we have already mentioned in section 1.2, the amplitudes of individual Cepheids (see Fig. 1.5) decrease with the wavelength of the observation, this is due to a much decreased sensitivity of the infrared surface brightness to the temperature. For exactly the same reason, the observed width of the PL relation decreases dramatically with the wavelength (see Fig 1.7). In the infrared bands the PL relation shows a remarkably small scatter (± 0.2 mag). Thus, Cepheids observed at long wavelengths and at random points in their cycle are closer to their time-averaged mean magnitudes than the equivalent observation at shorter wavelengths. From *B* band to *K* band the width of the PL relation decreases from 1.2 mag to 0.5 mag. As a result, for distance determinations even single, random-phase observations of known Cepheids, when made in the near-infrared, are comparable in accuracy to complete time-averaged magnitudes (derived from a dozen or more observations) in the blue.

1.6.1 The metallicity problem

The debate on the role played by the chemical composition on the pulsational properties of Cepheids is still open, with different theoretical models and observational results leading to markedly different conclusions.

From the theoretical point of view pulsational models by different groups lead to substantially different results. Linear models (e.g. Chiosi et al 1992; Sandage et al 1999; Baraffe & Alibert 2001), based on non adiabatic pulsational models, suggest a moderate dependence of the PL relation on the metallicity. The predicted change is less than 0.1 mag over the metallicity¹⁸ interval from $Z = 0.004$ to $Z = 0.02$ at $\log(P) = 1$, independent of wavelengths. Non-linear convective models (e.g. Bono et al 1999; Caputo et al 2000; Caputo 2008) instead predict a larger dependence on the same interval of metallicity: the change is 0.4 mag in *V*, 0.3 mag in *I* and 0.2 mag in *K*, again at $\log(P) = 1$. Moreover, the predicted change in these latter models is such that metal-rich Cepheids are fainter than metal-poor ones, at variance with the results of the linear models. Fiorentino et al (2002) and, more recently, Marconi, Musella & Fiorentino (2005) investigations, also based on non-linear models, suggested that there may be also a dependence on the helium abundance.

On the observational side, the majority of the constraints comes from indirect measurements of the metallicity, mostly in external galaxies, such as oxygen nebular abundances derived from spectra of *HII* regions at the same Galactocentric distance of the Cepheid field (e.g. Sasselov et al 1997; Kennicutt et al 1998; Sakai et al 2004). These analyses indicate that metal-rich Cepheids are brighter than metal-poor ones (hence at variance with the predictions of non-linear convective models), but it is important to note that the results span a disappointingly large range of values (see Table 1.1 and Fig. 1.8). In order to better constrain a possible dependence of the Cepheid PL relation on the metallicity, a better approach

¹⁸The metallicity of an object is the proportion in mass of its matter made up of chemical elements other than hydrogen and helium. It is indicated with *Z*.

Table 1.1: Overview of recent results for the metallicity sensitivity of Cepheid distances. In the first column is listed the variation of the distance modulus μ per dex of metallicity, the negative sign indicates that the true distance is longer than the one obtained neglecting the effect of the metallicity. In the second column is listed the elemental abundance used as reference for the metallicity. The third and fourth columns give the method and the reference of the different studies. See also Fig. 1.8

$\delta\mu/\delta[M/H]$ (mag/dex)		Method	Reference
-0.32 ± 0.21	[Fe/H]	Analysis of Cepheids in 3 fields of M31 (<i>BVRI</i> bands)	Freedman & Madore (1990)
-0.88 ± 0.16	[Fe/H]	Comparison of Cepheids from 3 fields of M31 and LMC (<i>BVRI</i> bands)	Gould (1994)
-0.40 ± 0.20	[O/H]	Simultaneous solution for distances to 17 galaxies (<i>UBVRIJHK</i> bands)	Kochanek (1997)
$-0.44^{+0.10}_{-0.20}$	[O/H]	Comparison of EROS observations of SMC and LMC Cepheids (<i>VR</i> bands)	Sasselov et al. (1997)
-0.24 ± 0.16	[O/H]	Comparison of HST observations of inner and outer fields of M101	Kennicutt et al. (1998)
-0.12 ± 0.08	[O/H]	Comparison of 10 Cepheid galaxies with Tip of the Red Giant Branch distances	Kennicutt et al. (1998)
-0.20 ± 0.20	[O/H]	Value adopted for the HST Key Project final result	Freedman et al. (2001)
0	[Fe/H]	OGLE result comparing Cepheids in IC1613 and MC (<i>VI</i> bands)	Udalski et al. (2001)
0	[O/H]	Comparison of Planetary Nebula luminosity function distance scale and Surface Brightness fluctuation distance scale	Ciardullo et al. (2002)
-0.24 ± 0.05	[O/H]	Comparison of 17 Cepheid galaxies with Tip of the Red Giant Branch distances	Sakai et al. (2004)
-0.21 ± 0.19	[Fe/H]	Baade-Wesselink analysis of Galactic and SMC Cepheids (<i>VK</i> bands)	Storm et al. (2004)
-0.23 ± 0.19	[Fe/H]	Baade-Wesselink analysis of Galactic and SMC Cepheids (<i>I</i> band)	Storm et al. (2004)
-0.29 ± 0.19	[Fe/H]	Baade-Wesselink analysis of Galactic and SMC Cepheids (<i>W</i> index)	Storm et al. (2004)
-0.27 ± 0.08	[Fe/H]	Compilation from the literature of distances and metallicities of 53 Galactic and MC Cepheids (<i>VIWK</i> bands)	Groenewegen et al. (2004)
-0.39 ± 0.03	[Fe/H]	Cepheid distances to SNe Ia host galaxies	Saha et al. (2006)
-0.29 ± 0.09	[O/H]	Cepheids in NGC 4258 and [O/H] gradient from Zaritsky et al. (1994)	Macri et al. (2006)
-0.10 ± 0.03	[Fe/H]	Weighted mean of Kennicutt, Macri and Groenewegen estimates	Benedict et al. (2007)
-0.017 ± 0.113	[O/H]	Comparison between Cepheid and TRGB distances for 18 galaxies	Tammann et al. (2007)
0	[Fe/H]	Comparison between the slopes of Galactic and LMC Cepheids	Fouqué et al. (2007)
$+0.05 \pm 0.03$	[Fe/H]	Predicted Period-Wesenheit (<i>V, I</i>) relation	Bono et al. (2008)

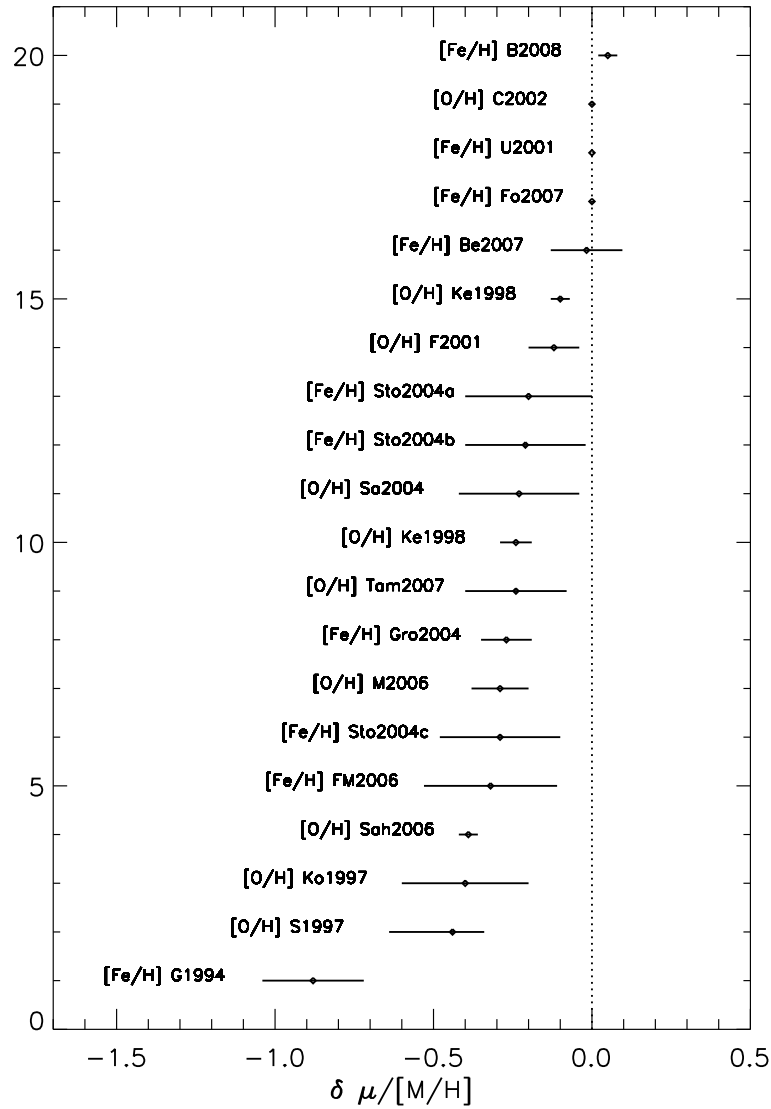


Figure 1.8: Comparison of recent results for the metallicity sensitivity of Cepheid distances. FM1990: Freedman & Madore (1990); G1994: Gould (1994); Ko1997: Kochanek (1997); S1997: Sasselov et al. (1997); Ke1998: Kennicutt et al. (1998); F2001: Freedman et al. (2001); U2001: Udalski et al. (2001); C2002: Ciardullo et al. (2002); Sa2004: Sakai et al. (2004); Sto2004: Storm et al. (2004); Gro2004: Groenewegen et al. (2004); M2006: Macri et al. (2006); Sah2006: Saha et al. (2006); Be2007: Benedict et al. (2007); Fo2007: Fouqué et al. (2007); Tam2007: Tammann et al. (2007); B2008: Bono et al. (2008). See Table 1.1

is to measure directly the metal content of Cepheid stars, which, so far, has been attempted only by few studies, primarily focused on stars of our own Galaxy (cf Fry & Carney 1997; Andrievsky et al 2002a, 2002b, 2002c and 2004; Luck et al 2003). Fry & Carney (1997, hereafter FC97), for instance, have derived iron and α element¹⁹ abundances for 23 Galactic Cepheids from high resolution and high signal-to-noise spectra. They found a spread in $[\text{Fe}/\text{H}]$ ²⁰ of about 0.4 dex, which they claim it is real. With approximately half of their sample (stars belonging to clusters or associations) they have made a preliminary evaluation of metallicity effects on the zero point of the PL relation, finding that metal-rich Cepheids are brighter than metal-poor ones at the same period. Thus, finding a result similar to the studies based on indirect measurements of the metallicity.

The impressive observational effort carried out by Andrievsky and collaborators (Andrievsky et al 2002a, 2002b, 2002c; Luck et al 2003; Andrievsky et al 2004) has instead taken advantage of high resolution spectra of 130 Galactic Cepheids (collected with different instruments at different telescopes) in order to determine their chemical composition and study the Galactic abundance gradient (see also section 1.7). In relation to our work, it is important to note that Andrievsky and collaborators did not investigate the effects of the chemical composition on the Cepheid PL relation: on the contrary, they used the PL relation to determine the distances of their stars. Outside our Galaxy, Luck & Lambert (1992, hereafter LL92) have studied 10 Cepheids in the Magellanic Clouds (5 in LMC and 5 in the SMC). For LMC, they found a mean $[\text{Fe}/\text{H}]$ of -0.36 dex with a dispersion of 0.3 dex, while for the SMC the mean $[\text{Fe}/\text{H}]$ is -0.6 dex with a rather small dispersion (less than 0.15 dex). In subsequent investigation, Luck et al. (1998, hereafter L98), based on ten LMC Cepheids and six SMC Cepheids, four of which in common with LL92, confirmed the mean $[\text{Fe}/\text{H}]$ value of LMC (-0.30 dex), found very little evidence of a significant metallicity dispersion in the LMC (contrary to LL92, but similarly to the SMC) and slightly revised downwards the mean $[\text{Fe}/\text{H}]$ of the SMC (-0.74 vs -0.60 from LL92).

It is worth mentioning two studies that have followed slightly different approaches. Groenewegen et al (2004) have selected from the literature a sample of 37 Galactic, ten LMC and six SMC Cepheids for which individual metallicity estimates and *BVIK* photometry were known. Their work aimed at investigating the metallicity dependence of the PL relation using individual metallicity determinations as well as good individual distance estimates for Galactic Cepheids. They inferred a metallicity effect of about -0.27 ± 0.08 mag/dex in the zero point in the *V*, *I*, *K* bands and the Wesenheit index W ²¹, in the sense that metal-rich Cepheids are brighter than the metal-poor ones (see Table 1.1 and Fig. 1.8, for a comparison with other studies). Also Storm et al (2004) discussed the effect of the metallicity on the PL relation using 34 Galactic and five SMC Cepheids, for which they determined accurate individual distances with the Baade-Wesselink method. Using an average abundance for the SMC Cepheids of $[Fe/H] = -0.7$ and solar metallicity for the Galactic ones, they determined, in a purely differential way, the following corrections: -0.21 ± 0.19 mag/dex for the *V* and *K* bands, -0.23 ± 0.19 mag/dex for the *I* band and -0.29 ± 0.19 mag/dex for the Wesenheit index *W*. These are in quite good agreement with Groenewegen et al (2004). More recently Macri et al. (2006) found, by adopting a large sample of Cepheids in two different fields of NGC 4258 and the $[\text{O}/\text{H}]$ gradient based on *HII* regions provided by Zaritsky et al. (1994), a metallicity effect of $\gamma = -0.29 \pm 0.09$ mag/dex. This galaxy has been adopted as a benchmark for estimating the metallicity effect, since an accurate geometrical distance based on water maser emission is available (Herrnstein et al. 2005). However, in a thorough investigation Tammann et al. (2007) suggested that the flat slope of the Period-Color relation of the Cepheids located in the inner metal-rich field could be due to a second parameter, likely helium, other than the metal abundance. Furthermore, Bono et al. (2008) found, using the new and more accurate nebular oxygen abundances

¹⁹Isotopes that are integer multiples of the mass of the helium nucleus: C, O, Mg, Si, S, Ar, Ca, Ti

²⁰ $[\text{Fe}/\text{H}] = \log_{10}(Z_{\text{star}}/Z_{\odot})$, where $Z_{\odot} = 0.0198$

²¹Reddening-free index defined as: $W = V - 2.42 \cdot (V - I)$, where 2.42 is the value of $\frac{A_V}{E(V-I)}$.

for a good sample of *HII* region in *NGC4258* provided by Díaz et al. (2000), a shallower abundance gradient. In particular, the new estimates seem to suggest that both the inner and the outer field might have a mean oxygen abundance very similar to LMC. They also found a very good agreement between predicted and observed Period-Wesenheit (V, I) relation. Nonlinear convective models predict for this relation a metallicity effect of $\gamma = +0.05 \pm 0.03$ mag/dex. On the basis of independent distances for 18 galaxies based on Cepheid and on the Tip of the Red Giant Branch, Tammann et al. (2007) found a small metallicity effect ($\gamma = 0.017 \pm 0.113$ mag/dex). On the other hand, Fouqué et al. (2007) using a sample of 59 Galactic Cepheids whose distances were estimated using different methods - HST trigonometric parallaxes (Benedict et al. 2007), revised Hipparcos parallaxes (van Leeuwen et al. 2007), infrared surface brightness method (Fouqué & Gieren 1997), and interferometric Baade-Wesselink method (Kervella et al. 2004), zero-age-main-sequence fitting of open clusters (Turner & Burke 2002) - found no significant difference between optical and Near-Infrared (NIR) slopes of Galactic and LMC Cepheids (Udalski et al. 1999; Persson et al. 2004).

Despite these ongoing observational efforts, it is important to underline that none of the observational studies undertaken so far has directly determined elemental abundances of a large sample of Cepheids in order to explicitly infer the metallicity effect on the PL relation, taking advantage of a sample that has been homogeneously analyzed. Therefore, this kind of analysis is the necessary step to improve our knowledge about the metallicity effect and put tight constraints to the theoretical models. The novelty of our approach consists exactly in this, i.e. in the homogeneous analysis of a large sample of stars (more than 300) spanning a factor of ten in metallicity and for which we have high-resolution and high-signal-to-noise spectra and optical and NIR photometry. Preliminary results based on a subsample of the data discussed here were presented by Romaniello et al. (2005) and Romaniello et al. 2008.

1.7 The disk abundance gradient

Abundance gradients as observational characteristics of the Galactic disc are among the most important input parameters in any theory of Galactic chemical evolution. Chemodynamical evolutionary models provide interesting predictions concerning the formation and evolution of the Milky Way. However, the plausibility and accuracy of these predictions need to be validated with observational data. Further development of theories of Galactic chemodynamics is dramatically hampered by the scarcity of this observational data, their large uncertainties and, in some cases, apparent contradictions between independent observational results. For these reasons, many questions concerning the present-day abundance distribution in the galactic disc, its spatial properties, and evolution with time, still have to be answered. The most commonly adopted observables are the star formation rate and the abundance gradients across the Galactic disk. In recent years the problem of radial abundance gradients in spiral galaxies has emerged as a central problem in the field of Galactic chemodynamics.

1.7.1 A brief review

Abundance gradients were discovered first by Searle (1971) in six external galaxies using *HII* regions. However, their occurrence in our Galaxy remained controversial as they are not easy to observe due to the fact we are embedded in the Galactic disk. Other discussions of the galactic abundance gradient, as

determined from several studies, were provided by Friel (1995), Gummersbach et al. (1998), Hou et al. (2000). Here we briefly summarize some of the more pertinent results.

1. A variety of objects (planetary nebulae, cool giants/supergiants, F-G dwarfs, old open clusters) seem to give evidence that an abundance gradient exists. Using *DDO*, Washington, *UBV* photometry and moderate resolution spectroscopy combined with metallicity calibrations for open clusters and cool giants the following gradients were derived ($d[Fe/H]/dR_G$): -0.05 dex kpc^{-1} (Janes 1979), -0.095 dex kpc^{-1} (Panagia & Tosi 1981), -0.07 dex kpc^{-1} (Harris 1981), -0.11 dex kpc^{-1} (Cameron 1985), -0.017 dex kpc^{-1} (Neese & Yoss 1988), -0.13 dex kpc^{-1} (Geisler et al. 1992), -0.097 dex kpc^{-1} (Thogersen et al. 1993), -0.09 dex kpc^{-1} (Friel & Janes 1993), -0.091 dex kpc^{-1} (Friel 1995), -0.09 dex kpc^{-1} (Carraro et al. 1998), -0.06 dex kpc^{-1} (Friel 1999; Phelps 2000). The slopes based on old Open Clusters still show a large spread. By adopting a sample of 40 clusters distributed between the solar circle and $R_G \sim 14$ kpc, Friel et al. (2002) found a slope of -0.06 dex kpc^{-1} . More recently, Carraro et al. (2007) using new accurate metal abundances for five old open clusters located in the outer disk together with the sample adopted by Friel et al. (2002) found a much shallower global iron gradient, namely -0.018 dex kpc^{-1} . One must also add that there have been attempts to derive the abundance gradient (specially $d[Fe/H]/dR_G$) using high-resolution spectroscopy of cool giant and supergiant stars. Harris & Pilachowski (1984) obtained -0.07 dex kpc^{-1} , while Luck (1982) found a steeper gradient of -0.13 dex kpc^{-1} . The latest slopes based on Planetary Nebulae range from -0.05 dex kpc^{-1} (Costa et al., 2004) to the lack of a Galactic metallicity gradient (Stanghellini et al., 2006). Oxygen and sulphur gradients determined from observations of planetary nebulae are -0.058 dex kpc^{-1} and -0.077 dex kpc^{-1} respectively (Maciel & Quireza 1999), with slightly flatter values for neon and argon, as in Maciel & Köppen (1994). A smaller slope was found in an earlier study of Pasquali & Perinotto (1993). According to those authors the nitrogen abundance gradient is -0.052 dex kpc^{-1} , while that of oxygen is -0.030 dex kpc^{-1} .
2. From young B main sequence stars, Smartt & Rolleston (1997) found a gradient of -0.07 dex kpc^{-1} , while Gehren et al. (1985), Fitzsimmons et al. (1992), Kaufer et al. (1994) and Kilian-Montenbruck et al. (1994) derived significantly smaller values: -0.03 - 0.00 dex kpc^{-1} . No systematic abundance variation with Galactocentric distance was found by Fitzsimmons et al. (1990). The studies of Gummersbach et al. (1998) and Rolleston et al. (2000) support the existence of a gradient (-0.07 dex kpc^{-1}). The elements in these studies were *C - N - O* and *Mg - Al - Si*. More recently, Daflon et al. (2004) obtained a slope value of -0.042 dex kpc^{-1} .
3. Studies of the abundance gradient (primarily nitrogen, oxygen, sulphur) in the Galactic disc based on young objects such as *HII* regions give positive results: either significant slopes from -0.07 to -0.11 dex kpc^{-1} according to: Shaver et al. (1983) for nitrogen and oxygen, Simpson et al. (1995) for nitrogen and sulphur, Rudolph et al. (1997) for nitrogen and sulphur, or intermediate gradients of about -0.05 to -0.06 dex kpc^{-1} according to: Simpson & Rubin (1990) for sulphur, Aerbach et al. (1997) for oxygen and sulphur; and negative ones: weak or nonexistent gradients as concluded by Fich & Silkey (1991); Vilchez & Esteban (1996), Rodriguez (1999). Peña et al. (2000) derived oxygen abundances in several *HII* regions and found a rather flat distribution with Galactocentric distance (coefficient -0.04 dex kpc^{-1}). The same results were also reported by Deharveng et al. (2000).
4. From a theoretical point of view, Cescutti et al (2007), modeled the abundance gradients in the disk for several chemical elements (O, Mg, Si, S, Ca, Sc, Ti, Co, V, Fe, Ni, Zn, Cu, Mn, Cr, Ba,

La and Eu). They adopted a chemical evolution model able to well reproduce the main properties of the solar vicinity. The model assumes that the disk formed inside-out with a timescale for the formation of the thin disk of 7 Gyr in the solar vicinity, whereas the halo formed on a timescale of 0.8 Gyr. They computed, for the first time, the abundance gradients for all the mentioned elements in the Galactocentric distance range 4-22 kpc. The flat gradients at large Galactocentric distances (> 12 kpc), as traced by the Cepheids, open cluster and red giant data, allowed them to conclude that a model where the density of the halo stellar component is constant in the inner 20 kpc should be preferred.

As one can see, there is no conclusive argument that can allow us to reach a firm conclusion about whether or not a significant abundance gradient exists in the Galactic disc, at least for all elements considered and within the whole observed interval of Galactocentric distances.

1.7.2 The Cepheid contribution

Compared to other objects supplying us with an information about the radial distribution of elemental abundances in the galactic disc, Cepheids have several advantages:

1. they are primary distance calibrators which provide excellent distance estimates;
2. they are luminous stars allowing the study of the gradient over a large range of Galactocentric distances;
3. the abundances of many chemical elements can be measured from Cepheid spectra (many more than from *HII* regions or B stars). This is important for investigation of the distribution in the galactic disc of absolute abundances and abundance ratios. Additionally, Cepheids allow the study of abundances past the ironpeak which are not generally available in *HII* regions or B stars;
4. lines in Cepheid spectra are sharp and well-defined which enables one to derive elemental abundances with high reliability.

Indeed, some studies were in favor of Galactic gradients, like D'Odorico et al. (1976) and Janes (1979) whereas others found no correlation between distance and metallicity (Clegg & Bell (1973), Jennens & Helfer (1975)). Today, the existence of Galactic abundance gradients seems widely accepted, even if some recent studies still report no evidence of such gradients, but the empirical determinations of their shapes and slopes is strongly debated. The global iron slopes based on Cepheids are very homogeneous, and indeed dating back to the first estimates by Harris (1981, 1984), who found a slope of $-0.07 \text{ dex } kpc^{-1}$, the more recent estimates provide slopes ranging from $-0.06 \text{ dex } kpc^{-1}$ (Andrievsky et al., 2002c; Luck et al., 2003; Andrievsky et al., 2004; Luck et al., 2006) to $-0.07 \text{ dex } kpc^{-1}$ (Lemasle et al. (2007)). The Andrievsky sample covers a range of Galactocentric distances from 4 to 14 kpc. The emerging picture can be best described by a relatively steep gradient (about $-0.14 \text{ dex } kpc^{-1}$) for Galactocentric distances less than 7 kpc, followed by a much shallower slope ($-0.03 \text{ dex } kpc^{-1}$) between 7 and 10 kpc, a discontinuity at approximately 10 kpc and a nearly constant metallicity of about $-0.2 \text{ dex } kpc^{-1}$ towards larger Galactocentric distances, out to about 14 kpc. Their results on the abundance

gradient from the Cepheids, have been also helpful to constrain the structure and age of the bar, and its influence on the metallicity gradient.

1.7.3 The linear gradient

As far as the shape of the gradient is concerned, current findings are even more controversial. In particular, the hypothesis of a linear gradient is still lively debated. Several investigations based on different stellar tracers - *HII* regions, Vilchez & Esteban (1996); Open Clusters, Twarog et al. (1997), Carraro et al. (2007); Cepheids, Andrievsky et al. (2004); Planetary Nebulae, Costa et al. (2004) - indicate a flattening of the Galactic gradient beyond 10-12 kpc (Vilchez & Esteban (1996)). This flattening is well reproduced by chemodynamical evolutionary models (Cescutti et al., 2007). More recently, Young et al. (2006) measured metallicities and detailed chemical compositions for stars in the outer Galactic disk. An analysis of the radial velocities and chemical abundance patterns of four old open clusters with Galactocentric distances between 12 and 23 kpc was presented in Yong et al. (2005). From these analyses, two main findings were reached:

1. at large Galactocentric distances, $R_{GC} \geq 10$ kpc, the expected metallicity gradient vanishes, and the stars exhibit a constant value of $[Fe/H] \sim -0.5$;
2. field and cluster stars in the outer Galactic disk show enhancements for the α -elements, $[\alpha/Fe] \sim 0.2$. Their interpretation was that these abundance patterns reflected the episodic growth of the disk via accretion or merger events. These events triggered rapid star formation with Type II supernovae preferentially contributing to the chemical enrichment.

Moreover, we know that the open clusters have ages between 2 and 6 Gys. The ages of the field giants are unknown, but presumably these stars are as old as the open clusters. The absence of the radial abundance gradient inferred from this sample of distant field and cluster stars may therefore not reflect the current situation in the outer disk. The time variation of the Galactic radial abundance gradient offers a more comprehensive test of Galactic evolution models than a single-epoch (or time-integrated) abundance gradient. The possibility of an ongoing merger event in the outer disk (e.g., Newberg et al. 2002; Ibata et al. 2003; Yanny et al. 2003) reinforces the need to analyze a sample of young stars at large distances and to measure detailed abundance ratios $[X/Fe]$ in addition to the metallicity $[Fe/H]$. Cepheids are intermediate-mass stars whose short lifetimes ensure that their atmospheres reflect the present-day composition of the interstellar medium (ISM). Abundance analyses of Cepheids appear feasible (Fry & Carney 1997; Andrievsky et al. 2002a, 2002b, 2002c, 2004; Luck et al. 2003), and the Cepheid period-luminosity relation allows for accurate distance determinations. Due to their luminosity, high-resolution spectroscopic observations of Cepheids located at large distances can be performed with modest-sized telescopes. Yong et al. (2006) present metallicities, $[Fe/H]$, and elemental abundance ratios, $[X/Fe]$, for a sample of two dozen Cepheids with Galactocentric distances $12kpc \leq R_{GC} \leq 17.2kpc$. These Cepheids allow us to study the Galactic radial abundance gradient as a function of time. Detailed abundance ratios $[X/Fe]$ offer an insight into the events currently taking place in the outer disk, and such abundance ratios may reveal the signatures of recent merger events. On the other hand, independent studies do not show evidence of a flattening toward the outer disk, like Rolleston et al. (2000) based on O/B stars or Deharveng et al. (2000) based on *HII* regions. Moreover, a discontinuity in the metallicity gradient at $R_G \sim 10 - 12$ kpc has also been suggested by Twarog et al. (1997) according to Open Clusters

photometry. Instead of a regular decrease from the inner to the outer disk, they bring forward a 2 zones distribution with an abrupt discontinuity of -0.2 dex at about 10-12 kpc and a shallower gradient inside each zone. This hypothesis was supported by Andrievsky et al. (2002c), Luck et al. (2003) and by Andrievsky et al. (2004). Such a variety may be due to the fact that the different tracers adopted to estimate the gradient present only a handful of objects toward the outer disk, i.e. at $R_G \geq 12$ kpc. Abundance analyses of nearby field stars (Edvardsson et al. 1993; Reddy et al. 2003), open clusters (Friel 1995), planetary nebulae (Henry et al. 2004), and *HII* regions (Shaver et al. 1983) have provided insight into the mean metallicity and metallicity gradient of younger and older stars and stellar remnants. Radial abundance gradients, as measured in disk stars, provide crucial constraints for models of the formation and evolution of our Galaxy (Hou et al. 2000; Chiappini et al. 2001). However, to explore the origin and continuing evolution of the Galactic disk, we need much more information than mean metallicities alone can provide. We need detailed elemental abundance ratios, which contain vital information on the relative contributions of Type II supernovae, Type Ia supernovae, and asymptotic giant branch (AGB) stars.

1.8 This thesis project

This thesis project moves along two different paths: to assess the influence of the stellar iron content on the PL relation in the *V* and *K* bands and to constrain the Galactic iron gradient between 5 and 15 kpc, using homogeneous iron abundance measurements for more than 250 Galactic Cepheids located along the disk together with accurate distance determinations based on Baade-Wesselink method.

The novelty of the approach adopted in this project consists in the homogeneous analysis of the largest, up to now, sample of Cepheids (~ 300) observed in three galaxies (the Milky Way, the Large Magellanic Cloud and the Small Magellanic Cloud), spanning a factor of ten in metallicity and for which multi-wavelength photometry and high-resolution spectra are available. To fulfill our goals, firstly, we have selected a big sample of Cepheids for which accurate photometry (in optical and NIR bands), distances and high-resolution spectroscopy were available both in the literature and in the ESO archive. Secondly, we have directly measured iron abundance from few spectra, we have determined mean magnitudes and mean radial velocity from light and radial velocity curves and we have also estimated distances using BW technique.

With these results in hands:

- we make a comparison with previous works on the chemical composition of Cepheids;
- we investigate the effect of the metallicity on the PL relation in the *V* and *K* bands, studying the behavior of the residuals in two bands determined from the photometry for our sample and the standard PL relations from the literature as a function of the measured metallicity.
- we investigate the behavior of the radial abundance gradient using metallicity estimates based both on high resolution spectroscopy and Walraven photometry.

This thesis is organized as follows:

Chapter 1 We introduced the study of Cepheids, their characteristics and evolution. Moreover we gave

a review of the problematics related to the Cepheids distance scale and the use of Cepheids as chemical tracers.

Chapter 2 We discussed the observational aspect of this thesis. The selection criteria of the data set are described along with telescopes and instruments used to collect the stellar spectra and the photometry.

Chapter 3 We outlined a general overview of the spectra analyses: assembling the line list, determining the equivalent widths and the stellar parameters. We also give a detailed description of the methodology used to estimate the elemental abundances and their uncertainties.

Chapter 4 We presented the results of our investigation about the effect of the iron content on the PL relation in the visual and infrared bands, namely V and K bands. We examined the effects on the slope and zero point of the relation and compared our outcomes with two different hypothesis currently reported in the literature.

Chapter 5 We presented our results on the Baade-Wesselink method.

Chapter 6 We presented new calibrations of the Metallicity-Index Color (MIC) relations and we showed the results about the Galactic iron gradient compared with most recent estimates.

Chapter 7 We summarize the work done and the results obtained.

Appendix A Includes all the tables and light curves of our Walraven sample.

Appendix B Includes the complete line list we used to measure radial velocities and metallicities.

CHAPTER 2

Observations

Significant progress has been made in the past few years towards the understanding and the characterization of the Cepheid Period-Luminosity (PL) relation and the existence of the radial abundance gradient, both on the observational and theoretical sides, but the debate on the role played by the chemical composition is far from being settled. In particular, from an observational point of view, the subjects have been approached in essentially two ways: either by direct measurements of the elemental abundances in nearby Cepheids, or by measuring a secondary metallicity indicator in external galaxies known to contain Cepheids, under the assumption that they would have the same chemical composition. Regrettably, the direct determination of chemical abundances has been attempted, up to now, only by few studies, mainly focused on stars of our own Galaxy (see section 1.6). This approach requires high quality spectra of the stars under scrutiny and these are easier to obtain, from ground-based telescopes, for Cepheids that are close to the Sun, limiting the range in metallicity that can be explored. Therefore, to further tackle the effect of chemical composition on the PL relation, we decided to undertake a detailed chemical analysis (focusing on iron) of a large sample of Cepheids in the Galaxy and the Magellanic Clouds, adopting the first of the two approaches described above: the direct determination of abundances. In order to do this we have obtained high quality spectra, i.e. with high resolution and high signal-to-noise, that have been collected using the highly advanced facilities of the European Southern Observatory (ESO) in Chile.

For the problems related with the radial abundance gradient, we used a different approach. We calibrated a new method to estimate metallicity based on Walraven photometry of Galactic Cepheids. Thus, we used data collected between 1960 and 1970-71, at the 36" Lightcollector telescope in the Leiden Southern Station (South Africa).

2.1 Telescopes and instruments

We collected our data sample using many different telescopes and instruments. The spectroscopic data came from the La Silla and the Paranal Observatories, while the photometric data are taken from the South African Astronomical Observatory (SAAO). The Galactic Cepheids are bright stars and a small telescope is sufficient to collect their spectra and images, then they have been observed at the La Silla, the Dutch and the SAAO observatory, while the Magellanic Cepheids are fainter and needed a larger

Table 2.1: The main parameters and the performances for the Fiber-fed Extended Range Optical Spectrograph (FEROS).

Wavelength range in one exposure (object + sky)	356 - 920 nm (39 orders, 2 fibers)
Resolving Power (with 2-slice image slicer)	R=48000
Entrance Aperture	2.7 arcsec
Fiber Input/Output Focal Ratio	F/4.6
Spectrograph Beam Size	136 mm diameter
Off-axis Collimators	F/11, cut from one parent paraboloid
Echelle	R2, 79 lines/mm, 154 mm by 306 mm
Crossdisperser Prism	LF5 glass, 55°: apex angle
Dioptric Camera	
Wavelength range	350 - 900 nm
F/#	F/3.0
Focal Length	410 mm
Field Diameter	69 mm
Image Quality (E80)	< 25 μ m
Efficiency	> 85%
CCD	2048 x 4096, 15 μ m, thinned
Detection Efficiency (without telescope)	7% (3700 \AA), 27% (5000 \AA), 8% (9000 \AA)
Limiting Magnitudes at the ESO 1.52	16 mag in V (S/N = 15, 2 h) 12.5 mag in V (S/N = 15, 2 h)
Radial-Velocity Accuracy	< 30 m/s

telescope such as the VLT at Paranal Observatory. In the next sections we will illustrate the principal characteristics of each telescopes and instruments.

2.1.1 The ESO-1.5m telescope and FEROS

The ESO-1.5m telescope is one of the several telescopes of the La Silla Observatory, which is located at the southern extremity of the Atacama desert in Chile at an altitude of 2400 meters. This telescope is a Cassegrain reflector and is mounted in an English cradle. It has a Cassegrain focus with a focal ratio of f/14.9. The Fibre-fed, Extended Range, Echelle Spectrograph (FEROS, Pritchard 2004) is a bench-mounted, thermally controlled, prism-cross dispersed Echelle spectrograph. It has been mounted at the ESO-1.52m telescope (we collected our data sample in 2001) till October of 2002 then it was transferred to the MPG/ESO-2.20m telescope, where is now permanently mounted. It is a high resolution ($R \sim 48,000$), high efficiency (20%), versatile spectrograph providing in a single spectrogram almost the complete spectral coverage from 350 nm to 920 nm (see Table 2.1). The mechanical and thermal stability of FEROS allow for a precise wavelength calibration based on daytime calibrations and for most purposes additional calibrations during the night are not necessary, thus ensuring a high productivity in terms of scientific data produced. It is possible to obtain radial velocities with accuracies of 25 m/s or better. FEROS is fed by two fibres providing simultaneous spectra of object plus either sky or one of the two calibration lamps (wavelength calibration and flat-field). The fibres are illuminated via 2.0 arcsec apertures on the sky separated by 2.9 arcmins. A small amount of rotation of the telescope adapter is

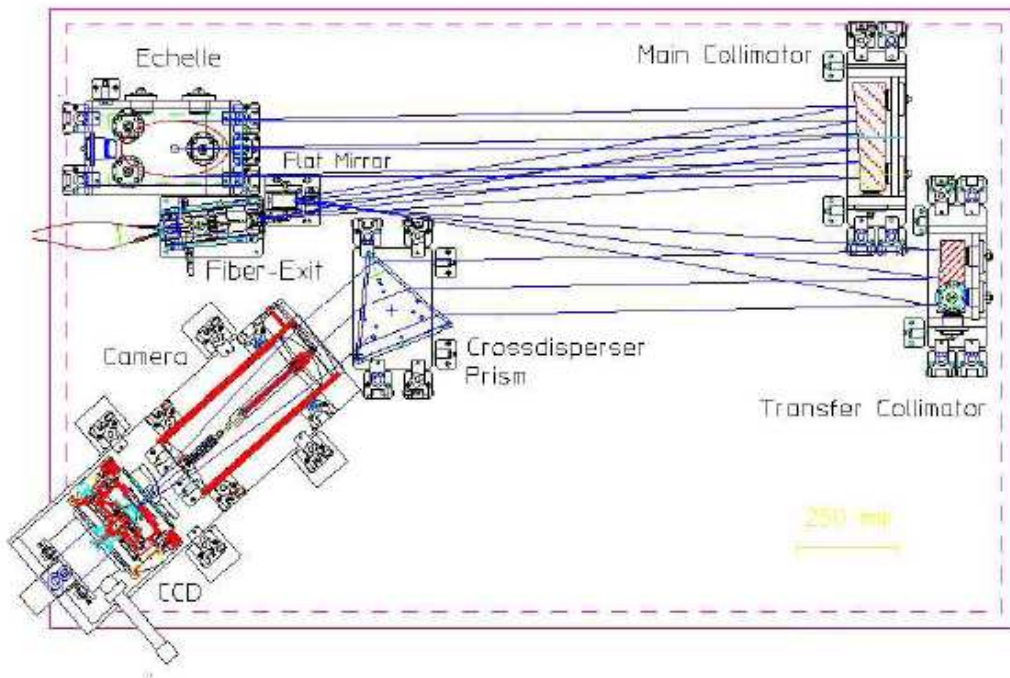


Figure 2.1: The FEROS complete system as seen from the top.

possible in the rare case that a field star by chance falls on the sky fibre. The resolving power of 48,000 is achieved with a two-slice image slicer (a device that reshapes the circular image of each fibre into a narrow and long segment that behaves like a slit, but with minimum rejection of light) over the spectral range of 350 nm to 920 nm spread over 39 Echelle orders (with a typical order value of 40). The detector is an EEV 2048 x 4096 CCD. Calibration lamp light is delivered to the science fibres in the FEROS Fibre Head via the calibration fibres from the FEROS Calibration Unit. As we have already mentioned, FEROS provides almost complete spectral coverage from 350 nm to 920 nm. Only the two spectral ranges 853.4 nm to 854.1 nm and 886.2 nm to 887.5 nm are lost due to non overlap of the spectral orders. The main capabilities of FEROS are summarized in Table 2.1 and a schematic overview of the spectrograph can be seen in Fig 2.1.

2.1.2 The ESO-VLT telescope and UVES

The ESO Very Large Telescope (VLT) is located on Cerro Paranal in the Atacama desert in the northern part of Chile (600 km from La Silla), at an altitude of 2600 meters. The VLT consists of an array of four 8-meter telescopes (Antu, Kueyen, Melipal and Yepun) which can work independently or in combined mode. The telescopes may be used in interferometric mode providing extremely high spectral resolution corresponding to baselines of several hundred meters. Each unit telescope has an alt-azimuth mount and a Ritchey-Chretien optical system. The VLT can operate in either Cassegrain or Nasmyth focus. The VLT uses active optics: the optical quality of the image is continually monitored by an image analyzer using a reference star and the contributions of the various optical aberrations are computed and corrected for. UVES (Dekker et al 2000; Kaufer et al 2004), the Ultraviolet and Visual Echelle Spectrograph

Table 2.2: The main parameters and the performances for the Ultraviolet and Visual Echelle Spectrograph (UVES).

	Blue Arm	Red Arm
Wavelength range	300 - 500 nm	420 - 1100 nm
Resolving power-slit product	41,400	38,700
nm/pixel	0.0019 nm at 450 nm	0.0025 nm at 600 nm
Max. Resolving power (2-pixel sampling)	80,000	110,000
Throughput at blaze (TEL+UVES, no slit, no atm.)	12% at 400 nm	14% at 600 nm
Limiting magnitude (90m exp. time, S/N=10, 0.7 arcsec slit, seeing 0.7)	18 R=58,000 at 360 nm	19.5 R=62,000 at 600 nm
CCDs	2048 4096 (windowed to 2048 3000)	two 2048 4096 (mosaic of different types)
Pixel (15μm) scale		
disp. dir. (varying along order)	0.215 \pm 20%	
along slit (dep. on cross-disp.)	0.25'' (CD1 and CD2)	0.18'' (CD3), 0.17'' (CD4)
Echelle (R4 mosaic)	41.59 g/mm	31.6 g/mm
Cross dispersers	CD1: 1000 g/mm	CD3: 600 g/mm
Blaze wavelength	430 nm	560 nm
	CD2: 660 g/mm	CD4: 312 g/mm
Blaze wavelength	460 nm	770 nm
Typ. wavel. cov. CD1 and CD3 (CD2 and CD4 in parenthesis)	85 (126) nm in 33 (31) orders	200 (403) nm in 37 (33) orders
Min. order separation (standard setup)	10 arcsec (40 pixel)	9 arcsec (51 pixel)

located at Nasmyth platform B of the second Unit Telescope (Kueyen) of the VLT, is a crossdispersed Echelle spectrograph designed to operate with high efficiency from the atmospheric cut-off at 300 nm to the long-wavelength limit of the CCD detectors of 1100 nm. To this purpose, the light beam coming from the telescope is split into two arms (UV-Blue and Visual-Red) within the instrument. The two arms can be operated separately or in parallel with a dichroic beam splitter. The resolving power is 40,000 when a 1 arcsec slit is used. The maximum resolution (to be obtained with a narrower slit or with the use of an image slicer) is 80,000 or 110,000 in the Blue and the Red Arm, respectively. The instrument is built for maximum mechanical stability and for accurate calibration of the wavelength scale down to an accuracy of at least 50 m/s. An iodine cell can be inserted in the light beam for observations requiring higher accuracy. The main capabilities of the two UVES arms are summarized in Table 2.2 and Fig 2.2 shows a scheme of the spectrograph. In 2003, a new mode of operation involving multi-object spectroscopy was implemented. Eight fibers (input diameter 1 arcsec) coming from the fibre positioner of FLAMES, the instrument mounted at the opposite Nasmyth platform, can feed the red arm of the UVES spectrograph. UVES consists of two main parts: the first part is mounted on the rotator (which remains stationary while the telescope adapter rotates to follow the field rotation). It includes the calibration system, a removable

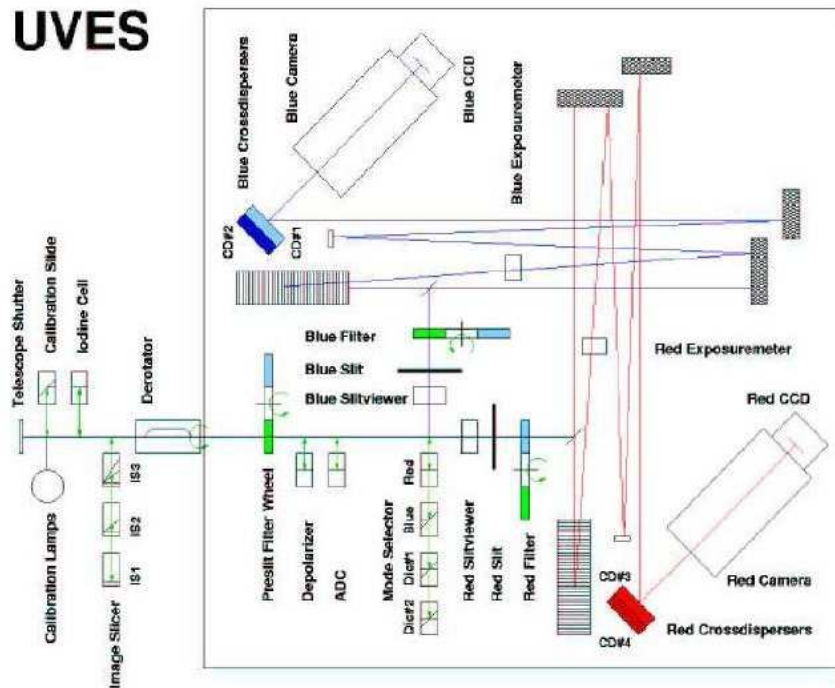


Figure 2.2: Schematic overview of the UVES spectrograph.

iodine cell, a slide with image slicers and an optical derotator which is permanently installed in the beam. The second part, the two arms cross-dispersed Echelle spectrograph, is mounted on a steel table fixed to the floor of the Nasmyth platform and is covered by a light-tight enclosure which also provides thermal insulation and protection from dust. The light beam from the telescope is focused on the red arm entrance slit or is directed to the blue arm slit by a mirror. On the fixed table in the pre-slit area, additional optical components are available for insertion in the optical beam: filters, a depolarizer, an Atmospheric Dispersion Compensator (ADC) and two pupil stops of different size. Two dichroics are available to work in parallel with the two arms. The blue arm (300-500 nm) and the red arm (420-1100 nm) have an identical layout. They are folded and cross each other to minimize the size of the table on the platform. The two-arm solution gives high efficiency because it permits to optimize the spectral response of coatings, gratings and detectors in each arm. With a beam of 200 mm, the off-axis parabolic collimators illuminate the Echelle gratings of 214 x 840 x 125 mm with a large blaze angle (76 °). The Echelle R4 gratings are the largest ever made of this type. They are operated in quasi-Littrow mode, that is with the angle of incidence and diffraction equal but in a different plane, to maximize efficiency. The grating cross-dispersers provide an order separation larger than 10 arcsec at any wavelength in the spectral range 300 - 1100 nm. This separation allows to perform semi-long-slit spectroscopy of compact objects, the use of image slicers, a good sampling of sky emission at red wavelengths and the possibility of accurate inter-order background estimates. The cameras are dioptric (no central obstruction) and provide an external focal plane for easy detector interfacing and upgrading during the lifetime of the instrument, together with a large field, good image quality and high optical transmission. The blue CCD detector format is 2048 x 4096 pixels, windowed to 2048 x 3000. In the red, a mosaic of two 4096 x 2048 pixels CCDs is offered, separated by about 1 mm (loss of one order in the gap). The direction of the spectral dispersion (= echelle orders) is along the larger dimension of the CCDs.



Figure 2.3: The Walraven five-channel photometer and the 91-cm ‘Dutch Telescope’, shortly after their transfer to ESO, La Silla, in 1979. The ‘L-shape’ of the photometer optics layout can be recognized. The blue cylinder below the cassegrain focus is the coldbox for the L channel. The two other coldboxes for the (B, W) and (V, U) photomultipliers are mounted to the side of the telescope tube. The coldboxes use dry-ice cooling.

2.1.3 The Dutch telescope and the Walraven photometer

Observations with the Walraven five-channel photometer, attached to the 91-cm ‘Lightcollector’ reflector, started in 1958 at the Leiden Southern Station in Broederstroom, South-Africa. After 20 years in South-Africa the telescope (now re-baptized to ‘Dutch Telescope’) and photometer were moved to the ESO La Silla observatory in Chile, where the photometric observations were resumed in March 1979 and continued for another 12 years until the decommissioning of the photometer in 1991. Due to the much better photometric conditions on La Silla, this last phase of the operational life of the instrument was particularly fruitful. Although the *VBLUW* photometric system had originally been designed for the study of early-type stars, it had soon become clear that the system had very attractive properties for F/G stars as well. This resulted in a wide variety of photometric programs. During 32 years of almost uninterrupted observations, a very large amount of high-quality data was obtained for many types of stars, but the emphasis was on OB-associations, clusters, Cepheids (both in the Galaxy and in the LMC/SMC), RR

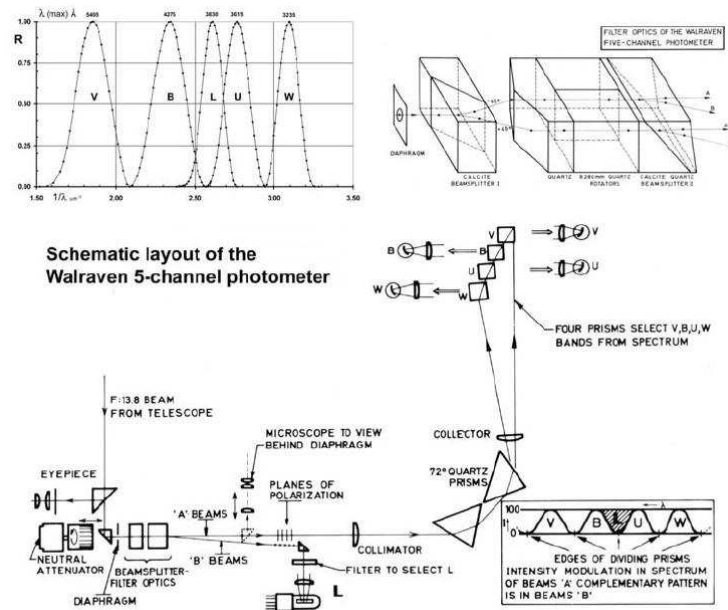


Figure 2.4: Overview and schematic optical layout of the Walraven photometer (figure from Pel & Lub 2007). The passbands (upper left) are produced by a set of polarizing crystal optics (upper right). The channels V, B, U and W are separated in a prism spectrograph, L is selected from the complementary pair of beams by an additional filter.

Lyrae stars and faint F/G stars in the Galactic thick disk and inner halo. The Walraven photometer has always been a ‘white elephant’, partly by its unique design, but also due to the fact that the instrument remained literally unique as copies were never built. In addition, during its whole life the photometer was mounted permanently on the same telescope that had been built specifically for this instrument. In fact, as can be seen in Fig. 2.3, mounting of the photometer to that telescope was so special that a transfer to any other telescope would have required major modifications. When Walraven started designing the photometer around 1955 his primary goals were: optimum matching of photometric passbands to the properties of stellar (in particular: early type) spectra, high instrumental throughput and observing efficiency, and high photometric stability. He met these requirements remarkably well by a very original design of which we give a short overview in Fig. 2.4. This figure summarizes the main properties and optical layout of the instrument. The heart of the photometer is the ingenious set of quartz/calcite crystal optics (upper right panel) which define the passbands of the five channels V, B, L, U and W (upper left). These delicate and very small components (together only a few cm^3 !) were manufactured by Theodore and Johanna Walraven themselves. The combination of polarizing beamsplitters and polarization rotators splits the incoming light into two pairs of beams (‘A’ and ‘B’) which are 100% linearly polarized and have complementary intensity modulations in the spectrum. Since the polarization rotation in crystal quartz is temperature-insensitive, this modulation is extremely stable. Due to the properties of the filter optics, the passband profiles are close to sinusoidal on a frequency scale. The V, B, U and W channels are selected from the ‘A’ beams and spatially separated in a prism spectrograph. Because the dispersing prisms are used at the Brewster angle and the light is fully polarized in the appropriate plane, this spectrograph has $> 90\%$ throughput over the full wavelength range of 6500-3100 Å. By placing the edges of the selection prisms in the light minima, small movements of the spectrum (e.g. due to seeing) have no effect on the passbands. The L channel is selected by an additional filter from the complementary ‘B’

Table 2.3: The bandwidths and effective wavelengths of the five photometric passbands.

	V	B	L	U	W
(λ_{eff}^{-1}) (Å)	5405	4280	3825	3630	3240
$\Delta\lambda$ (Å)	695	435	220	235	150

beams. All channels are recorded simultaneously by five photomultipliers in coldboxes cooled by dry ice. At the photometer entrance a neutral optical attenuator (fast rotating slotted drum) can be moved into the beam in order to extend the dynamic range for bright stars by 3 magnitudes. It is useful here to mention briefly the most important features of the *VBLUW* system. The bandwidths and the effective wavelengths (for the energy distribution of an unreddened *O* star, observed in the zenith) of the five photometric passbands are given in table 2.3. These bands determine spectral indices very similar to those used in Paris Classification of Chalonge, Barbier and co-workers (Chalonge 1958): the slopes of the Paschen and Balmer continua ($(V - B)$ and $(U - W)$, respectively), the Balmer jump ($B - U$), and the strength of the line absorption in the region of the higher Balmer lines ($B - L$). It should be noted that the *VBLUW* convention is, to express brightness and colors in $^{10}\log(Intensity)$ rather than in magnitudes. The zero-points on this $^{10}\log$ scale are fixed by defining the brightness and colors of the primary standard star *HD 144470* ($= \omega^1 Sco$).

The passbands are defined by special filter, which makes use of polarization optics. Separation of the wavelength regions takes place in a quartz-prism spectrograph, and the five corresponding signals are measured simultaneously by separated photomultipliers. In the design of the photometer, Dr. Walraven has aimed especially at high wavelength-stability (Lub & Pel 1977). For more details we refer to Walraven & Walraven (1960), Pel (1978), Lub & Pel (1977) and for a more recent review Pel & Lub (2007).

2.1.4 The SAAO-0.75m telescope and the Mk II IR photometer

The 0.75-m reflector, built by Grubb Parsons, was added to the Multiple Refractor Mounting (MRM) in 1974. The multiple photographic refractors originally placed on this mounting in 1964 have now been removed. Position read-out and telescope pointing are now controlled by electronics from DFM Engineering. The telescope's secondary mirror delivers a Cassegrain focus with an f ratio of f/15. A photo of the 0.75m with the UCT CCD mounted at the Cassegrain focus is shown in figure 2.5. The right ascension (RA) drive is a single stage of worm gears driven by a stepping servo motor through two timing belts and pulley stages. The hour angle (HA) encoder is driven off the worm shaft. The declination (Dec) drive is a chain drive and the Dec encoder is driven off this via a sprocket. Prior to the 2006 upgrade, the switching of dome power, dome tracking, lights, and movement of focus position was done manually. Opening of the shutter was done via a manual switch and the mirror cover was removed by hand. Movement of the telescope was controlled via a DOS based interface. The 2006 refurbishment has provided:

1. An upgrade of the 0.75m's previous DOS-based TCS to a WindowsTM-based TCS. The TCS, named WinTCS and provided by DFM engineering, allows for more userfriendly control of the telescope and PC control of the focus, dome, lights and mirror cover.
2. The installation of a new position encoding system which enables self-automated initialization of



Figure 2.5: The 0.75m telescope with the UCT CCD mounted below it.

the telescope. This is useful to use in the event that the telescope loses pointing during observations.

3. A Programmable Logic Controller (PLC) box to manage the telescope peripheral subsystem. That is the PLC box:

- implements (via a radio) PC control of the dome shutter, lights and mirror cover,
- facilitates the safeguarding of the peripheral subsystem from behaving unpredictably following power outages or TCS failure,
- and enables the addition of a rain sensor to initiate an emergency shut down procedure on detection of rain.

The Mk II infrared photometer is an improved version of the Mk I, designed primarily to cover the JHKL bands (1.25, 1.6, 2.2 and 3.4 microns). It uses an InSb cell cooled with nitrogen slush, and a sectored mirror focal plane chopper. Liquid nitrogen is supplied by SAAO. Data acquisition is via the program BRUCE, which runs in DOS on the 486 PC. BRUCE also provides online reductions, making corrections for atmospheric extinction and for zero-point. Comprehensive lists of appropriate JHKL standard star magnitudes should be available in the dome, but the wary observer may wish to get a copy in Cape Town. This is an updated version of the data published by Carter (1990). In Table 2.4 we report some useful details on *MkII* System. A full description of the Mk I photometer, which is very similar to the Mk II, can be found in Glass (1973).

Table 2.4: Mk II System Parameters.

Mk II System Parameters	
Filters	<i>JHKLML</i>
Apertures	1, 1.5, 2.0, 3.0, 4.0 mm diameter
Detector	InSb photoconductor
Fabry Lens	Calcium flouride
Chopping Speed	12.5 Hz
Acquisition Field	40 mm diameter (about 12 arcmin)
Offset Guider Field	Also 12 arcmin
Integration Time	Adjustable, normally 10 seconds
Performance	10% accuracy at $K = 10.4$ after 4 modules (160 s) with a 2.0 mm (37 arcsec) aperture

2.2 Data

As we have already mentioned in chapter 1 this thesis project has many topics. For this reason we divided our dataset in three sample depending on their goals.

1. **PL-data:** first sample has been used to constrain the metallicity effect on the PL relation in the V and K bands with Galactic and Magellanic Cepheids for which accurate distances was available in literature. This dataset includes a total of 68 stars: 32 Galactic, 22 LMC and 14 SMC Cepheids. The observing time was allocated in October 2000 and in January-February 2001. For each star we have a single epoch observation. The spectra of the 32 Galactic stars were collected at the ESO 1.5 m telescope on Cerro La Silla with the Fibre-fed Extended Range Optical Spectrograph (FEROS, Pritchard 2004, see also section 2.1.1) in two runs by Martin Groenewegen and Emanuela Pompei. The spectra of the Magellanic Cepheids were obtained at the VLT-Kueyen telescope on Cerro Paranal with the UV-Visual Echelle Spectrograph (UVES, Dekker et al 2000; Kaufer et al 2004, see also Section 2.1.2) in Service Mode (observations are carried out by the staff of Paranal Observatory, see table 2.5 and 2.6).
2. **BW-data:** second dataset was to estimate the distances applying the Baade-Wesselink method. It includes multiphase observations (more than 25 spectra for each object) for four Galactic Cepheids (see table 2.7). The observing runs were collected with FEROS@1.5m between May and September 2005 in Service Mode.
3. **Walraven-data:** aim of the third dataset was to estimate metallicity from Walraven photometry to improve the sample to study the Galactic abundance gradient. We provide new empirical and theoretical calibrations of two photometric metallicity indices. The empirical calibration relies on a sample selected from the observing runs 1962 (Walraven et al. 1964) and 1970-1971 (Pel 1976) at the Leiden Southern Station (SAAO, South Africa). The Station's main instrument used to collect this data was the 36" (91-cm) Lightcollector, equipped with Walraven's simultaneous five-channel photometer (see section 2.1.3). The sample includes 173 Galactic Cepheids and it is 82% complete for all known Cepheids brighter than $V = 11.0$ mag at minimum and south of declination $+15$ deg.

The theoretical calibration relies on an homogeneous set of scaled-solar evolutionary tracks for intermediate-mass stars and on pulsation predictions concerning the topology of the instability strip.

In order to constrain the possible occurrence of systematic errors in the optical photometry we are also collecting accurate multiband *JHK* NIR data (see also tables in appendix A).

More details on the three samples will be presented in the following sections.

2.2.1 PL-data: the Galactic sample

To assemble the Galactic sample we have collected a total of 32 Galactic stars at the ESO 1.5m telescope on Cerro La Silla with FEROS (see section 2.1.1). The 2-D raw spectra were run through the respective instrument Data Reduction softwares, yielding 1-D extracted, wavelength calibrated and rectified spectra. The normalization of the continuum was refined with the IRAF task continuum. The 1-D spectra were corrected for heliocentric velocity using the *rvcorr* and *dopcor* IRAF tasks. The latter was also used to apply the radial velocity correction, which was derived from 20 unblended narrow lines well spread over the spectrum, selected among the species FeI, FeII and MgI. The measured signal-to-noise ratios vary between 70 and 100. The selected Cepheids span a wide period range, from 3 to 99 days. For the Galactic Cepheids we have adopted periods, optical and NIR photometry from Laney & Stobie (1994), Storm et al. (2004), Groenewegen et al. (2004), Benedict et al. (2007) and Fouqué et al. (2007). In order to obtain the absolute magnitudes of our Cepheids, which allow us to investigate the effects of the chemical composition on the PL relation, it is crucial to know the distances and reddening to the individual stars. In this sense, we have adopted two different sets of distances and reddenings. The "Old set" was assembled as follow (see columns 4 and 5 in Table 2.5):

i) 25 objects have distance moduli (μ) provided by Storm et al. (2004, see their Table 3) and by Groenewegen et al. (2004, see their Table 3). These individual distances have been obtained using the Baade-Wesselink (BW) method (see section 1.5). We note that the distance scale based on the calibrations used by Storm et al (2004) and Groenewegen et al (2004) provides, within the errors, the same distances.

ii) the remaining seven objects had not distance estimates available in the literature. For five of them we determined the distance by combining the linear diameter from Laney & Stobie (1995) with the *V, K* unreddened magnitudes from Laney & Stobie (1994), using two surface brightness-color calibrations:

- from Groenewegen (2004): we have combined Eq. 1 and Eq. 2 with Table 3 coefficients marked with the filled circle (the *V* vs. *V – K* relation)
- from Fouqué & Gieren (1997): we have combined Eq. 1 with Eq. 27 (the *V* vs. *V – K* relation)

The distance moduli derived with the two calibrations mentioned above agree very well (within 1%) and we have adopted the distances determined with Groenewegen's calibration (these are the values listed in Table 2.5).

For the "New set" we have considered (see columns 6 and 7 in Table 2.5):

i) 24 objects: distance moduli based on the infrared surface brightness method provided by Fouqué et al. (2007, see their Table 7).

ii) 3 objects: the trigonometric parallaxes for ι Car, β Dor, and ζ Gem have been provided by Benedict et al. (2007).

Table 2.5: Pulsation phases (ϕ) and intrinsic parameters of the Galactic Cepheids. Both AP Pup and AX Vel were not included in the analysis of the metallicity effect because accurate distance estimates are not available in literature. In particular, for AP Pup we only listed the apparent mean magnitudes. In the last column is listed the duplicity status according to Szabados (2003): B - spectroscopic binary, Bc - spectroscopic binary that needs confirmation, O - spectroscopic binary with known orbit, V - visual binary

ID	$\log P$	ϕ	μ_{Old}	$E(B - V)_{Old}$	μ_{New}	$E(B - V)_{New}$	M_B	M_V	M_K	Duplicity
l Car	1.5509	0.580	8.99 ^d	0.170 ^d	8.56 ^b	0.147 ^a	-4.17	-5.28	-7.53	...
U Car	1.5891	0.490	10.97 ^d	0.283 ^d	10.87 ^a	0.265 ^a	-4.50	-5.41	-7.44	B
V Car	0.8259	0.375	9.84 ^e	0.174 ^h	10.09 ^a	0.169 ^a	-2.54	-3.24	-4.86	B
WZ Car	1.3620	0.745	12.92 ^d	0.384 ^d	12.69 ^a	0.370 ^a	-3.80	-4.58	-6.52	...
V Cen	0.7399	0.155	9.18 ^d	0.289 ^c	8.91 ^a	0.292 ^a	-2.41	-2.99	-4.49	...
KN Cen	1.5319	0.867	13.12 ^d	0.926 ^d	12.84 ^a	0.797 ^a	-4.63	-5.46	-7.59	B
VW Cen	1.1771	0.967	12.80 ^d	0.448 ^d	12.76 ^a	0.428 ^a	-2.93	-3.85	-6.08	B
XX Cen	1.0395	0.338	11.11 ^d	0.260 ^d	10.90 ^a	0.266 ^a	-3.19	-3.91	-5.58	B
β Dor	0.9931	0.529	7.52 ^c	0.040 ^c	7.50 ^b	0.052 ^a	-3.16	-3.91	-5.57	...
ζ Gem	1.0065	0.460	7.78 ^c	0.010 ^c	7.81 ^b	0.014 ^a	-3.16	-3.94	-5.72	V
GH Lup	0.9675	0.031	10.05 ^e	0.364 ^h	10.25 ^a	0.335 ^a	-2.77	-3.66	-5.54	B
T Mon	1.4319	0.574	10.82 ^d	0.209 ^c	10.71 ^a	0.181 ^a	-4.16	-5.15	-7.25	O
S Mus	0.9850	0.266	9.81 ^e	0.147 ^h	9.57 ^a	0.212 ^a	-3.48	-4.10	-5.62	O
UU Mus	1.0658	0.865	12.59 ^d	0.413 ^d	12.41 ^a	0.399 ^a	-3.12	-3.86	-5.70	...
S Nor	0.9892	0.343	9.91 ^d	0.189 ^c	9.87 ^a	0.179 ^a	-3.23	-4.00	-5.77	B
U Nor	1.1019	0.422	10.72 ^d	0.892 ^d	10.46 ^a	0.862 ^a	-3.14	-3.90	-5.72	...
X Pup	1.4143	0.232	12.36 ^e	0.443 ^h	11.64 ^a	0.402 ^a	-3.57	-4.38	-6.34	...
AP Pup	0.7062	0.109	... ^f	... ^f	... ^f	... ^f	7.37	6.78	5.26	B
AQ Pup	1.4786	0.436	12.52 ^d	0.512 ^c	12.41 ^a	0.518 ^a	-4.53	-5.35	-7.27	B
BN Pup	1.1359	0.397	12.95 ^d	0.438 ^c	12.93 ^a	0.416 ^a	-3.55	-4.33	-6.14	...
LS Pup	1.1506	0.012	13.55 ^d	0.478 ^d	13.39 ^a	0.461 ^a	-3.60	-4.37	-6.18	B
RS Pup	1.6174	0.944	11.56 ^d	0.446 ^c	11.30 ^a	0.457 ^a	-4.71	-5.69	-7.81	...
VZ Pup	1.3649	0.816	13.08 ^d	0.471 ^c	12.84 ^a	0.459 ^a	-3.93	-4.63	-6.31	...
KQ Sco	1.4577	0.446	12.36 ^c	0.839 ^c	12.23 ^g	0.869 ^a	-4.05	-5.11	-7.55	...
EU Tau	0.3227	0.414	10.27 ^c	0.170 ^c	10.27 ^c	0.170 ^d	-2.26	-2.74	-4.05	Bc
SZ Tau	0.4981	0.744	8.73 ^c	0.290 ^c	8.55 ^a	0.295 ^a	-2.38	-2.93	-4.33	B
T Vel	0.6665	0.233	9.80 ^d	0.281 ^c	10.02 ^a	0.289 ^a	-2.24	-2.88	-4.47	B
AX Vel	0.5650	0.872	10.76 ^f	0.224 ^h	... ^f	0.224 ^a
RY Vel	1.4496	0.704	12.02 ^d	0.562 ^c	11.73 ^a	0.547 ^a	-4.23	-5.05	-6.96	...
RZ Vel	1.3096	0.793	11.02 ^d	0.335 ^c	10.77 ^a	0.299 ^a	-3.78	-4.61	-6.56	...
SW Vel	1.3700	0.792	11.00 ^d	0.349 ^c	11.88 ^a	0.344 ^a	-4.02	-4.83	-6.75	...
SX Vel	0.9800	0.497	11.44 ^e	0.250 ^h	11.41 ^g	0.263 ^a	-3.33	-3.95	-5.49	...

^a Fouqué et al. (2007).

^b Benedict et al. (2007).

^c Groenewegen et al. (2004).

^d Storm et al. (2004).

^e Laney & Stobie (1995) and Groenewegen (2004).

^f Not included in the analysis of the metallicity effect.

^g Groenewegen (2007).

^h Fernie et al. (1995).

Table 2.6: Pulsation phases (ϕ) and intrinsic parameters of the Magellanic Cepheids. Periods ($\log P$), apparent mean magnitudes and reddenings come from Laney & Stobie (1994). The mean K-band magnitudes were transformed into the 2MASS photometric system using the transformation provided by Koen et al. (2007, see eq. 5.6).

ID	$\log P$	ϕ	B_0	V_0	K_0	$E(B - V)$
LMC						
HV 877	1.654	0.682	14.06	12.98	10.77	0.12
HV 879	1.566	0.256	14.12	13.15	11.03	0.06
HV 971	0.968	0.237	14.86	14.24	12.68	0.06
HV 997	1.119	0.130	14.94	14.19	12.37	0.10
HV 1013	1.382	0.710	14.39	13.46	11.41	0.11
HV 1023	1.425	0.144	14.48	13.51	11.45	0.07
HV 2260	1.112	0.144	15.19	14.43	12.67	0.13
HV 2294	1.563	0.605	13.19	12.45	10.74	0.07
HV 2337	0.837	0.861	13.27	0.07
HV 2352	1.134	0.201	14.49	13.84	12.25	0.10
HV 2369	1.684	0.136	13.15	12.29	10.38	0.10
HV 2405	0.840	0.037	13.43	0.07
HV 2580	1.228	0.119	14.33	13.67	11.92	0.09
HV 2733	0.941	0.411	14.85	14.34	13.00	0.11
HV 2793	1.283	0.917	14.49	13.58	11.75	0.10
HV 2827	1.897	0.880	13.19	12.03	9.80	0.08
HV 2836	1.244	0.059	14.85	14.02	12.04	0.18
HV 2864	1.041	0.055	15.16	14.42	12.77	0.07
HV 5497	1.997	0.321	12.73	11.63	9.43	0.10
HV 6093	0.680	0.024	15.74	15.16	13.71	0.06
HV 12452	0.941	0.860	15.25	14.60	12.83	0.06
HV 12700	0.911	0.342	15.62	14.87	13.12	-0.01
SMC						
HV 817	1.277	0.298	14.13	13.59	12.12	0.08
HV 823	1.504	0.873	14.46	13.60	11.58	0.05
HV 824	1.818	0.315	13.06	12.27	10.33	0.03
HV 829	1.931	0.348	12.61	11.81	9.92	0.03
HV 834	1.866	0.557	12.95	12.14	10.20	0.02
HV 837	1.631	0.822	13.95	13.10	11.11	0.04
HV 847	1.433	0.500	14.40	13.66	11.83	0.08
HV 865	1.523	0.108	13.55	12.93	11.21	0.06
HV 1365	1.094	0.184	15.39	14.79	13.20	0.07
HV 1954	1.223	0.847	14.13	13.62	12.12	0.07
HV 2064	1.527	0.279	14.28	13.50	11.61	0.07
HV 2195	1.621	0.135	13.85	13.07	11.09	-0.02
HV 2209	1.355	0.822	13.99	13.42	11.84	0.04
HV 11211	1.330	0.516	14.36	13.64	11.83	0.06

iii) 3 objects: for EU Tau, we adopted the distance by Groenewegen et al. (2004), while for KQ Sco and SX Vel we adopted distances calculated by Dr. Martin Groenewegen, following the general method outlined in G07, but using the SB-relation and projection-factor from Fouqué et al. (2007) for consistency.

iv) 2 object: the Cepheid AP Pup was not included in the analysis of the metallicity effect because an accurate estimate of its linear diameter is not available. For this object in Table 2.5 we only listed the apparent magnitudes. The same outcome applies to AX Vel, since Laney & Stobie (1995) mentioned that the quality of the radius solution for this object was quite poor.

Accurate reddening estimates for Galactic Cepheids have been recently provided by Laney & Caldwell (2007), however, we typically adopted the reddening estimates used to determine individual Cepheid distances. The current Cepheid sample includes objects that are classified in the literature as fundamental pulsators, except EU Tau and SZ Tau, which are classified as first overtone pulsators, and AX Vel that is classified as one of the few double-mode pulsators in the Galaxy (Ferne et al. 1995; Sziládi et al. 2007). Their observed periods have been "fundamentalised" using $P_0 = P_1 / (0.716 - 0.027 \cdot \log P_1)$ (Feast & Catchpole 1997).

From the database of the binaries among the Galactic Classical Cepheids (Szabados 2003) we found that 15 stars are spectroscopic binaries and one star (ζ Gem) is a visual binary (see last column of Table 2.5). According to current empirical evidence the companions are typically B and A-type main sequence stars, which are much less luminous (at least 3 mag) than our main Cepheid targets. Only in the case of the two most luminous B dwarf, companions respectively of KN Cen and S Mus, we have detected a small contribution to the continuum level of the Cepheid spectra.

2.2.2 PL-data: the Magellanic sample

The Magellanic sample consists of the 22 Cepheids in the LMC and the 14 Cepheids in the SMC, obtained at the VLT-Kueyen telescope on Cerro Paranal with UVES (see section 2.1.2) in service mode. The measured signal-to-noise ratios vary between 50 and 70. For these stars we have adopted periods, optical and NIR photometry from Laney & Stobie (1994). The pulsation phases at which our stars were observed and selected characteristics are listed in Table 2.6. As we have already mentioned, the good estimates of the distance of a star is crucial to know its absolute magnitude, which is essential for our analyses. For the Magellanic Cepheids, we adopted the distances of their parent galaxies, corrected for projection effects. This assumption is necessary due to the lack of individual determination of distance for our programme Cepheids in the Magellanic Clouds. Considering the values reported in the most recent literature (e.g. Benedict et al 2002; Walker 2003; Borissova et al 2004), we adopted as distance modulus of the barycentre of the LMC the value of 18.50 ± 0.10 mag (i.e. 50 ± 2.3 kpc). The SMC is taken to be 0.44 ± 0.10 mag (e.g. Cioni et al 2000) more distant than the LMC (i.e a total distance of 61 ± 2.9 kpc). This value of the relative distance between the two galaxies has confirmed the results of previous studies (Westerlund 1997 and reference therein). Depth and projection effects in the Magellanic Clouds were corrected for using the position angle and the inclination of each galaxy as determined by van der Marel & Cioni (2001, LMC) and Caldwell & Laney (1991, SMC).

2.2.3 BW-data

For the BW-data we have selected 4 Cepheids with super-solar composition as measured by Andrievsky et al (2002a, 2002b) and set out to measure their distances with the Baade-Wesselink technique, which

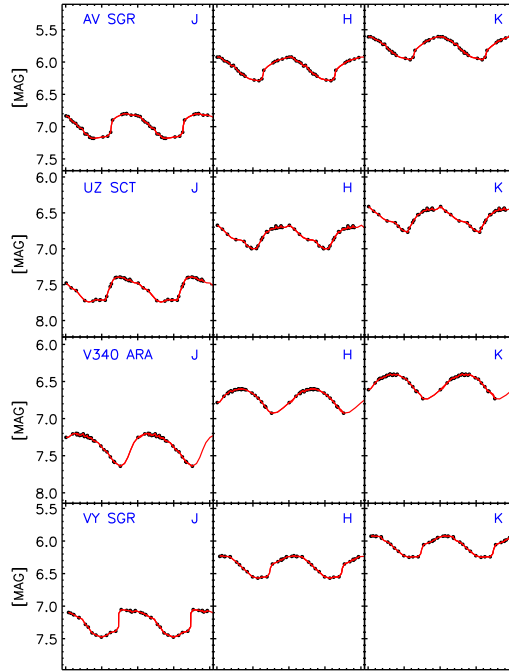


Figure 2.6: From left to right J,H,K-band light curves for the BW-data Galactic Cepheids. The symbols are the same as in Fig. 2.7.

Table 2.7: BW-data parameters.

NAME	α (J2000)	δ (J2000)	N.phase points	M_V	[Fe/H]
V340 ARA	16 45 19	-51 20 33	25+2	10.2	0.31
AV SGR	18 04 49	-22 43 00	28+2	11.3	0.34
VY SGR	18 12 05	-20 42 00	27+2	11.5	0.26
UZ SCT	18 31 22	-12 55 00	25+2	11.3	0.33

has proven to yield distances to the individual stars to better than 5% accuracy (e.g., Barnes & Evans 1976, Laney & Stobie 1995, Fouqué & Gieren 1997, Storm et al 2004). The stars we have chosen are the most metal-rich ones in the large sample for which Andrievsky et al. (2002) have measured the chemical composition, thus yielding the largest baseline in [Fe/H]. The accurate multi-epoch, multi-band optical and infrared photometric data needed for the Baade-Wesselink technique was collected at the SAAO by team member Laney for all of our targets and are currently being reduced and analyzed. Figure 2.6 shows the J , H and K -band light curves for our program Cepheids while Table 2.7 listed their main parameters. The second ingredient for the Baade-Wesselink method, namely accurate radial velocity curves along the pulsational cycle, was the object of our successful proposal 075.D-0676 (PI Romaniello, 18.5h with FEROS, class A). The goal there was to obtain, for each of the 4 target stars, radial velocity measurements with an accuracy of 1 km/s at 20 epochs to reach the target accuracy of 5% in distance as stated above. The quality of each spectrum at each epoch ($S/N \sim 70$) will only allow for a crude determination of the metal content. For this reason we decided to add two more spectra (“+2” in column 4 of table 2.7) for each target with higher signal-to-noise ratio ($S/N \sim 150$) and used an average of them to measure the metallicities for these stars in an homogeneous way with respect to the PL sample (same line list, gf

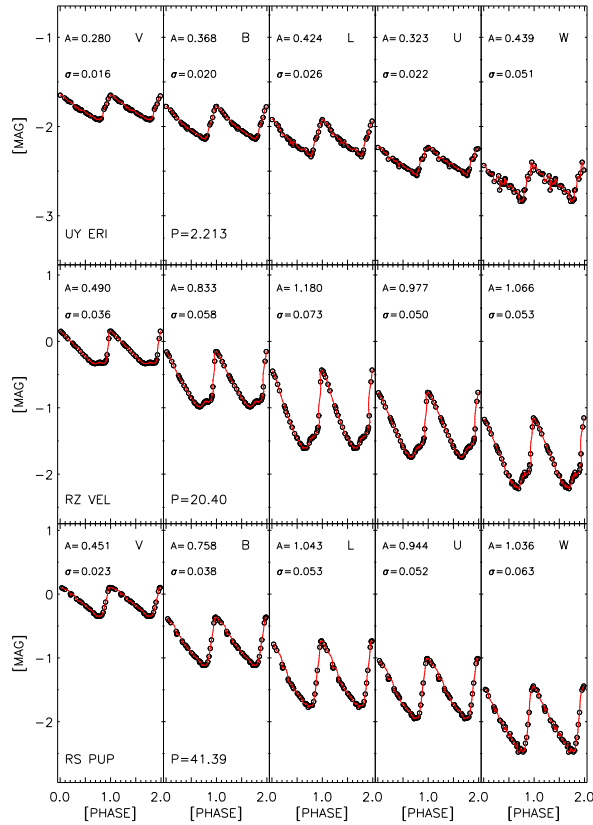


Figure 2.7: From left to right light curves in the Walraven V,B,L,U,W bands for three Cepheids. From top to bottom short, intermediate, and long period Cepheids (see labeled values). For each band are also plotted the intrinsic scatter of the fit with a cubic spline and the amplitude.

values, tools to derive the chemical abundances, etc.). In this way the metallicity will be determined to a satisfactory precision (0.1 dex).

2.2.4 Walraven-data

The Walraven optical sample include 173 Galactic Cepheids for which *VBLUW*-bands photometry were collected. Fig. 2.7 shows the light curves in the five bands for three (of 173) Cepheids of our sample, namely FW LUP, RZ VEL and RS PUP. The light curves and the tables with physical parameters, mean Walraven and mean NIR magnitudes of the whole sample are shown in Appendix A. Data plotted in figure 2.7 show that individual simultaneous *VBLUW* measurements present an accuracy of the order of few millimag. For each object have been collected at least 30 phase points that properly cover the entire pulsation cycle. This means that the intrinsic accuracy of the mean magnitudes estimated by fitting a cubic spline is of the order of a few hundredths of magnitude. As we have already mentioned, we used NIR mean magnitudes to estimate the distances of our empirical set. Making in comparison the data from *MkII@0.75m* archive and the whole Walraven sample, we found accurate NIR magnitudes only for 65 Cepheids. For these the uncertainties of each phase point range from 0.005 to 0.007 for $K < 6$

mag, deteriorating to about 0.012 at $K = 8.6$ mag. This implies an accuracy in the mean magnitudes of about 0.002 - 0.005, depending on the number of points. However, the dominant uncertainty on the mean magnitudes is probably due to the absolute calibration which is 0.01. The mean magnitude of the other Cepheids are based on 2MASS photometry and they were estimated using the template light curves provided by Soszýnski et al. (2005) together with the V -band amplitude and the epoch of maximum available in the literature.

CHAPTER 3

Overview of the analysis of stellar spectra

Following Alloin (in "Astrophysical & laboratory spectroscopy", 1988), Kaler ("Stars and their spectra", 1989), Gray ("The observation and analysis of stellar photospheres", 1992), Jaschek & Jaschek ("The behavior of chemical elements in stars", 1995) and Emerson ("Interpreting astronomical spectra", 1996), we will give a brief general overview about stellar spectra and their analysis. The stellar spectra are typically absorption spectra. A star can be described as a layered body, characterized by different physical conditions (pressure, temperature, density) in the different layers, and its resulting spectrum is the combination of the radiation emerging from its different parts. The deep layers are gases under high pressure and they produce a continuum spectrum, going outwards through the external layers (called atmosphere) the pressure and the density drop and the radiation is absorbed by the atoms of the atmosphere gas. However this picture is a rough simplification, in reality, the pressure drops slowly in the outward direction and the layers overlap, gradually merging one into another. Each line actually is formed at a somewhat different depth in the stellar atmosphere. For example, lines of ions must be produced in layers that are deeper than those that generate neutral features, as higher temperatures are required to strip electrons from atoms through collisions. The interpretation of a stellar spectrum consists of deriving from the observed quantities (shape of the continuum, intensity and profile of the lines) the physical parameters which describe the stellar atmosphere: its dynamical and thermodynamical state and its chemical composition. Historically, the first studies and classifications of stellar spectra have been done from an observational point of view, starting from the spectrum of the Sun in the early 1800s. The rapidly improving instrumentation and the increasing number of studied stars changed the classification of stellar spectra through the decades. At the beginning, it was based only on the color of the stars and the presence of particular lines (the Harvard classes: *OBAFGKM*), then it became a two-dimensional classification adopting also luminosity classes (from luminous supergiants Ia to white dwarfs VII). In Fig 3.1 are shown examples of spectra of well-studied stars with their spectral class. The changes through the spectral sequence from hot stars (B) to cool stars (M) are quite evident. Figure 3.2 displays the average locations of stars of the various luminosity classes in the Hertzsprung-Russell diagram, obtained using the absolute visual magnitude vs the spectral type. Cepheids belong to a range of spectral classes from *F* to *K*. Being variable stars their color (i.e. temperature) varies with the phase, so their spectral type will be different depending on when the stars are observed. Their luminosity class is between Ia (luminous supergiants) and II (bright giants). Figure 3.3 shows three Galactic Cepheids of our sample characterized by different temperatures (4705 K, 5555 K and 6130 K) but with a similar metallicity. It can be seen the

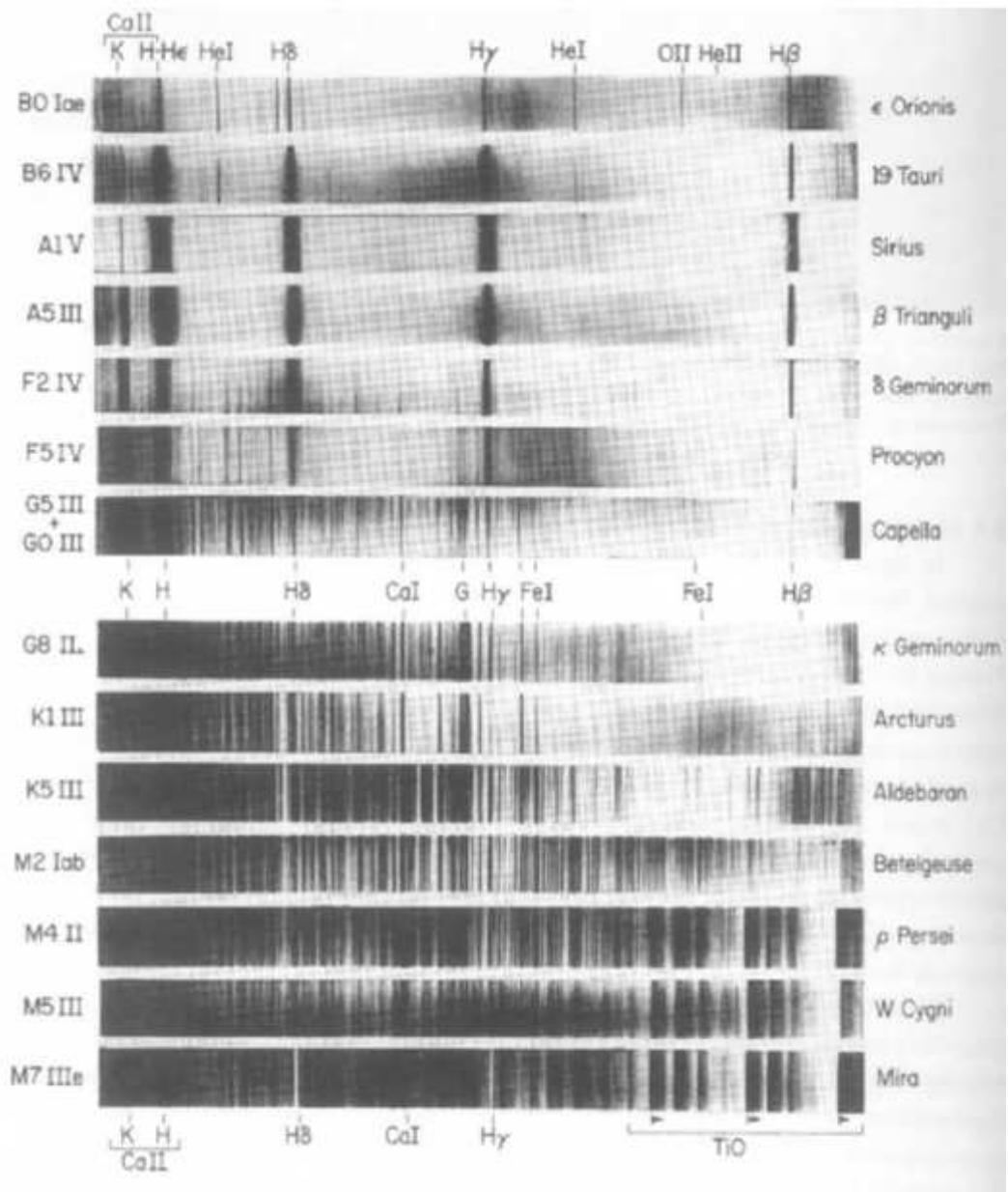


Figure 3.1: The spectral sequence is illustrated with representative stellar spectra in the blue and violet region. Hydrogen, calcium, iron and oxygen lines are indicated. The cool M stars spectra show also the violet edges of molecular TiO bands (from Kaler 1989).

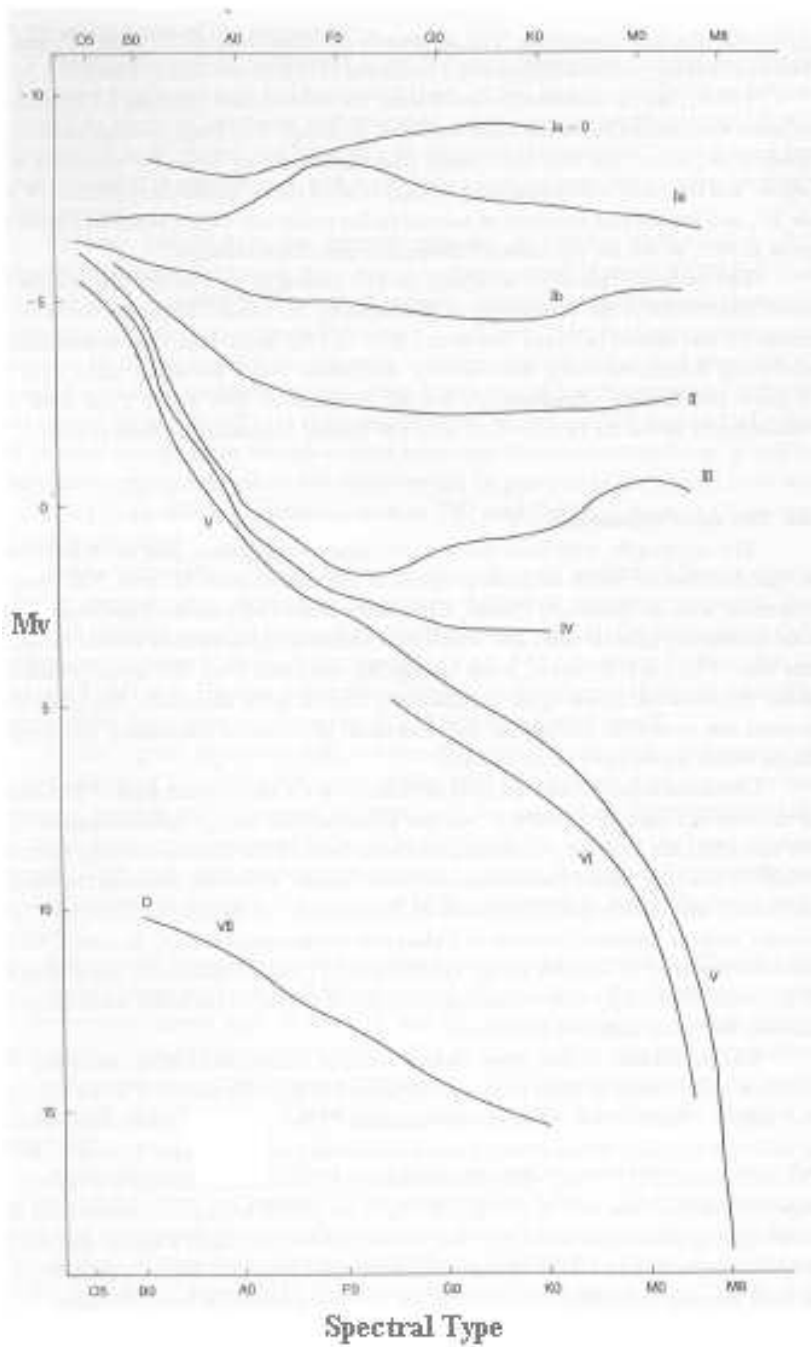


Figure 3.2: The Hertzsprung-Russell diagram with the average locations of the stars of the various luminosity classes. The y-axis is the absolute visual magnitude while the x-axis is the spectral type. The stars actually occupy broad bands centered on the solid lines. The supergiant (Ia-Ib) and giant (II-III) zones are especially broad (Figure 3.8 from Kaler 1989). Cepheids belong to a range of spectral classes from F to K

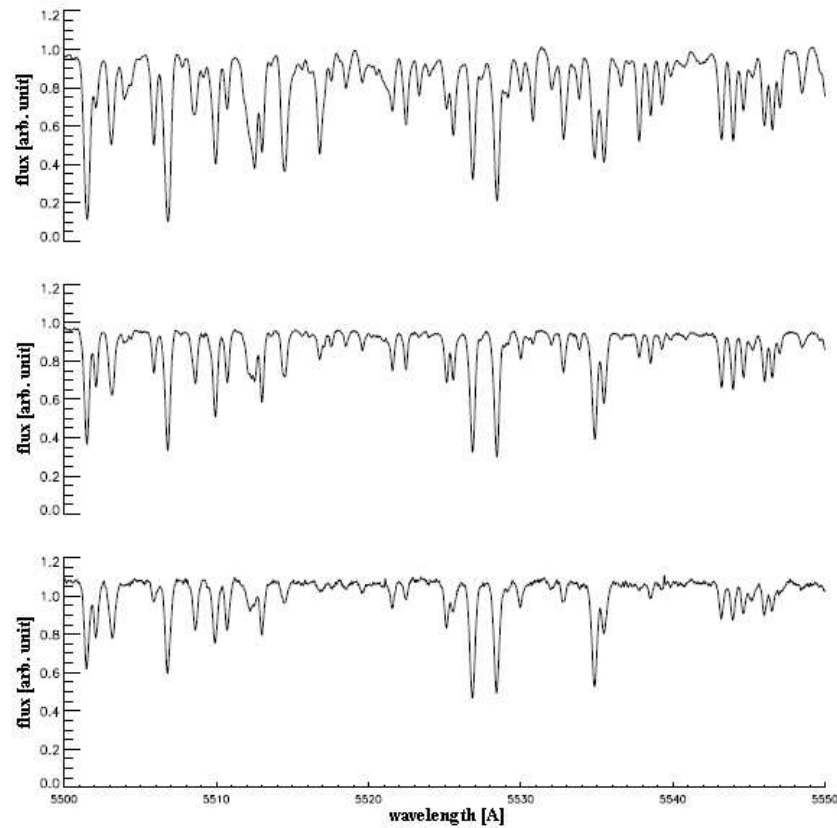


Figure 3.3: The same spectral range as observed in three Galactic Cepheids (with a solar metallicity) of our sample characterized by different temperatures top: 4705 K, middle: 5555 K, bottom: 6130 K. The intensity of the lines decreases as the temperature increases.

decrease of the intensity of the lines as the temperature increases. The luminosity and the temperature of a Cepheid vary along the pulsational cycle so the intensity of its spectral lines change with the phase. Number and intensity of the spectral lines depend also on the chemical composition of the variable. The physical origin of a stellar spectrum has been unraveled in the first part of the twentieth century, when the equations relating ionization and excitation to temperature and density have been derived and solved. From that time on a whole body of work has been done to describe and reveal the nature of a stellar spectrum from a theoretical point of view, with the development of models of the stellar atmospheres. The modern analysis of a stellar spectrum uses a reverse approach compared to the empirical classification mentioned above. First it is necessary to build a stellar atmosphere model and predict values for the observable quantities and, secondly, to compare these values with real observations and readjust the physical parameters of the model to match the observations. The intensity or strength of a line can be characterized by the so-called equivalent width (see section 3.1.2). The equivalent width of a line (W) is defined as the surface enclosed in the line profile:

$$W = \int_{\lambda_1}^{\lambda_2} \frac{I_c - I_l}{I_c} d\lambda \quad (3.1)$$

where I_c is the continuum intensity and I_l is the line intensity at every λ between λ_1 and λ_2 (the limits of the line). In other words the equivalent width is the measure of the flux of the line in units of the density of the flux of the continuum. If we assume the continuum background as unity, it is the width of a rectangle

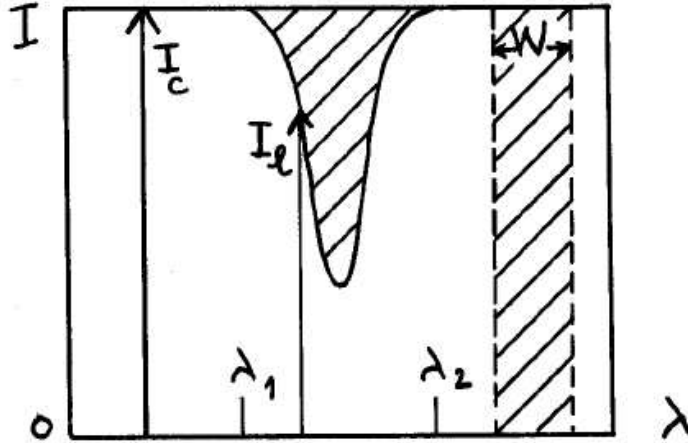


Figure 3.4: Definition of the equivalent width W . I_c is the continuum intensity and I_l is the line intensity at every λ between λ_1 and λ_2 (from Alloin 1988).

with height 1. The abscissa in Fig. 3 can be expressed either in terms of wavelength or on a frequency scale. The equivalent width is given in the same units as the abscissa and can thus be expressed in \AA or cm^{-1} . The difficulties in measuring equivalent widths usually come from the tracing of the continuum, because of line crowding (typical of late type stars) or of superpositioning of neighboring lines (rapid rotating or pulsating stars). Also, it can be problematic to recover the true continuum measuring lines in the vicinity of a strong line with broad wings. As we shall see, the W of a line is linked to the abundance of that element and this is one of the way to determine the elemental abundance of a star from its spectrum. An alternative technique is the spectral synthesis, particularly useful in case of severe line blending. The strength or equivalent width of a line in a stellar spectrum depends on the chemical abundance, the temperature, the absorption coefficient, the number of absorbers and atomic constants. The change in the line profile and equivalent width is not a simple proportionality, but depends on the optical depth of the line. In Fig 3.5 we see an example of the theoretical behavior of the profile and equivalent width of an *FeI* line. The top panel shows the so-called curve of growth, which, typically, is a log-log plot of equivalent width (W) versus abundance (A). The line strength increases with an increase in the chemical abundance and we can distinguish three different phases of the line growth. For weak lines, the depth and the equivalent width of the line is proportional to A . The second phase is entered as the central depth approaches the maximum value and the line saturates. The saturation grows asymptotically towards a constant value. The third stage of the behavior starts as the optical depth in the line wings becomes significant compared to ratio of the line absorbers to the continuum opacity. At this stage the equivalent width will grow approximately proportional to $A^{1/2}$. Thus, to determine the elemental abundance is crucial to accurately measure equivalent widths of weak lines, in order to remain in the first phase of the line growth, where there is a direct proportionality between W and A . The behavior of this part of the curve of growth is described by the following expression (from Gray, 1992):

$$\log\left(\frac{W}{\lambda}\right) = \text{const} + \log A + \log gf \lambda - \Theta_x \chi - \log \kappa_\nu \quad (3.2)$$

where A is the chemical abundance, $\Theta_x = 5040/T$ (where T is the temperature), χ is the excitation potential for the atomic level, gf is the oscillator strength (related to the atomic transition probability and different for each atomic level), κ_ν is the ratio of the line absorbers to the continuum opacity and the absorption coefficient is lumped in the constant. κ_ν depends on the electron pressure that, in turn,

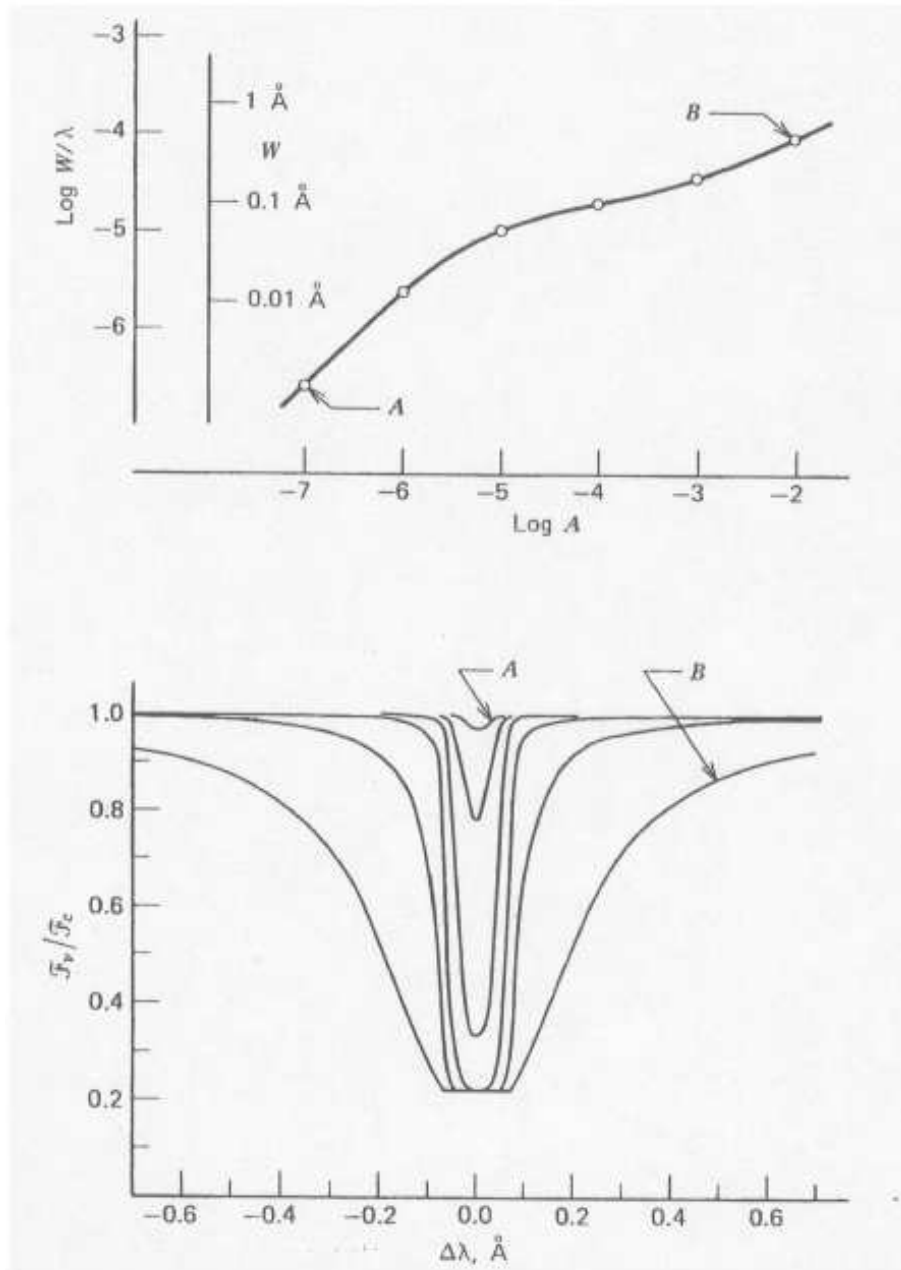


Figure 3.5: Both the equivalent width (top) and the profile (bottom) change with the chemical abundance of the absorbing species. The circles on the curve of growth correspond to the profiles below (Fig.13.12 from Gray, 1992).

is controlled by the surface gravity. On the other hand, the absorption coefficient is a function of the thermal and microturbulent velocities, the latter is a small-scale non-thermal velocity that parameterize the spectral line broadening (see Gray, 1992, chapters 13, 14 and 18 for an in-depth discussion of the above mentioned quantities and their derivation). Thus, the equivalent width and the chemical abundance are then related to the stellar parameters (temperature, gravity and microturbulent velocity), which are also used to characterize a model atmosphere. Knowing these parameters and the physical characteristic of the line of interest and its equivalent width, it is then possible to calculate the correspondent elemental abundance using Eq. 3.2. This equation also tell us that, for a given star, curves of growth for lines of the same species, where A is constant, will differ only in the displacements along the abscissa according to their individual values of gf , λ , χ and κ_v . From the model atmosphere point of view, we can choose a line (it has a fixed gf , λ and χ and the model fixes Θ_x and κ_v) and vary the equivalent width to generate its curve of growth. In this way it is also possible to investigate how changes in the temperature, in the gravity or in the microturbulent velocity can affect the chemical composition. A few more words must be added on the general subject of chemical composition. The quantity normally derived from observations of stellar spectra is the number of atoms of some elements as a fraction of the number of atoms of hydrogen. Abundances are expressed relative to hydrogen because in the vast majority of the stars hydrogen atoms are close to 90% of all atoms, and spectral lines are measured relative to the continuum, whose intensity is usually directly or indirectly related to the hydrogen abundance. The total abundance of all the elements heavier than helium relative to hydrogen does vary considerably between stars. This quantity is called metallicity because lines of iron are often the easiest to detect in faint stars. The metallicity or the iron abundance, like all the other elements, is commonly quoted relative to its value in the Sun. The terminology commonly employed is $[X/H]$, where X generally indicates a chemical element, which means $\log(NX/NH)_{star} - \log(NX/NH)_{\odot}$. Usually stars with a low (negative) value of this quantity are described as being metal poor, while stars with a high (positive) value are called metal rich. It is important to stress that all these observed abundances refer to the surface of the star. Below we present the methodologies used to calculate the elemental abundances of our sample of Cepheids both from spectra analysis (assembling the line lists, determining the equivalent widths and temperatures and computing the abundance with the adopted model atmospheres) and from Metallicity Index Color (MIC) relations based on Walraven photometry.

3.1 Line list

A crucial step of any spectral analysis in order to derive elemental abundances is a careful assembling of a line list. It is fundamental to select unblended lines to prevent undesirable contribution from other elements that can affect the determination of the abundance, making them larger than they should be. As a starting point, we have assembled two line lists (FeI-II and α -elements) choosing lines used in previous studies on Cepheids and RR Lyrae from Clementini et al (1995), Fry & Carney (1997, hereafter FC97), Kiss & Vinko (2000) and Andrievsky et al (2002a) plus a selection of iron lines from VALD (Vienna Atomic Line Database; Kupka et al 1999). The Vienna Atomic Line Database is a critical collection of atomic line parameters of astronomical interest and provides tools for selecting subsets of lines for typical astrophysical applications (line identification, chemical composition and radial velocity measurements, model atmosphere calculations, etc). The VALD lines have been selected for effective temperatures typical of Cepheid stars (4500-6500 K). We have, then, visually inspected each line on the observed spectra, in order to check their profile and to avoid blended lines. In order to do so, we have searched the VALD database for all the existing lines between 4800 and 7900 Å on stellar spectra characterized

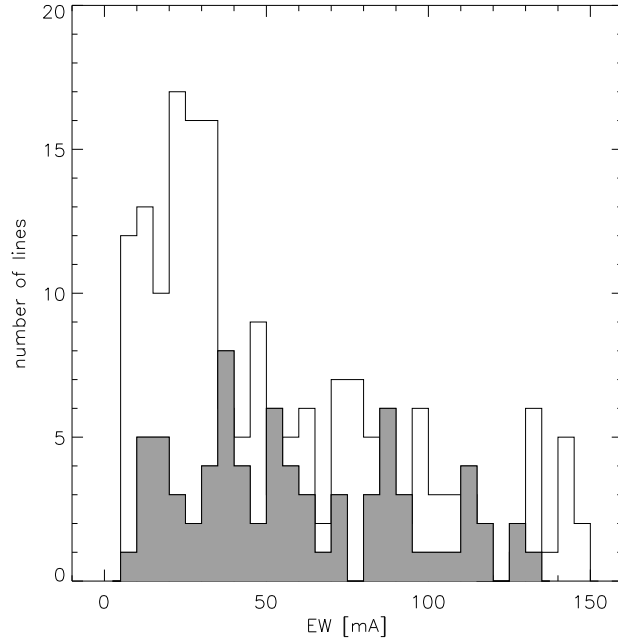


Figure 3.6: The distributions of the equivalent widths (EW) of our lines (empty histogram) and Fry & Carney’s lines (1997, dark grey histogram), in the case of the same star (VCen).

by stellar parameters typical of Cepheids ($T_{\text{eff}}=4500$ K, 5500 K and 6500 K, $\log g=2$ and $v_t=3$ km/s). We then overplotted all the lines found in VALD, that fall within $\pm 3 \text{ \AA}$ from each of our iron lines, and checked for their possible contribution to the equivalent width of our iron line. This test was carried out on 3 different observed spectra, characterized by effective temperatures (as found in the literature from previous analyses) close to 4500 K, 5500 K and 6500 K, respectively. Any contribution larger than 5% of the line strength made us discard the iron line under scrutiny. There remains, of course, the possibility that some weak lines could be missing in the VALD compilation, but these are expected to be only weak lines, whose contribution would, then, be negligible.

Our final lists includes 275 FeI lines, 37 FeII lines, 5 OI lines, 4 NaI lines, 6 MgI lines, 4 AlII lines, 49 SiII lines, 28 CaI lines, 53 TiI lines and 18 TiII lines, spanning a spectral range from 4800 \AA to 7900 \AA which is the range covered by our FEROS spectra. Our UVES spectra cover a narrower spectral range for which we can use 217 FeI lines, 30 FeII lines, 2 OI lines, 2 NaI lines, 5 MgI lines, 2 AlII lines, 27 SiII lines, 22 CaI lines, 42 TiI lines and 12 TiII lines. For all the lines, we have adopted the physical properties (oscillator strengths, excitation potentials) listed in VALD. A high number of lines for each element reduces the internal errors on the final determination of the abundance. Figure 3.6 compares the distribution of the equivalent widths of our iron lines with those from Fry & Carney (1997), in the case of the same star, the Galactic Cepheid V Cen. As it can be clearly seen, our list is significantly larger and well samples the best range of equivalent widths (at around 20 m \AA as suggested by Cayrel 1988 for the determination of elemental abundances) to obtain iron abundances. The complete lists of lines are given in Appendix B where the four columns list respectively the wavelength, the ion identification, the excitation potential and the gf values of each line.

3.2 Equivalent widths

The second crucial step of our spectral analysis is the measurement of the equivalent widths (EW) of the iron lines we have assembled in our final list. Because of the large number of lines and spectra, our final EW measurements were derived by using a semi-interactive routine (*fitline*, see section 3.1.4) developed by one of our collaborators Prof. Patrick Francois: *fitline*, that greatly increases the efficiency while yielding accurate measurements. All the UVES spectra have been smoothed to improve the quality of the Gaussian fit (smooth_step = 11 pix using *splot* task in IRAF). All the useful information from the spectra are preserved in the process. The selected iron lines, even on the smoothed spectra, do not show any contamination from other line. However, for about 15% of the lines, the Gaussian profile performed by *fitline*, could not satisfactorily reproduce the observed profile (see Fig 3.7, panel (d)). The equivalent widths of these lines, usually very broad or asymmetric, were measured manually with the *splot* task. The mean difference, as computed for those lines for which both methods could be applied, is around 1.5 mÅ, comparable to the average error on the EW inferred from the quality of the data (Equation 7, Cayrel 1988). We can then safely use all our EW measurements, independently of the method we used to derive them.

For the determination of the metallicities, we have selected only lines with equivalent widths between 5 and 150 mÅ. The lower limit was chosen to be a fair compromise between the spectral characteristics and the need for weak lines for an optimal abundance determination. The upper limit was selected in order to avoid the saturated portion of the curve of growth. We note that a slightly higher upper limit (200 mÅ) was chosen for T Mon, SZ Tau and KQ Sco because these stars have very strong lines. This was done in order to keep the number of selected lines similar to the one used for the rest of the sample, after checking that this higher upper limit does not have any effect on the final metallicities derived for these three stars.

Considering the mean difference on the EW obtained with *fitline* and *splot* and the uncertainty in the continuum placement from two measurements of the EW (carried out independently by two of us) we assume ± 3 mÅ as error on the equivalent widths for the lines below 100 mÅ and ± 5 mÅ for the stronger features.

3.3 Stellar Parameters

The stellar parameters were derived spectroscopically. We have determined the stellar effective temperature T_{eff} by using the line depth ratios method described in Kovtyukh & Gorlova(2000). It is based on weak neutral metal lines (in our case, less than 100 mÅ in equivalent width in order to exclude line broadening effects) with low excitation potentials, selected to obtain as close as possible pairs in wavelength space. The depth ratios of these lines are very sensitive to the effective temperature, thus they can be used as temperature indicators. The application of this method is rather simple, it consists in measuring the depths of the lines selected by Kovtyukh & Gorlova (32 pairs), determining their ratios and calculating the T_{eff} using this relation:

$$T_{\text{eff}} = a + b \cdot r + c \cdot r^2 + d \cdot r^3 \quad (3.3)$$

where r is the line depth ratio, a , b , c and d are the coefficients of the calibration for each pair. The final effective temperature is the mean value of the outcomes from each pair of lines. Since the calibration of this method has been done using the FC97 scale of temperatures, our temperature scale is linked to theirs. The line depth ratios have the advantage of being independent of interstellar reddening and metal-

licity effects, uncertainties that instead plague other methods like the integrated flux method or colors calibrations (Gray 1994). The main uncertainties of the calibration of the line depth ratios, instead, lie in the accuracy of its zero point and slope, which have been thoroughly tested either with different color-temperature relations or diameters measurements by Kovtyukh & Gorlova (2000).

The total number of line depth ratios adopted to estimate the temperature ranges from 26 to 32 and from 20 to 28 for Galactic and Magellanic Cepheids, respectively. From this method, we have obtained effective temperatures with an intrinsic accuracy of about 40 K for the Galactic Cepheids and 50 K for the Magellanic ones (errors on the mean). Table 3.1 and Table 3.2 list our final effective temperatures for Galactic and Magellanic Cepheids, respectively.

Microturbulent velocity (v_t) and gravity ($\log g$) were constrained by minimizing the $\log([\text{Fe}/\text{H}])$ vs EW slope (using the FeI abundance) and by imposing the ionization balance, respectively. These two procedures are connected and require an iterative process (on average, between 5 and 7 iterations, depending on the star). We first achieved the minimization of the $\log([\text{Fe}/\text{H}])$ vs EW slope and, subsequently, the ionization balance. As first guess for the microturbulent velocity and the gravity, we adopted values typical of Cepheids ($v_t=3$ km/s, $\log g = 2$) as inferred from previous studies (FC97 and Andrievsky et al. 2002a, 2002b). We first assumed the ionization balance to be fulfilled when the difference between $[\text{FeI}/\text{H}]$ and $[\text{FeII}/\text{H}]$ is less than the standard error on $[\text{FeII}/\text{H}]$ (typically, 0.08-0.1 dex). However, we noticed that for most stars this condition was usually satisfied by more than one value of $\log g$, suggesting that our conditions for fulfillment might be too conservative and not very informative. We then checked which $\log g$ value satisfies the ionization balance within the standard error on $[\text{FeI}/\text{H}]$ (typically, 0.02 dex). For 55 stars out of 68 we were able to reach the FeI-FeII balance within few hundredths of a dex. The corresponding $\log g$ values are the final gravity values quoted in Table 3.1 and Table 3.2. For the remaining 13 objects, we assumed as our final $\log g$ the value giving the "best" ionization balance, i.e. the one with the smallest difference between $[\text{FeI}/\text{H}]$ and $[\text{FeII}/\text{H}]$. Also, it is worth noticing that for two stars (HV 2827 and HV 11211) we had to increase the temperatures as determined from the line depth ratios by 50 K (which is still within the estimated error on the determination of T_{eff}), in order to fulfill our requirements for a satisfactory ionization balance.

In order to determine the errors on the microturbulent velocity and the gravity, we have run several iterations for each star, slightly modifying the values of these two quantities that fulfill the requirements mentioned above. We have estimated errors in v_t to be 0.1 km/s and in $\log g$ to be 0.10 dex.

3.4 FITLINE

Fitline is a code based on genetic algorithms, which mimic how DNA can be affected to make the evolution of species (Charbonneau 1995). It uses a Gaussian fit, which is defined by four parameters: central wavelength, width, depth and continuum value of the line. A top-level view of the algorithm is as follows:

1. Compute an initial set of Gaussians, picking random values of the four parameter (scaled to vary between 0 and 1) and calculate the χ^2 with the observed line for each Gaussian.
2. Compute a new set of Gaussian from the 20 best fit of the previous "generation" introducing random modification in the values of the parameters ("mutation").
3. Evaluate the "fitness" of the new set (χ^2 calculation for each Gaussian) and replace the old set with the new one.

Table 3.1: Stellar parameters and FeI and FeII abundances of our Galactic sample. The FeI values have been adopted as final $[Fe/H]$. We compare our results, where it is possible, with previous investigations: Fry & Carney (1997); Andrievsky et al. (2002a,b,c), Luck et al. (2003).

ID	T_{eff}	v_t	$\log g$	[FeI/H]	[FeII/H]	[Fe/H] _{FC}	[Fe/H] _A
1 Car	4750	3.60	0.4	0.00	0.00
U Car	5980	3.00	1.2	+0.17	+0.13
V Car	5560	3.05	1.8	-0.07	-0.02
WZ Car	4520	1.80	2.1	+0.08	+0.19
V Cen	6130	2.80	1.9	+0.04	-0.03	-0.12	+0.04 ^a
KN Cen	5990	3.80	1.6	+0.17	+0.09
VW Cen	5240	4.20	1.2	-0.02	+0.07
XX Cen	5260	2.95	1.3	+0.04	+0.04
β Dor	5180	3.00	1.3	-0.14	-0.11	...	-0.01 ^a
ζ Gem	5180	3.70	1.4	-0.19	-0.14	-0.04	+0.06 ^a
GH Lup	5480	3.60	1.5	+0.05	+0.01
T Mon	4760	3.80	0.6	-0.04	-0.03	+0.09	+0.21 ^b
S Mus	5780	2.75	1.8	+0.13	+0.19
UU Mus	5900	3.05	1.7	+0.11	+0.05
S Nor	5280	2.80	1.1	+0.02	+0.04	-0.05	+0.06 ^a
U Nor	5230	2.60	1.1	+0.07	+0.13
X Pup	5850	3.30	1.4	+0.04	-0.05	...	0.00 ^a
AP Pup	6070	3.05	2.1	-0.07	-0.07
AQ Pup	5170	3.10	0.8	-0.07	-0.09	...	-0.14 ^b
BN Pup	5050	2.95	0.6	-0.10	-0.07	...	+0.01 ^c
LS Pup	6550	3.50	2.2	-0.16	-0.10
RS Pup	4960	3.50	0.7	+0.09	+0.10	...	+0.16 ^b
VZ Pup	5230	3.25	1.1	-0.17	-0.15	...	-0.16 ^c
KQ Sco	4840	3.60	0.7	+0.21	+0.27	...	+0.16 ^d
EU Tau	6060	2.30	2.1	+0.04	+0.02	...	-0.03 ^a
SZ Tau	5880	2.80	1.7	+0.07	+0.04	-0.02	+0.06 ^a
T Vel	5830	2.55	1.8	+0.10	+0.03	...	-0.04 ^b
AX Vel	5860	3.10	1.8	+0.02	-0.06
RY Vel	5250	4.10	1.2	-0.07	-0.06	...	-0.03 ^b
RZ Vel	5140	4.40	1.6	-0.19	-0.14	...	-0.11 ^b
SW Vel	6590	3.75	1.7	-0.24	-0.17	-0.10	-0.05 ^b
SX Vel	5380	2.55	1.2	+0.02	-0.02	...	-0.04 ^b

^a Luck et al. (2003).

^b Andrievsky et al. (2002a).

^c Andrievsky et al. (2002c).

^d Andrievsky et al. (2002b).

Table 3.2: Stellar parameters and FeI, FeII abundances of our Magellanic Cepheids. The FeI values were adopted as final $[Fe/H]$. When available the value from previous studies is also reported ($[Fe/H]_L$, where L stands for Luck & Lambert 1992; Luck et al. 1998). In the last column are listed the same values (as in column # 7), but rescaled to the iron solar abundance adopted in our work.

ID	T_{eff}	v_t	$\log g$	[FeI/H]	[FeII/H]	$[Fe/H]_L$	$[Fe/H]_{Lc}$
LMC							
HV 877	4690	5.40	0.5	-0.44	-0.47
HV 879	5630	3.05	1.0	-0.14	-0.14	-0.56 ^b	-0.46
HV 971	5930	2.30	1.4	-0.29	-0.29
HV 997	5760	3.10	1.2	-0.21	-0.22
HV 1013	4740	5.35	0.2	-0.59	-0.60
HV 1023	5830	3.10	1.1	-0.28	-0.27
HV 2260	5770	3.40	1.6	-0.38	-0.36
HV 2294	5080	3.90	0.5	-0.42	-0.42	-0.06 ^a	+0.10
HV 2337	5560	3.30	1.6	-0.35	-0.36
HV 2352	6100	3.65	1.6	-0.49	-0.47
HV 2369	4750	6.00	0.3	-0.62	-0.63
HV 2405	6170	4.20	2.3	-0.27	-0.28
HV 2580	5360	2.75	0.7	-0.24	-0.25
HV 2733	5470	2.90	1.8	-0.28	-0.27
HV 2793	5430	2.90	0.9	-0.10	-0.11
HV 2827	4790	4.00	0.0	-0.38	-0.33	-0.24 ^b	-0.14
HV 2836	5450	2.85	1.0	-0.16	-0.19
HV 2864	5830	2.80	1.5	-0.19	-0.20
HV 5497	5100	3.40	0.3	-0.25	-0.24	-0.48 ^b	-0.38
HV 6093	5790	4.50	1.5	-0.60	-0.60
HV 12452	5460	2.90	1.0	-0.35	-0.37
HV 12700	5420	3.15	1.4	-0.36	-0.35
SMC							
HV 817	5850	3.25	1.0	-0.82	-0.84
HV 823	5990	3.80	1.4	-0.80	-0.81
HV 824	5170	3.00	0.7	-0.73	-0.74	-0.94 ^b	-0.84
HV 829	5060	3.30	0.2	-0.76	-0.73	-0.61 ^b	-0.51
HV 834	5750	2.95	1.2	-0.63	-0.64	-0.59 ^b	-0.49
HV 837	5140	2.90	0.0	-0.83	-0.80	-0.91 ^b	-0.81
HV 847	4790	2.80	0.0	-0.75	-0.77
HV 865	6130	1.90	0.5	-0.87	-0.82	-0.44 ^a	-0.28
HV 1365	5340	2.48	0.6	-0.82	-0.84
HV 1954	5890	2.47	1.0	-0.76	-0.75
HV 2064	5550	3.10	0.7	-0.64	-0.64
HV 2195	5970	2.90	1.0	-0.67	-0.68	-0.45 ^a	-0.29
HV 2209	6130	2.30	1.1	-0.65	-0.67
HV 11211	4830	2.60	0.0	-0.83	-0.81

^a Luck & Lambert (1992).

^b Luck et al. (1998).

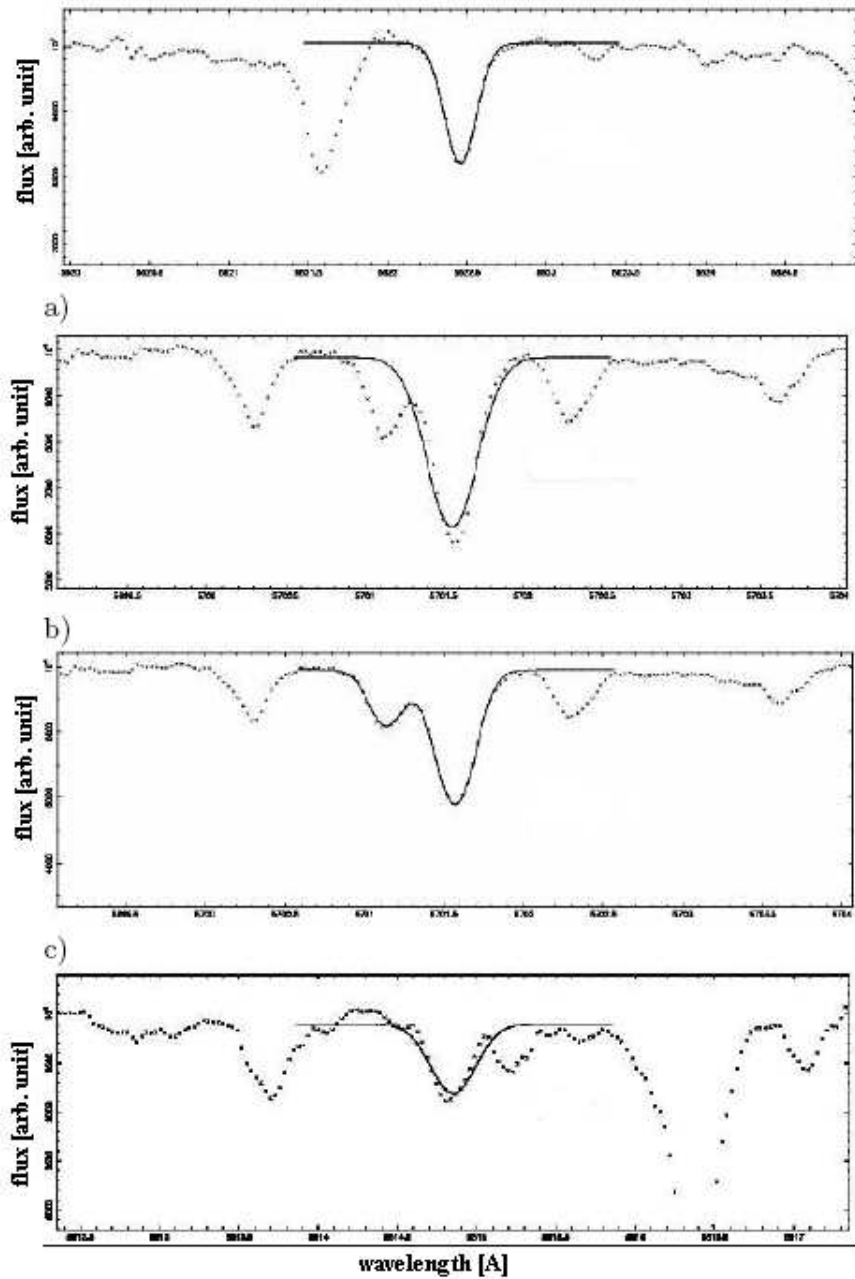


Figure 3.7: Examples of measurements of equivalent widths with fitline. Panel (a) shows a good fit from the first fitline session, panel (b) a bad fit from the first fitline session, panel (c) a good fit from the second fitline session and panel (d) a bad fit from the second fitline session.

4. Iterate the process (100 to 200 “generations”) to get the best fit (lowest χ^2) for each observed line.

The final equivalent widths are determined in three steps: running fitline a first time to obtain preliminary evaluation of the equivalent widths, feeding these results to a routine that allows to inspect and interactively correct the position of the continuum for each line (visually inspecting the observed spectrum with the best fit superimposed) and, as last step, the algorithm calculates the final equivalent widths. These steps include a complete session of fitline. The necessary inputs to run this program are the 1-D spectrum of the star (possibly already normalized) and the line list. The program’s parameters that can be adjusted to achieve the best results are the width of the gaussians and the tolerance range for the search of a blend. After several tests we found that the best approach was to run two sessions of fitline, using two different values for the width of the gaussian fitting (typically 32 and 26 pixels) and the tolerance range (typically 0.15 and 0.9 Å):

1. the first session gives measures of EW of the complete line list for a set of parameters, in Fig 3.7 an example of a good fit from the first session is shown (a);
2. the lines that present a bad fit as output of the first session are re-measured adopting different values of the width of the gaussian, usually smaller, and the tolerance range, usually bigger. In this way, during the interactive process, it is easier to get a better fit of the lines of interest using the program feature for the measure of blended lines. Fig 3.7 shows example of a bad fit from the first session (b) and a good fit from the second session adopting a smaller width and a bigger tolerance range (c).

3.5 Abundances and their uncertainties

Our final iron abundances, together with the adopted stellar parameters, are listed in Table 3.1 and Table 3.2 for the Galactic and Magellanic Cepheids, respectively.

For our **Galactic** sample, we find that the mean value of the iron content is solar ($\sigma = 0.10$, see Fig. 3.8, upper panel), with a range of values between -0.18 dex and +0.25 dex. These two extremes are represented respectively by 2 and 1 stars (out of the 32 in total). Our Galactic Cepheids span a narrow range of Galactocentric distances (the mean Galactocentric distance of our sample is 7.83 ± 0.88 kpc), thus preventing us from giving any indications about the metallicity gradient in the Galactic disc. For the **LMC** sample, we find a mean metallicity value of ~ -0.33 dex ($\sigma = 0.13$, see Fig. 3.8, middle panel), with a range of values between -0.62 dex and -0.10 dex. Here, the more metal-rich extreme is just an isolated case, while the metal-poor end of the distribution is represented by 3 stars.

For the **SMC** sample, we find that the mean value is about ~ -0.75 dex ($\sigma = 0.08$, see Fig. 3.8, lower panel), with a range of values between -0.87 and -0.63. As we have already mentioned, there are two binary stars (KN Cen and S Mus) among our Galactic sample with a bright B dwarf as a companion. In the spectral range covered by our spectra, these bright companions give a contribution only to the continuum level, because all their absorption lines fall in the ultra-violet region (these are very hot stars, with effective temperature $\sim 20,000$ K). In order to test the effect of this contribution, we have subtracted from the observed spectrum of the two binaries the estimated optical spectrum of the B dwarf, which only consists of a continuum without any line. On the resulting spectra, which we assume to be the true spectra of our Cepheids, we have then re-measured the EWs of a sub-set of iron lines and derived the metallicity. In the case of KN Cen the differences in the EWs measured on the observed spectrum and the

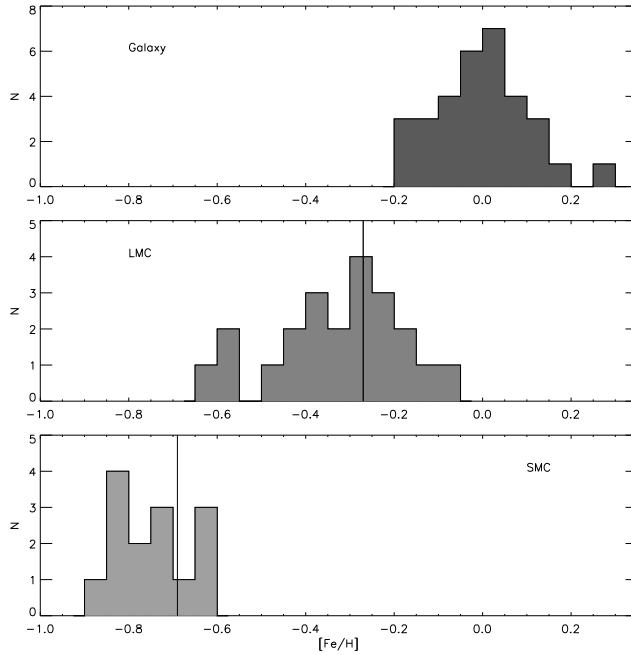


Figure 3.8: Histograms of the $[Fe/H]$ ratios derived for all the stars of our sample in the Galaxy, the LMC and the SMC. The solid lines indicate the mean values found using *F* and *K* supergiants by Hill et al. (1995) and Hill (1997) (see Table 3.4). We found a good agreement with the results obtained for non-pulsating stars of the same age of Cepheids.

Table 3.3: Effects on measured *FeI* and *FeII* abundances caused by changes in atmospheric parameters.

	$\Delta[FeI/H]$	$\Delta[FeII/H]$
$\Delta T_{\text{eff}} = +100$ K	+0.07 dex	+0.00 dex
$\Delta \log g = +0.1$ dex	+0.00 dex	+0.04 dex
$\Delta v_t = +0.1$ Km/s	-0.03 dex	-0.02 dex

true Cepheid spectrum are negligible (i.e. within the errors), thus the iron content we have derived for this star is robust. Regarding S Mus, instead, the EWs measured on the true spectrum are 12-15% larger than the ones measured on the spectrum we have observed. Thus, the true iron abundance of this Cepheid star should be 0.1 dex higher than the one we have derived. This happens because the intensity of the lines (due only to the Cepheid contribution) when compared to the continuum of the combined spectra is, in percentage, less than the intensity of the lines compared to the continuum of the Cepheid alone. In other words the contribution of the companion makes the lines of the Cepheid weaker. Please note that the iron content reported for S Mus in Table 3.1 has already been corrected for the above mentioned effect. The internal uncertainties in the resulting abundances are due to errors in the atomic data (*gf*-values) and EW measurements. We have estimated, on average, an internal error in the $[Fe/H]$ determination of 0.10 dex. It is also important to understand the effects of potential systematic errors in the stellar parameters on the final derived abundances (see Table 3.3). In order to do so we have determined curves of growth for different effective temperatures, microturbulent velocities and gravities for both *FeI* and *FeII*. As expected, we find that *FeI* abundances marginally depend on the gravity, whereas *FeII* does not depend

on the effective temperature. An increase in temperature of 100 K, at fixed v_t and $\log g$, results in an increase in $[\text{FeI}/\text{H}]$ of about 0.07 dex. An increase in v_t of 0.1 km/s gives a decrease in $[\text{FeI}/\text{H}]$ of about 0.03 dex, for constant T_{eff} and $\log g$, and we obtain a decrease of 0.02 dex for $[\text{FeII}/\text{H}]$. An increase in $\log g$ of about 0.1 dex produces an increase in $[\text{FeII}/\text{H}]$ of about 0.04 dex (with fixed v_t and T_{eff}).

An additional potential source of uncertainty and concern comes from the fact that our metallicities have been derived from single epoch observations. However, we note that FC97 did not find any significant difference in their derived $[\text{Fe}/\text{H}]$ as a function of phase (the test was performed on four of their longest period cepheids) and Luck & Andrievsky (2004) and Kovtyukh et al. (2005) show that the elemental abundances for Cepheids with a period between 6 and 68 days are consistent for all pulsation phases.

We have also compared our results to previous works. For this purpose, we have selected the chemical analyses of FC97, Andrievsky et al. (2002a, 2002b, 2002c) and Luck et al. (2003) for the Galactic Cepheids and LL92 and L98 for the Magellanic Clouds. When necessary, we have rescaled the literature $[\text{Fe}/\text{H}]$ values to the solar iron abundance we have adopted ($\log[n(\text{Fe})] = 7.51$). In total, for the Galactic sample, we have 6 stars in common with FC97 and 18 with the entire sample of Andrievsky's group, while for the MC sample, we have 3 stars in common with LL92 and 7 with L98.

For **Galactic** Cepheids we obtained that:

the mean difference between our results and those of FC97 and Andrievsky analyses is comparable to the difference between FC97 and Andrievsky's values (0.08 ± 0.02). In more detail, the mean difference between our iron abundances and FC97 is 0.09 ± 0.02 , which is satisfactory. For 4 stars (V Cen, S Nor, T Mon, ζ Gem) the agreement is at 1σ level, for the remaining 2 stars the agreement is well within the quoted uncertainties. We note that our derived abundances for V Cen and S Nor are more in agreement with the metallicity derived by Andrievsky et al. than with FC97. When comparing our results to Andrievsky's, we obtain a mean difference of 0.07 ± 0.05 . For 14 stars (out of 18), the iron abundances agree quite well within the associated errors. Of the remaining 4 stars, we note that SW Vel, β Dor, and T Mon agree within the standard deviation ($\sigma=0.20, 0.19, 0.22$ dex respectively) instead of the standard error, that is the condition suggested by Kovtyukh et al. (2005a) for the independence of the elemental abundance on the phase. This is not the case for ζ Gem, for which we cannot explain the difference (0.20 dex) but for which we find instead an agreement with FC97.

In the comparison of **Magellanic** Cepheids we found that:

In order to properly compare our results for the Magellanic Cepheids with the values obtained by LL92 and L98, we first had to rescaled the latter values for the difference in the adopted solar iron abundance between us (7.51) and them (7.67 and 7.61, respectively). These revised values are listed in the last columns of Table 3.2. In general, the mean metallicities that L98 found with their complete sample (-0.30 dex and -0.74 dex for the LMC and SMC, respectively) are in very good agreement with our results (-0.33 dex and -0.75 dex). They also found a similar spread in iron for the MCs. With LL92, instead, there is a good agreement in the case of LMC but a difference for the metallicity of the SMC (0.15 dex greater than our mean value). Our derived abundances are always smaller than the values derived by LL92. However, the number of objects in common is too small to constrain the effect on a quantitative basis. When we move to a star-by-star comparison, larger differences emerge. The comparison with L98 abundances discloses a very good agreement for one object (HV 837) and a plausible agreement, i.e. within the standard deviation error, for other 3 stars (HV 5497, HV 824 and HV 834). Regrettably, this is not the case of HV 879, HV 2827 and HV 829 for which we note rather large discrepancies ($\sim 0.2 - -0.3$ dex) that remain unexplained. However, we note that L98 used different

Table 3.4: Comparison of the mean metallicities of the Magellanic Clouds with previous studies. The number of studied stars are also listed. RB89: Russell & Bessell (1989), RD92: Russell & Dopita(1992), R93: Rolleston et al. (1993), H95: Hill et al. (1995), H97: Hill (1997), K00: Korn et al. (2000), A01: Andrievsky et al. (2001), R02: Rolleston et al. (2002), G06: Grocholski et al. (2006), T07: Trundle et al. (2007), P08: Pompéia et al. (2008).

Reference	[Fe/H] _{LMC}	[Fe/H] _{SMC}	Notes
This work	-0.33±0.13	-0.75 ± 0.08	22+14 Cepheids
RB89	-0.30±0.20	-0.65 ± 0.20	8+8 F supergiants
R93	...	-0.80 ± 0.20 ^a	4 B stars
H95	-0.27±0.15	...	9 F supergiants
H97	...	-0.69 ± 0.10	6+3 K supergiants
K00	-0.40±0.20	-0.70 ± 0.20	6 B stars
A01	-0.40±0.15	...	9 F supergiants
R02	-0.31±0.04	...	5 B stars
G06	-0.3 – -2.0 ^b	...	200 giants
T07	-0.29±0.08	-0.62±0.14	13+5 cluster giants
P08	-0.3 – -1.8	...	59 red giants

^aMean metallicity based on oxygen.

^bMetallicity based on calcium triplet.

analytical codes, different oscillator strengths, and different values of the stellar gravity (they adopted the "physical" gravity calculated from the stellar mass, the luminosity and the temperature). A combination of all these three factors could well account for the observed differences. As already mentioned, larger differences (0.4 - 0.6 dex) are found with respect to LL92, for the 3 stars we have in common. For these reason we performed a more quantitative comparison for the three Cepheids in common with LL92, namely HV 865, HV 2195 and HV 2294. The calibrated spectra were kindly provided in electronic form by R.E. Luck. By adopting the same atmospheric parameters used by LL92 we find the following iron abundances: [FeI/H]= -0.75 (HV 865), -0.60 (HV 2195) and -0.15 (HV 2294). The comparison with the iron abundances provided by LL92 (see the last column in Table 3.2) indicates that the new measurements are ~ 0.3 dex systematically more metal-poor. They also agree, within the errors, reasonably well with current measurements (see column 5 in Table 3.2). Thus supporting the arguments quoted above to account for the difference between the two different iron measurements. Moreover, one should keep in mind that the quality of the LL92 data set is significantly lower than ours ($R \approx 18,000$ vs 40,000) and that their oscillator strengths may differ from our selection: they were taken from the critical compilations of Martin, Fuhr & Wiese (1988) and Fuhr, Martin & Wiese (1988), which are included in VALD but not among the references used for our gf-values. Moreover, they have used different analytical tools: MARCS model atmospheres (Gustafsson et al. 1975) and a modified version of the LINES line-analysis code and MOOG (Sneden 1973) synthesis code. They also state that their method overestimates the equivalent widths of the weak lines.

For completeness, we make a comparison different stellar populations in the Magellanic Clouds. The mean metallicities of our sample are in good agreement with previous results obtained for *F*, *K* supergiants and *B* stars in the Magellanic Clouds (see Table 3.4). Russell & Bessell (1989) found a mean [Fe/H]= -0.30 ± 0.2 dex in the LMC and [Fe/H]= -0.65 ± 0.2 dex in the SMC, analyzing high-resolution

spectra of 16 *F* supergiants (8 for each galaxy). In 1995 Hill et al. obtained, from 9 *F* supergiants from the field of the LMC, a mean iron abundance of -0.27 ± 0.15 dex and Hill (1997) found a mean $[\text{Fe}/\text{H}] = -0.69 \pm 0.1$ dex, analyzing 6 *K* supergiants in the SMC. Andrievsky et al. (2001) re-analyzed the sample of *F* LMC supergiants studied by Hill et al. (1995) and obtained a slightly lower mean value: $[\text{Fe}/\text{H}] = -0.40 \pm 0.15$ dex. Regarding the *B* type stars, Rolleston et al. (1993) and Rolleston et al. (2002) found, from the analysis of 4 stars in the SMC and 5 stars in the LMC, respectively, mean values of metallicity of -0.8 ± 0.20 dex and -0.31 ± 0.04 dex. Korn et al. (2000) obtained for the LMC (from 6 *B* stars) a mean $[\text{Fe}/\text{H}] = -0.40 \pm 0.2$ dex and $[\text{Fe}/\text{H}] = -0.70 \pm 0.2$ dex for the SMC (from 3 *B* stars). Grocholski et al. (2006) using homogeneous calcium triplet measurements for 200 stars belonging to 28 different LMC clusters covering a broad range of cluster ages, found by transforming the Ca abundance in iron abundance that the metallicity ranges from $[\text{Fe}/\text{H}] \sim -0.3$ to $[\text{Fe}/\text{H}] \sim -2.0$. More recently, Trundle et al. (2007) collected high resolution spectra with FLAMES@VLT for a good sample of Magellanic giants and found a mean metallicity of $[\text{Fe}/\text{H}] = -0.62 \pm 0.14$, 5 giants in the SMC cluster NGC 330, and of $[\text{Fe}/\text{H}] = -0.29 \pm 0.08$, 13 giants in the LMC cluster NGC 2004. By using similar data for 59 red giant stars in the LMC inner disk, Pompéia et al. (2008) found that their metallicity ranges from $[\text{Fe}/\text{H}] \sim 0.0$ to $[\text{Fe}/\text{H}] \sim -1.80$. In conclusion, the mean iron content of Cepheids, for the Magellanic Clouds, agree very well with the results obtained for non variable stars of similar age and stars that are Cepheid's progenitors. Cepheids do not show any difference with these two other populations.

 CHAPTER 4

The effect of metallicity on the PL relation

The effect of the metallicity on the Cepheid PL relation has been a matter of conjectures and debate for several years from a theoretical and an observational point of view, as we have already discussed in section 1.6.1.

Using the iron abundances that we have determined for our sample of Galactic and Magellanic Cepheids, we investigate this effect in the V and K bands. Our test in these two bands aims to verify if there is a change of the influence of the metallicity as wavelength increases, since theoretical models by Bono et al (1999) predict a smaller effect in the infrared bands than in the optical one. Our sample of stars covers a range in metallicity of about 1 dex (see section 3.1.5), allowing us to use a rather wide baseline.

We determine PL relations using all the stars with magnitudes corrected for the reddening effect (see Table 2.5 and 2.6) and with periods between 3 and 70 days. This selection in period has been done following theoretical results from Bono et al (1999) that show a linear behavior of the PL relations up to $\log P = 1.8$. Above this value (i.e. in the region of long period Cepheids) the PL relations start to bend due to the shift of the instability strip towards redder colors (see in Fig. 1.6 the shape and position of the instability strip in the HR diagram).

We then use for our study of the PL relation 61 out of 68 stars.

Figure 4.1 shows the linear regressions we have obtained for our sample of Cepheids in B , V and K bands. We can see the decrease of the intrinsic scatter from the blue band to the infrared band. We note that the short-period end of these relations (i.e. below $\log P = 0.9$) is less populated, this is due to an effect of selection in magnitude: only the brightest SMC Cepheids (i.e. with long periods) have been observed. We choose for our analysis the V and K bands, as representative of the optical and infrared ranges of wavelengths.

To investigate the effect of the iron content on the PL relations in the V and K bands we have adopted the following approach: we calculate the residuals in both bands, $\delta(M_V)$ and $\delta(M_K)$, as the difference of the absolute magnitude of our Cepheids and the absolute magnitude determined from the standard PL relations of Freedman et al (2001) and Persson et al (2004), respectively.

We have adopted these relations as point of reference because they are among the most recent observational results in the current literature and are determined from large samples of stars of the Large Magellanic Cloud, which is the first rung of the extragalactic distance ladder.

The absolute magnitudes of our Cepheids are determined from the observed magnitudes (corrected for

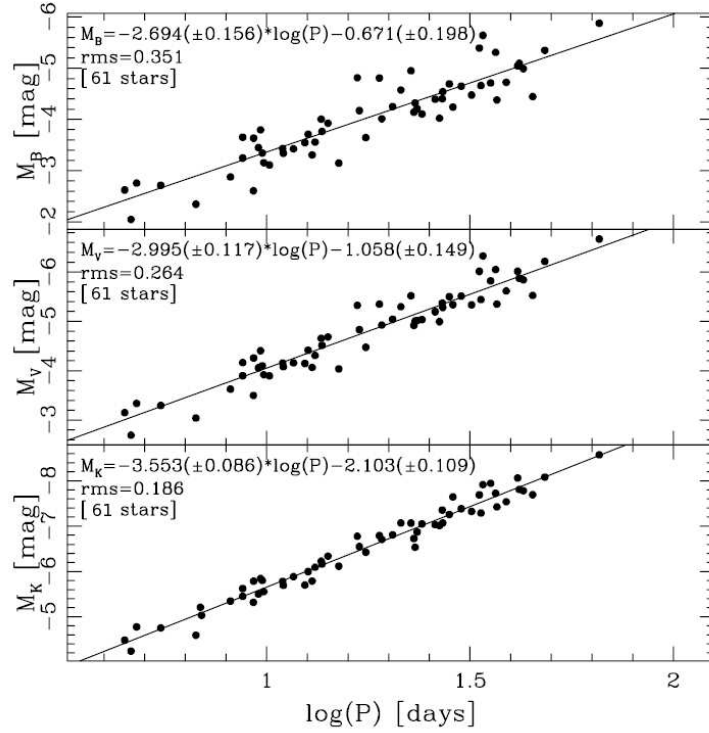


Figure 4.1: PL relations determined for our sample of Cepheids in the B, V and K bands (top, middle and bottom panel, respectively). The decrease of the intrinsic scatter with the increase of the filter can be seen.

the reddening effect) and the distance of the star, as follows:

$$M = m - \log d + 5 \quad (4.1)$$

where m is the apparent magnitude, M is the absolute magnitude and d is the distance of the star. The quantity $\mu = m - M$ is called distance modulus. The absolute magnitudes used as reference are calculated from standard PL relations mentioned above in the V and K band using the pulsational period of our programme stars. Then we study the trends of the V-band and the K-band residuals as a function of the iron abundance. $\delta(M_V)$ and $\delta(M_K)$ are, effectively, the corrections to be applied to a standard PL relation as a function of the iron content.

4.1 The adopted standard PL relations

As we have already mentioned in Chapter 1 the LMC is the first rung of the extragalactic distance ladder and its Cepheid PL relations are widely used as standard relations to determine distances or calibrate secondary distance indicators. The advantages of using this galaxy as testbed are the following:

- in this galaxy, Cepheids are bright enough for accurate photometry even with small telescopes;
- it has little depth along the line of sight (i.e. it is a fair approximation to use its distance for its Cepheids, van der Marel & Cioni 2001);

- the foreground Galactic extinction towards it is low.

Freedman et al (2001) and Persson et al (2004) have both adopted as distance modulus of the LMC the value of 18.50 mag (i.e. 50 kpc), in agreement with the most recent results about the distance of this galaxy.

The PL relation in the V band by Freedman and collaborators is:

$$M_V = -2.760[\pm 0.03] \cdot (\log P - 1) - 4.218[\pm 0.02] \quad (4.2)$$

where M_V is the absolute magnitude in the V band and P is the period, with $rms = \pm 0.16$. They have calculated it from a sample of 650 LMC Cepheids from the Optical Gravitational Lensing Experiment database (OGLE, Udalski et al 1999) with well-determined mean magnitudes in B , V and I band and periods between 2 and 32 days.

Persson and collaborators determined the PL relation in the K band from 92 LMC Cepheids, with periods between 3 and 100 days. For this sample of stars they have accurate J , H and K mean magnitudes and reddenings. Their result in the K band is :

$$M_K = -2.449[\pm 0.05] \cdot \log P - 3.281[\pm 0.04] \quad (4.3)$$

where M_K is the absolute magnitude in the K band and P is the period, with $rms = \pm 0.11$.

The infrared data obtained by Persson et al. are on the LCO (Las Campanas Observatory) photometric system¹ (Persson et al 1998) while the infrared data for our sample of Cepheids are on the SAAO (South Africa Astronomical Observatory) photometric system (Carter 1990; Carter & Meadows 1995). The K_s band in the LCO system is $0.32 \mu\text{m}$ wide and it is centered at $2.16 \mu\text{m}$, it is called short because it has a cut-off at $\sim 2.3 \mu\text{m}$ in order to reduce the noise contribution from the thermal background. Thus observation in this band are less sensitive to variation in the ambient temperature. The K band in the SAAO system is centered at $2.2 \mu\text{m}$ with a width of $0.70 \mu\text{m}$.

To avoid systematic differences we decided to transform both systems in the 2MASS (Two Micron All Sky Survey) system, since this survey provides photometry for million of galaxies and nearly a half-billion stars over the entire sky and represents an important point of reference. We utilize the following color transformations calculated by Carpenter (2001) for the LCO system:

$$(K_s)_{2MASS} = (K_s)_{LCO} + (-0.002 \pm 0.002) \cdot (J - K_s)_{LCO} - 0.010 \pm 0.004 \quad (4.4)$$

and by Koen et al. (2007) for the SAAO system:

$$(K_s)_{2MASS} = (K_s)_{SAAO} + (0.017 \pm 0.006) \cdot (J - K_s)_{SAAO} - 0.024 \pm 0.003 \quad (4.5)$$

4.2 Results

As we have already mentioned, to assess the effect of the iron content on the Cepheid PL relation we select, among our sample, only the stars with periods between 3 and 70 days (61 stars out of 68), populating, in this way, the linear part of the PL relation, i.e. the one useful for distance determinations (e.g.

¹The infrared photometric systems are less well-standardized than systems in the optical and each observatory will often define its own system which differs slightly from the others. These differences arise because the atmospheric windows, which are transparent at infrared wavelengths, are themselves different at different observatories and, in particular, vary with altitude.

Bono et al. 1999; Marconi et al. 2005).

By using the values given in the current literature (e.g. Benedict et al. 2002; Walker 2003; Borissova et al. 2004; Sollima et al. 2008; Catelan & Cortes 2008; Groenewegen et al. 2008), we adopted for the barycentre of the LMC a true distance modulus (μ_{LMC}) of 18.50 mag (with an error of ± 0.10). This is also consistent with the standard PL relations (Freedman et al. 2001; Persson et al. 2004) used as comparison. The SMC is considered 0.44 ± 0.10 mag more distant than the LMC (e.g. Cioni et al. 2000; Bono et al. 2008). This value of the relative distance between the two galaxies has confirmed the results of previous studies (Westerlund 1997, and references therein). For all the Galactic Cepheids we have individual distances, as mentioned in section 2.2.1

It is necessary to divide our Cepheid sample into bins of metallicity to investigate its effect on the PL relation. The number of bins needs to be chosen taking into account two competing effects. On the one hand, dividing the stars in more bins in principle allows to disentangle finer details. On the other, however, each bin needs to contain enough stars so that the instability strip is well populated and, hence, spurious sampling effects are negligible. We choose two bins with about 30 stars each as best compromise between a detailed investigation and statistical significance. This choice is justified by the simulations described in the next section.

Our results for the V and K bands are presented in Figures 4.2 and 4.3, respectively. In the top panels are shown the PL relations in each metallicity bin calculated with a linear regression. In each panel are also indicated the average iron content of the bin, the root mean square of the linear regression and the number of stars. The bottom panels of Figures 4.2 and 4.3 show the magnitude residuals $\delta(M)$ in the V and K band, respectively, as a function of $[Fe/H]$. These magnitude residuals are calculated as the difference between the observed absolute magnitude and the absolute magnitude as determined from its period using a standard PL relation, namely the PL_V from Freedman et al. (2001) and the PL_K from Persson et al. (2004). In practice, $\delta(M)$ is the correction to be applied to a universal, $[Fe/H]$ -independent PL relation to take into account the effects of metallicity. A positive δ means that the actual luminosity of a Cepheid is fainter than the one obtained with the standard PL relation. The filled squares in the bottom panels of Figures 4.2 and 4.3 represent the mean values of $\delta(M)$ in each metallicity bin, the vertical error-bars are the errors on the mean and the solid line is the null value, which corresponds to an independence of the PL relation on the iron content. The horizontal bars indicate the size of the metallicity bins.

Data plotted in the bottom right panel of Fig. 4.2 indicate that the magnitude residuals of the V band in the individual bins are positive and located at $\approx 2\sigma$ (metal-poor) and $\approx 9\sigma$ (metal-rich) from zero. Moreover, the $\delta(M_V)$ in the two bins differ from each other at the 3σ level. Our data, then, suggest that metal-rich Cepheids in the V band are, at a fixed period, fainter than metal-poor ones. Data plotted in the bottom left panel indicate that this finding is marginally affected by uncertainties in the Galactic Cepheid distance scale. The use of Cepheid distances provided by Groenewegen (2008) provides a very similar trend concerning the metallicity effect. Moreover, the magnitude residuals based on the "Old Sample" are located $\approx 1.5\sigma$ (metal-poor) and $\approx 4\sigma$ (metal-rich) from zero and the difference in the two bins is larger than one σ .

The results for the K band are displayed in Fig. 4.3.

The near-infrared data are on different photometric systems, therefore, we transformed them into the 2MASS (Two Micron All Sky Survey) photometric system. In particular, the apparent K magnitudes were transformed using the transformation provided by Koen et al. (2007, see eq. 4.5), while the PL_K relation by Persson was transformed using the transformation provided by Carpenter (2001, see eq. 4.4). The correction are typically of the order of ~ 0.02 mag. Data plotted in the bottom right panel of Fig. 4.3 indicate that the metal-poor bin is within 1σ consistent with zero. On the other hand, the metal-rich bin differs from the null hypothesis by $\approx 4\sigma$. Moreover, the magnitude residuals in the two metallicity bins differ by $\approx 2\sigma$. This finding is at odds with current empirical (Persson et al. 2004; Fouqué et al. 2007) and theoretical (Bono et al. 1999, 2008; Marconi et al. 2005) evidence suggesting that the PL_K relation

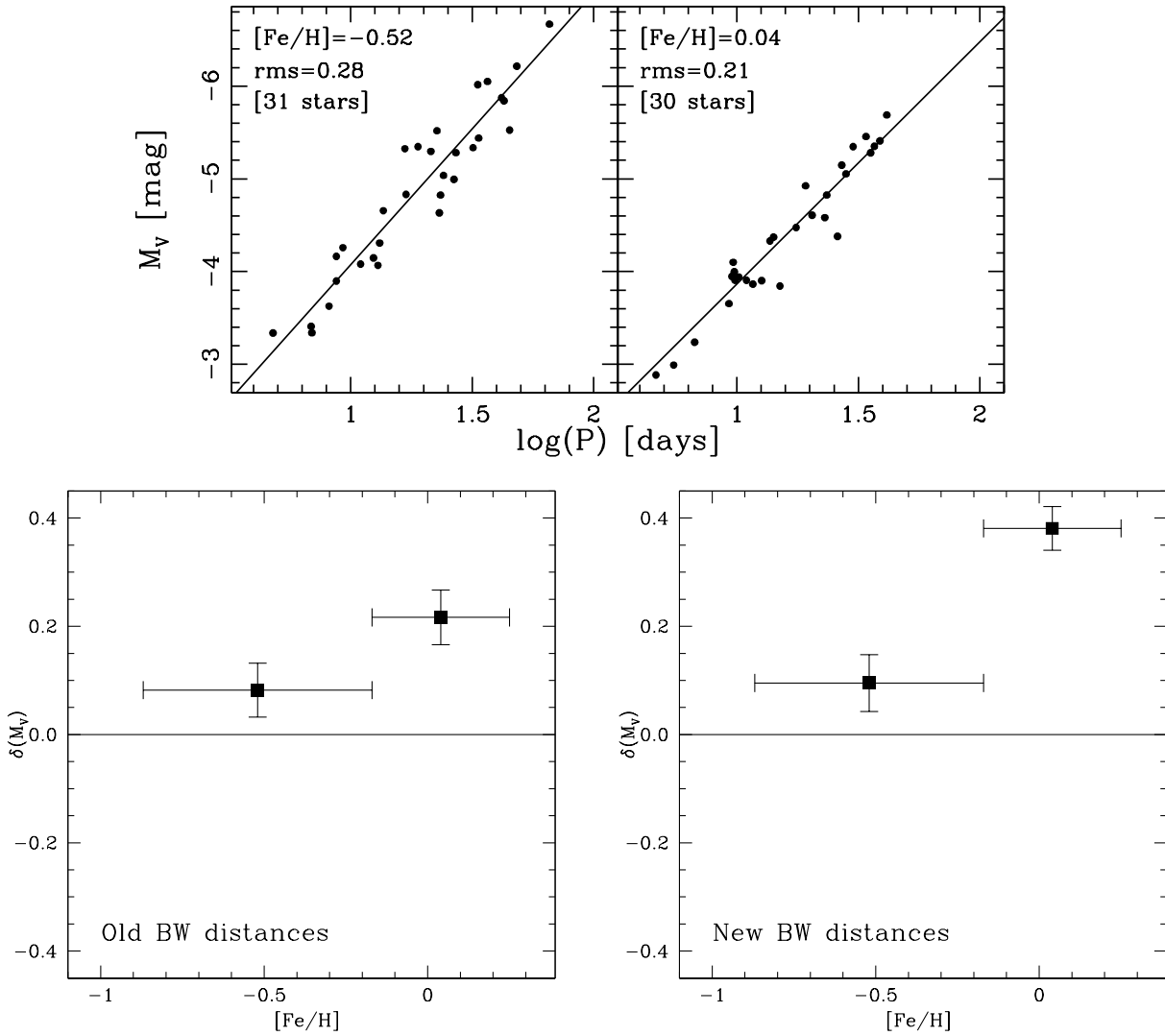


Figure 4.2: The top panels show the PL relations calculated in each bin for the V band. The bottom panels show the residuals $\delta(M_V)$ as a function of the iron abundance for both the "Old" and the "New" Galactic Cepheid distances. The mean values of $\delta(M_V)$ in each metallicity bin are plotted as filled squares, with the vertical error-bars representing its associated errors. The horizontal bars indicate the dimension of the bins. The horizontal solid lines indicate the null value which corresponds to an independence of the PL relation from the iron content.

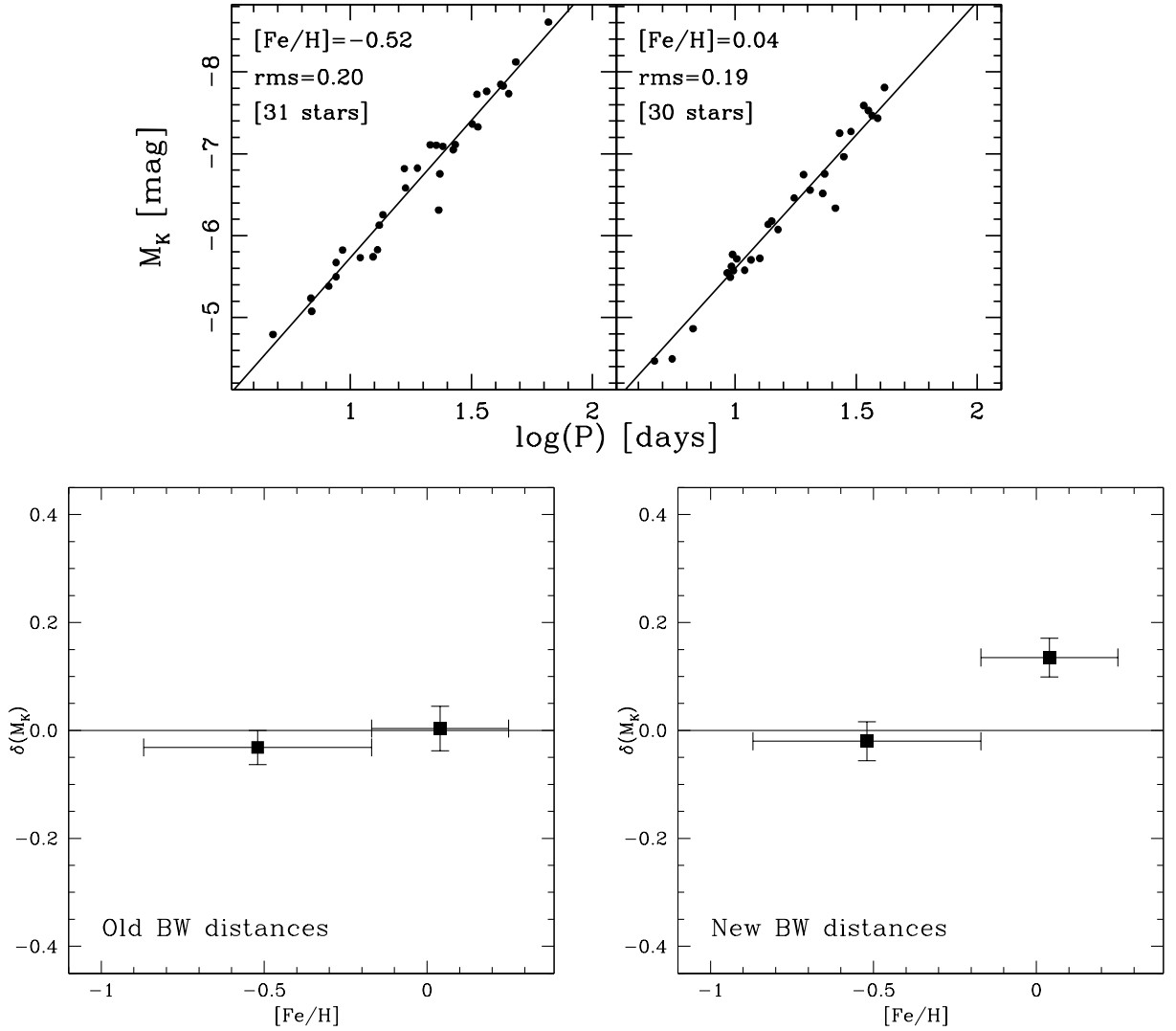


Figure 4.3: The top panels show the PL relations calculated in each bin for the K band. The bottom panels show the residuals $\delta(M_K)$ as a function of the iron abundance for both the "Old" and the "New" Galactic Cepheid distances. The mean values of $\delta(M_K)$ in each metallicity bin are plotted as filled squares, with the vertical error-bars representing its associated errors. The horizontal bars indicate the dimension of the bins. The horizontal solid lines indicate the null value which corresponds to an independence of the PL relation from the iron content.

is marginally affected by metal abundance. In order to constrain this effect we also adopted the "Old Sample" distances. The magnitude residuals plotted in the bottom left panel of Fig. 4.3 show that the two metallicity bins are, within the errors, consistent with no metallicity effect. Unfortunately, current error budget (distance, metal abundance) does not allow us to reach firm conclusions concerning the metallicity dependence of the PL_K relation.

4.3 Uncertainties

The error on the residuals showed in Fig. 4.2 and Fig. 4.3 is characteristic of the particular sample of stars we have used. In this section we describe the simulations we have performed in order to assess the impact of different samplings of the PL relation.

In order to do so, we have extracted random subsamples composed by different numbers of stars from a sample of observed Cepheid that populate well the PL relation. We choose as reference a sample of 771 LMC Cepheids from the OGLE database (Udalski et al. 1999) for the test in the V -band and the sample of 92 LMC Cepheids (Persson et al. 2004) for the test in the K -band. The latter is the largest observed sample of Cepheids in the near-infrared bands. For each extraction a linear regression was performed to derive the slope and the zero point of the resulting PL relation. Also, we calculated the magnitude residuals $\delta(M_V)$ and $\delta(M_K)$ as defined above for the actual observed programme stars. We have, then, compared these quantities with those derived for the whole sample in order to estimate the error due to random sampling and to optimize the number of bins we can divide our sample into. It is worth noticing here that this procedure will somewhat *overestimate* the sampling error. This is because some of the random extractions will generate a subsample that covers a small range of periods, while we have carefully selected our sample in order to cover a broad period range.

After performing 1 million extractions in each of the bands, V and K , for several bin sizes, we have settled for two metallicity bins of about 30 stars each. With this choice, $\delta(M_V)$ results to being less than 0.1 mag in 95% of the cases and never larger than 0.15. The mean value of the distribution is 0.03 mag. These results imply that the non-zero result for the high metallicity bin in Figure 4.2 cannot be due to insufficient sampling of the PL relation.

As for the K band, the simulations indicate that $\delta(M_K)$ is smaller than 0.04 mag in 95% of the cases and never larger than 0.06 mag, with a mean of 0.01 mag. Also in this case, then, the results discussed above and displayed in Figure 4.3 are not significantly affected by sampling errors.

4.4 Comparison with previous results

We compare our results with two different behaviors (see Fig. 4.4) as examples of the effects of the metallicity on the PL relation currently available in the literature: independence from the iron content and a monotonic decreasing trend (e.g. Kennicutt et al. 1998; Sakai et al. 2004; Storm et al. 2004; Groenewegen et al. 2004; Macri et al. 2006; Sandage & Tammann 2008), in the sense that metal-rich Cepheids are brighter than metal-poor ones.

We use for the comparison the classical results of Kennicutt et al. (1998) adopted by the HST Key Project to determine extragalactic distances with Cepheids (Freedman et al. 2001). They have analyzed two Cepheid fields in M101, with average values of metallicity around -0.4 dex and 0.28 dex (determined from measurements of oxygen in HII regions in the two fields). They have observed 29 Cepheids in the

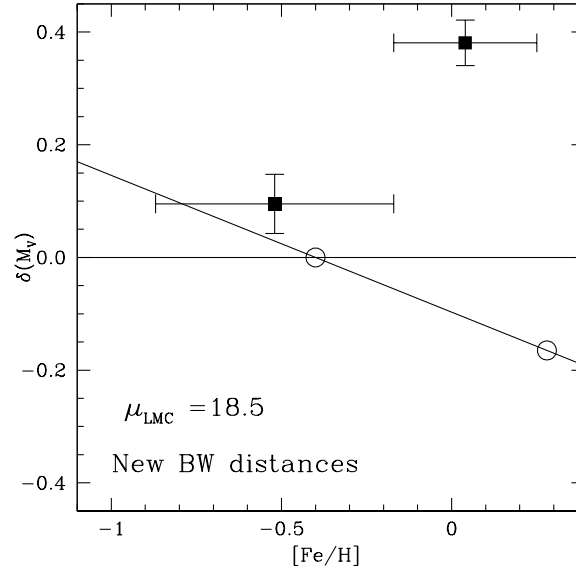


Figure 4.4: The V-band residuals compared to Freedman et al. (2001) PL relation are plotted against the iron content measured from observed spectra (bottom right panel in Fig. 5.2). The filled squares display the mean value in each metallicity bin, with its associated errorbar. The metallicity dependence estimated by Kennicutt et al. (1998) using two Cepheid fields in M101 (open circles) is shown as a full line.

outer field (low metallicity) and 61 Cepheids in the inner field (high metallicity) with periods between 10 and 60 days. Considering the outcome of our simulations, the two Cepheid samples observed by Kennicutt and collaborators are comparable to our sub-samples in each bin, it is then reasonable to compare the qualitative indications about the effect of the metallicity that can be derived from the two analyses. The complete comparison is possible only in the V-band.

As we have already mentioned the error due to the sampling of the PL relation is much smaller than the one on the residuals. Data plotted in Figures 4.2, 4.3 and 4.4 disclose several circumstantial evidence. This means that the increasing trend of the latter in the V-band, as a function of the iron content, is real with a confidence level of 99%.

i) V-band case

- *No dependence of $\delta(M_V)$ on $[Fe/H]$* : A null effect on the metal abundance (solid line in fig. 4.4) would imply that the residuals of the two bins should be located, within the errors, along the independence line. Current findings and the outcome of the simulations mentioned in the previous section, indicate that this hypothesis can be excluded completely. The increasing trend of the residual in the V-band, as a function of the iron content, is real with a confidence level larger than 95%.
- *Monotonically decreasing $\delta(M_V)$* : we compare the classical results of Kennicutt et al. (1998, open circles in Fig. 4.4) with our data. Since the increasing trend of our residuals is real, this hypothesis is incompatible with our results. In passing, we also note that the reddening estimates adopted by Kennicutt et al. (1998) are based on the observed mean colors. However, metal-poor Cepheids are, at fixed period, hotter than metal-rich ones. Therefore, Kennicutt et al. would have underestimated the reddenings and the luminosities of his metal-poor sample, producing an

apparent under-luminosity for metal-poor Cepheids.

ii) *K*-band case

- Current data do not allow us to reach a firm conclusion concerning the metallicity effect.

To summarize, we found an increasing trend of the *V*-band residuals with the iron content. This result is in disagreement with an independence of the PL relation on iron abundance and with the linearly decreasing trend found by other observational studies in the literature (e.g. Kennicutt et al. 1998).

4.5 LMC distances: "short" vs "long" scale

Regrettably we can find in the recent literature values of the LMC distance modulus ranging from 18.1 to 18.8, not always obtained with different techniques. Those studies finding a distance modulus less than 18.5 support the so-called "short" distance scale, whereas those finding it greater than 18.5 support the "long" distance scale (for a review of the results and methods see Benedict et al. 2002; Gibson 2000). More recently, Schaefer (2008) found that distance estimates to the LMC published before 2001 present a large spread ($18.1 \leq \mu \leq 18.8$). On the other hand, distances published after 2002 tightly concentrate around the value adopted by the HST Key Projects ($\mu = 18.5$, Freedman et al. 2001; Saha et al. 2006). In order to overcome this suspicious bias, we decided to investigate the different behavior of the PL relation depending on the adopted LMC distance scale. In order to do that, we have repeated our calculation of the *V*-band residuals assuming a distance modulus for LMC of 18.3 (representative of the "short" scale) and of 18.7 (for the "long" scale). The results are shown in Fig. 4.5. In the left and right panel, the *V*-band residuals refer to the "short" and the "long" distance scale, respectively. For μ_{LMC} of 18.3, the *V*-band residuals are located at least at 5σ from zero. The difference between the metal-poor and the metal-rich bin is of the order of one σ . This trend is similar to the trend we obtained using $\mu_{LMC}=18.5$, however, the distance from zero of the metal-poor bin is significantly larger. This result disagrees with an independence of the PL relation on the iron abundance and the monotonic decreasing behavior at the 99.99 % level (according to the χ^2 method). On the other hand, the $\delta(M_V)$ values for μ_{LMC} of 18.7 are located at ≈ 2 (metal-poor) and ~ 8 (metal-rich) σ from zero. The difference between the two bins is at least at 4σ level. The data trend is slightly steeper than for $\mu_{LMC}=18.5$. Using again a χ^2 technique, we find that this result disagrees with an independence of the PL relation on iron abundance and with the linearly decreasing trend often quoted in the literature (e.g. Kennicutt et al. 1998).

The results based on the tests performed assuming different LMC distances are the following:

- **Short scale** - Data plotted in the left panel of Fig. 4.5 indicate that *V*-band PL relation does depend on the metal content. Indeed, the two bins are located at least at 5σ from zero. This means that the zero-point of the quoted PL relations does depend on the metal abundance. However, the difference between the two bins is small and of the order of one σ . This indicates that the metallicity effect supported by the short scale is mainly caused by a difference in the zero-point. This result would imply a significant difference in the zero-point of Magellanic Cepheids. However, such a difference is not supported by current empirical (Laney & Stobie 1994; van Leeuwen et al. 2007; Fouqué et al. 2007; Sandage & Tammann 2008) and theoretical evidence.

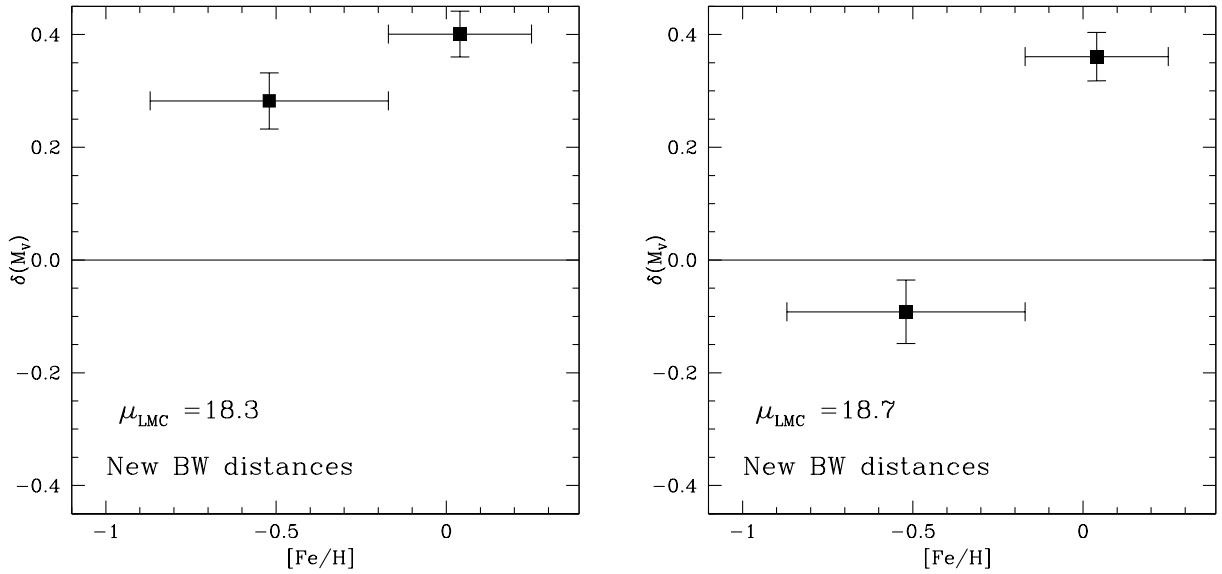


Figure 4.5: The V-band residuals compared to the Freedman et al. (2001) PL relation versus the iron content measured from observed spectra, assuming an LMC distance modulus of 18.3 (left) and of 18.7 (right). The filled squares represent the mean value in each metallicity bin, with its associated errorbar.

- **Long scale** - Data plotted in the right panel of Fig. 4.5 indicates that V-band PL relation does depend on the metal content. The difference from zero ranges from ~ 2 for the metal-poor bin to more than 8σ for the metal-rich bin. Moreover, the two bins differ at 4.5σ level. This means that the metallicity effect supported by the long scale is mainly caused by a difference in the slope. This finding, taken at face value, would imply that metal-poor Cepheids (e.g. Cepheids in IC 1613, $-1.3 \leq [Fe/H] \leq -0.7$, Skillman et al. 2003) should be, at fixed period, ≈ 0.5 (V) mag brighter than Galactic Cepheids. This difference is not supported by current empirical (Dolphin et al. 2003; Antonello et al. 2006; Pietrzynski et al. 2006; Saha et al. 2006; Fouqué et al. 2007) and theoretical evidence.

The quoted results suggest that the V-band PL relation is affected by metal abundance. This finding is marginally affected by the adopted LMC distance. It is worth mentioning that recent empirical estimates based on robust primary standard candles indicate that the true LMC distance is 18.5 ± 0.1 (Alves 2004; Benedict et al. 2007; van Leeuwen et al. 2007; Catelan & Cortes 2008; Feast et al. 2008; Groenewegen et al. 2008; Sollima et al. 2008). In view of this convergence on the LMC distance and on the results based on the "short" and on the "long" distance scale, the results based on $\mu_{LMC} = 18.5$ appear to be the most reliable ones.

4.6 Conclusions

We have directly measured the iron abundances for 68 Galactic and Magellanic Cepheids from FEROS and UVES high resolution and high signal-to-noise spectra. We have used these measurements to assess the influence of the stellar iron content on the Cepheid PL relation in the V and in the K band. In order to do this we have related the V -band and the K -band residuals from the standard PL relations of Freedman et al. (2001) and Persson et al. (2004), respectively, to $[\text{Fe}/\text{H}]$. Differently from previous studies, we can constrain the PL relation using Cepheids with known distance moduli and chemical abundances, homogeneously measured, that cover almost a factor of ten in metallicity.

Our results includes:

- **Galactic sample:** we find that the mean value of the iron content is solar ($\sigma = 0.10$, see Fig. 3.8), with a range of values between -0.18 dex and $+0.25$ dex;
- **LMC sample:** we find that the mean value is about ~ -0.33 dex ($\sigma = 0.13$, see Fig. 3.8), with a range of values between -0.62 dex and -0.10 dex.
- **SMC sample:** we find that the mean value is about ~ -0.75 dex ($\sigma = 0.08$, see Fig. 3.8), with a range of values between -0.87 and -0.63 .

We have compared our results with the analyses of FC97, Andrievsky et al. (2002a, 2002b, 2002c) and Luck et al. (2003) for the Galactic Cepheids and LL92 and L98 for the Magellanic Clouds. Regarding the Galactic sample, our results are marginally more in agreement with Andrievsky's values than with FC97 and the differences, on average, appear rather small. Considering the Magellanic Cepheids, we have a poor agreement with LL92, which could be in part accounted for by different analytical tools and data quality. Our data are in better agreement with L98 results and the spread of our iron abundances in the LMC and SMC is similar to the one they reported. We note that the mean metallicity that they found with their complete sample (-0.30 dex and -0.74 dex) is in very good agreement with our results.

Our main results concerning the effect of the iron abundance on the PL relation are summarized in Fig. 4.2 and Fig. 4.3 (bottom panels) and they hold for a LMC distance modulus of 18.50. In Fig. 4.4 is also showed the comparison in the V -band with the empirical results of Kennicutt et al. (1998) in two Cepheid fields of M101 (open circles and solid line). The main findings can be summarized as follows:

- The V -band PL relation does depend on the metal abundance. This finding is marginally affected by the adopted distance scale for the Galactic Cepheids and by the LMC distance.
- Current data do not allow us to reach a firm conclusion concerning the dependence of the K -band PL relation on the metal content. The use of the most recent distances for Galactic Cepheids (Benedict et al. 2007; Fouqu e et al. 2007; van Leeuwen et al. 2007) indicates a mild metallicity effect. On the other hand, the use of the old distances (Storm et al. 2004) suggest a vanishing effect.
- Residuals based on a canonical LMC distance ($\mu_{LMC} = 18.5$) and on the most recent distances for Galactic Cepheids present a well defined effect in the V -band. The metal-poor and the metal-rich bin are $\approx 2\sigma$ and $\approx 9\sigma$ from the null hypothesis. Moreover, the two metallicity bins differ at the 3σ level.

- By assuming a "short" LMC distance ($\mu_{LMC} = 18.3$) the residuals present a strong metallicity dependency in the zero-point of the V -band PL relation. By assuming a "long" LMC distance ($\mu_{LMC} = 18.7$) we found a strong metallicity effect when moving from metal-poor to metal-rich Cepheids. This indicates a significant change in the slope and probably in the zero-point. The findings based on the "short" and on the "long" LMC distance are at odds with current empirical and theoretical evidence, suggesting a smaller metallicity effect.
- Metal-rich Cepheids in the V -band are systematically fainter than metal-poor ones. This evidence is strongly supported by the canonical, the "short" and the "long" LMC distance.

The above results together with recent robust LMC distance estimates indicate that the behaviors based on the canonical distance appear to be the most reliable ones.

In order to constrain on a more quantitative basis the metallicity dependence of both zero-point and slope of the optical PL relations is required a larger number of Cepheids covering a broader range in metal abundances. Moreover, for each metallicity bin Cepheids covering a broad period range are required to reduce the error on the residuals and to constrain on a quantitative basis the fine structure of the PL relation in optical and NIR photometric bands.

 CHAPTER **5**

Baade-Wesselink method

As we have already mentioned, we used the Baade-Wesselink (BW) method to measure the distances of our targets. The version that we apply is explained in Groenewegen et al. 2007 (G07). The two main ingredients to apply this technique are radial velocities and color index, namely $V - K$. In the following sections, we briefly repeated the fundamental points of the model, we explained the methodology used to obtain radial velocities and color index and we presented our results.

5.1 The model

The V -, K - and RV data with error bars are fitted with a function of the form:

$$F(t) = F_0 + \sum_{i=1}^{i=N} (A_i \sin(2\pi t e^{if}) + B_i \cos(2\pi t e^{if})) \quad (5.1)$$

where $P = e^{-f}$ is the period (in days). Typically, P is determined from the fit to the available optical photometry as this dataset is usually most extensive. The period is then fixed when fitting Eq. 5.1 to the K -band and RV data.

The determination of the parameters is done using the *MRQMIN* routine (using the Levenberg-Marquardt method) from Press et al. (1992) written in Fortran77, which minimizes

$$\chi^2 = \sum_{i=1}^{i=n} (F_i - F(t_i))^2 / (\sigma_{F_i})^2, \quad (5.2)$$

with F_i the measurement at time t_i which has an error bar σ_{F_i} .

Also the reduced χ^2 is defined:

$$\chi_r^2 = \frac{\chi^2}{(n - p)} \quad (5.3)$$

and the quantity

$$BIC = \chi^2 + (p + 1) \ln(n), \quad (5.4)$$

where $p = 2N + 2$ is the number of free parameters ($p = 2N + 1$ when fitting the RV and K light curve). As the number N of harmonics to be fitted to the data is a priori not known, one could obtain ever better fits (lower χ^2) by increasing N . The Bayesian information criterion (Schwarz 1978) is a formalism that penalizes this, and N (for the V , K and RV curve independently) is chosen such that BIC reaches a minimum. The number of harmonics used varies between 3 and 10 in the optical, 1 and 5 in the NIR , and 2 and 9 for the RV curves.

Given the analytical form of Eq. 5.1, the radial velocity curve can be integrated exactly to obtain the variation in radius as a function of time (phase):

$$\Delta(t, \delta\Theta) = -p \int_{t_0}^{t + P\delta\Theta} (v_R - \gamma) dt \quad (5.5)$$

where γ is the systemic velocity, v_R the radial velocity, p the projection factor and $\delta\Theta$ allows for a phase shift between the RV curve and the angular diameter variations determined via the SB relation. Then, the equation

$$\Theta(t) = 9.3038 \text{ mas} \left(\frac{R_0 + \Delta R(t, \delta\Theta)}{d} \right) \quad (5.6)$$

is fitted with Θ the angular diameter in mas, R_0 the stars radius in solar radii and d the distance in pc. The fitting is done using the linear bi-sector (using the code *SIXLIN* from Isobe et al. 1990) as used and preferred by e.g. Storm et al. (2004), Barnes et al. (2005) and Gieren et al. (2005). In some cases a phase range around 0.85-0.95 was excluded from the fit.

In G07 the p-factor was determined chiefly using six Cepheids with interferometrically measured angular diameter variations and HST based accurate parallaxes (Benedict et al. 2007). It was concluded that, formally, there was no need for a period-dependent p-factor, and $p = 1.27 \pm 0.05$ fitted the available data. On the other hand, a moderate dependence of $p \sim -0.03 \log P$ as used in the Gieren et al. papers (1993, 1997, 1998; Storm et al. 2004; Barnes et al. 2003), or $p \sim -0.064 \log P$ as advocated by Nardetto et al. (2007) are also consistent with the available data.

The Nardetto et al. (2007) theoretical investigation suggest that there is a difference between the p-factor to be used with wide-band interferometry (like in G07) and with RV data (when applying the SB technique as in the present study). In our case, we considered the G07 value for the p-factor: $p = 1.33$. An SB relation can be defined as follows (see van Belle 1999):

$$\Theta_0 = \Theta \times 10^{m_1/5}, \quad (5.7)$$

where Θ is the LD angular diameter (in mas), and m_1 a dereddened magnitude (for example, V_0). The logarithm of this quantity (the zero magnitude angular diameter) is plotted against a de-reddened color (for example, $(V - K)_0$):

$$\log \Theta_0 = a \times (m_2 - m_3) + b. \quad (5.8)$$

The distances and radii obtained applying this method are presented in the next sections.

5.2 Radial velocities

To estimate the distances of our four Cepheids, we need, first of all, radial velocity measurements. We provide two sets of radial velocities. The first one has been obtained using *fitline* (see section 3.1.4) i.e. by cross-correlation between the lines of each spectra and the line list that we assembled (see section 3.1.1 and Table B.1 in Appendix B). The second set has been measured again by cross-correlation but using the best S/N spectra as reference. We have to note that in this case we obtained the RVs normalized to the reference spectrum. In figure 5.1 we show the radial velocity curves of our targets. On the left panel we plotted the radial velocity curves performed by *fitline*. The red stars on this plot, indicate the two more spectra with highest S/N (~ 150) that we add to obtain a satisfactory precision in the determination

Table 5.1: Distances and radii from the BW-analysis for program Cepheids. The errors listed take into account the errors in the fit and the errors quoted basing on a Monte Carlo simulation where new datasets are generated based on the error bar in each individual V , K , RV measurement.

Name	$d(\text{pc})$	$\Delta d(\text{pc})$	R_0/R_\odot	$\Delta(R_0/R_\odot)$	$d(\text{pc})_{\text{And}}$
V340 Ara	4063	129	106.2	3.4	4321
AV Sgr	2345	84	95.8	3.4	2250
UZ Sct	3268	104	82.5	2.6	2867
VY Sgr	2617	49	89.6	1.7	2187

of iron content. On the right panel of the same figure, we show the radial velocities obtained by cross-correlation with one of the spectra as reference. Figures from 5.2 to 5.5 illustrate the main ingredients to apply this technique. The upper panels show the optical and near infrared bands light curves while the lower panels plot radial velocity curves. V , K , and RV curve as a function of phase for our program stars. Figures from 5.6 to 5.9 show the variation of the angular diameter against phase (lower panels) and the change in angular diameter derived from the Surface-Brightness relation against the change in radius (upper panels) from integration of the RV curve from which the distance is derived (see Eq. (5.6)). The absolute magnitudes have been derived in a self-consistent way from the Fourier fit to the data.

5.3 Distances

Table 5.1 lists the distances and radii obtained and the comparison with previous estimates. For the distance and radius, the errors listed (columns 3 and 5 of table 5.1) take into account the errors in the fit and the errors quoted basing on a Monte Carlo simulation where new datasets are generated based on the error bar in each individual V , K , RV measurement. This errors quoted are the one σ dispersion in the derived quantities. In the last column of this table we reported the most recent estimates of the distance of our Cepheids (Andrievsky et al. 2002b). We note that Andrievsky and collaborators used a different method to estimate the distances. They derived the heliocentric distance d as:

$$d = 10^{-0.2 \cdot (M_V - \langle V \rangle - 5 + A_V)} \quad (5.9)$$

where they estimated the absolute magnitude (M_V) of program Cepheids from the "absolute magnitude - pulsational period" relation of Gieren et al. (1998). $E(B-V)$, $\langle B - V \rangle$, mean visual magnitudes and pulsational periods were from Fernie et al. (1995) and they used for A_V an expression from Laney & Stobie (1993):

$$A_V = [3.07 + 0.28 \cdot (B - V)_0 + 0.04 \cdot E(B - V)] \cdot E(B - V) \quad (5.10)$$

Taking into account the differences between our and Andrievsky approach to determine the distances, we can conclude that our results agree quite well with their values. Moreover, using the Baade-Wesselink method we obtained an accuracy on distance estimates of 3%.

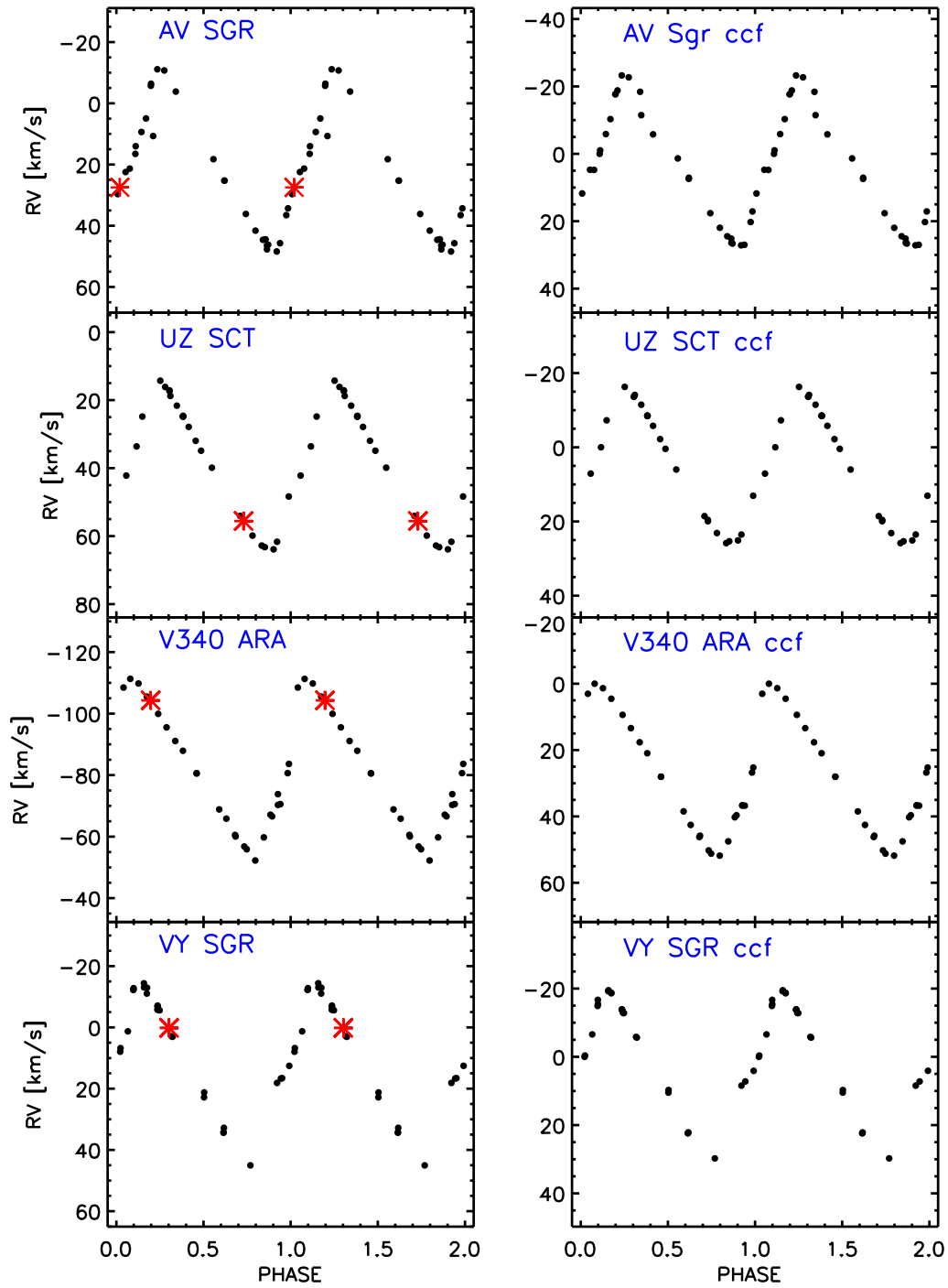


Figure 5.1: The radial velocity curves for our program Cepheids. Left Panel: Radial velocity curves obtained by cross-correlation with the line list (FITLINE). The red stars indicate the spectra used to measure the metallicity which have the best S/N (~ 150). Right Panel: Radial velocity curves obtained by cross-correlation between spectra.

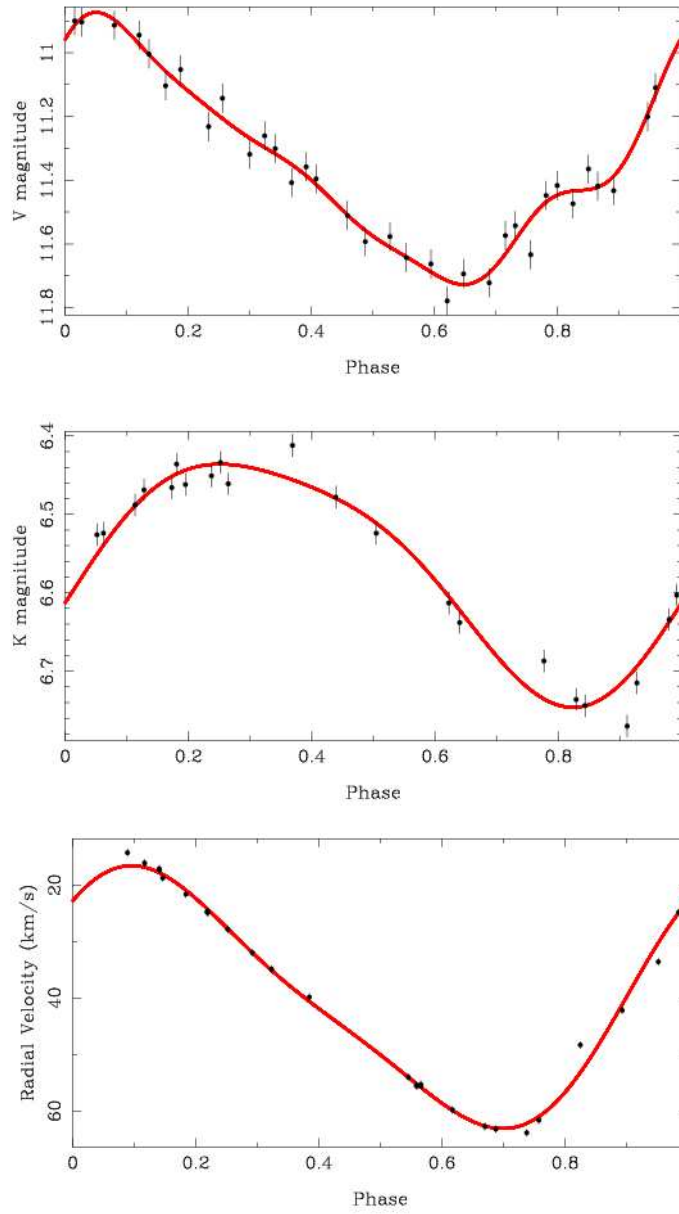


Figure 5.2: The phased curves in V, K and RV are shown for UZ Sct. Data points are shown with errors bars and the line shows the harmonic fit.

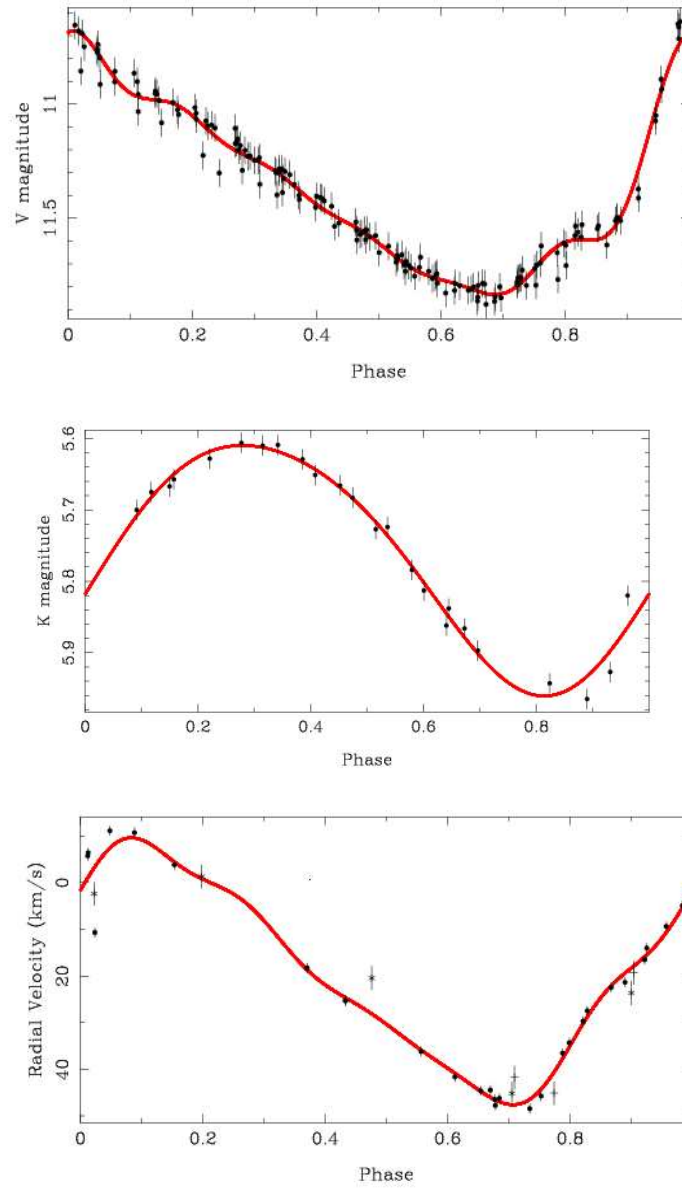


Figure 5.3: The phased curves in V, K and RV are shown for AV Sgr. Data points are shown with errors bars and the line shows the harmonic fit.

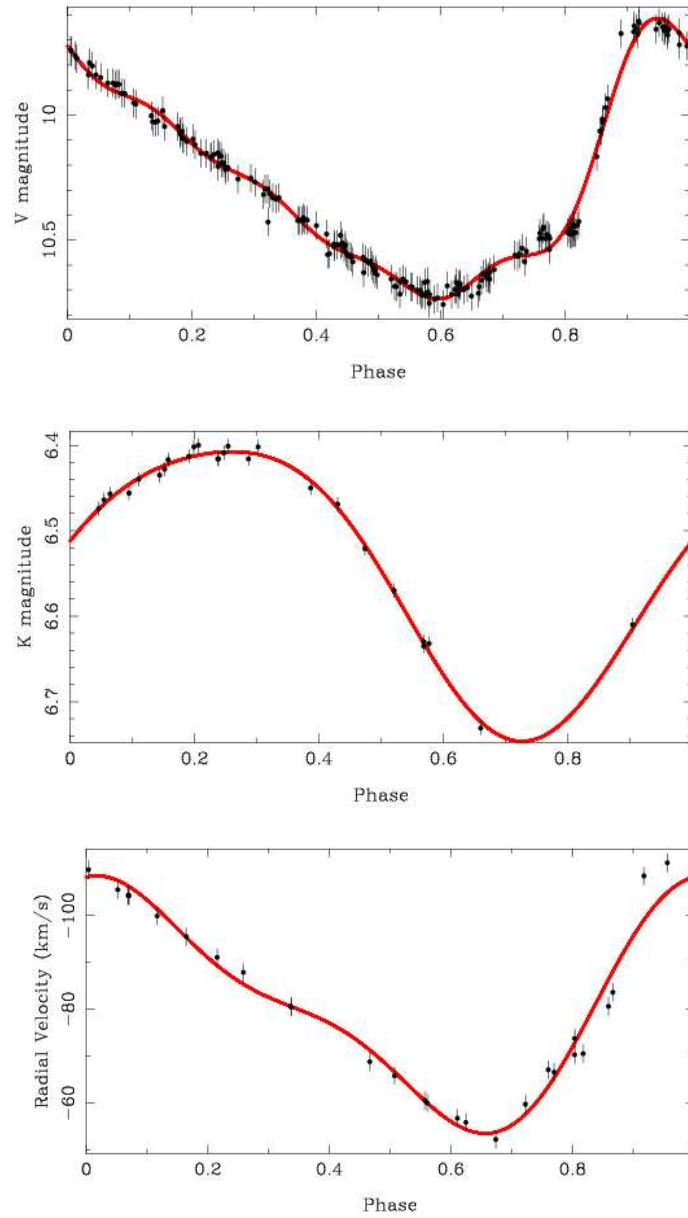


Figure 5.4: The phased curves in V, K and RV are shown for V340 Ara. Data points are shown with errors bars and the line shows the harmonic fit.

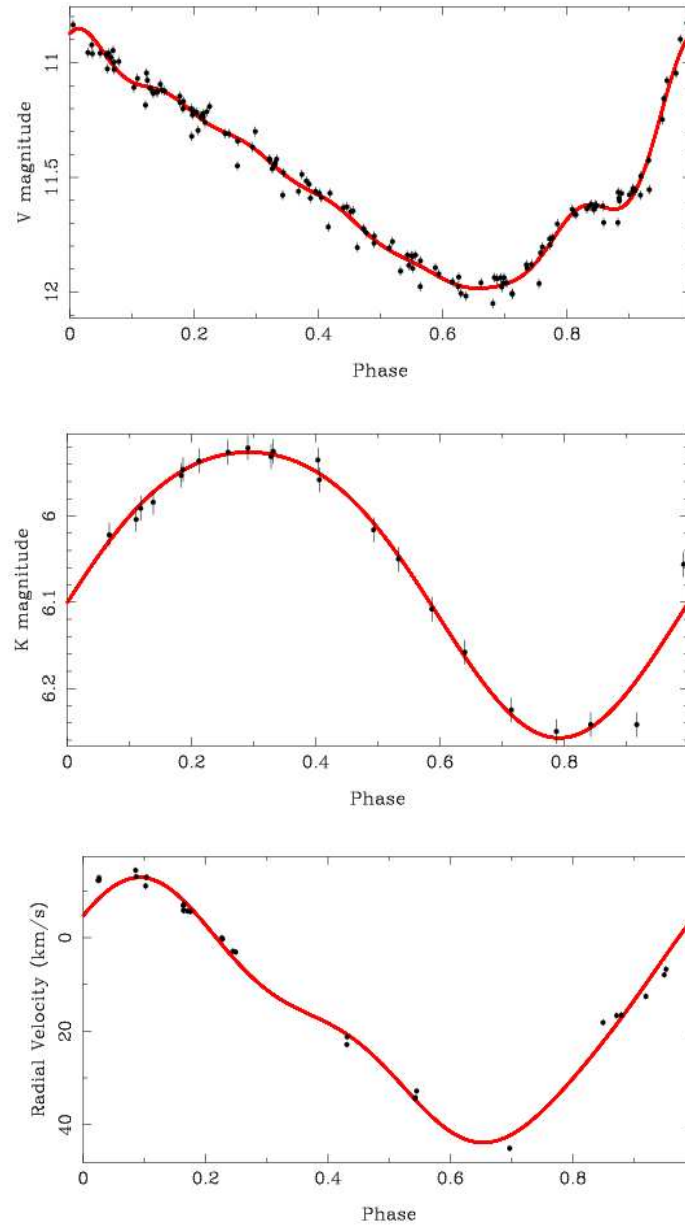


Figure 5.5: The phased curves in V, K and RV are shown for VY Sgr. Data points are shown with errors bars and the line shows the harmonic fit.

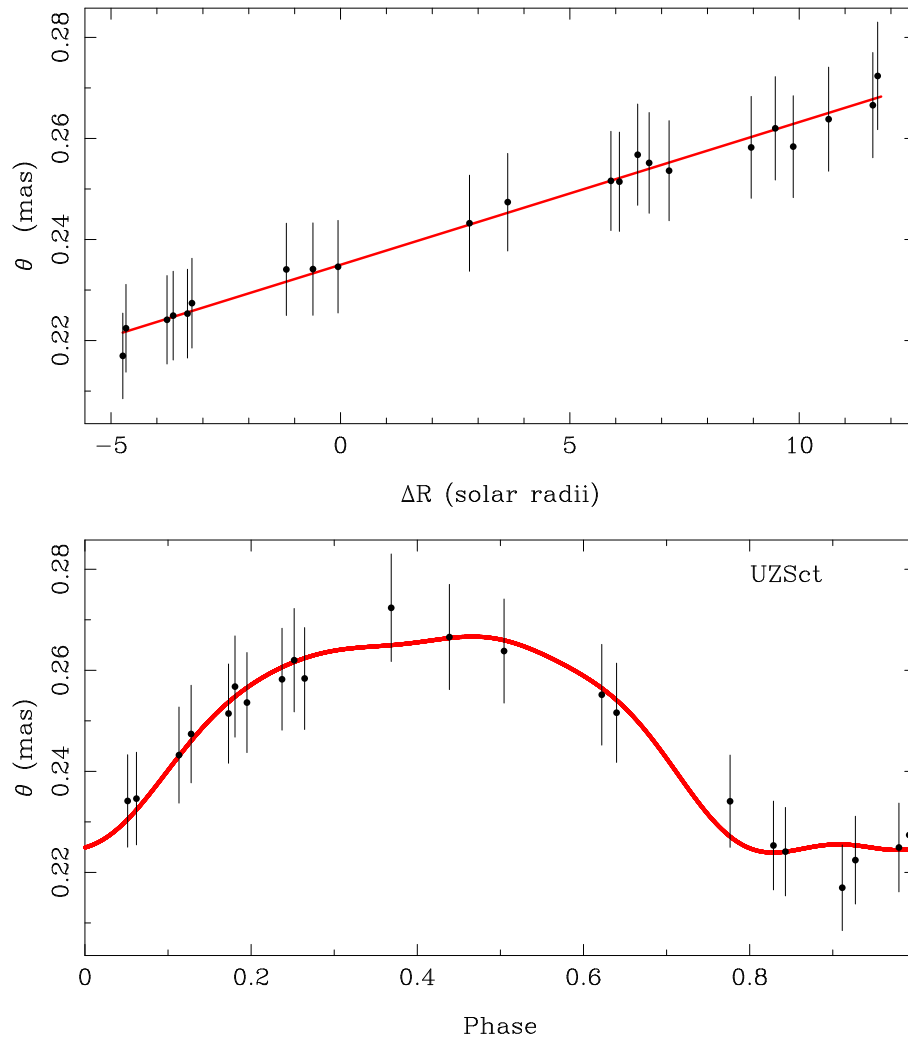


Figure 5.6: For UZ Sct, the top panel shows the linear-bisector fit to the angular diameter as a function of radial displacement. The bottom panel shows the angular diameter against phase. Crosses represent data-points not considered in the fit.

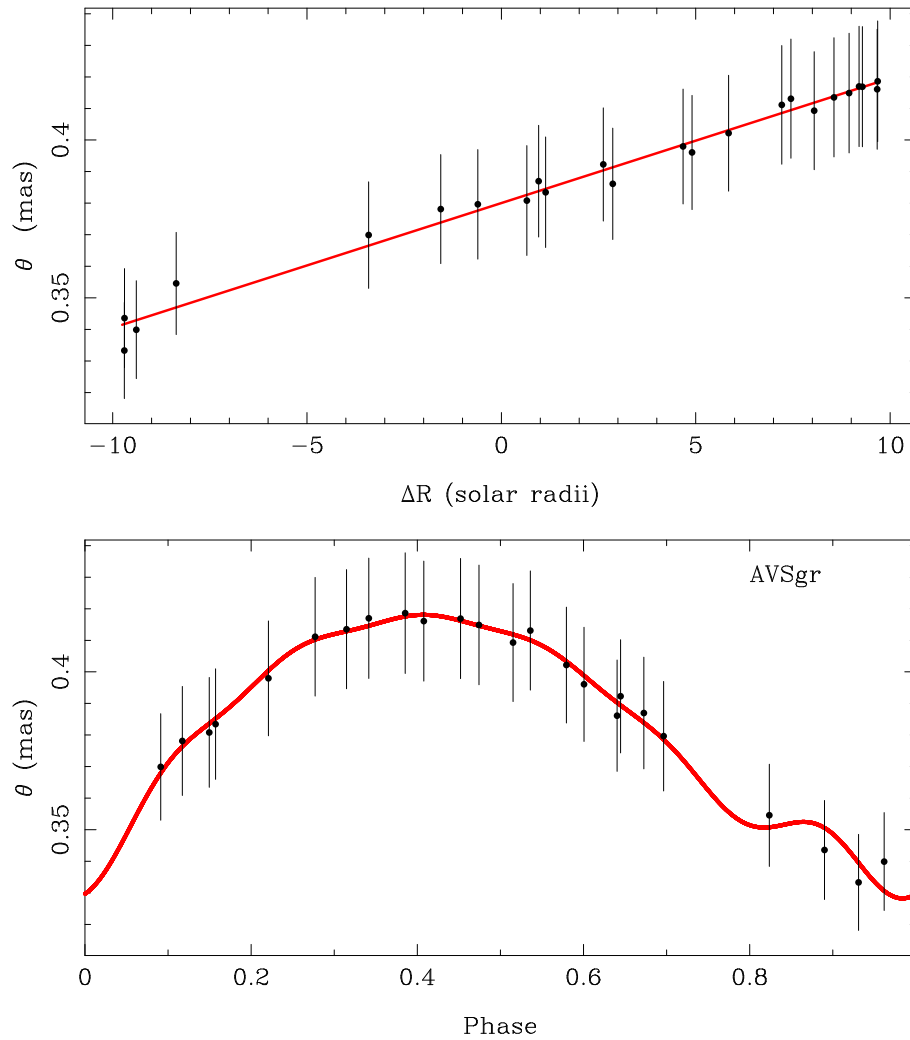


Figure 5.7: For AV Sgr, the top panel shows the linear-bisector fit to the angular diameter as a function of radial displacement. The bottom panel shows the angular diameter against phase. Crosses represent data-points not considered in the fit.

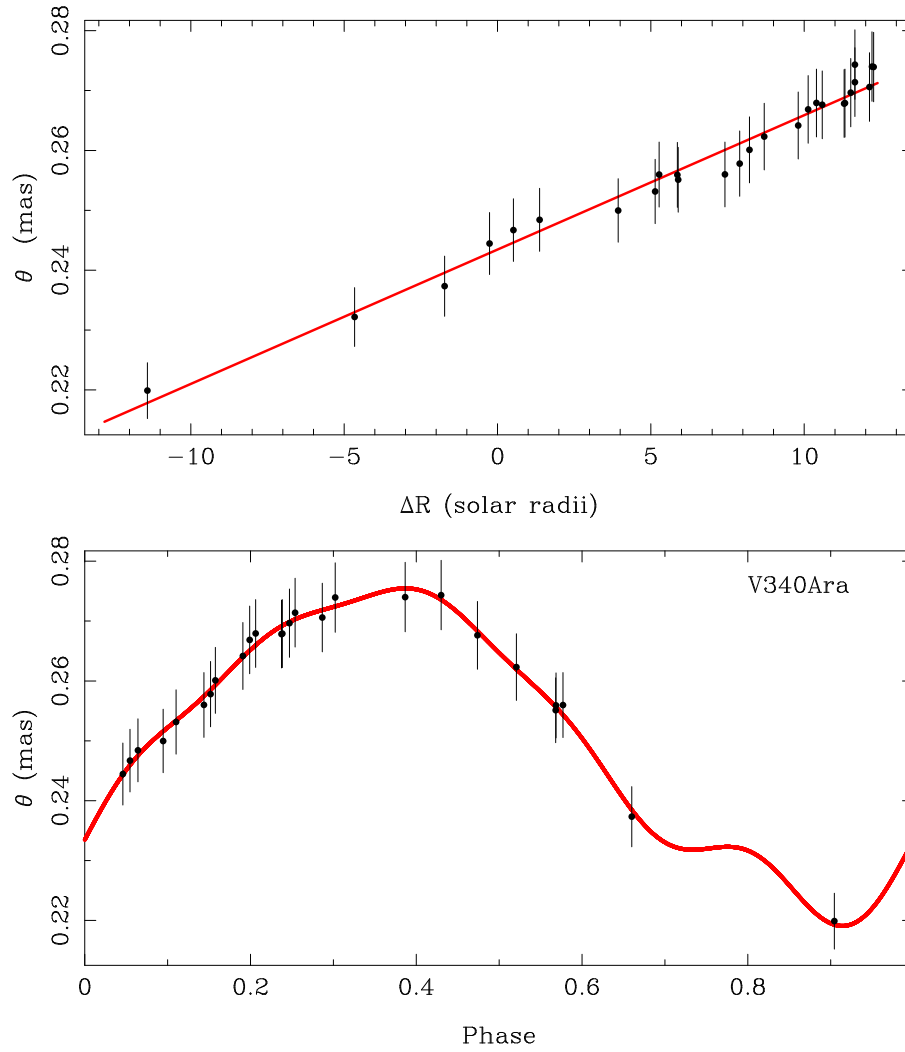


Figure 5.8: For V340 Ara, the top panel shows the linear-bisector fit to the angular diameter as a function of radial displacement. The bottom panel shows the angular diameter against phase. Crosses represent datapoints not considered in the fit.

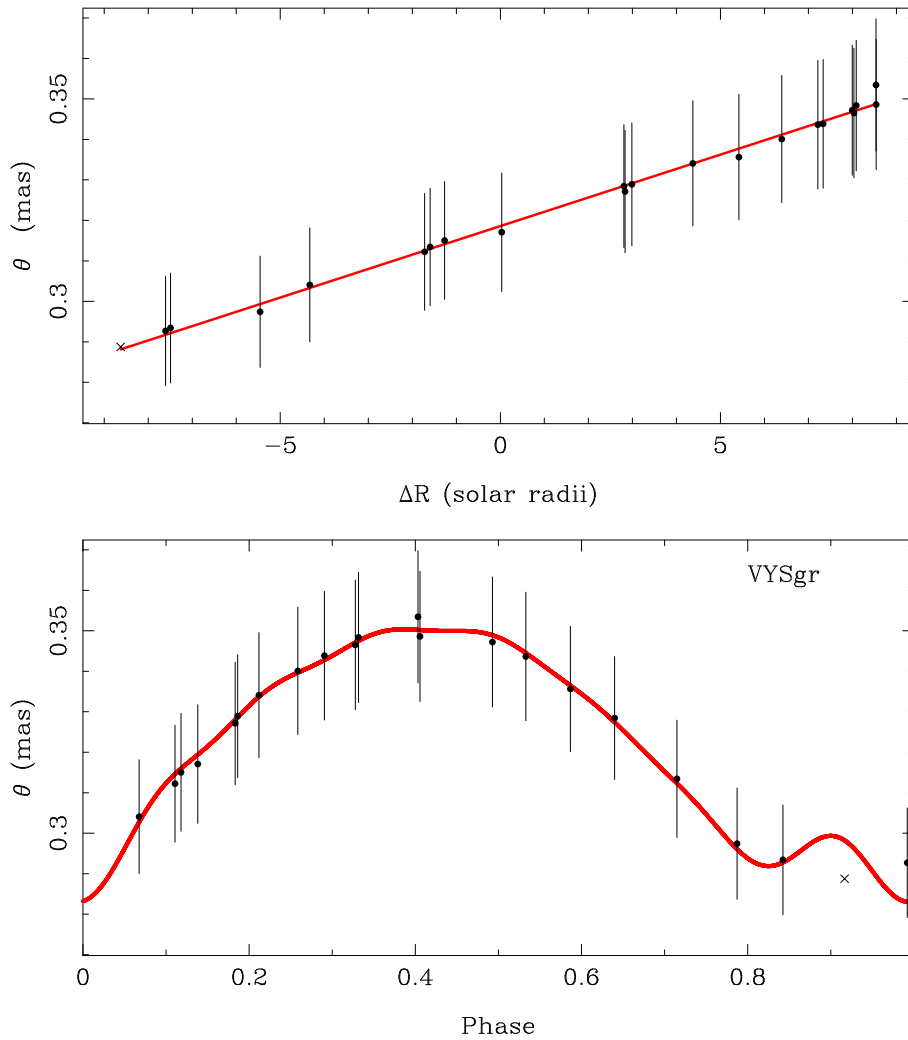


Figure 5.9: For VY Sgr, the top panel shows the linear-bisector fit to the angular diameter as a function of radial displacement. The bottom panel shows the angular diameter against phase. Crosses represent datapoints not considered in the fit.

5.4 Conclusions

We have derived distances and radii for four metal-rich Cepheids, namely V340 Ara, AV Sgr, UZ Sct and VY Sgr. To estimate these parameters we have used the Baade-Wesselink technique with the most recent surface brightness relation and projection factor. The method used is explained in Groenewegen 2007 and we summarized it in section 5.1. The different steps to apply the Baade-Wesselink are shown in figures from 5.2 to 5.9 for each target. Our results are listed in Table 5.1. In the same table (last column) we have also listed the distances obtained from Andrievsky et al. 2002b, for comparison. We underline that the method used by Andrievsky and collaborators is based on the "absolute magnitude - pulsational period" relation of Gieren et al. (1998). Considering this point, our distances are more accurate and they agree quite well with literature determinations. Moreover, we have used these results to improve the number of chemical tracers in the study of Galactic abundance gradient, in particular these Cepheids are fundamental to investigate the inner region of the disk.

The Galactic abundance gradient

In section 2.2 we have presented the dataset used to calibrate new empirical and theoretical Metallicity-Index Color (MIC) relations. In the following, we will explain the theory and methodology adopted.

6.1 Interstellar reddening corrections

Before any physical information can be derived from photometric data, all colors and magnitudes have to be corrected for interstellar reddening. In order to constrain the absorption coefficients, detailed observations of a sizable sample of standard stars in the southern hemisphere have been performed during three different periods (1960-61, 1970-71, 1980-81). There are very small differences between these three absolute calibrations of the Walraven system and transformations are very well studied. The zero-point was set by the measurements of one B star passing through the zenith in South Africa (ω^1 Sco, spectral type B1.5V, $V_J = 3.96$ and $(B - V)_J = -0.04$, HD 144470). We underline that we used the data from South Africa (1970-71) transformed into the photometric system as valid for La Silla (1979-1991) and then we were able to apply the relations between Johnson and Walraven systems. On the basis of the quoted data the following relations were derived by Lub and Pel between magnitudes, colors and color excesses in the Johnson and in the Walraven systems:

$$V_J = 6.886 - 2.5 \cdot V - 0.082 \cdot (V - B) \quad (6.1)$$

$$(B - V)_J = 2.571 \cdot (V - B) - 1.020 \cdot (V - B)^2 + 0.050 \cdot (V - B)^3 \quad (6.2)$$

$$\frac{E(B - V)_J}{E(V - B)} = 2.375 - 0.169 \cdot (V - B) \quad (6.3)$$

$$\frac{A_{V_w}}{E(V - B)} = 3.17 - 0.16 \cdot (V - B) - 0.12 \cdot E(V - B) \quad (6.4)$$

while the ratios between different color excess in the Walraven system are the following:

$$\frac{E(B - U)}{E(V - B)} = 0.61 \quad (6.5)$$

$$\frac{E(U - W)}{E(V - B)} = 0.45 \quad (6.6)$$

$$\frac{E(B - L)}{E(V - B)} = 0.39 \quad (6.7)$$

We have also adopted the usual relations for the extinctions according to Cardelli et al. (1989):

$$\frac{A_{V_J}}{E(B - V)_J} = 3.1 \quad (6.8)$$

$$\frac{A_{J_J}}{A_{V_J}} = 0.28 \quad (6.9)$$

$$\frac{A_{H_J}}{A_{V_J}} = 0.19 \quad (6.10)$$

$$\frac{A_{K_J}}{A_{V_J}} = 0.11 \quad (6.11)$$

It should be noted that, the Walraven system uses units of $\log_{10}(\text{Intensity})$ instead of magnitudes ($-2.5 \cdot \log_{10}(\text{Intensity})$), therefore for transforming the distance moduli based on Johnson photometry we adopt $DM_W = -0.4 \cdot DM_J$.

To check the validity of our extinction and distance modulus relations we make a comparison theory and observations. The transformation of the evolutionary models into the observational plane was performed by adopting a set of atmosphere with the same chemical composition (Castelli & Kurucz 2003). The reader interested in a detailed discussion concerning the input physics is referred to Pietrinferni et al. (2004). Fig. 6.1 shows the comparison between theory and observations for both the Johnson V_J, B_J -bands (top) and the Walraven V, B -bands (bottom). Individual distances were estimated using NIR mean magnitudes and the empirical NIR PL relations provided by Persson et al. (2004) and the reddening corrections provided by Fernie (1995). The dashed lines display the predicted first overtone blue edge (hotter) and the fundamental red edge (cooler) of the Cepheid instability strip (Bono et al. 2005). As the figure shows all the empirical data are inside the instability strip.

6.2 MIC Relations

As we have already mentioned, in order to avoid systematic uncertainties in the metallicity estimate we adopted the reddenings given in the Catalog of Classical Cepheids (Fernie et al. 1995) and removed the objects that were members of binary systems (Szabados et al. 2003). We ended up with a sample of 122 Cepheids for which we searched in the literature for iron measurements based on high resolution spectra. We found accurate iron abundances for 51 (of 122) Cepheids (Andrievsky et al. 2002a,b,c; Andrievsky et al. 2004; Luck et al. 2006; Lemasle et al. 2007; Romaniello et al. 2008). The calibrating Cepheids covered a broad range in metallicity, namely $-0.4 < [Fe/H] < 0.4$. However, only few stars present iron abundances $> +0.15$ (1 Cepheid) and < -0.25 (4 stars), it means that the 90% of the sample, within errors, present solar metal content.

For the empirical calibration we performed a multilinear regression fit between the observed (B-L) color, spectroscopic iron abundance and an independent color index (CI). In particular, we estimated the coefficients of the following MIC relation:

$$[Fe/H]_{ph} = \alpha + \beta \cdot (B - L)_0 + \gamma \cdot CI_0 + \delta \cdot (B - L)_0^2 + \epsilon \cdot CI_0^2 \quad (6.12)$$

where the symbols have the usual meaning, and CI_0 indicates an unreddened color index. For this investigation, we chose two different CIs, namely (V-B) and (V-K) since they are good temperature indicators. As we have already mentioned, to estimate the theoretical MIC relations we used an homogeneous set of evolutionary models for intermediate-mass stars with scaled-solar chemical composition. The adopted stellar masses range from $M = 3.5$ to $10.0 M_\odot$ (by steps of $0.5 M_\odot$), while the metal and helium content are $Z = 0.002, 0.004, 0.008, 0.0198, 0.04$ and $Y = 0.248, 0.251, 0.256, 0.273, 0.303$. For each set of tracks we selected, at fixed metallicity, all the points located inside the predicted edges of the instability

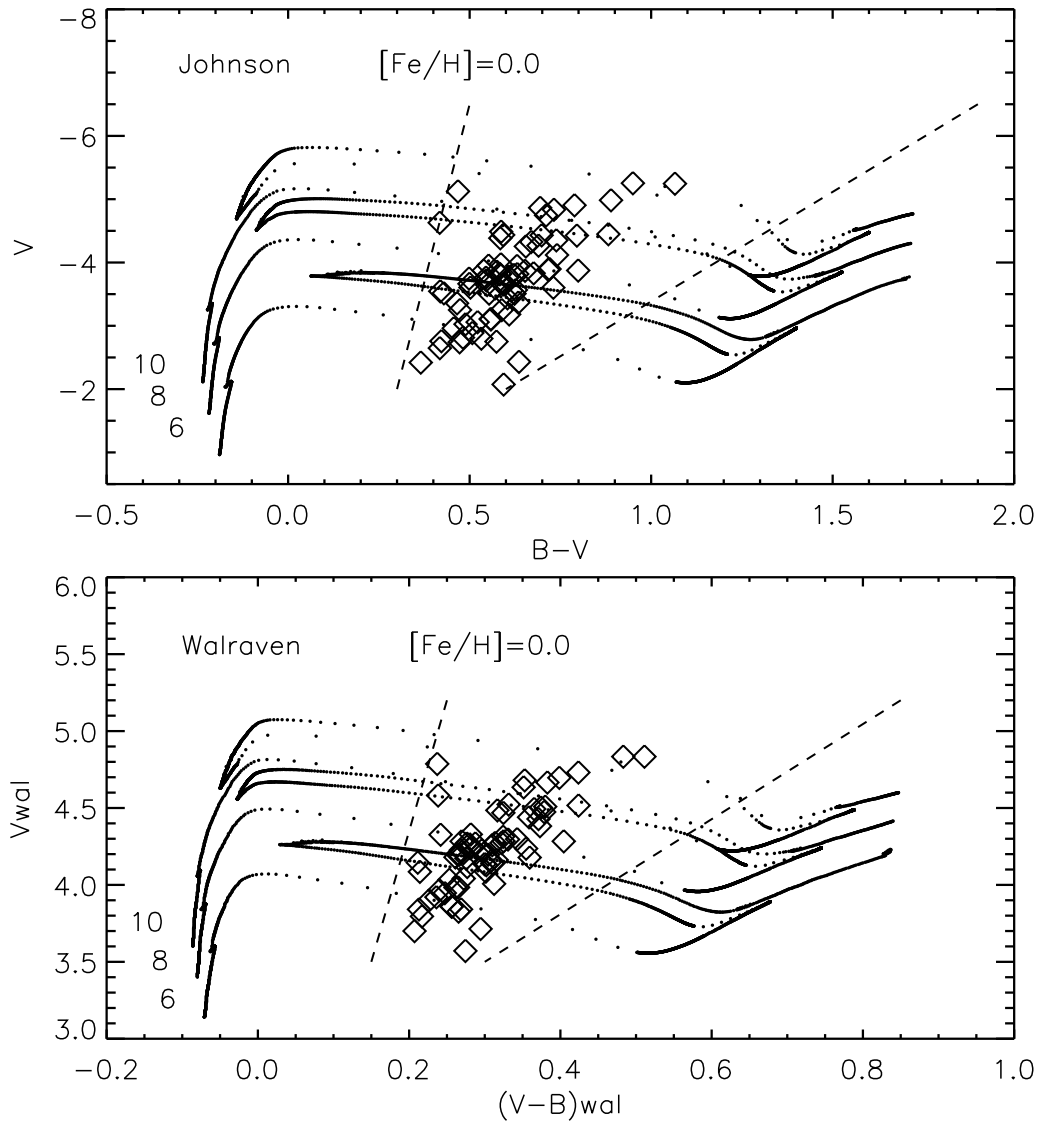


Figure 6.1: Top panel: $V_J, B_J - V_J$ Johnson Color-Magnitude Diagram for calibrating Cepheids (diamonds). Solid lines display evolutionary tracks at solar chemical composition ($Y=0.273, Z=0.0198$) and different stellar masses (see labeled values). Individual distances for calibrating Cepheids were estimated using the NIR PL relations by Persson et al. (2004) and reddening estimates provided by Fernie (1995). The dashed lines show the edges of the instability strip. Bottom panel: Same as the top, but for the Walraven V, B -bands.

Table 6.1: Coefficients and Multi-correlations of the MIC relations: $[Fe/H] = \alpha + \beta \cdot (B - L) + \gamma \cdot CI_0 + \delta \cdot (B - L)^2 + \epsilon \cdot CI_0^2$

MICs	α	β	γ	δ	ϵ	MCORR
$MIC_{(V-B)}^{Theo}$	-1.90 ± 0.09	-2.78 ± 0.76	10.32 ± 0.39	-8.67 ± 0.02	-0.72 ± 0.47	97%
$MIC_{(V-K)}^{Theo}$	-0.58 ± 0.08	-0.86 ± 0.43	7.98 ± 0.78	-0.16 ± 0.11	-3.22 ± 0.83	98%
$MIC_{(V-B)}^{Emp}$	-0.38 ± 0.09	3.86 ± 0.22	-3.02 ± 0.44	-10.06 ± 0.23	9.42 ± 0.65	62%
$MIC_{(V-K)}^{Emp}$	-1.02 ± 0.07	-0.05 ± 0.11	5.29 ± 0.51	-0.13 ± 0.35	-3.41 ± 0.17	67%

Table 6.2: Mean values and dispersions of the residuals of MIC relations.

Calibrations	$\delta[Fe/H]$	σ	σ_{MIC}
$MIC_{(V-B)}^{Theo}$	$< 10^{-6}$	0.11	0.09
$MIC_{(V-K)}^{Theo}$	$< 10^{-6}$	0.11	0.08
$MIC_{(V-B)}^{Emp}$	$< 10^{-7}$	0.10	0.09
$MIC_{(V-K)}^{Emp}$	$< 10^{-7}$	0.09	0.07

strip (Bono et al. 2005, Caputo et al. 2005). Moreover, to obtain the same number of stars for each metallicity we have selected, ten points located at the same distance in color (cyan diamonds in the upper panels of fig. 6.2 and 6.3). Then we performed the regression fit (Eq. 6.12) between the quoted metallicities and the predicted CIs. In table 6.1 we listed the values of the coefficients and multi-correlations (MCORR) for the different MIC relations. As the table shows, MCORR is very good for theoretical calibrations both using (V-B), $\sim 97\%$ and (V-K) color, $\sim 98\%$, while for empirical MIC relation is 62% using (V-B) and 67% for (V-K). These low values for can be explained by the fact that the calibrating Cepheids are concentrated around $[Fe/H] \sim 0$.

6.3 Metallicity estimates

To check the validity of our results we estimated the photometric metallicity applying each MIC relations and we calculated the residual between photometric and theoretical or spectroscopic measurements.

For the theoretical calibrations, the residuals are showed in figures 6.2 for (V-B) and 6.3 for (V-K) colors. In the upper panels of these figures, we showed the distribution of theoretical colors at different metallicities. As the panels show the theoretical data cover a greater range in color ($-0.96 \leq [Fe/H] \leq +0.40$) then the one covered by empirical sample. Moreover, the color distributions as a function of metallicity are more concentrated in the plane (B-L) vs (V-B) then in the (B-L) vs (V-K). Middle panels plotted the theoretical residuals as a function of theoretical metallicities for the (V-B) and (V-K) MIC relations, respectively. The dashed lines indicate the 1σ level. In the lower panels we showed the histograms of the residuals and we labeled the MIC relations used and the values of $\delta[Fe/H]$ and σ of the relations.

In Table 6.2 we listed the mean values of the residual distribution and the standard deviations. From

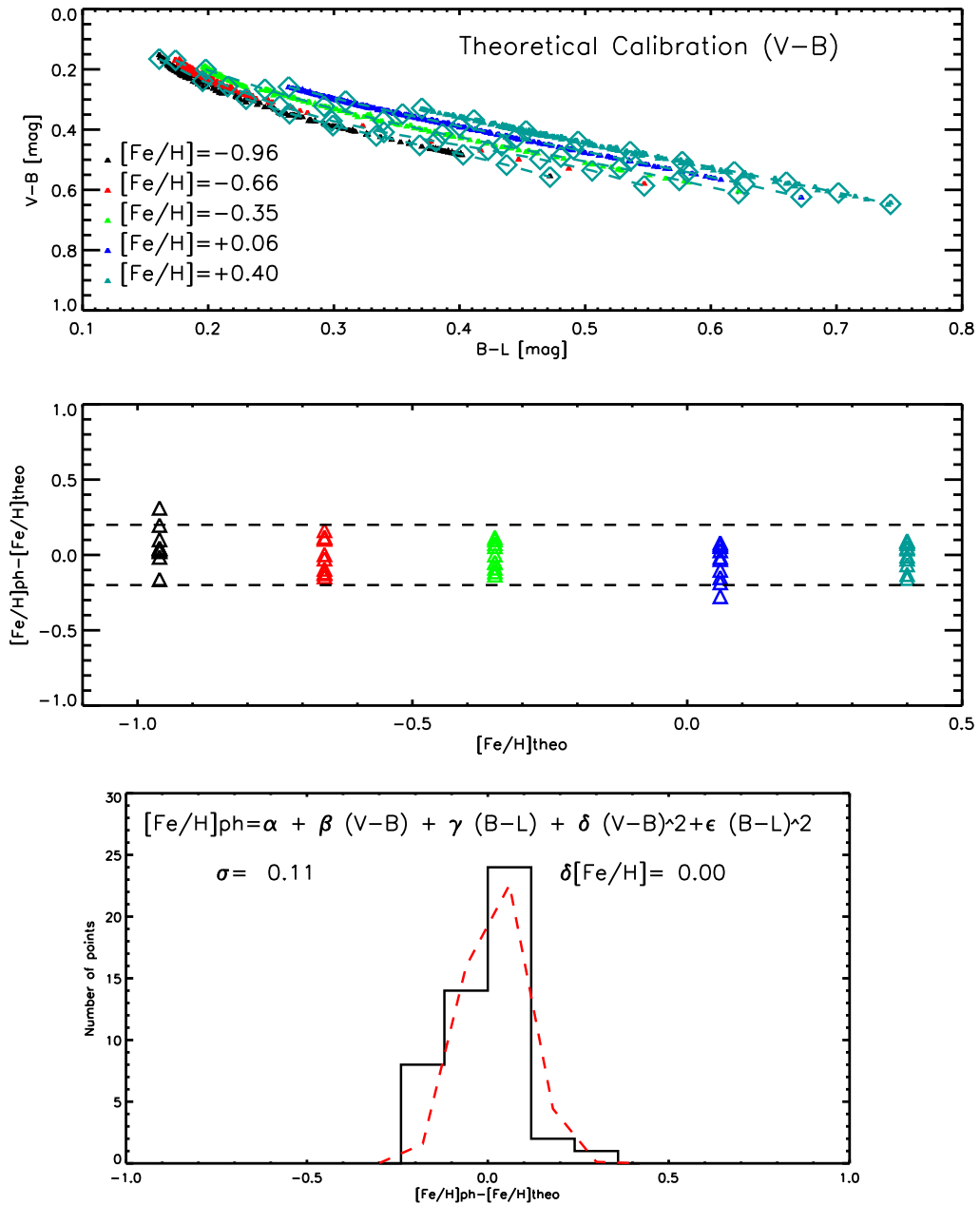


Figure 6.2: Theoretical MIC relation in (V-B) color. Top panel: theoretical sample in the color-color plane (V-B) vs (B-L). The different colors of the points indicate the different metallicities: Black are $[\text{Fe}/\text{H}] = -0.96$; Red are $[\text{Fe}/\text{H}] = -0.66$; Green are $[\text{Fe}/\text{H}] = -0.35$; Blue are $[\text{Fe}/\text{H}] = +0.06$; Cyan are $[\text{Fe}/\text{H}] = +0.40$. The cyan diamonds indicate the 10 points sampled for the multilinear regression. Middle panel: residuals between photometric and theoretical metallicities. The dashed lines show the levels at ± 0.2 . Bottom panel: Histogram of the residuals. In this panel we also plotted the MIC relation used and the values of mean $\delta[\text{Fe}/\text{H}]$ and σ of the relation.

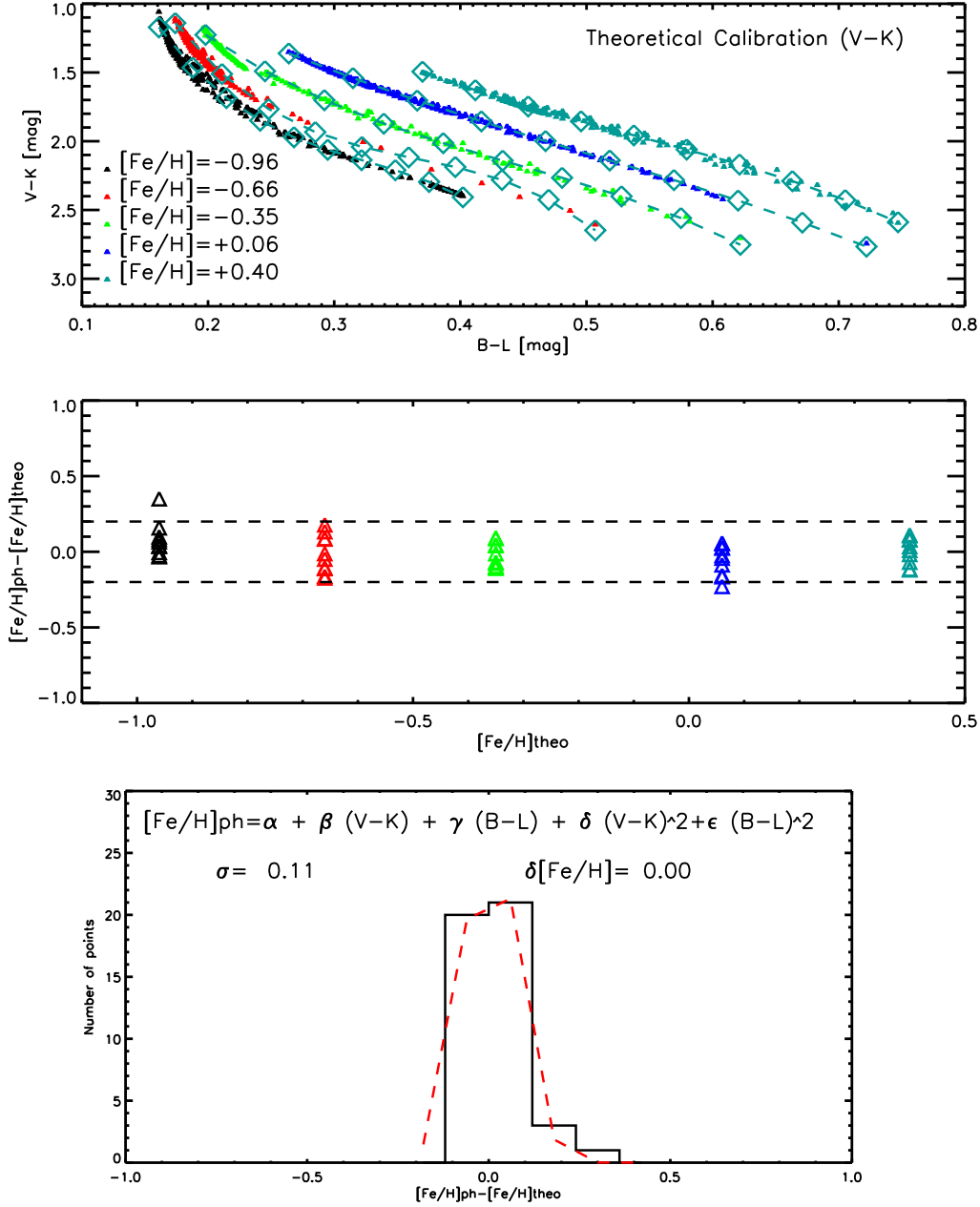


Figure 6.3: Theoretical MIC relation in (V-K) color. Top panel: theoretical sample in the color-color plane (V-K) vs (B-L). Middle panel: residuals between photometric and theoretical metallicities. Bottom panel: Histogram of the residuals, MIC relation used and the values of mean δ $[\text{Fe}/\text{H}]$ and σ of the relation.

Table 6.3: Mean values and dispersion of residuals applying theoretical MIC relations to the calibrating Cepheids.

Calibrations	$\delta[\text{Fe}/\text{H}]$	σ
$MIC_{(V-B)}$	0.004	0.15
$MIC_{(V-K)}$	0.005	0.13

this table, we can conclude that the residuals for theoretical calibrations are concentrated around zero ($\delta[\text{Fe}/\text{H}] < 10^{-6}$) and the intrinsic accuracy of MIC relations is ~ 0.1 dex.

The same methodology has been apply to calibrate the empirical MIC relations. We discuss here, only the calibration in (V-K) color because very similar results have been obtained with the (V-B) relation. We considered the distributions of the empirical colors at different metallicity bins (see labeled values in fig. 6.4, upper panels). Then we performed, once again, the multilinear regression (Eq. 6.12) between the spectroscopic metallicities and the color indices for 51 calibrating Cepheids. The coefficients and the value of the multi-correlations for the empirical MIC relations, are still listed in table 6.1. Applying the empirical coefficients we estimated, also in this case, the photometric metallicities and the residuals between them and the spectroscopic measurements. As figure 6.4 shows, there is a degeneracy in iron content. It depend on the abundance range covered by data. Theoretical calibrations spanned ~ 1.5 dex while in this case the range covered is ~ 0.4 dex. To improve the empirical MIC relations more spectroscopic data are needed. In the middle panels of figure 6.4 we plotted the residuals as a function of spectroscopic metallicities for (V-K) MIC relation. The slope showed from these panel indicate the degeneracy and the lack of metal-rich or metal-poor Cepheids. In the lower panels we shown the histograms of these residuals and we labeled the MIC relations used and the values of $\delta[\text{Fe}/\text{H}]$ and σ of the relations.

All these values are listed in Table 6.2. Also in this case, the residual are around zero and the intrinsic accuracy of the empirical MIC relations is about 0.1 dex.

We underline that these dispersions (see column 3 in table 6.2) are mainly due to the standard deviation of the multilinear regression (see column 4 in table 6.2). Moreover, to validate the theoretical MIC relations we applied them to the calibrating Cepheids and we calculated again the photometric metallicities. The results are shown in fig. 6.5 for the MIC relation using (V-B) color and in fig. 6.6 for the one using (V-K) color. The top panels show the residuals as a function of spectroscopic metallicities and in the bottom panels we plotted the histograms of this residuals. We found that the residuals are still around zero and the dispersion is less then 0.2 dex. In particular, for the (V-B) MIC relation we obtained $\delta[\text{Fe}/\text{H}] = 0.004$ and $\sigma = 0.15$ and using the (V-K) color we found $\delta[\text{Fe}/\text{H}] = 0.005$ and $\sigma = 0.13$. In table 6.3 we listed all these values. Our results suggest that the theoretical and empirical MIC relations based on different color indices do agree quite well. Moreover and even more importantly, the metallicity range covered by the photometric abundances is, within empirical and theoretical uncertainties, in good agreement with spectroscopic measurements (Andrievsky et al. 2002; Yong et al. 2006; Lemasle et al. 2007).

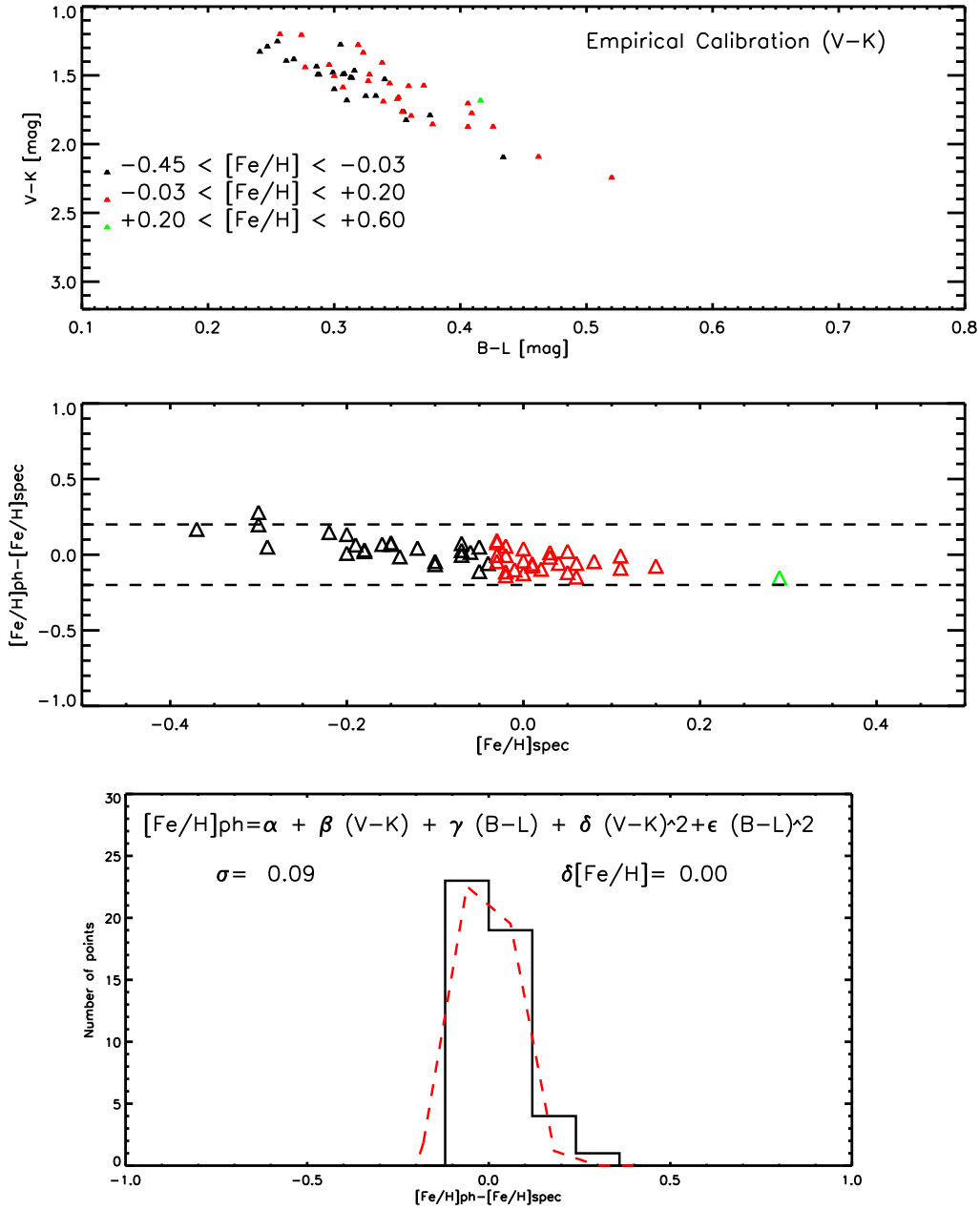


Figure 6.4: Empirical MIC relation in (V-K) color. Top panel: Empirical color-color plane (V-K) vs (B-L). Middle panel: residuals between photometric and spectroscopic metallicities. Bottom panel: Histogram of the residuals, MIC relation used and the values of mean $\delta [Fe/H]$ and σ of the relation.

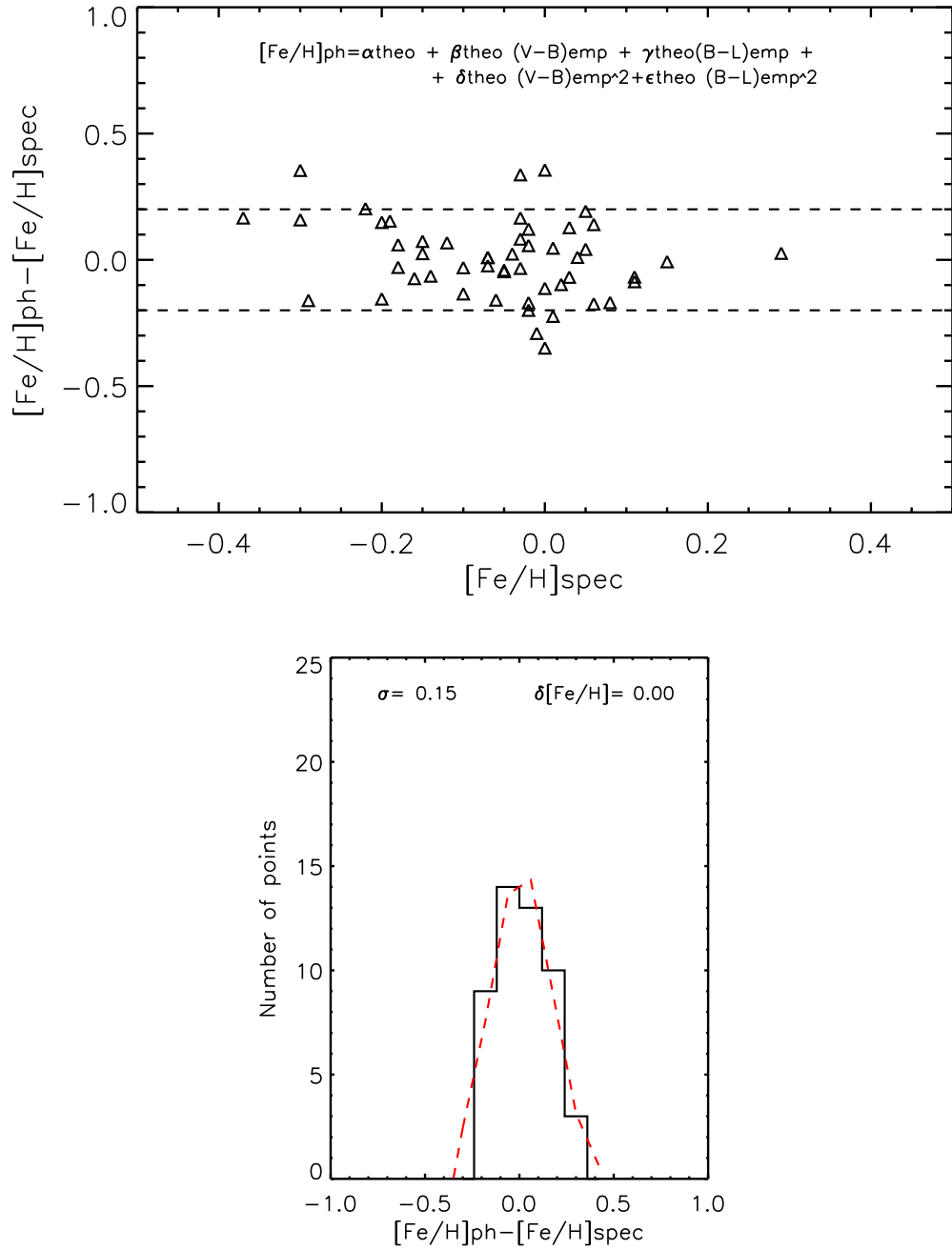


Figure 6.5: Theoretical MIC relation in (V-B) color applied to the calibrating Cepheids. Top panel: residuals between photometric and spectroscopic metallicities. Bottom panel: Histogram of the residuals and the values of mean $\delta [\text{Fe}/\text{H}]$ and σ .

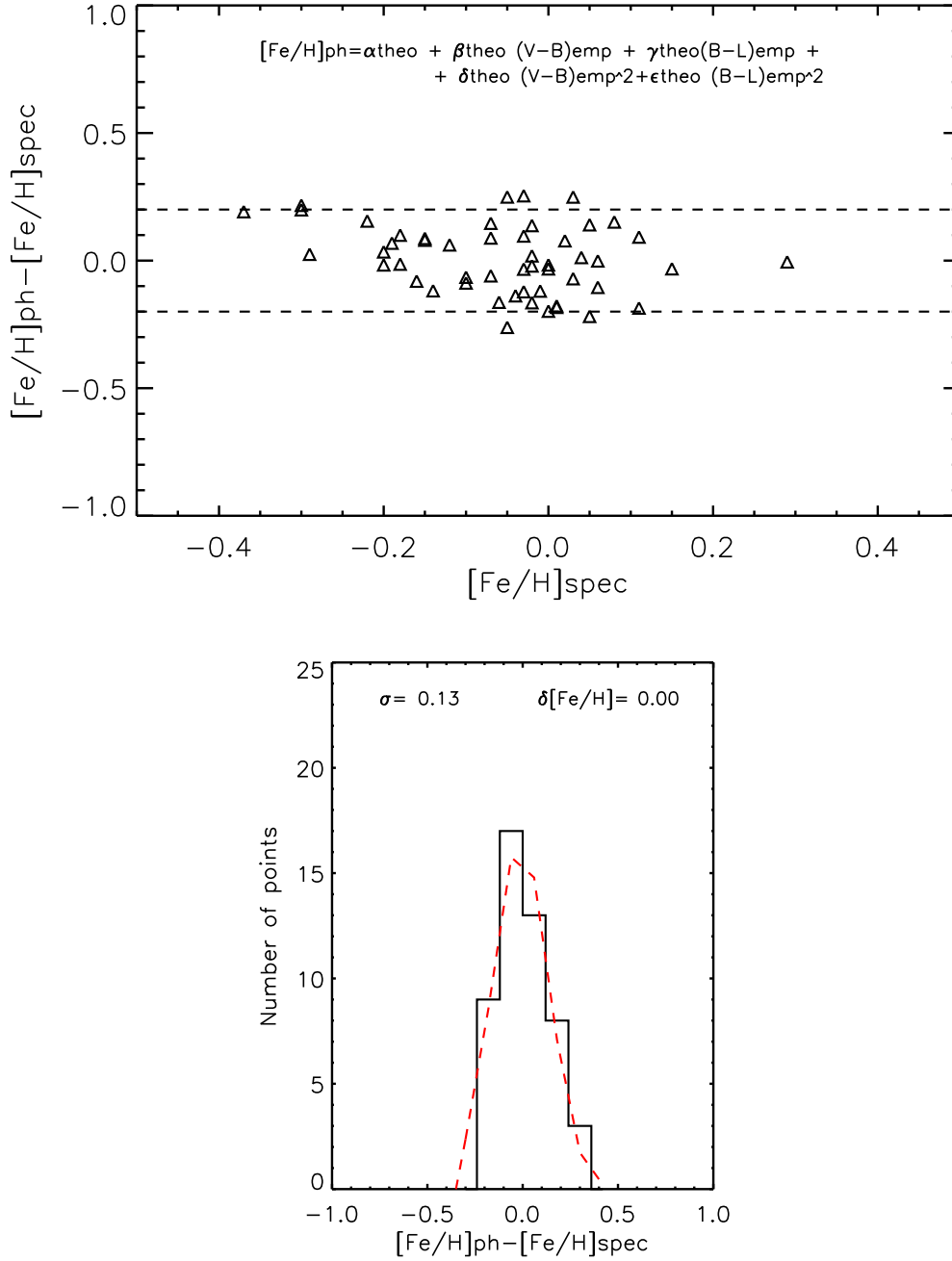


Figure 6.6: Theoretical MIC relation in (V-K) color applied to the calibrating Cepheids. Top panel: residuals between photometric and spectroscopic metallicities. Bottom panel: Histogram of the residuals and the values of mean $\delta [\text{Fe}/\text{H}]$ and σ .

6.4 The Galactic abundance gradient

According to Lemasle et al. 2008 and Andrievsky et al. 2002 (a, b, c) we estimated the individual distances using the near infrared (J -; H -; K -band) Period-Luminosity (PL) relations provided by Persson et al. (2004) and by assuming an LMC distance modulus of 18.50, a conservative value adopted by the HST Key Project (Freedman et al., 2001). Note that the quoted PL relations were also transformed into the 2MASS photometric system using the transformations provided by Carpenter (2001, see Eq. 4.4). In order to estimate the distance of first overtone Cepheids, their periods were fundamentalised (Feast & Catchpole 1997). Using the PL relations from Persson et al. (2004) for Galactic Cepheids is not a problem, although they are based on a large and homogeneous sample of LMC Cepheids. Our results and current empirical and theoretical findings indicate that the slope and the zero-point of NIR PL relations marginally depend on metallicity (Bono et al., 1999; Persson et al., 2004; Fouqué et al., 2007; Romaniello et al., 2008). Moreover, the near-infrared PL relations present an intrinsic dispersion that is significantly smaller than the dispersion of the optical PL relations. The difference is due to the fact that the former ones are, at fixed period, marginally affected by the intrinsic width in temperature of the instability strip. Finally, Cepheid distances based on near-infrared PL relations are more accurate than optical ones because they are marginally affected by uncertainties in reddening estimates. We adopted the individual Cepheid reddenings provided either by Laney & Caldwell (2007) or listed in the Fernie's database (Fernie et al., 1995). These two sets of reddenings are not homogeneous as recent results provided by Laney & Caldwell (2007) are corrected from metallicity effects whereas reddenings from Fernie et al. (1995) do not account for metallicity effects. The relative absorption in the V -band, was estimated using Eq. 6.8, and then according to Cardelli et al. (1989) we estimated the absorption in J , H , and K -band (see Eq. 6.9, 6.10 and 6.11). Pulsation periods are from the Fernie's database (Fernie et al., 1995). The heliocentric distance of the stars adopted in the following is the mean value between the three distances in J , H , and K -bands to limit random errors. The Galactocentric distance is finally calculated with the classical formula assuming a Galactocentric distance of 8.5 kpc for the sun (Feast & Whitelock, 1997):

$$R_G = (R_{G_\odot}^2 + (d \cdot \cos(b))^2 - 2 \cdot R_{G_\odot} \cdot d \cdot \cos(b) \cdot \cos(l))^{1/2} \quad (6.13)$$

This determination (whose error bars are 0.5 kpc) was based on the analysis of the Hipparcos proper motion of 220 Cepheids. Recent studies give Galactocentric distances for the sun between 7.62 ± 0.32 kpc (Eisenhauer et al., 2005) and 8.8 ± 0.3 kpc (Collinge et al., 2006). For a recent review of the distance to the Galactic Center, see Groenewegen et al. (2008).

To investigate the Galactic abundance gradient, we included 71 new metallicity estimates based on (V-K) MIC relation. We added four metal-rich Cepheids for which we collected high resolution spectra and for which we derived accurate distances based on the Baade-Wesselink technique. Moreover, to improve the number of tracers, we have also included 116 Cepheids from Andrievsky et al. (2002), 63 from Lemasle et al. (2007), 10 from Romaniello et al. (2008) and 6 from Sziládi et al. (2007) to end up with 270 Galactic Cepheids. Figure 6.7 shows our results on the Galactic abundance gradient. In the upper panel we plotted the entire dataset with different symbols and colors: Andrievsky et al. (2002, cyan open circles); Walraven data are the photometric metallicities (blue stars); BW-data are the four metal-rich Cepheids from our Baade-Wesselink analysis (green cruxes); Lemasle et al. (2007, full black points), Romaniello et al. (2008, red triangles) and Sziládi et al. (2007, gold diamonds). This figure indicates that the iron gradient in the Galactic disk presents a slope of $-0.048 \pm 0.004 \text{ dex } kpc^{-1}$ which is in very good agreement with the most recent literature values. The middle panel shows the distribution of our sample across the disk. On the x-axis we plot the Galactocentric longitude (l) and the y-axis indicates the altitude above the Galactic plane (z)¹. From this figure, we can conclude that the sample we collected is homogeneously distributed across the entire Galactic disk.

However, the hypothesis of a linear gradient is still widely debated. Several investigations suggest a

¹The altitude above the Galactic plane is $z = d \cdot \sin(b)$, where b is the Galactic latitude

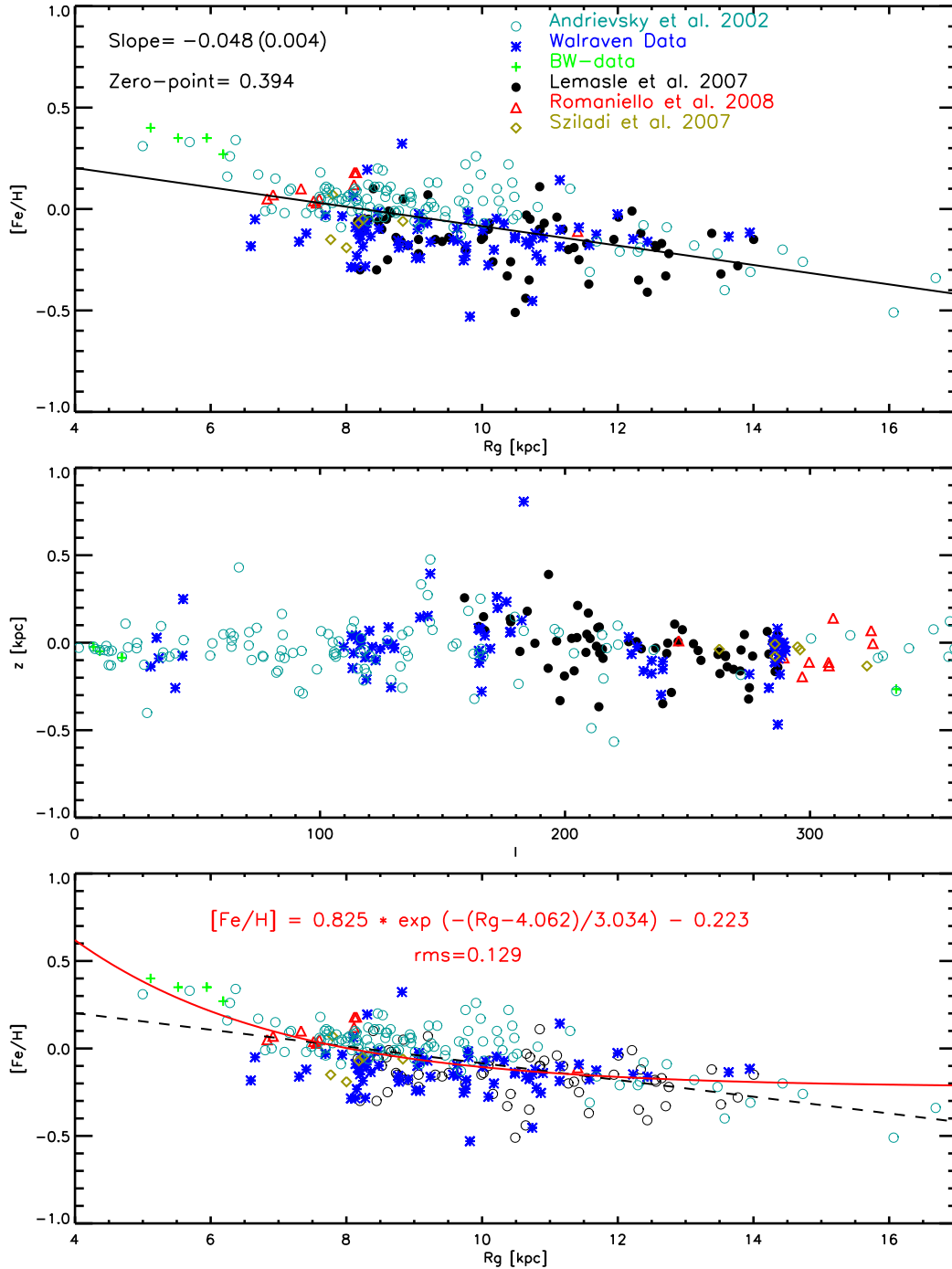


Figure 6.7: Galactic abundance gradient from the entire sample. Different symbols and colors identify different set of data: Andrievsky et al. (2002) cyan open circles; blue stars for photometric metallicities; BW-data are the four metal-rich Cepheids from our Baade-Wesselink analysis (green cruxes); Lemasle et al. (2007), full black points; Romaniello et al. (2008), red triangles and Sziládi et al. (2007), gold diamonds. Upper panel: the Galactic abundance gradient linear fit. We have also labeled the values of the slope and zero-point. Middle panel: Cepheid distribution across the Galactic disk. Lower panel: exponential fit of the Galactic abundance gradient (red line). We overplotted, for comparison also the linear fit (black dashed line) and the formula of exponential distribution obtained for minimum rms.

bimodal distribution with a steeper slope toward the bulge and a flattening of the gradient toward the outer disk with a discontinuity at $R_G \sim 10$ kpc. Our data do not support the discontinuity hypothesis (see fig. 6.7, upper panel) but we have found a large spread in metal abundance (~ 0.8 dex) for Cepheids located approximately at the same distance ($R_g \sim 10$ kpc), but covering a broad range of Galactocentric longitude. Current findings show that Cepheids present an increase in the spread in iron abundance and that it may depend on the Galactocentric longitude. The occurrence of this spread indicates that linear radial gradients should be cautiously treated to constrain the chemical evolution of the Galactic disk. Finally, we decided to fit the Galactic abundance gradient with an exponential distribution. The lower panel of figure 6.7 shows this fit. The formal expression of this fit is:

$$[Fe/H] = 0.825 \cdot e^{-\frac{R_G - 4.062}{3.034}} - 0.223 \quad (6.14)$$

where the symbols have the usual meaning. We calculated these values for the exponential parameters to obtain the minimum root-mean-square (rms=0.129).

6.5 Conclusions

High resolution spectra, multibands Walraven photometry and accurate distance determinations based on both infrared photometry and Baade-Wesselink method allowed us to extend the study of the Galactic iron abundance gradient toward the disk.

The comparison between iron abundance estimates based on theoretical and empirical MIC relations brings forward two interesting findings:

- *i) Empirical Calibrations* – Cepheid iron abundances based on the empirical calibration agree quite well with spectroscopic measurements. The differences are on average less than 10^{-7} dex with an intrinsic dispersion $\sigma = 0.10$ dex for the relation using the (V-B) color and $\sigma = 0.09$ dex for the relation using the (V-K) color. However, to validate these relations, new spectroscopic measurements with high S/N and resolution are mandatory.
- *ii) Theoretical Calibration* – Metallicities based on the theoretical MIC relations agree very well with theoretical abundances. The differences are less than 10^{-6} dex with intrinsic dispersions of $\sigma = 0.11$ dex for both the relation using the (V-B) color and the (V-K) color.

Current sample includes 270 Cepheids located between 5 and 17 kpc from the Galactic center (see Fig. 6.7). This sample include: 71 new Cepheid from photometric measurements of metallicity, 4 from our Baade-Wesselink investigation (to improve the sampling in the inner disk), 116 from Andrievsky et al. (2002), 63 from Lemasle et al. (2007), 10 from Romaniello et al. (2008) and 6 from Sziládi et al. (2007). Using the entire sample we investigated the working hypothesis of a linear gradient and we have obtained a slope of -0.048 ± 0.004 dex kpc^{-1} , in very good agreement with previous studies (see fig. 6.7). Moreover and even more importantly, data plotted in figure do not show evidence of a gap over the Galactocentric distances covered by the current Cepheid sample.

However, the Galactic iron abundance gradient is better described by an exponential distribution that present a steeper slope toward the bulge and a flattening toward the outer disk.

Data plotted in figure 6.7 indicates that:

- The spread in metallicity is larger in the outer disk, in particular around 10 kpc.
- There is no evidence of a gap over the Galactocentric distances covered by the current sample.

Current findings are suggesting to be very cautious in using the slopes of Galactic gradients. A significant improvement in the sample of inner and outer disk Cepheids implies a systematic photometric survey to detect new Cepheids. This goal can be achieved with the new generation of automatic telescopes such as HAT (Hungarian-made Automated Telescope; <http://cfawww.harvard.edu/gbakos/HAT/index.html>) or ASAS (All Sky Automated Survey; <http://archive.princeton.edu/asas/>) and with spectroscopic follow up of the new targets.

Conclusions

Aim of this thesis was the study of Cepheids both as distance indicators and chemical tracers of the Galactic Disk.

In particular we focused on:

- The study about the influence of the stellar iron content on the PL relation in the V and K bands.
- Distances and radii determinations by Baade-Wesselink technique.
- The investigation on Galactic abundance gradient between 5 and 16 kpc, using homogeneous iron abundance measurements for 270 Galactic Cepheids located along the disk together with accurate distance determinations.

A huge sample of object (270) has been analyzed, covering the range of metallicity around one dex. We have presented and analyzed photometric and spectroscopic data. The available photometric data set consists on accurate optical (*VBLUW*-Walraven photometric system) and NIR data of 173 Cepheids. The available spectroscopic data set includes on a huge number of spectra, 68 for the investigation on PL-relation and more then 100 for the Baade-Wesselink analysis. They have been obtained with many different instruments. One side the large variety of instruments used has required a long and careful work of data reduction and calibration, on the other side the final data set results free from systematic effects due to specific instrumentation.

The most important conclusions are the following:

- **PL relation:** In order to asses the influence of the stellar iron content on the Cepheid PL relation, we have related the V -band and the K -band residuals from the standard PL relations of Freedman et al. (2001) and Persson et al. (2004), respectively, to $[\text{Fe}/\text{H}]$.
For the **Galactic** sample we found that the mean value of the iron content is solar ($\sigma = 0.10$, see Fig. 3.8), with a range of values between -0.18 dex and +0.25 dex;
For the **LMC** sample we found that the mean value is about ~ -0.33 dex ($\sigma = 0.13$, see Fig. 3.8), with a range of values between -0.62 dex and -0.10 dex.

For the **SMC** sample we find that the mean value is about ~ -0.75 dex ($\sigma = 0.08$, see Fig. 3.8), with a range of values between -0.87 and -0.63 .

- **PL relation:** We have compared our results with the analyses of FC97, Andrievsky et al. (2002a, 2002b, 2002c) and Luck et al. (2006) for the Galactic Cepheids and LL92 and L98 for the Magellanic Clouds. Regarding the Galactic sample, our results are marginally more in agreement with Andrievsky's values than with FC97 and the differences, on average, appear rather small. Considering the Magellanic Cepheids, we have a poor agreement with LL92, which could be in part accounted for different analytical tools and data quality. Our data are in better agreement with L98 results and the spread of our iron abundances in the LMC and SMC is similar to the one they reported. We note that the mean metallicity that they found with their complete sample (-0.30 dex and -0.74 dex) is in very good agreement with our results.

- **PL relation:** Our main results concerning the effect of the iron abundance on the PL relation are summarized in Fig. 4.2 and Fig. 4.3 (bottom panels) and they hold for a LMC distance modulus of 18.50.

The V -band PL relation does depend on the metal abundance. This finding is marginally affected by the adopted distance scale for the Galactic Cepheids and by the LMC distance. Current data do not allow us to reach a firm conclusion concerning the dependence of the K -band PL relation on the metal content. The use of the most recent distances for Galactic Cepheids (Benedict et al. 2007; Fouqu e et al. 2007; van Leeuwen et al. 2007) indicates a mild metallicity effect. On the other hand, the use of the old distances (Storm et al. 2004) suggest a vanishing effect. Residuals based on a canonical LMC distance ($\mu_{LMC} = 18.5$) and on the most recent distances for Galactic Cepheids present a well defined effect in the V -band. The metal-poor and the metal-rich bin are $\approx 2\sigma$ and $\approx 9\sigma$ from the null hypothesis. Moreover, the two metallicity bins differ at the 3σ level. These findings support the evidence that the Cepheid PL relation is not Universal.

- **PL relation:** By assuming a "short" LMC distance ($\mu_{LMC} = 18.3$) the residuals present a strong metallicity dependency in the zero-point of the V -band PL relation. By assuming a "long" LMC distance ($\mu_{LMC} = 18.7$) we found a strong metallicity effect when moving from metal-poor to metal-rich Cepheids. This indicates a significant change in the slope and probably in the zero-point. The findings based on the "short" and on the "long" LMC distance are at odds with current empirical and theoretical evidence, suggesting a smaller metallicity effect. Metal-rich Cepheids in the V -band are systematically fainter than metal-poor ones. This evidence is strongly supported by the canonical, the "short" and the "long" LMC distance.
- **BW:** We have derived distances for four metal-rich Cepheids using the Baade-Wesselink technique with the most recent surface brightness relation and estimates for the projection factor. Our results are shown in Table 5.1 and they agree very well with previous distance determinations (see column 2 and 6 in table 5.1). We used these results on the study of Galactic abundance gradient to investigate the inner disk region.
- **Galactic abundance Gradient:** High resolution spectra, multibands Walraven photometry and accurate distance determinations, allowed us to extend the study of the Galactic iron abundance gradient toward the disk.

The comparison between iron abundance estimates based on theoretical and empirical MIC relations brings forward two interesting findings:

i) Empirical Calibrations – Cepheid iron abundances based on the empirical calibration agree quite well with spectroscopic measurements. The differences are on average less than 10^{-6} dex with an intrinsic dispersion $\sigma \sim 0.09$ dex for the relation using the $(V-B)$ color and $\sigma \sim 0.07$ dex for the

relation using the (V-K) color. *ii) Theoretical Calibration* – Iron abundances based on the theoretical MIC relations agree very well with spectroscopic measurements. The differences are less than 10^{-7} dex with an intrinsic dispersion of $\sigma = 0.11$ dex for both (V-B) and (V-K) color relations.

- **Galactic abundance Gradient:** We investigated the working hypothesis of a linear gradient and we calculated the iron Galactic gradient using 270 Cepheids which include: metallicity estimates based on (V-K) MIC relation for 71 new Cepheids, 4 from our Baade-Wesselink analysis, 116 from Andrievsky et al. (2002), 63 from Lemasle et al. (2007), 10 from Romaniello et al. (2008) and 6 from Sziládi et al. (2007). Our results are showed in figure 6.7. We found a slope of $-0.048 \pm 0.004 \text{ dex kpc}^{-1}$ that is in very good agreements with recent estimates. Moreover and even more importantly, data plotted in this figure do not show evidence of a gap over the Galactocentric distances covered by the current Cepheid sample.
- **Galactic abundance Gradient:** Current findings showed that the Galactic iron abundance gradient is better described by a bimodal distribution with a steeper slope toward the bulge and a flattening of the gradient toward the outer disk. For this reason, we investigated, also, the working hypothesis of an exponential gradient. The fit agree very well with the data and have given $rms = 0.129$.

Although we are confident to have given a significant contribution to the understanding of Cepheids both as distance indicators and chemical tracers, much work remains to be done. In order to constrain on a more quantitative basis the metallicity dependence of both zero-point and slope of the optical PL relations is required a larger number of Cepheids covering a broader range in metal abundances. Moreover, for each metallicity bin Cepheids covering a broad period range are required to reduce the error on the residuals and to constrain on a quantitative basis the fine structure of the PL relation in optical and NIR photometric bands. Moreover, the natural continuation of the project on the Galactic abundance gradient is its extension to metal-rich Cepheids.

Moreover, current findings are suggesting to be very cautious in using the slopes of Galactic gradients. A significant improvement in the sample of inner and outer disk Cepheids implies a systematic photometric survey to detect new Cepheids. This goal can be achieved with the new generation of automatic telescopes such as HAT (Hungarian-made Automated Telescope; <http://cfawww.harvard.edu/gbakos/HAT/index.html>) or ASAS (All Sky Automated Survey; <http://archive.princeton.edu/asas/>) and with spectroscopic follow up of the new targets.

APPENDIX A

Light Curves

Table A.1: Physical parameters of 161 Walraven Cepheids.

Name	Log(P)	l	b	E(B-V)	$[Fe/H]_{spec}$	$[Fe/H]_{phot}$	DM_J	DM_H	DM_K
U Aql	0.8466	30.91	-11.62	0.399	...	-0.04	9.230	9.158	9.068
η Aql	0.8559	35.60	-2.34	0.149	+0.06 ^a	+0.06	7.248	7.248	7.199
FF Aql	0.6504	36.00	-3.14	0.224	+0.02 ^c	+0.10	8.197	8.241	8.087
FM Aql	0.7863	49.20	6.36	0.646	+0.08 ^c	+0.23	10.348	10.195	10.067
FN Aql	0.9769	44.34	0.89	0.510	-0.02 ^c	+0.12	11.255	11.089	10.988
SZ Aql	1.2340	38.54	-3.11	0.641	+0.15 ^c	+0.12	11.523	11.516	11.483
TT Aql	1.1385	34.73	-5.58	0.495	+0.11 ^c	+0.20	10.436	10.300	10.195
V336 Aql	0.8636	34.19	-2.14	0.644	...	-0.05	12.100	11.863	11.742
V496 Aql	0.8330	32.99	-1.65	0.413	+0.05 ^c	+0.19	10.351	10.248	10.145
V600 Aql	0.8597	28.20	-7.13	0.869	+0.03 ^f	+0.28	11.748	11.641	11.413
l Car	1.5509	41.35	-2.16	0.170	+0.00 ^a	-0.03	8.637	8.585	8.561
U Car	1.5885	43.89	-2.63	0.283	...	-0.12	11.057	11.088	11.073
V Car	0.8259	43.14	3.79	0.174	-0.04 ^a	-0.18	10.378	10.406	10.375
Y Car	0.5611	33.30	1.08	0.178	...	-0.16	10.834	10.899	10.855
AQ Car	0.9898	46.19	1.64	0.161	-0.30 ^b	-0.08	12.420	12.376	12.312
CC Car	0.6776	29.42	-18.60	0.526	13.859	13.646	13.493
CN Car	0.6931	44.14	4.45	0.419	...	-0.18	12.674	12.503	12.421
CR Car	0.9895	39.15	-2.57	0.504	14.207	13.880	13.824
DY Car	0.6697	38.27	-17.59	0.391	13.436	13.320	13.213
ER Car	0.8875	40.94	-13.07	0.101	...	-0.03	10.319	10.308	10.257
FI Car	1.1290	335.19	-3.75	0.726	14.024	13.816	13.603
FN Car	0.6614	330.85	-11.22	0.581	13.342	13.180	13.044
FO Car	1.0152	166.75	4.33	0.461	12.887	12.317	12.162
FQ Car	1.0117	183.15	8.92	0.868	...	-0.14	13.802	13.550	13.390
FR Car	1.0301	165.77	-1.28	0.351	...	-0.03	12.879	12.761	12.661
GH Car	0.7578	164.75	2.14	0.414	...	-0.16	11.766	11.775	11.633
GX Car	0.8571	167.28	0.94	0.405	...	-0.14	12.056	11.953	11.812
GZ Car	0.6190	164.88	-0.99	0.419	...	-0.19	12.278	12.171	12.058
IT Car	0.8770	177.61	1.99	0.193	...	-0.05	11.235	11.178	11.102
SX Car	0.6866	182.31	3.67	0.326	...	-0.14	11.546	11.492	11.452
UW Car	0.7280	177.86	1.61	0.457	...	-0.17	11.819	11.722	11.598
UX Car	0.5661	158.99	5.89	0.123	-0.10 ^b	-0.17	10.938	10.977	10.923
UY Car	0.7438	176.08	5.93	0.189	...	-0.15	11.817	11.750	11.740
VY Car	1.2768	160.53	1.98	0.243	-0.06 ^b	-0.22	11.388	11.381	11.348
WW Car	0.6699	165.47	1.73	0.398	...	-0.25	12.013	11.931	11.837
WZ Car	1.3620	162.40	-0.98	0.384	+0.18 ^a	...	13.094	13.105	13.076
XX Car	1.1963	165.95	-3.98	0.349	...	-0.16	13.109	13.032	12.937
XY Car	1.0946	165.02	-2.19	0.417	...	-0.09	12.527	12.377	12.264
XZ Car	1.2214	172.46	4.26	0.367	...	-0.10	12.263	12.127	12.025
YZ Car	1.2592	169.49	-0.63	0.396	...	-0.18	12.563	12.475	12.377
RW CMa	0.7581	172.22	3.98	0.544	...	-0.15	13.045	12.870	12.715
RY CMa	0.6701	144.85	3.80	0.248	-0.12/-0.20 ^b	-0.06	10.670	10.627	10.553
RZ CMa	0.6289	145.90	4.70	0.464	-0.20 ^b	-0.22	11.655	11.632	11.438

Continue ...

Name	Log(P)	l	b	E(B-V)	$[Fe/H]_{spec}$	$[Fe/H]_{phot}$	DM_J	DM_H	DM_K
SS CMa	1.0921	145.02	6.15	0.549	...	-0.13	12.974	12.813	12.693
TV CMa	0.6693	143.94	3.23	0.583	...	-0.23	12.297	12.193	11.996
TW CMa	0.8448	141.26	2.03	0.357	-0.51 ^b	...	12.430	12.338	12.258
V Cen	0.7399	141.25	3.32	0.289	-0.05 ^a	+0.20	8.909	9.316	9.638
AZ Cen	0.5068	140.85	5.30	0.160	...	-0.23	10.981	11.001	10.940
BB Cen	0.6018	232.05	-3.82	0.396	...	-0.20	12.038	11.933	11.816
KK Cen	1.0857	226.01	0.28	0.642	...	-0.12	14.300	14.052	13.968
KN Cen	1.5319	231.15	-1.10	0.788	12.773	12.740	12.698
TX Cen	1.2328	239.23	-4.20	1.058	...	+0.14	13.213	13.060	12.886
UZ Cen	0.5230	227.21	-2.37	0.275	...	-0.16	11.042	11.025	10.892
VW Cen	1.1771	229.12	0.12	0.448	+0.05 ^a	...	13.075	13.018	12.966
XX Cen	1.0395	227.56	-3.26	0.260	+0.04 ^a	...	11.162	11.194	11.170
V339 Cen	0.9762	239.86	-4.44	0.428	...	-0.10	11.593	11.452	11.339
V381 Cen	0.7058	239.91	-4.92	0.205	...	-0.07	10.529	10.523	10.465
V419 Cen	0.7409	235.38	-3.46	0.176	...	-0.15	11.167	11.224	11.099
V496 Cen	0.6458	235.35	-5.07	0.568	...	-0.18	11.632	11.496	11.361
R Cru	0.7654	229.43	-1.46	0.192	...	-0.07	9.834	9.824	9.767
S Cru	0.6711	289.06	0.04	0.163	...	-0.11	9.363	9.343	9.280
T Cru	0.8282	275.25	-12.28	0.193	...	-0.02	9.713	9.637	9.570
X Cru	0.7938	285.69	-0.33	0.286	...	-0.05	11.178	11.110	10.986
AD Cru	0.8060	286.73	1.33	0.680	...	-0.15	12.896	12.686	12.478
AG Cru	0.5840	285.59	-1.76	0.211	...	-0.18	10.676	10.660	10.592
SV Cru	0.8454	284.78	0.16	0.845	...	-0.19	13.775	13.577	13.421
SU Cru	1.1088	299.21	-0.65	10.737	10.531	10.471
VW Cru	0.7214	287.23	-3.24	0.675	...	-0.11	11.241	11.015	10.869
VX Cru	1.0868	287.29	-2.31	0.957	14.111	13.812	13.666
β Dor	0.9931	286.55	1.21	0.044	-0.01 ^a	...	7.621	7.638	7.624
W Gem	0.8984	288.20	0.01	0.283	+0.04 ^a	+0.05	10.182	10.125	10.065
DX Gem	0.4966	289.30	-1.18	0.451	-0.02 ^g	-0.00	12.486	12.385	12.282
FW Lup	-0.3150	331.33	13.47	9.160	9.237	9.074
GH Lup	0.9675	291.29	-4.88	0.364	+0.03 ^a	-0.04	10.379	10.358	10.318
T Mon	1.4318	291.42	-3.86	0.209	+0.11 ^a	-0.08	10.660	10.629	10.599
AC Mon	0.9039	290.30	-0.77	0.508	-0.07 ^c	-0.13	12.636	12.459	12.336
CS Mon	0.8281	285.58	-1.39	0.528	...	-0.10	13.401	13.252	13.109
CV Mon	0.7307	285.77	-3.30	0.714	-0.04 ^a	...	11.227	11.236	11.190
EK Mon	0.5975	289.38	-1.59	0.584	-0.10 ^e	-0.19	12.571	12.409	12.208
SV Mon	1.1828	289.44	-0.39	0.249	-0.03 ^c	+0.07	12.200	12.207	12.067
TX Mon	0.9396	283.56	-1.29	0.511	-0.14 ^e	-0.26	13.561	13.472	13.392
TZ Mon	0.8709	286.24	-1.73	0.441	-0.03 ^e	-0.06	13.406	13.244	13.119
XX Mon	0.7369	285.67	-0.37	0.596	-0.18 ^e	-0.19	13.863	13.653	13.499
R Mus	0.8757	285.61	0.17	0.120	...	-0.07	9.826	9.827	9.784
S Mus	0.9850	287.63	-2.77	0.147	+0.08 ^a	...	9.591	9.635	9.615
RT Mus	0.4894	289.49	-0.87	0.328	...	-0.29	10.885	10.810	10.712
UU Mus	1.0658	288.80	-0.95	0.413	+0.05 ^a	...	12.658	12.666	12.632
S Nor	0.9892	290.09	1.47	0.189	+0.01 ^a	...	9.817	9.821	9.787
U Nor	1.1019	285.01	-4.32	0.892	+0.10 ^a	...	10.830	10.828	10.787

Continue ...

Name	Log(P)	l	b	E(B-V)	$[Fe/H]_{spec}$	$[Fe/H]_{phot}$	DM_J	DM_H	DM_K
GU Nor	0.5382	285.82	-3.49	0.684	...	-0.12	11.474	11.334	11.189
IQ Nor	0.9159	288.01	-2.09	0.672	...	+0.06	11.815	11.604	11.463
RS Nor	0.7923	286.93	0.59	0.580	...	-0.09	11.991	11.834	11.691
SY Nor	1.1019	288.41	-1.30	0.794	...	-0.29	12.273	12.073	11.925
TW Nor	1.0329	287.78	0.69	1.338	+0.03 ^a	...	11.875	11.869	11.838
Y Oph	1.2337	288.72	-0.37	0.655	+0.05 ^a	-0.17	8.881	8.959	8.957
BF Oph	0.6093	289.88	-0.96	0.247	+0.00 ^f	-0.20	9.533	9.567	9.534
GQ Ori	0.9353	289.61	-0.12	0.279	-0.03 ^c	...	11.821	11.695	11.671
RS Ori	0.8789	290.53	-2.09	0.389	-0.15 ^a	-0.07	11.287	11.173	11.124
X Pup	1.4143	290.92	-0.36	0.443	-0.04 ^a	...	12.408	12.405	12.377
AD Pup	1.1333	291.09	0.57	0.330	-0.20 ^b	-0.17	13.461	13.433	13.318
AP Pup	0.7062	288.40	0.32	0.208	-0.07 ^a	+0.02	10.176	10.145	10.085
AT Pup	0.8238	290.94	-0.25	0.183	-0.22 ^b	-0.06	11.158	11.136	11.079
BN Pup	1.1359	290.26	2.54	0.438	+0.01 ^a	-0.17	12.972	12.979	12.954
HW Pup	1.1289	289.16	-1.83	0.723	-0.29 ^e	-0.27	15.061	14.874	14.724
RS Pup	1.6169	289.14	0.36	0.446	+0.17 ^a	...	11.241	11.241	11.223
VW Pup	0.6320	281.57	-3.06	0.514	-0.19 ^e	-0.12	13.168	12.979	12.882
VZ Pup	1.3649	285.74	-1.95	0.471	-0.16 ^a	-0.24	13.413	13.454	13.441
WW Pup	0.7417	290.11	-0.48	0.398	-0.18 ^e	-0.08	13.191	13.136	13.042
WX Pup	0.9512	285.28	-1.80	0.319	-0.15 ^b	-0.06	12.294	12.215	12.139
WY Pup	0.7202	287.67	-2.25	0.270	...	-0.14	13.375	13.348	13.263
S Sge	0.9234	288.19	-0.75	0.127	+0.10 ^c	...	9.255	9.263	9.228
U Sgr	0.8290	290.07	-4.40	0.403	+0.03 ^a	+0.19	8.953	8.991	8.971
W Sgr	0.8805	289.11	-0.84	0.111	-0.01 ^a	-0.13	8.180	8.189	8.149
X Sgr	0.8459	298.34	-0.94	0.197	+0.02 ^f	...	7.795	7.786	7.731
Y Sgr	0.7614	291.35	-3.92	0.205	+0.06 ^c	...	8.629	8.597	8.521
AP Sgr	0.7040	291.47	-1.11	0.192	9.728	9.707	9.639
AV Sgr	1.1879	286.86	-8.91	1.267	+0.34 ^d	-0.23	12.784	12.349	12.073
AY Sgr	0.8175	283.20	-7.00	0.919	...	-0.28	11.897	11.646	11.361
BB Sgr	0.8220	114.47	0.78	0.284	+0.08 ^f	...	9.558	9.583	9.549
VY Sgr	1.1322	129.03	-4.57	1.283	+0.26 ^d	-0.12	12.887	12.465	12.203
WZ Sgr	1.3394	115.29	-3.25	0.467	+0.00 ^a	-0.02	11.362	11.309	11.257
YZ Sgr	0.9802	133.47	8.52	0.292	+0.05 ^c	...	10.776	10.743	10.547
V1833 Sgr	1.6890	1.33	-6.77	16.895	16.848	16.802
RV Sco	0.7826	109.67	-1.61	0.342	+0.10 ^f	+0.32	9.710	9.643	9.557
RY Sco	1.3079	118.19	-4.11	0.777	+0.09 ^f	...	10.595	10.649	10.633
V470 Sco	1.2112	134.84	-1.18	1.517	12.011	11.656	11.408
V482 Sco	0.6559	118.93	-11.40	0.360	...	-0.10	10.205	10.130	10.036
V500 Sco	0.9693	125.49	-1.55	0.599	-0.02 ^c	-0.04	11.258	11.085	10.956
V636 Sco	0.8323	130.36	-2.12	0.217	...	-0.03	9.693	9.647	9.575
X Sct	0.6230	124.63	-1.07	0.619	...	-0.25	11.591	11.429	11.278
Y Sct	1.0146	122.74	-2.74	0.823	...	-0.05	11.833	11.600	11.429
Z Sct	1.1106	120.87	0.11	0.542	+0.29 ^f	+0.28	12.679	12.565	12.434
CK Sct	0.8701	120.13	1.50	0.795	...	-0.07	12.256	12.091	11.861
EV Sct	0.4901	125.85	-1.11	0.679	-0.37 ^a	-0.18	10.847	10.902	10.889
RU Sct	1.2945	127.94	2.58	0.957	...	-0.53	11.433	11.469	11.462

Continue ...

Name	Log(P)	l	b	E(B-V)	$[Fe/H]_{spec}$	$[Fe/H]_{phot}$	DM_J	DM_H	DM_K
SS Sct	0.5648	118.00	-0.96	0.337	+0.06 ^f	-0.04	10.259	10.194	10.099
TY Sct	1.0435	118.41	-1.56	1.014	...	-0.07	12.650	12.448	12.219
UZ Sct	1.1686	125.37	2.84	1.071	+0.33 ^d	...	13.332	13.021	12.815
R Tra	0.5301	127.40	-0.25	0.127	...	-0.18	9.089	9.078	9.016
S Tra	0.8010	129.55	-0.73	0.100	...	-0.04	9.708	9.704	9.655
T Vel	0.6665	115.48	1.10	0.281	...	-0.24	10.203	10.215	10.175
V Vel	0.6406	116.56	-1.00	0.209	-0.02 ^a	-0.19	10.202	10.177	10.115
AE Vel	0.8533	116.56	-1.00	0.667	-0.30 ^b	-0.10	12.424	12.250	12.089
AH Vel	0.6261	116.58	-0.99	0.074	...	-0.16	8.703	8.770	8.735
AP Vel	0.4952	116.85	-1.31	0.515	-0.06/-0.03 ^b	...	11.553	11.399	11.280
AX Vel	0.5650	112.90	1.64	0.224	...	-0.24	10.529	10.610	10.593
BG Vel	0.8403	119.40	0.52	0.448	-0.07 ^a	+0.08	10.220	10.108	10.000
CP Vel	0.9931	113.87	1.96	0.917	-0.10 ^b	...	14.580	14.319	14.110
CX Vel	0.7963	114.70	0.67	0.759	...	-0.14	12.953	12.732	12.548
DD Vel	1.1204	271.51	-1.38	+0.22	14.956	14.636	14.448
DR Vel	1.0492	116.78	0.49	0.685	...	-0.02	12.052	11.846	11.699
EX Vel	1.1217	136.04	1.51	0.814	-0.01 ^b	...	14.058	13.773	13.672
EZ Vel	1.5383	120.27	-2.55	0.822	...	-0.31	15.522	15.398	15.220
FG Vel	0.8098	113.30	-2.07	0.851	...	-0.45	13.230	13.004	12.828
RZ Vel	1.3096	113.78	-2.21	0.335	...	-0.16	10.972	10.982	10.949
RY Vel	1.4493	117.21	-0.42	0.562	-0.07 ^a	...	11.927	11.971	11.950
ST Vel	0.7678	117.78	-6.25	0.503	-0.03 ^a	-0.15	11.836	11.645	11.513
SV Vel	1.1491	118.75	-1.80	0.392	...	-0.11	12.154	12.078	11.985
SW Vel	1.3700	121.23	-0.55	0.349	...	-0.28	12.075	12.085	12.055
SX Vel	0.9800	132.93	-2.07	0.250	-0.05 ^a	...	11.533	11.587	11.566
XX Vel	0.8441	134.40	-0.15	0.572	-0.03 ^a	...	13.072	12.914	12.788

Table A.2: Physical parameters of the 12 Walraven type II Cepheids.

Name	Log(P)	l	b	E(B-V)	[Fe/H]	DM_J	DM_H	DM_K
T Ant	0.7707	264.54	+11.12	12.505	12.512	12.469
EV Aql	1.5885	47.96	+3.44	16.134	15.913	15.812
KL Aql	0.7859	55.09	-7.60	13.105	13.044	12.978
PP Aql	1.3804	51.33	-7.45	15.439	15.360	15.316
PZ Aql	0.9422	30.88	-2.31	13.773	13.675	13.494
AB Ara	0.7751	330.29	-7.27	15.570	15.472	15.409
TX Del	0.7900	50.96	-24.26	...	+0.24 ^c	12.263	12.440	12.407
UY Eri	0.3450	193.34	-52.63	13.469	13.488	13.420
κ Pav	0.9588	328.29	-25.39	8.366	8.299	8.195
CE Pup	1.6949	259.22	-4.42	...	-0.40 ^h	15.909	15.703	15.571
CO Pup	1.2046	250.44	+4.52	14.473	14.402	14.347
EN TrA	1.5628	313.90	-8.68	14.230	14.097	13.551

Table A.3: Mean VBLUW magnitudes of the 161 type I Cepheids.

Name	V	σ_V	B	σ_B	L	σ_L	U	σ_U	W	σ_W
U Aql	0.141	0.019	-0.285	0.029	-0.682	0.039	-0.890	0.042	-1.245	0.039
η Aql	1.160	0.014	0.829	0.022	0.460	0.032	0.283	0.027	-0.028	0.017
FF Aql	0.584	0.015	0.281	0.018	-0.031	0.022	-0.273	0.017	-0.596	0.025
FM Aql	-0.613	0.013	-1.174	0.019	-1.607	0.027	-1.831	0.024	-2.252	0.046
FN Aql	-0.659	0.009	-1.189	0.012	-1.635	0.019	-1.836	0.018	-2.286	0.031
SZ Aql	-0.764	0.016	-1.399	0.025	-1.918	0.035	-2.147	0.035	-2.431	0.074
TT Aql	-0.163	0.018	-0.742	0.027	-1.233	0.039	-1.429	0.035	-1.881	0.032
V336 Aql	-1.234	0.017	-1.801	0.023	-2.251	0.030	-2.486	0.041	-2.745	0.082
V496 Aql	-0.387	0.007	-0.863	0.010	-1.304	0.014	-1.487	0.014	-1.864	0.017
V600 Aql	-1.312	0.012	-1.962	0.019	-2.431	0.035	-2.720	0.035	-2.985	0.143
I Car	1.219	0.004	0.639	0.007	0.090	0.007	-0.027	0.010	-0.429	0.012
U Car	0.175	0.046	-0.363	0.082	-0.857	0.118	-1.027	0.071	-1.456	0.073
V Car	-0.218	0.008	-0.564	0.013	-0.918	0.018	-1.106	0.024	-1.446	0.020
Y Car	-0.530	0.039	-0.784	0.055	-1.059	0.069	-1.277	0.055	-1.530	0.057
AQ Car	-0.819	0.026	-1.214	0.037	-1.617	0.057	-1.766	0.039	-2.131	0.059
CC Car	-2.112	0.263	-2.628	0.430	-2.909	0.552	-3.158	0.397
CN Car	-1.576	0.011	-2.048	0.016	-2.458	0.024	-2.648	0.028	-2.861	0.065
CR Car	-1.910	0.016	-2.435	0.023	-2.858	0.033	-3.040	0.035	-3.299	0.120
DY Car	-1.822	0.011	-2.225	0.013	-2.583	0.023	-2.803	0.022	-3.030	0.201
ER Car	-0.006	0.019	-0.367	0.026	-0.736	0.032	-0.887	0.061	-1.216	0.071
FI Car	-1.933	0.022	-2.596	0.026	-3.127	0.069	-3.193	0.105
FN Car	-1.906	0.020	-2.371	0.028	-2.732	0.046	-3.019	0.054	-3.233	0.203
FO Car	-1.584	0.013	-2.110	0.017	-2.542	0.022	-2.720	0.026	-2.912	0.126
FQ Car	-2.038	0.017	-2.708	0.028	-3.208	0.064	-3.511	0.083
FR Car	-1.156	0.006	-1.636	0.009	-2.090	0.016	-2.286	0.019	-2.485	0.056
GH Car	-0.949	0.004	-1.331	0.005	-1.669	0.008	-1.908	0.006	-2.277	0.029
GX Car	-1.035	0.016	-1.478	0.023	-1.868	0.037	-2.081	0.043	-2.459	0.050
GZ Car	-1.377	0.022	-1.781	0.033	-2.132	0.047	-2.356	0.026	-2.660	0.056
IT Car	-0.521	0.019	-0.930	0.020	-1.333	0.026	-1.492	0.025	-1.835	0.048
SX Car	-0.935	0.010	-1.313	0.010	-1.665	0.012	-1.875	0.014	-2.209	0.022
UW Car	-1.067	0.010	-1.477	0.014	-1.830	0.020	-2.073	0.019	-2.424	0.042
UX Car	-0.606	0.017	-0.881	0.024	-1.170	0.030	-1.371	0.020	-1.671	0.027
UY Car	-0.880	0.016	-1.222	0.023	-1.570	0.035	-1.752	0.026	-2.090	0.033
VY Car	-0.285	0.021	-0.807	0.032	-1.282	0.046	-1.483	0.034	-1.856	0.042
WW Car	-1.196	0.020	-1.579	0.027	-1.908	0.045	-2.133	0.025	-2.331	0.071
WZ Car	-1.000	0.028	-1.506	0.040	-1.957	0.052	-2.181	0.041	-2.362	0.068
XX Car	-1.017	0.042	-1.463	0.060	-1.858	0.080	-2.111	0.047	-2.340	0.098
XY Car	-1.032	0.028	-1.550	0.041	-2.013	0.062	-2.205	0.047	-2.482	0.137
XZ Car	-0.749	0.020	-1.298	0.028	-1.768	0.037	-1.975	0.036	-2.361	0.036
YZ Car	-0.794	0.024	-1.281	0.034	-1.693	0.045	-1.927	0.038	-2.314	0.038
RW CMa	-1.743	0.010	-2.269	0.017	-2.705	0.033	-2.912	0.026	-3.200	0.136
RY CMa	-0.521	0.010	-0.881	0.014	-1.231	0.016	-1.433	0.013	-1.770	0.031
RZ CMa	-1.162	0.007	-1.595	0.007	-1.936	0.009	-2.150	0.014	-2.484	0.042

Continue ...

Name	V	σ_V	B	σ_B	L	σ_L	U	σ_U	W	σ_W
SS CMa	-1.269	0.012	-1.803	0.018	-2.238	0.028	-2.467	0.025	-2.907	0.074
TV CMa	-1.537	0.013	-2.051	0.019	-2.438	0.036	-2.686	0.037	-2.973	0.158
TW CMa	-1.109	0.010	-1.518	0.015	-1.881	0.023	-2.089	0.028	-2.448	0.037
V Cen	-0.030	0.013	-0.410	0.020	-0.764	0.028	-0.958	0.020	-1.313	0.023
AZ Cen	-0.729	0.006	-0.998	0.006	-1.278	0.007	-1.511	0.008	-1.808	0.013
BB Cen	-1.307	0.004	-1.702	0.004	-2.054	0.006	-2.302	0.009	-2.583	0.035
KK Cen	-1.874	0.006	-2.420	0.010	-2.869	0.024	-3.000	0.042	-3.292	0.100
KN Cen	-1.234	0.011	-1.899	0.015	-2.335	0.028	-2.550	0.081	-2.809	0.025
TX Cen	-1.524	0.010	-2.287	0.016	-2.832	0.038	-2.968	0.070
UZ Cen	-0.790	0.032	-1.100	0.046	-1.408	0.056	-1.619	0.037	-1.904	0.042
VW Cen	-1.389	0.009	-1.975	0.016	-2.520	0.024	-2.692	0.026	-2.880	0.074
XX Cen	-0.442	0.017	-0.889	0.023	-1.284	0.032	-1.479	0.028	-1.856	0.028
V339 Cen	-0.797	0.016	-1.316	0.024	-1.763	0.035	-1.953	0.024	-2.358	0.047
V381 Cen	-0.378	0.023	-0.737	0.033	-1.088	0.042	-1.256	0.026	-1.589	0.033
V419 Cen	-0.557	0.003	-0.874	0.004	-1.193	0.005	-1.401	0.006	-1.730	0.016
V496 Cen	-1.286	0.022	-1.793	0.030	-2.191	0.048	-2.412	0.031	-2.734	0.101
R Cru	0.011	0.014	-0.324	0.020	-0.668	0.029	-0.835	0.024	-1.165	0.044
S Cru	0.071	0.023	-0.259	0.034	-0.599	0.041	-0.765	0.029	-1.098	0.039
T Cru	0.089	0.009	-0.291	0.013	-0.678	0.019	-0.830	0.025	-1.174	0.029
X Cru	-0.663	0.035	-1.088	0.044	-1.492	0.060	-1.661	0.045	-1.998	0.062
AD Cru	-1.721	0.021	-2.265	0.032	-2.714	0.060	-2.980	0.059	-3.279	0.131
AG Cru	-0.577	0.005	-0.890	0.007	-1.200	0.011	-1.418	0.011	-1.726	0.045
SV Cru	-2.144	0.006	-2.740	0.011	-3.181	0.047	-3.382	0.070
SU Cru	-1.218	0.013	-1.983	0.024	-2.512	0.046	-2.832	0.038	-3.085	0.091
VW Cru	-1.143	0.009	-1.700	0.014	-2.149	0.020	-2.405	0.019	-2.777	0.083
VX Cru	-2.103	0.012	-2.810	0.022	-3.139	0.096	-3.463	0.087
β Dor	1.230	0.016	0.971	0.014	0.520	0.021	0.383	0.015	0.044	0.022
W Gem	-0.073	0.023	-0.462	0.035	-0.838	0.051	-1.038	0.045	-1.393	0.045
DX Gem	-1.578	0.009	-1.971	0.012	-2.304	0.021	-2.562	0.017	-2.882	0.166
FW Lup	-0.871	0.006	-1.056	0.008	-1.277	0.010	-1.497	0.010	-1.712	0.015
GH Lup	-0.340	0.004	-0.846	0.005	-1.314	0.006	-1.487	0.011	-1.875	0.017
T Mon	0.262	0.009	-0.246	0.013	-0.744	0.018	-0.891	0.025	-1.242	0.029
AC Mon	-1.319	0.009	-1.828	0.013	-2.248	0.020	-2.473	0.019	-2.751	0.048
CS Mon	-1.678	0.010	-2.165	0.014	-2.571	0.029	-2.783	0.044	-3.061	0.121
CV Mon	-1.397	0.014	-1.951	0.023	-2.356	0.032	-2.634	0.033	-2.888	0.103
EK Mon	-1.702	0.017	-2.193	0.019	-2.580	0.037	-2.830	0.040	-3.084	0.089
SV Mon	-0.613	0.023	-1.093	0.034	-1.561	0.050	-1.723	0.049	-2.133	0.065
TX Mon	-1.678	0.020	-2.164	0.029	-2.551	0.042	-2.772	0.036	-2.962	0.065
TZ Mon	-1.601	0.010	-2.087	0.014	-2.512	0.024	-2.718	0.025	-3.009	0.096
XX Mon	-2.050	0.011	-2.543	0.014	-2.931	0.033	-3.161	0.035	-3.447	0.182
R Mus	0.195	0.006	-0.129	0.008	-0.472	0.011	-0.663	0.014	-0.969	0.036
S Mus	0.272	0.013	-0.074	0.018	-0.390	0.021	-0.555	0.017	-0.785	0.025
RT Mus	-0.900	0.018	-1.261	0.024	-1.566	0.028	-1.792	0.017	-2.118	0.046
UU Mus	-1.204	0.008	-1.695	0.010	-2.134	0.014	-2.340	0.028	-2.653	0.056
S Nor	0.154	0.013	-0.235	0.019	-0.628	0.027	-0.811	0.020	-1.157	0.026
U Nor	-1.011	0.008	-1.731	0.012	-2.207	0.018	-2.493	0.022	-2.791	0.061

Continue ...

Name	V	σ_V	B	σ_B	L	σ_L	U	σ_U	W	σ_W
GU Nor	-1.456	0.007	-1.999	0.008	-2.426	0.013	-2.665	0.012	-2.943	0.067
IQ Nor	-1.213	0.010	-2.000	0.017	-2.559	0.022	-2.682	0.029	-3.111	0.061
RS Nor	-1.323	0.014	-1.880	0.021	-2.344	0.036	-2.571	0.030	-2.882	0.142
SY Nor	-1.106	0.013	-1.687	0.017	-2.075	0.020	-2.266	0.018	-2.570	0.030
TW Nor	-1.991	0.371	-2.847	0.602	-3.376	0.808	-3.613	0.584
Y Oph	0.235	0.004	-0.347	0.006	-0.813	0.008	-1.076	0.007	-1.536	0.011
BF Oph	-0.232	0.008	-0.599	0.012	-0.948	0.017	-1.137	0.015	-1.470	0.034
GQ Ori	-0.894	0.577	-1.307	0.863	-1.728	1.719	-1.906	1.698	-2.240	1.698
RS Ori	-0.654	0.009	-1.078	0.012	-1.451	0.016	-1.680	0.014	-2.075	0.036
X Pup	-0.722	0.030	-1.300	0.047	-1.731	0.060	-1.959	0.046	-2.449	0.055
AD Pup	-1.235	0.027	-1.692	0.039	-2.103	0.055	-2.305	0.045	-2.561	0.124
AP Pup	-0.228	0.006	-0.583	0.010	-0.934	0.015	-1.108	0.010	-1.444	0.012
AT Pup	-0.459	0.011	-0.793	0.018	-1.137	0.025	-1.337	0.019	-1.669	0.035
BN Pup	-1.259	0.021	-1.809	0.032	-2.262	0.042	-2.467	0.042	-2.752	0.132
HW Pup	-2.118	0.020	-2.648	0.032	-3.012	0.048	-3.172	0.092
RS Pup	-0.124	0.023	-0.789	0.038	-1.303	0.053	-1.517	0.052	-2.013	0.063
VW Pup	-1.814	0.015	-2.256	0.022	-2.629	0.034	-2.864	0.029	-3.056	0.090
VZ Pup	-1.182	0.017	-1.725	0.027	-2.162	0.037	-2.365	0.028	-2.661	0.079
WW Pup	-1.515	0.034	-1.885	0.049	-2.207	0.068	-2.455	0.052	-2.849	0.080
WX Pup	-0.888	0.010	-1.297	0.014	-1.665	0.018	-1.870	0.028	-2.246	0.055
WY Pup	-1.507	0.011	-1.839	0.016	-2.165	0.021	-2.365	0.018	-2.657	0.041
S Sge	0.029	0.025	-0.445	0.034	-0.846	0.045	-1.055	0.057	-1.442	0.047
U Sgr	0.854	0.024	0.533	0.035	0.186	0.041	0.014	0.052	-0.301	0.042
W Sgr	0.881	0.027	0.557	0.031	0.238	0.033	0.039	0.028	-0.291	0.048
X Sgr	0.402	0.008	0.029	0.013	-0.353	0.020	-0.520	0.017	-0.858	0.020
Y Sgr	-0.074	0.015	-0.430	0.022	-0.766	0.031	-0.966	0.028	-1.295	0.052
AP Sgr	-1.902	0.418	-2.825	0.692	-3.308	0.691	-3.751	0.708
AV Sgr	-1.524	0.019	-2.170	0.031	-2.631	0.054	-2.919	0.042	-3.213	0.147
AY Sgr	-0.058	0.005	-0.463	0.008	-0.871	0.013	-1.044	0.012	-1.411	0.015
BB Sgr	-1.935	0.488	-2.823	0.827	-3.182	0.922	-3.582	0.872
VY Sgr	-0.498	0.028	-0.963	0.042	-1.446	0.054	-1.657	0.048	-2.097	0.042
WZ Sgr	-0.219	0.028	-0.643	0.040	-1.049	0.053	-1.244	0.043	-1.602	0.047
YZ Sgr	-2.313	0.205	-2.916	0.223	-3.547	0.375	-3.681	0.264	-4.313	0.395
V1833 Sgr	0.454	0.084	0.114	0.098	-0.256	0.094	-0.425	0.082	-0.755	0.116
RV Sco	-0.123	0.023	-0.381	0.033	-0.936	0.045	-1.120	0.034	-1.479	0.037
RY Sco	-0.530	0.021	-1.178	0.028	-1.641	0.032	-1.912	0.029	-2.306	0.040
V470 Sco	-1.766	0.392	-2.760	0.649	-3.091	0.664
V482 Sco	-0.466	0.007	-0.871	0.011	-1.244	0.015	-1.447	0.014	-1.817	0.021
V500 Sco	-0.800	0.021	-1.352	0.033	-1.805	0.045	-2.041	0.028	-2.494	0.045
V636 Sco	0.051	0.010	-0.347	0.015	-0.743	0.019	-0.897	0.028	-1.236	0.029
X Sct	-1.283	0.021	-1.756	0.029	-2.121	0.037	-2.408	0.027	-2.656	0.073
Y Sct	-1.154	0.010	-1.819	0.016	-2.319	0.023	-2.600	0.027	-2.888	0.069
Z Sct	-1.145	0.014	-1.723	0.023	-2.232	0.032	-2.442	0.032	-2.673	0.068
CK Sct	-1.547	0.004	-2.239	0.008	-2.750	0.022	-2.992	0.024	-3.270	0.120
EV Sct	-1.351	0.008	-1.831	0.006	-2.193	0.018	-2.489	0.020	-2.814	0.061
RU Sct	-1.121	0.027	-1.896	0.042	-2.387	0.056	-2.749	0.044	-3.007	0.131

Continue ...

Name	V	σ_V	B	σ_B	L	σ_L	U	σ_U	W	σ_W
SS Sct	-0.563	0.005	-0.954	0.008	-1.307	0.010	-1.514	0.007	-1.860	0.015
TY Sct	-1.647	0.377	-2.383	0.594	-2.911	0.884	-3.187	0.673
UZ Sct	-1.834	0.366	-2.641	0.594	-3.020	0.612	-3.355	0.663
R Tra	0.062	0.005	-0.239	0.007	-0.540	0.008	-0.733	0.006	-1.040	0.009
S Tra	0.174	0.010	-0.133	0.014	-0.478	0.019	-0.644	0.017	-0.966	0.035
T Vel	-0.501	0.021	-0.893	0.032	-1.248	0.041	-1.428	0.029	-1.773	0.039
V Vel	-0.316	0.006	-0.639	0.008	-0.951	0.010	-1.153	0.011	-1.487	0.015
AE Vel	-1.417	0.011	-1.962	0.018	-2.375	0.030	-2.645	0.026	-2.889	0.135
AH Vel	0.455	0.006	0.223	0.007	-0.051	0.008	-0.270	0.009	-0.565	0.011
AP Vel	-1.300	0.069	-1.723	0.102	-2.002	0.127	-2.275	0.099	-2.662	0.154
AX Vel	-0.546	0.029	-0.826	0.044	-1.109	0.055	-1.336	0.034	-1.637	0.021
BG Vel	-0.345	0.008	-0.841	0.012	-1.257	0.019	-1.449	0.023	-1.860	0.030
CP Vel	-2.408	0.265	-3.105	0.429	-3.461	0.536
CX Vel	-1.846	0.275	-2.445	0.456	-2.914	0.611	-3.086	0.413
DD Vel	-2.332	0.018	-3.019	0.028	-3.535	0.085	-3.826	0.086
DR Vel	-1.111	0.018	-1.782	0.029	-2.292	0.051	-2.510	0.032	-2.823	0.121
EX Vel	-1.947	0.018	-2.651	0.021	-2.994	0.091	-3.228	0.092
EZ Vel	-2.293	0.438	-3.056	0.661	-3.348	0.928
FG Vel	-2.018	0.006	-2.657	0.009	-3.041	0.031	-3.335	0.038
RZ Vel	-0.159	0.036	-0.702	0.058	-1.159	0.073	-1.345	0.050	-1.804	0.053
RY Vel	-0.696	0.018	-1.307	0.027	-1.752	0.036	-1.998	0.028	-2.473	0.028
ST Vel	-1.179	0.023	-1.694	0.038	-2.119	0.055	-2.335	0.027	-2.592	0.069
SV Vel	-0.726	0.033	-1.199	0.052	-1.613	0.071	-1.846	0.043	-2.086	0.136
SW Vel	-0.557	0.022	-1.102	0.036	-1.531	0.047	-1.733	0.045	-2.221	0.053
SX Vel	-0.600	0.119	-0.969	0.173	-1.321	0.209	-1.538	0.085	-1.903	0.100
XX Vel	-1.561	0.010	-2.055	0.015	-2.490	0.027	-2.706	0.021	-3.066	0.099

Table A.4: Mean VBLUW magnitudes of the 12 type II Cepheids.

Name	V	σ_V	B	σ_B	L	σ_L	U	σ_U	W	σ_W
T Ant	-1.018	0.013	-1.318	0.020	-1.623	0.027	-1.821	0.037	-2.147	0.049
EV Aql	-2.093	0.318	-2.782	0.497	-3.151	0.684	-3.401	0.724
KL Aql	-1.377	0.016	-1.781	0.025	-2.208	0.044	-2.377	0.037	-2.535	0.127
PP Aql	-2.073	0.475	-2.649	0.706	-3.062	0.718	-3.254	0.891
PZ Aql	-1.974	0.009	-2.603	0.013	-3.113	0.036	-3.399	0.042
AB Ara	-2.536	0.295	-2.953	0.463	-3.191	0.520	-3.398	0.518
TX Del	-0.961	0.053	-1.287	0.071	-1.689	0.106	-1.857	0.096	-2.210	0.108
UY Eri	-1.809	0.016	-1.997	0.020	-2.147	0.026	-2.402	0.022	-2.629	0.051
κ Pav	0.971	0.067	0.714	0.090	0.376	0.129	0.160	0.055	-0.140	0.083
CE Pup	-2.056	0.009	-2.812	0.018	-3.412	0.072	-3.328	0.097
CO Pup	-1.642	0.014	-2.070	0.022	-2.555	0.043	-2.697	0.031	-3.119	0.119
EN Tra	-0.759	0.044	-1.054	0.068	-1.350	0.092	-1.612	0.083	-1.937	0.088

Table A.5: Near Infrared Photometry of 161 Galactic Cepheids. For reference sources we indicate LS for Laney & Stobie 1994, transformed into the 2MASS photometric system using Koen et al. 2007; LSnew for new data from SAAO, transformed into the 2MASS photometric system using Koen et al. 2007; vL for van Leeuwen et al., 2007, transformed into the 2MASS photometric system; 2MASS for data from 2MASS catalogue + template and APnew for new data from Campo Imperatore Observatory.

Name	J	σ_J	H	σ_H	K	σ_K	Source
U Aql	4.400	0.010	4.002	0.010	3.844	0.010	LSnew
η Aql	2.388	0.010	2.062	0.010	1.945	0.010	vL
FF Aql	3.985	0.284	3.720	0.240	3.507	0.360	2MASS
FM Aql	5.708	0.010	5.234	0.010	5.041	0.010	vL
FN Aql	6.014	0.010	5.512	0.010	5.337	0.010	LSnew
SZ Aql	5.471	0.010	5.107	0.010	4.988	0.010	LS,APnew
TT Aql	4.685	0.010	4.200	0.010	4.014	0.010	vL
V336 Aql	7.216	0.020	6.652	0.023	6.463	0.030	APnew
V496 Aql	5.564	0.010	5.136	0.010	4.966	0.010	vL
V600 Aql	6.876	0.020	6.443	0.051	6.146	0.030	APnew
<i>l</i> Car	1.586	0.010	1.151	0.010	1.026	0.010	LS
U Car	3.887	0.010	3.533	0.010	3.415	0.010	LS
V Car	5.613	0.010	5.317	0.010	5.219	0.010	LS
Y Car	6.904	0.020	6.666	0.034	6.568	0.023	2MASS
AQ Car	7.138	0.010	6.757	0.010	6.618	0.010	vL
CC Car	9.562	0.025	9.037	0.024	8.824	0.021	2MASS
CN Car	8.328	0.027	7.844	0.034	7.701	0.038	2MASS
CR Car	8.926	0.019	8.262	0.029	8.131	0.023	2MASS
DY Car	9.163	0.033	8.736	0.051	8.570	0.017	2MASS
ER Car	5.360	0.010	5.020	0.010	4.899	0.010	vL
FI Car	8.303	0.029	7.747	0.055	7.453	0.025	2MASS
FN Car	9.096	0.024	8.623	0.069	8.428	0.034	2MASS
FO Car	7.525	0.029	6.616	0.040	6.385	0.027	2MASS
FQ Car	8.451	0.019	7.860	0.027	7.625	0.020	2MASS
FR Car	7.470	0.010	7.012	0.010	6.835	0.010	vL
GH Car	7.216	0.027	6.906	0.065	6.701	0.026	2MASS
GX Car	7.193	0.021	6.763	0.055	6.554	0.024	2MASS
GZ Car	8.165	0.018	7.751	0.042	7.581	0.027	2MASS
IT Car	6.309	0.010	5.924	0.010	5.779	0.010	vL
SX Car	7.220	0.034	6.854	0.031	6.753	0.021	2MASS
UW Car	7.363	0.020	6.950	0.034	6.763	0.018	2MASS
UX Car	6.992	0.010	6.728	0.010	6.620	0.010	vL
UY Car	7.311	0.021	6.927	0.042	6.854	0.026	2MASS
VY Car	5.201	0.010	4.834	0.010	4.713	0.010	LS
WW Car	7.740	0.026	7.347	0.036	7.193	0.024	2MASS
WZ Car	6.639	0.010	6.282	0.010	6.161	0.010	LS
XX Car	7.176	0.010	6.745	0.010	6.566	0.010	vL

Continue ...

Name	J	σ_J	H	σ_H	K	σ_K	Source
XY Car	6.915	0.010	6.419	0.010	6.227	0.010	vL
XZ Car	6.251	0.010	5.759	0.010	5.572	0.010	vL
YZ Car	6.432	0.010	5.985	0.010	5.800	0.010	vL
RW CMa	8.494	0.032	8.000	0.033	7.782	0.024	2MASS
RY CMa	6.396	0.010	6.042	0.010	5.908	0.010	vL,APnew
RZ CMa	7.511	0.020	7.180	0.019	6.929	0.030	APnew
SS CMa	7.370	0.010	6.863	0.010	6.664	0.010	vL
TV CMa	8.026	0.021	7.610	0.023	7.354	0.024	2MASS
TW CMa	7.605	0.010	7.188	0.010	7.040	0.010	vL
V Cen	4.415	0.010	4.505	0.010	4.764	0.010	LS
AZ Cen	7.222	0.010	6.944	0.010	6.831	0.010	vL
BB Cen	7.980	0.029	7.569	0.031	7.395	0.020	2MASS
KK Cen	8.716	0.021	8.123	0.024	7.960	0.027	2MASS
KN Cen	5.782	0.010	5.368	0.010	5.226	0.010	LS
TX Cen	7.165	0.011	6.655	0.031	6.395	0.009	2MASS
UZ Cen	7.232	0.023	6.916	0.027	6.730	0.021	2MASS
VW Cen	7.203	0.010	6.793	0.010	6.658	0.010	LS
XX Cen	5.723	0.010	5.414	0.010	5.313	0.010	LS
V339 Cen	6.354	0.010	5.877	0.010	5.690	0.010	vL
V381 Cen	6.143	0.010	5.822	0.010	5.703	0.010	vL
V419 Cen	6.670	0.026	6.410	0.031	6.222	0.018	2MASS
V496 Cen	7.435	0.027	6.989	0.031	6.796	0.023	2MASS
R Cru	5.260	0.010	4.931	0.010	4.810	0.010	vL
S Cru	5.086	0.010	4.755	0.010	4.632	0.010	vL
T Cru	4.941	0.010	4.541	0.010	4.407	0.010	vL
X Cru	6.514	0.030	6.125	0.049	5.936	0.018	2MASS
AD Cru	8.194	0.023	7.661	0.046	7.388	0.021	2MASS
AG Cru	6.674	0.010	6.353	0.010	6.230	0.010	LSnew
SV Cru	8.948	0.009	8.425	0.027	8.201	0.019	2MASS
SU Cru	5.080	0.010	4.527	0.010	4.387	0.010	LS
VW Cru	6.805	0.026	6.264	0.036	6.056	0.021	2MASS
VX Cru	8.523	0.027	7.879	0.031	7.654	0.025	2MASS
β Dor	2.329	0.010	2.008	0.010	1.920	0.010	LS
W Gem	5.188	0.010	4.802	0.010	4.671	0.010	vL,APnew
DX Gem	8.759	0.020	8.361	0.021	8.207	0.030	APnew
FW Lup	7.992	0.027	7.838	0.038	7.662	0.029	2MASS
GH Lup	5.167	0.010	4.811	0.010	4.698	0.010	LS
T Mon	3.985	0.010	3.581	0.010	3.455	0.010	LS
AC Mon	7.625	0.026	7.118	0.033	6.924	0.017	2MASS
CS Mon	8.629	0.021	8.156	0.051	7.946	0.017	2MASS
CV Mon	6.762	0.010	6.455	0.010	6.347	0.010	LS,2MASS,APnew
EK Mon	8.526	0.037	8.059	0.038	7.802	0.034	2MASS
SV Mon	6.310	0.021	5.964	0.057	5.740	0.016	2MASS
TX Mon	8.437	0.023	8.015	0.040	7.863	0.031	2MASS
TZ Mon	8.499	0.021	8.010	0.038	7.816	0.026	2MASS
XX Mon	9.379	0.027	8.852	0.044	8.635	0.023	2MASS

Continue ...

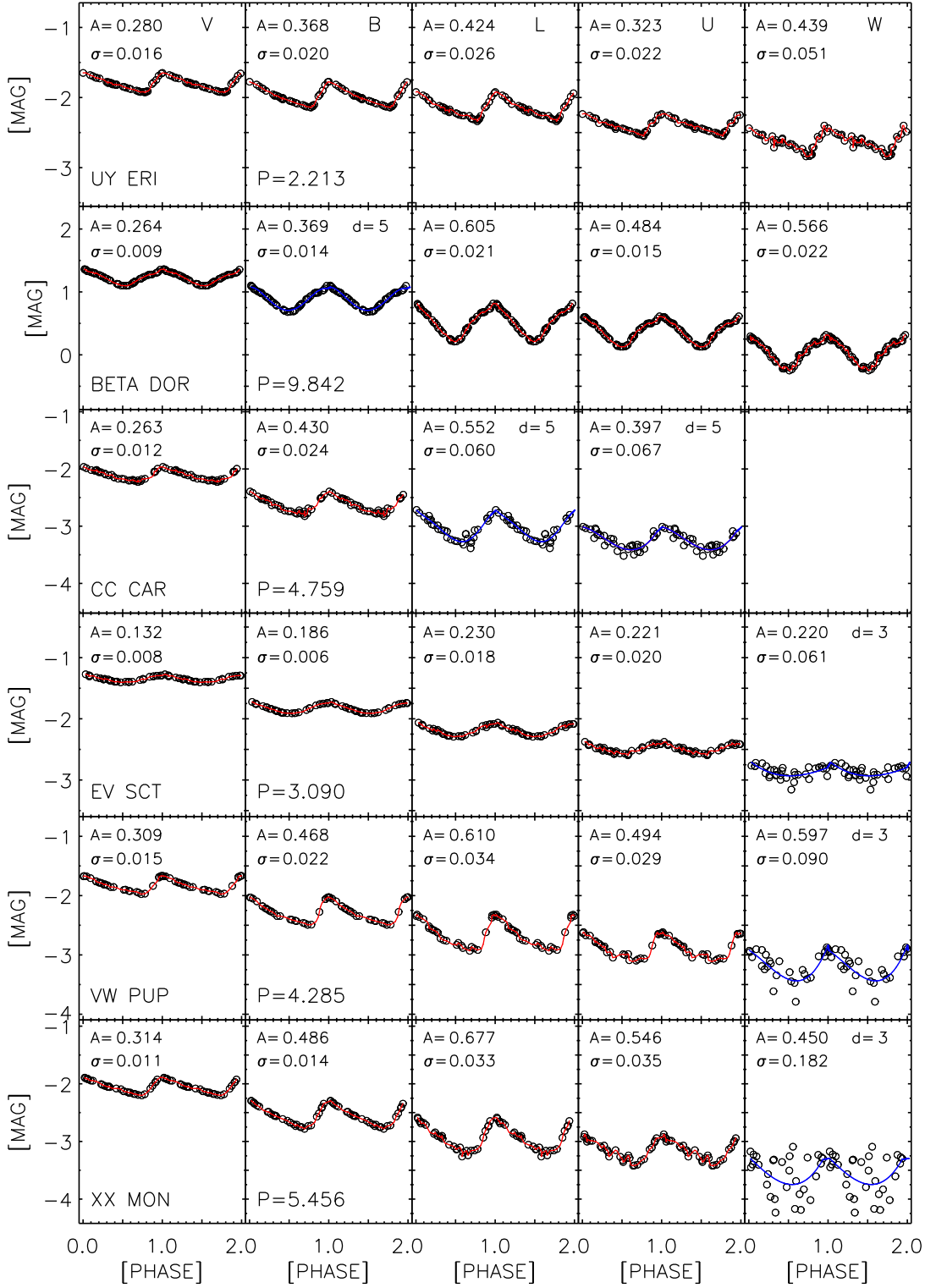
Name	J	σ_J	H	σ_H	K	σ_K	Source
R Mus	4.904	0.010	4.577	0.010	4.465	0.010	vL
S Mus	4.324	0.010	4.032	0.010	3.937	0.010	LS
RT Mus	7.181	0.010	6.809	0.010	6.660	0.010	vL
UU Mus	7.137	0.010	6.801	0.010	6.689	0.010	LS
S Nor	4.537	0.010	4.204	0.010	4.095	0.010	LS
U Nor	5.195	0.010	4.846	0.010	4.726	0.010	LS
GU Nor	7.616	0.019	7.175	0.026	6.977	0.023	2MASS
IQ Nor	6.766	0.023	6.224	0.033	6.012	0.047	2MASS
RS Nor	7.332	0.021	6.854	0.033	6.645	0.018	2MASS
SY Nor	6.638	0.010	6.091	0.010	5.864	0.010	vL
TW Nor	6.457	0.010	6.111	0.010	6.003	0.010	LS
Y Oph	2.830	0.010	2.551	0.010	2.463	0.010	LS,APnew
BF Oph	5.451	0.010	5.179	0.010	5.089	0.010	LS
GQ Ori	6.711	0.021	6.252	0.027	6.156	0.020	2MASS
RS Ori	6.355	0.026	5.913	0.049	5.794	0.026	2MASS,APnew
X Pup	5.788	0.010	5.413	0.010	5.291	0.010	LS
AD Pup	7.727	0.023	7.350	0.044	7.154	0.018	2MASS
AP Pup	5.788	0.010	5.443	0.010	5.322	0.010	vL
AT Pup	6.400	0.010	6.054	0.010	5.930	0.010	vL
BN Pup	7.230	0.010	6.887	0.010	6.781	0.010	LS
HW Pup	9.341	0.023	8.805	0.049	8.574	0.019	2MASS
RS Pup	3.982	0.010	3.594	0.010	3.472	0.010	LS
VW Pup	9.014	0.023	8.517	0.036	8.362	0.029	2MASS
VZ Pup	6.948	0.010	6.622	0.010	6.517	0.010	LS
WW Pup	8.691	0.027	8.319	0.047	8.162	0.026	2MASS
WX Pup	7.134	0.010	6.721	0.010	6.572	0.010	vL
WY Pup	8.943	0.021	8.601	0.038	8.454	0.029	2MASS
S Sge	4.183	0.010	3.859	0.010	3.752	0.010	vL
U Sgr	4.178	0.010	3.892	0.010	3.805	0.010	LS
W Sgr	3.243	0.010	2.923	0.010	2.814	0.010	vL
X Sgr	2.967	0.010	2.632	0.010	2.510	0.010	vL
Y Sgr	4.067	0.010	3.717	0.010	3.577	0.010	vL
AP Sgr	5.347	0.010	5.012	0.010	4.883	0.010	vL
AV Sgr	6.878	0.010	6.089	0.010	5.730	0.010	LSnew
AY Sgr	7.158	0.020	6.584	0.047	6.233	0.030	APnew
BB Sgr	4.805	0.010	4.507	0.010	4.406	0.010	LS,APnew
VY Sgr	7.156	0.010	6.385	0.010	6.042	0.010	LSnew,APnew
WZ Sgr	4.978	0.010	4.559	0.010	4.416	0.010	LS
YZ Sgr	5.524	0.018	5.155	0.076	4.885	0.023	2MASS
V1833 Sgr	9.409	0.018	8.968	0.020	8.814	0.017	2MASS
RV Sco	5.081	0.010	4.694	0.010	4.543	0.010	vL
RY Sco	4.310	0.010	4.001	0.010	3.896	0.010	LS
V470 Sco	6.031	0.021	5.321	0.019	4.988	0.017	2MASS
V482 Sco	5.976	0.010	5.591	0.010	5.438	0.010	vL
V500 Sco	6.041	0.010	5.532	0.010	5.330	0.010	vL
V636 Sco	4.908	0.010	4.537	0.010	4.398	0.010	vL

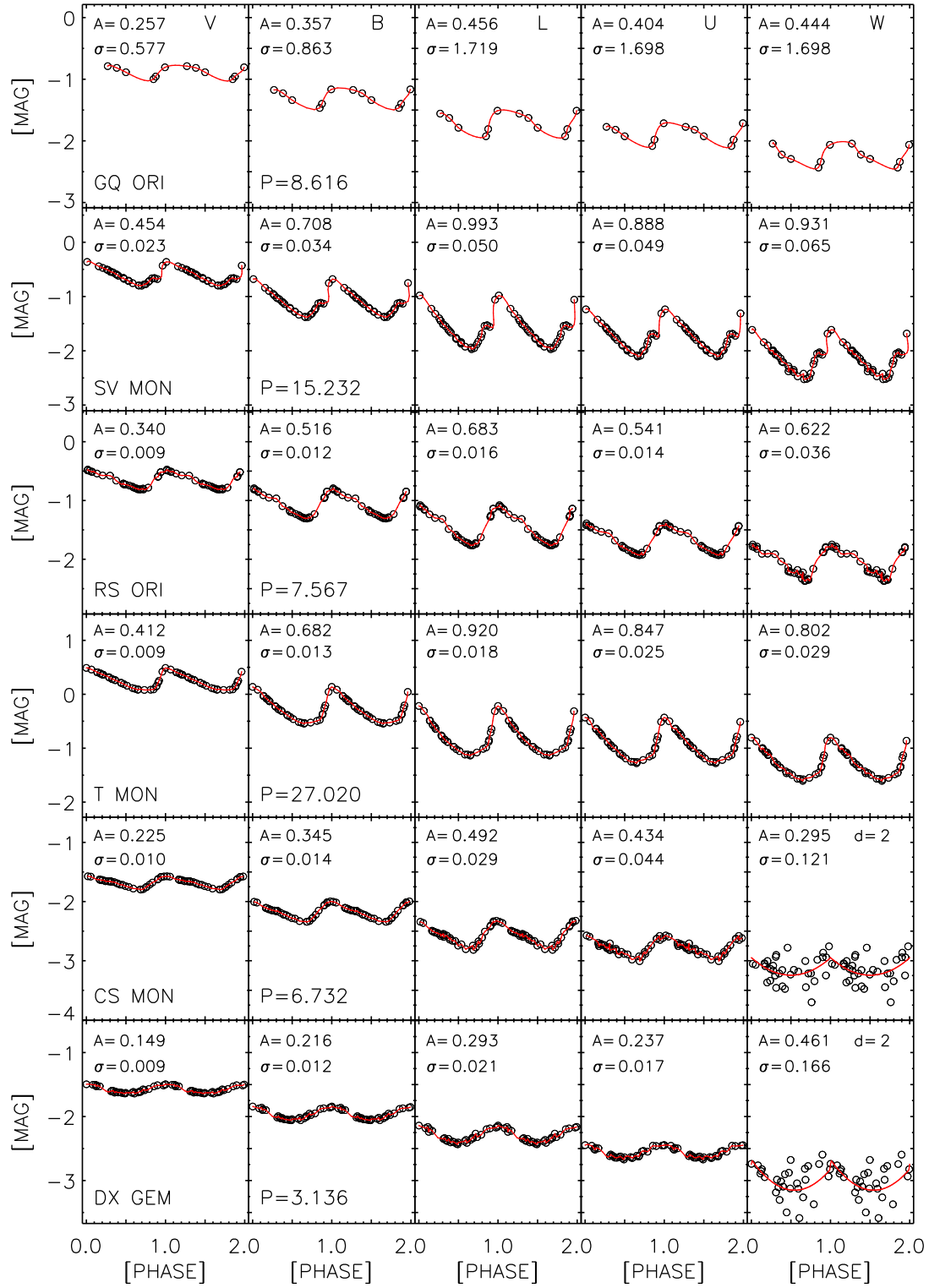
Continue ...

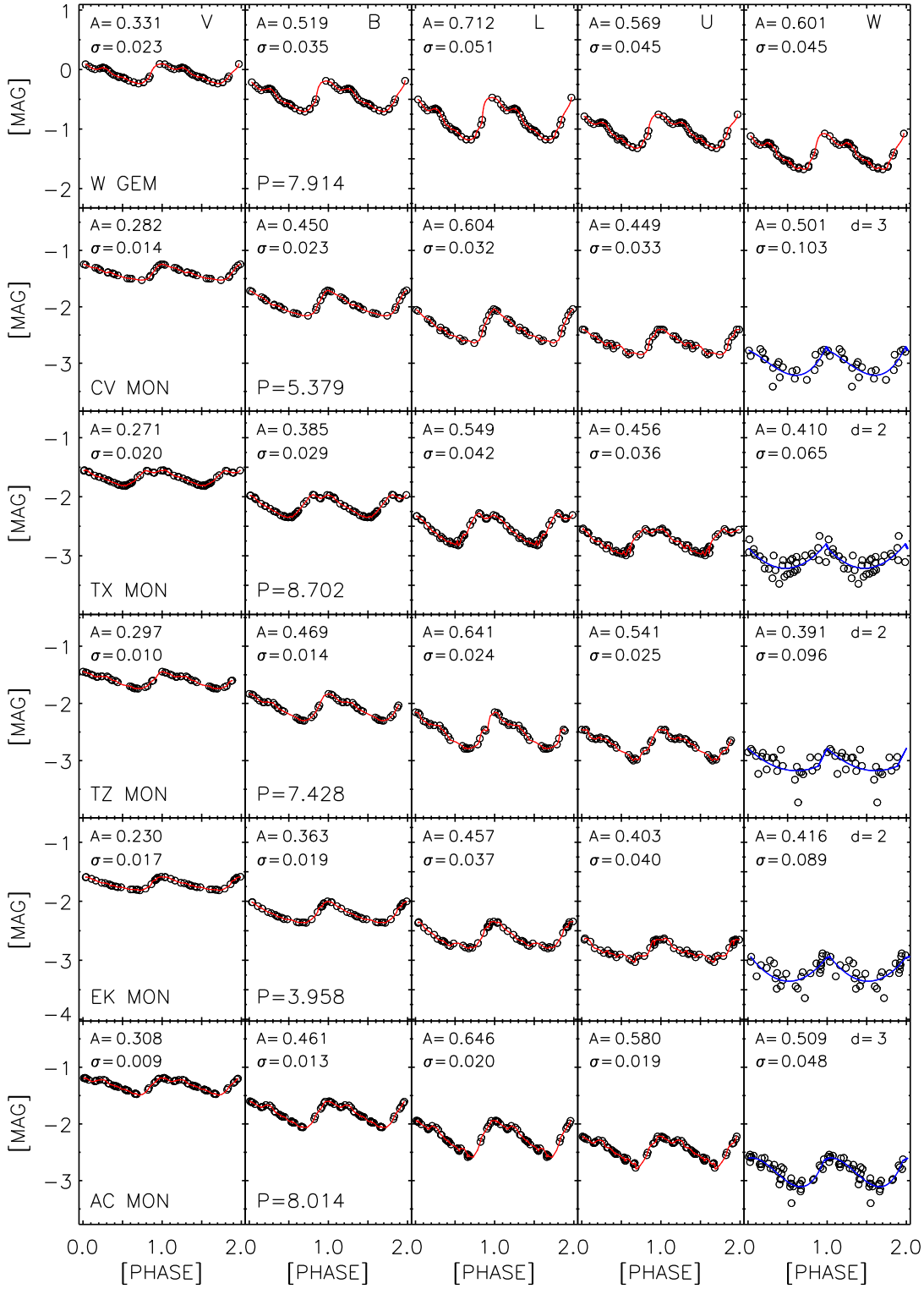
Name	J	σ_J	H	σ_H	K	σ_K	Source
X Sct	7.466	0.030	6.996	0.057	6.788	0.027	2MASS
Y Sct	6.473	0.010	5.901	0.010	5.654	0.010	vL,APnew
Z Sct	7.016	0.024	6.555	0.033	6.344	0.034	2MASS
CK Sct	7.352	0.020	6.859	0.051	6.560	0.030	APnew
EV Sct	7.141	0.010	6.899	0.010	6.835	0.010	LS,APnew
RU Sct	5.190	0.010	4.865	0.010	4.769	0.010	LS,APnew
SS Sct	6.317	0.010	5.949	0.010	5.800	0.010	vL
TY Sct	7.199	0.027	6.655	0.033	6.349	0.021	2MASS
UZ Sct	7.486	0.010	6.824	0.010	6.535	0.010	LSnew
R Tra	5.257	0.010	4.946	0.010	4.831	0.010	vL
S Tra	5.021	0.010	4.696	0.010	4.581	0.010	vL
T Vel	5.941	0.010	5.642	0.010	5.542	0.010	LS
V Vel	6.021	0.010	5.687	0.010	5.567	0.010	LSnew
AE Vel	7.573	0.023	7.072	0.051	6.843	0.027	2MASS
AH Vel	4.568	0.010	4.327	0.010	4.235	0.010	LSnew
AP Vel	7.831	0.026	7.380	0.059	7.209	0.017	2MASS
AX Vel	6.587	0.010	6.365	0.010	6.293	0.010	LS
BG Vel	5.410	0.010	4.972	0.010	4.797	0.010	vL
CP Vel	9.288	0.019	8.689	0.022	8.406	0.018	2MASS
CX Vel	8.281	0.015	7.739	0.041	7.489	0.015	2MASS
DD Vel	9.262	0.024	8.595	0.034	8.326	0.031	2MASS
DR Vel	6.583	0.010	6.035	0.010	5.811	0.010	vL
EX Vel	8.360	0.015	7.727	0.023	7.546	0.033	2MASS
EZ Vel	8.511	0.020	8.005	0.040	7.727	0.031	2MASS
FG Vel	8.516	0.021	7.967	0.049	7.725	0.025	2MASS
RZ Vel	4.682	0.010	4.329	0.010	4.206	0.010	LS
RY Vel	5.196	0.010	4.866	0.010	4.749	0.010	LS
ST Vel	7.254	0.021	6.744	0.044	6.548	0.029	2MASS
SV Vel	6.370	0.010	5.944	0.010	5.769	0.010	vL
SW Vel	5.594	0.010	5.236	0.010	5.114	0.010	LS
SX Vel	6.282	0.010	6.000	0.010	5.905	0.010	LS
XX Vel	8.250	0.035	7.766	0.071	7.573	0.027	2MASS

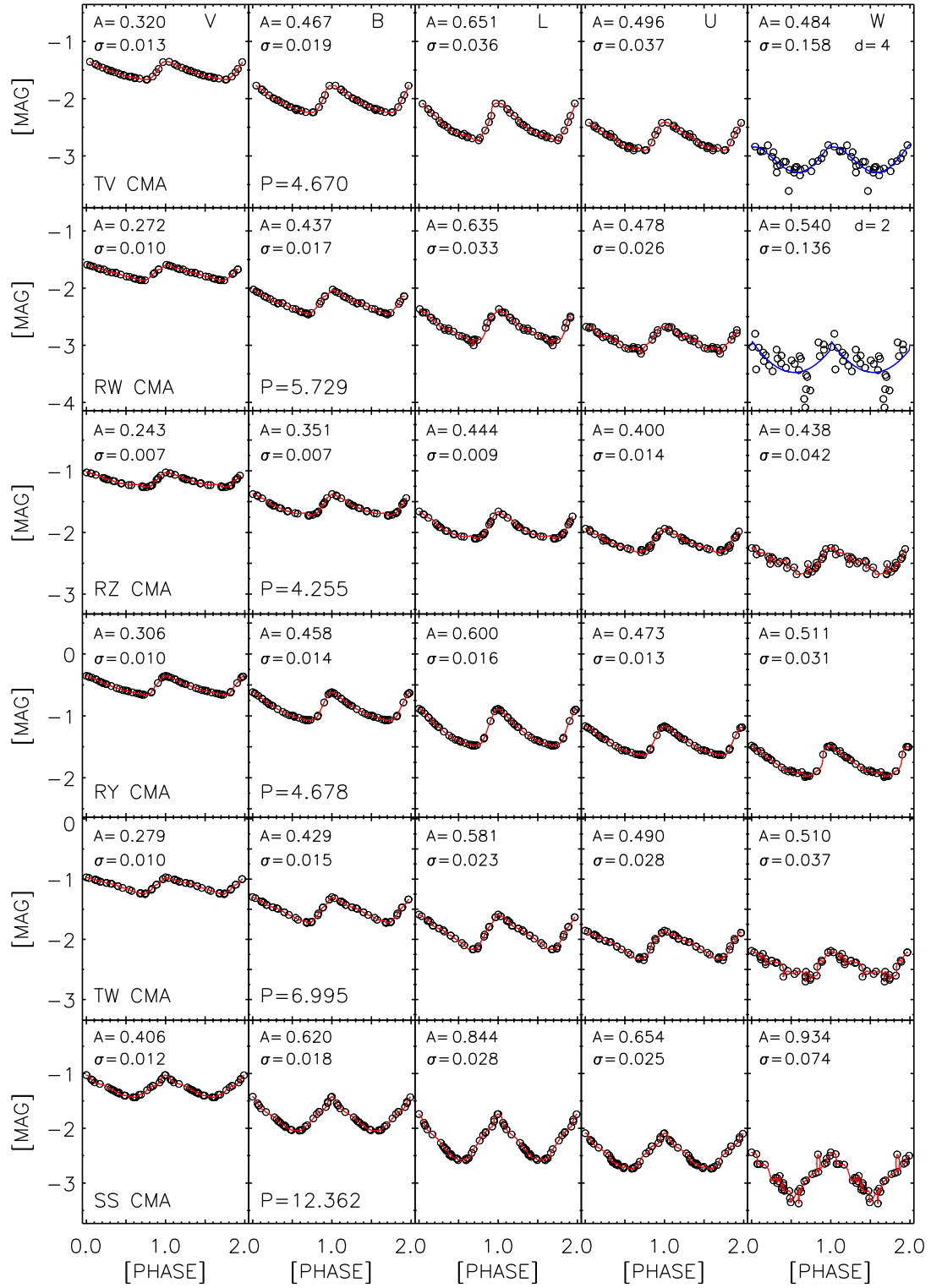
Table A.6: Near Infrared Photometry of 12 type II Cepheids. For reference sources see previous table (A.5).

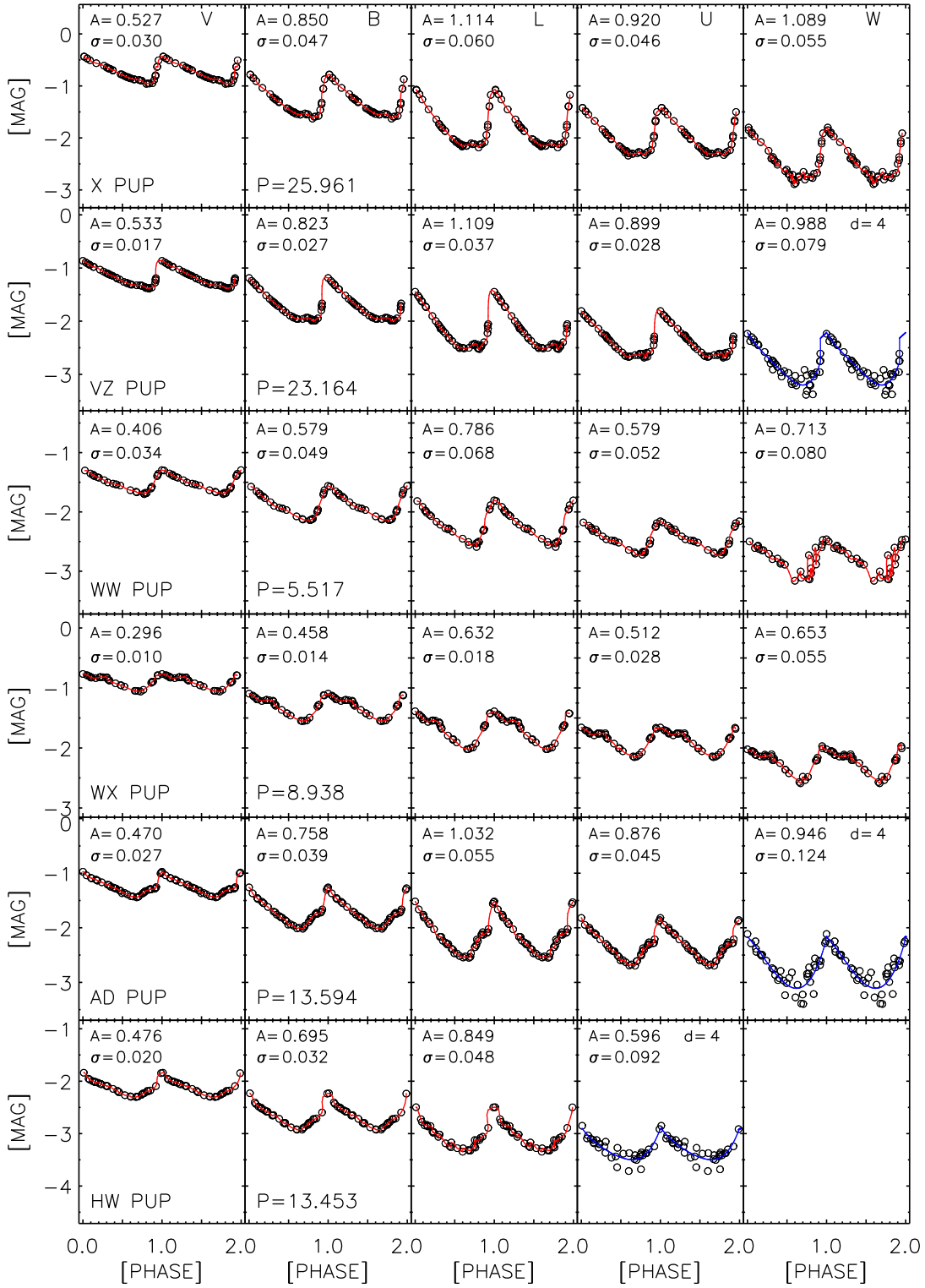
Name	J	σ_J	H	σ_H	K	σ_K	Source
T Ant	7.914	0.010	7.602	0.010	7.494	0.010	LSnew
EV Aql	8.964	0.018	8.358	0.005	8.154	0.017	2MASS
KL Aql	8.466	0.020	8.084	0.034	7.953	0.027	2MASS
PP Aql	8.926	0.021	8.478	0.021	8.341	0.017	2MASS
PZ Aql	8.641	0.011	8.210	0.031	7.957	0.023	2MASS
AB Ara	10.965	0.018	10.547	0.025	10.420	0.019	2MASS
TX Del	7.611	0.035	7.467	0.031	7.369	0.024	2MASS
UY Eri	10.220	0.022	9.954	0.022	9.842	0.019	2MASS
κ Pav	3.182	0.252	2.780	0.200	2.603	0.236	2MASS
CE Pup	8.404	0.011	7.804	0.015	7.564	0.017	2MASS
CO Pup	8.514	0.026	8.088	0.047	7.949	0.036	2MASS
EN Tra	7.141	0.018	6.625	0.029	5.977	0.021	2MASS

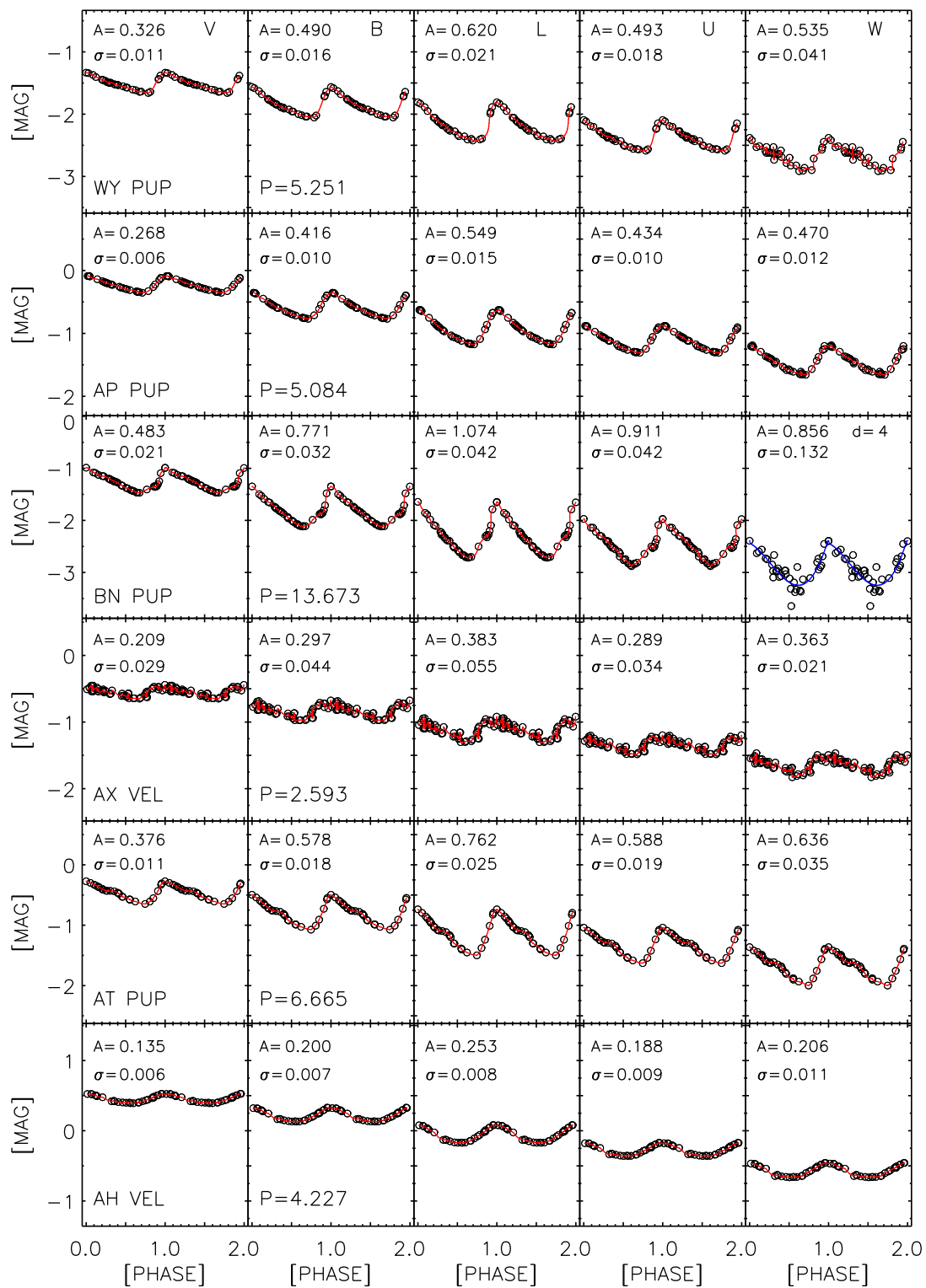


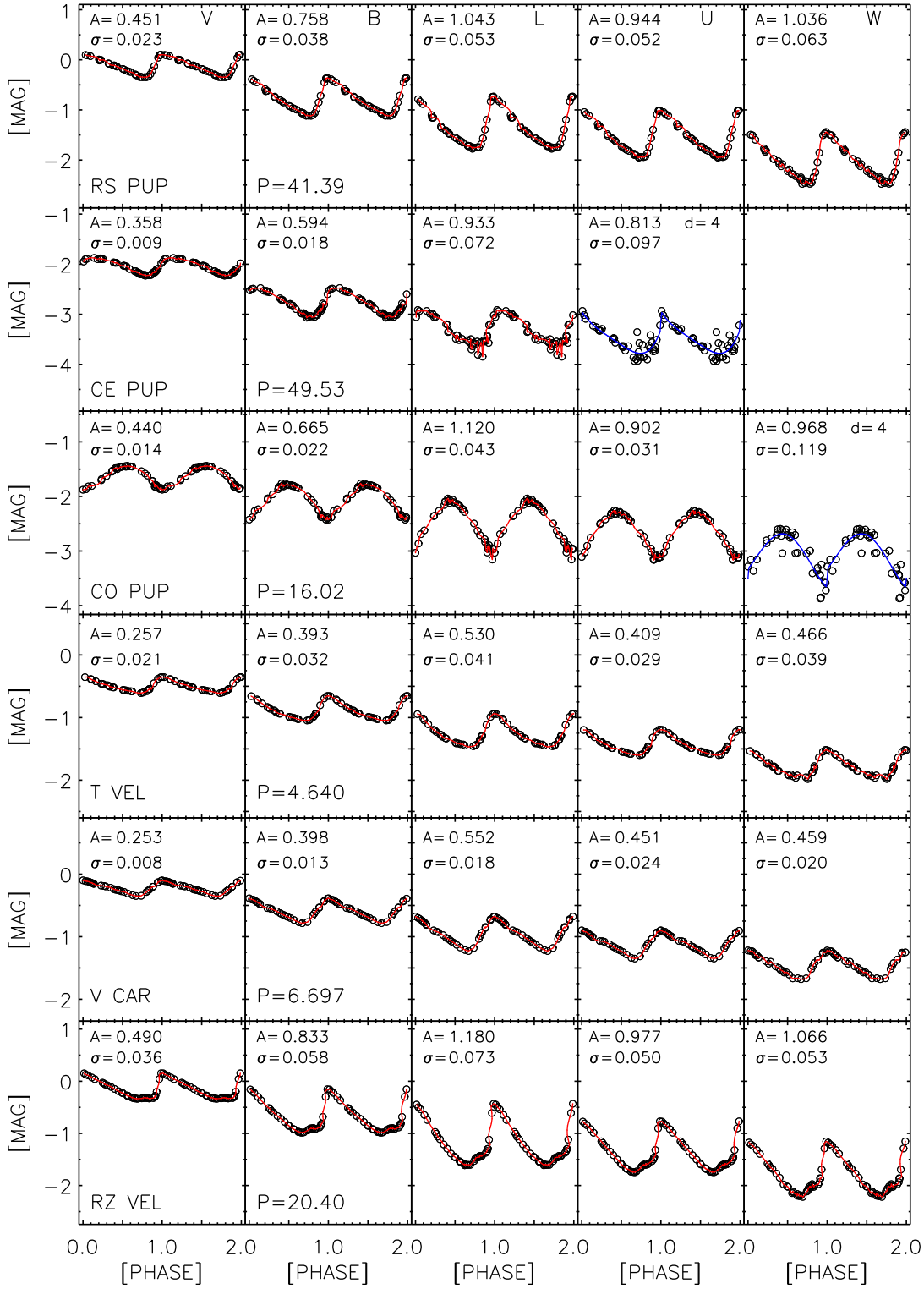


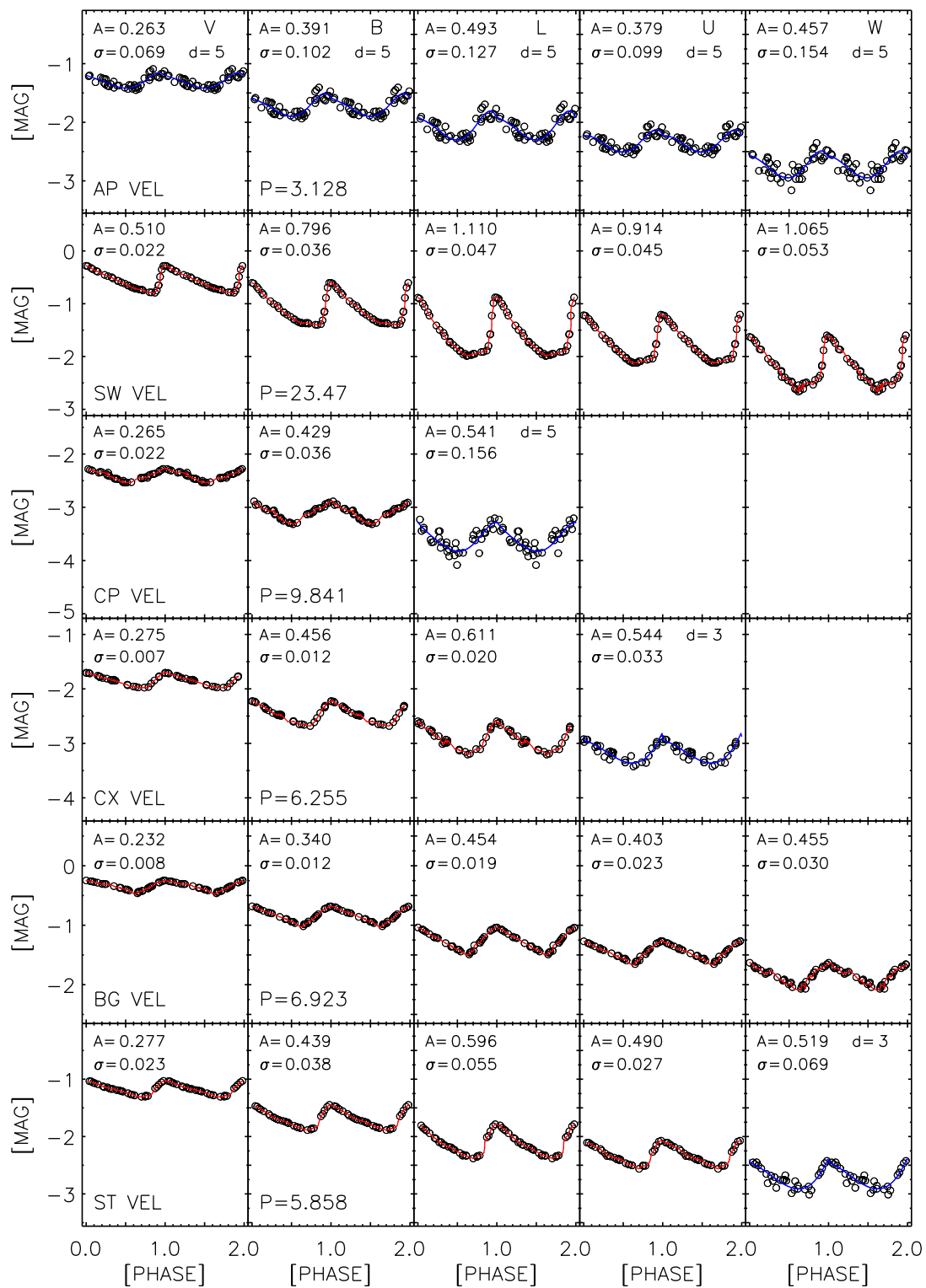


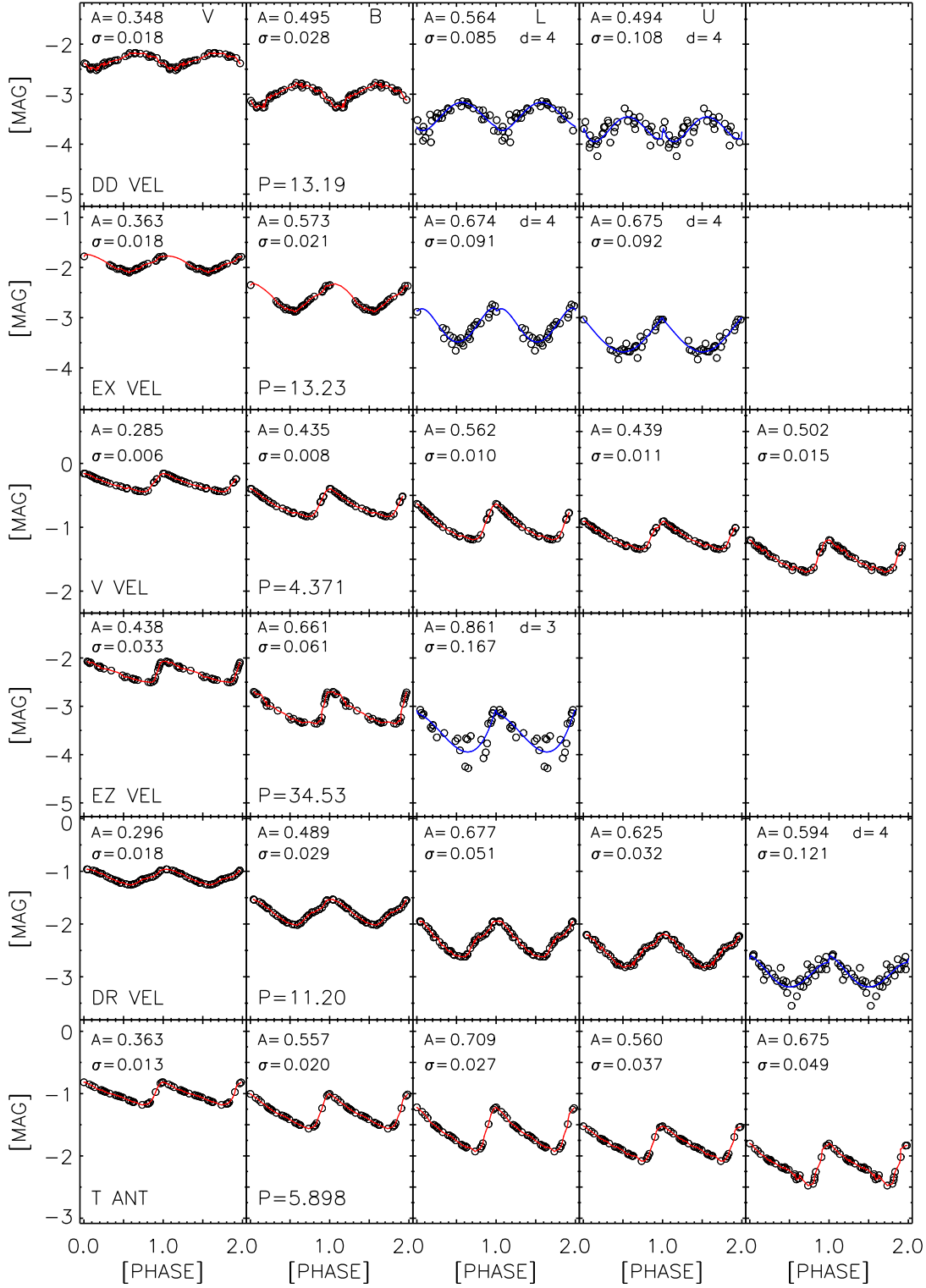


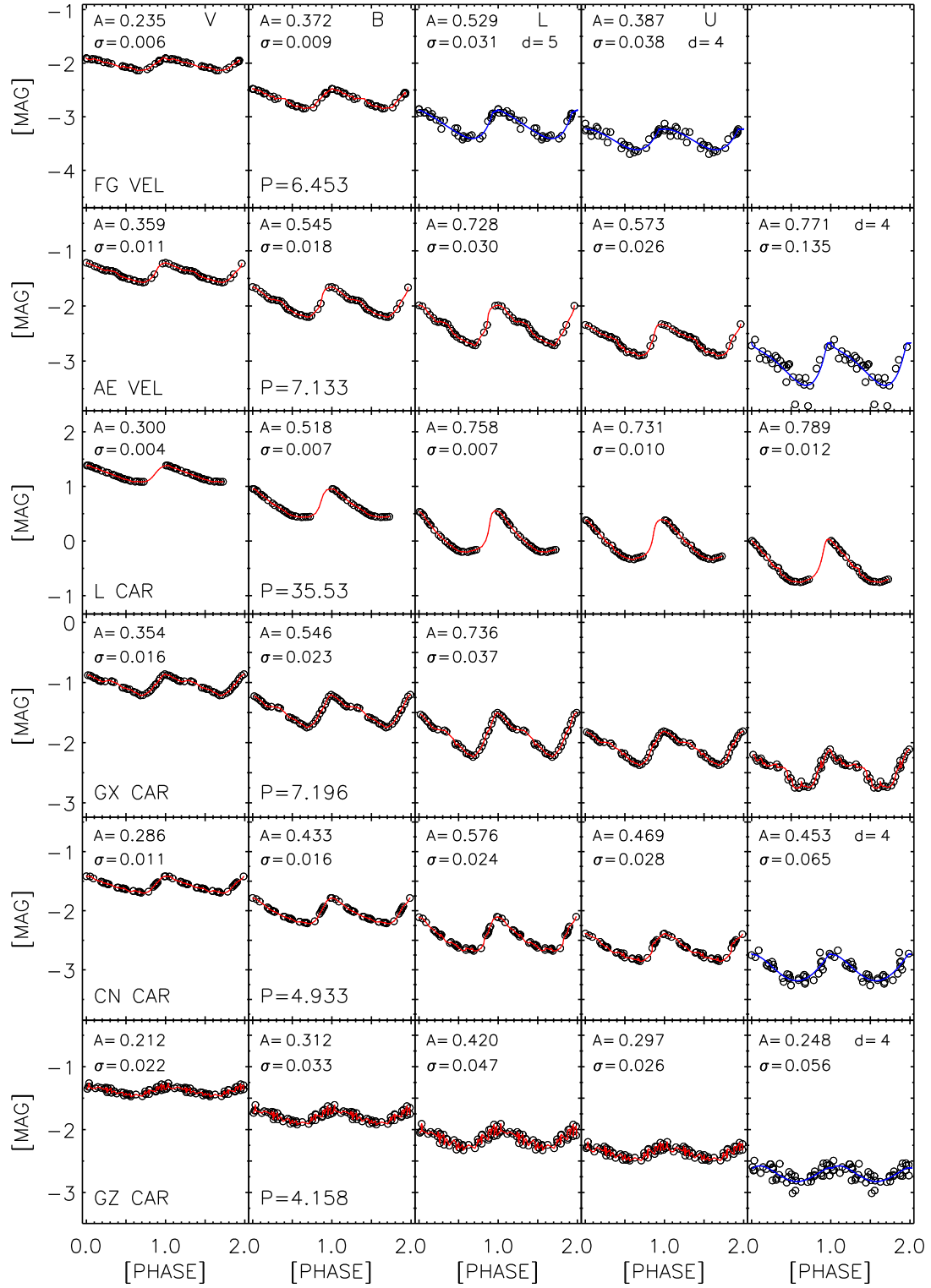


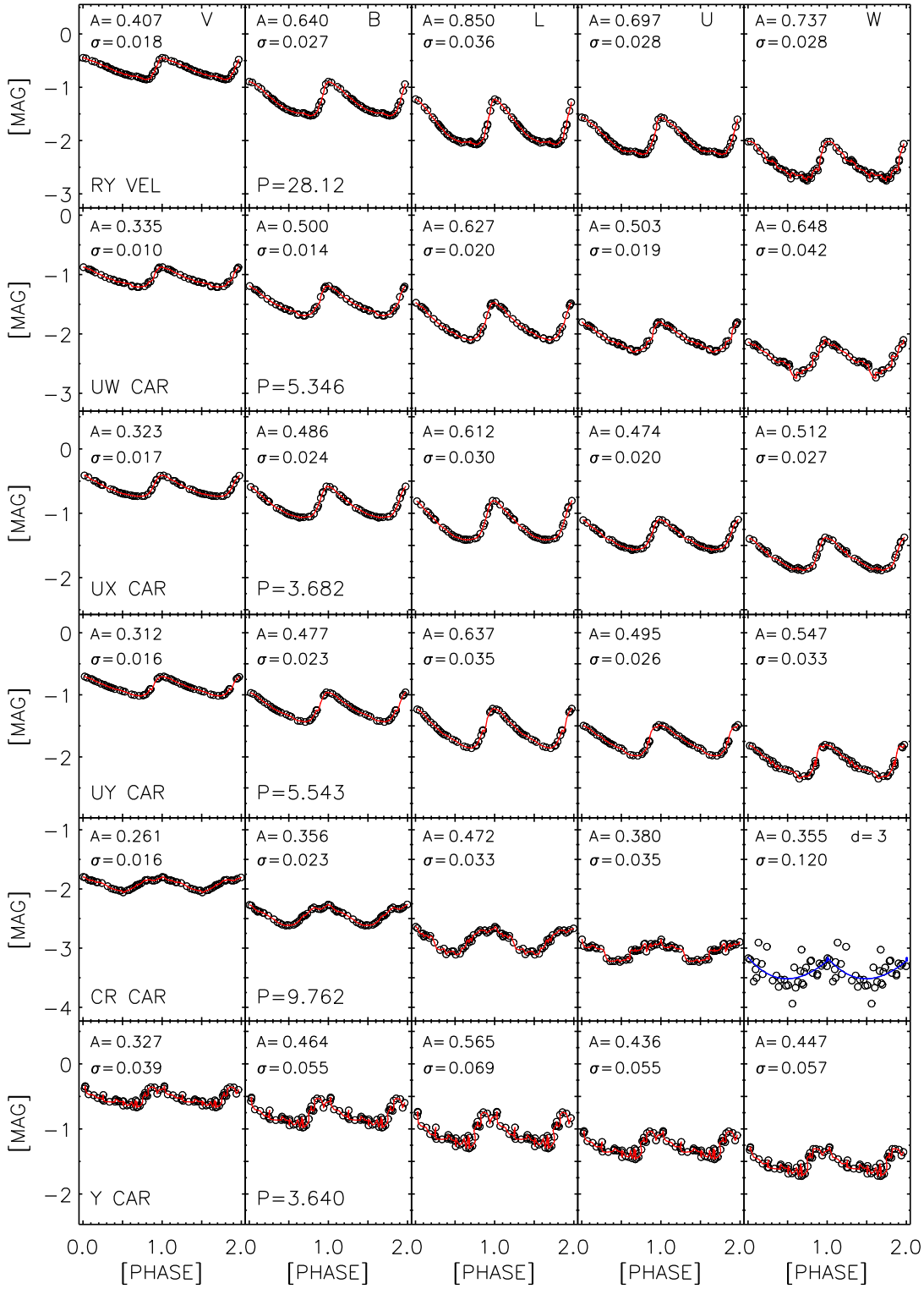


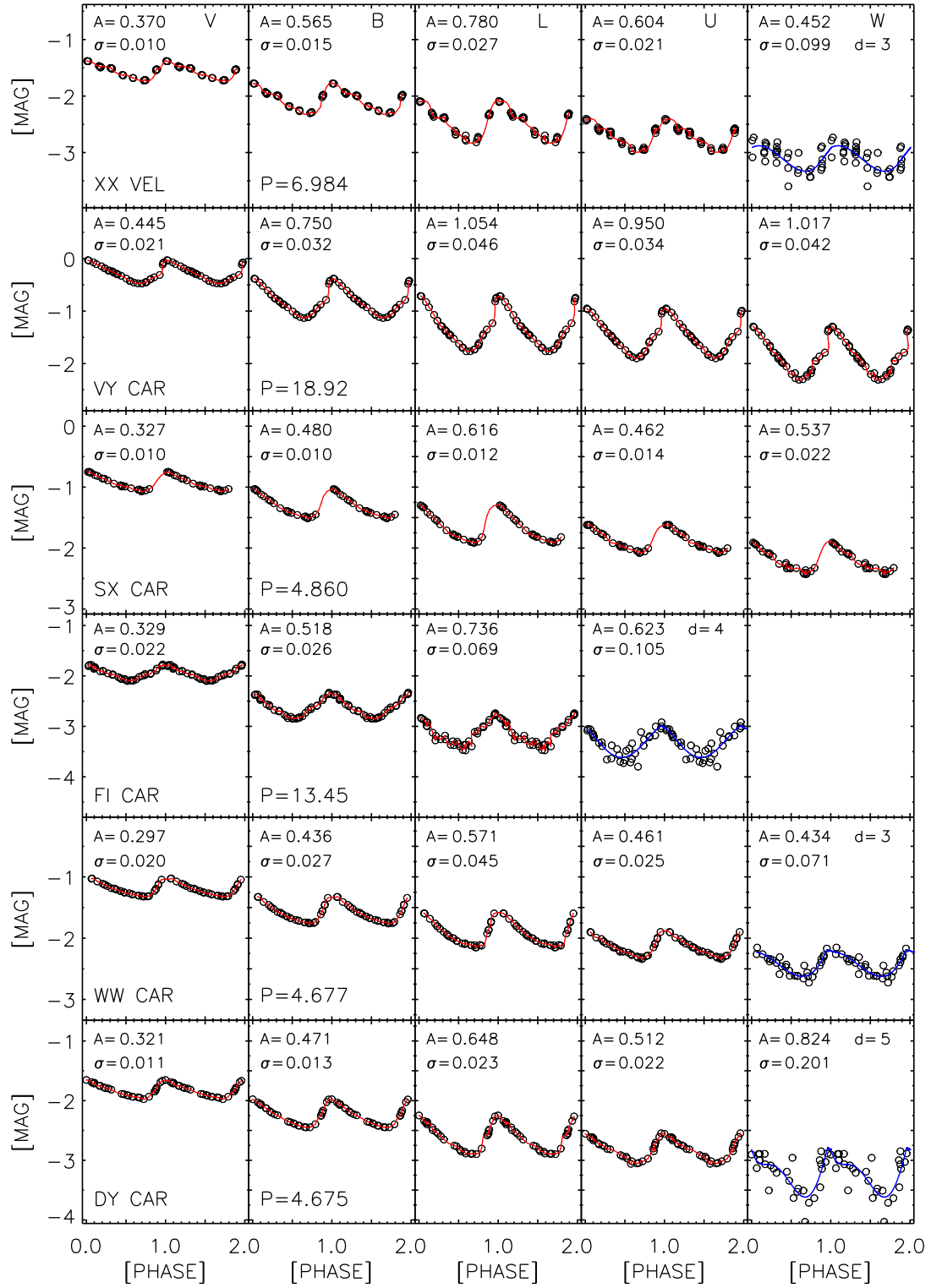


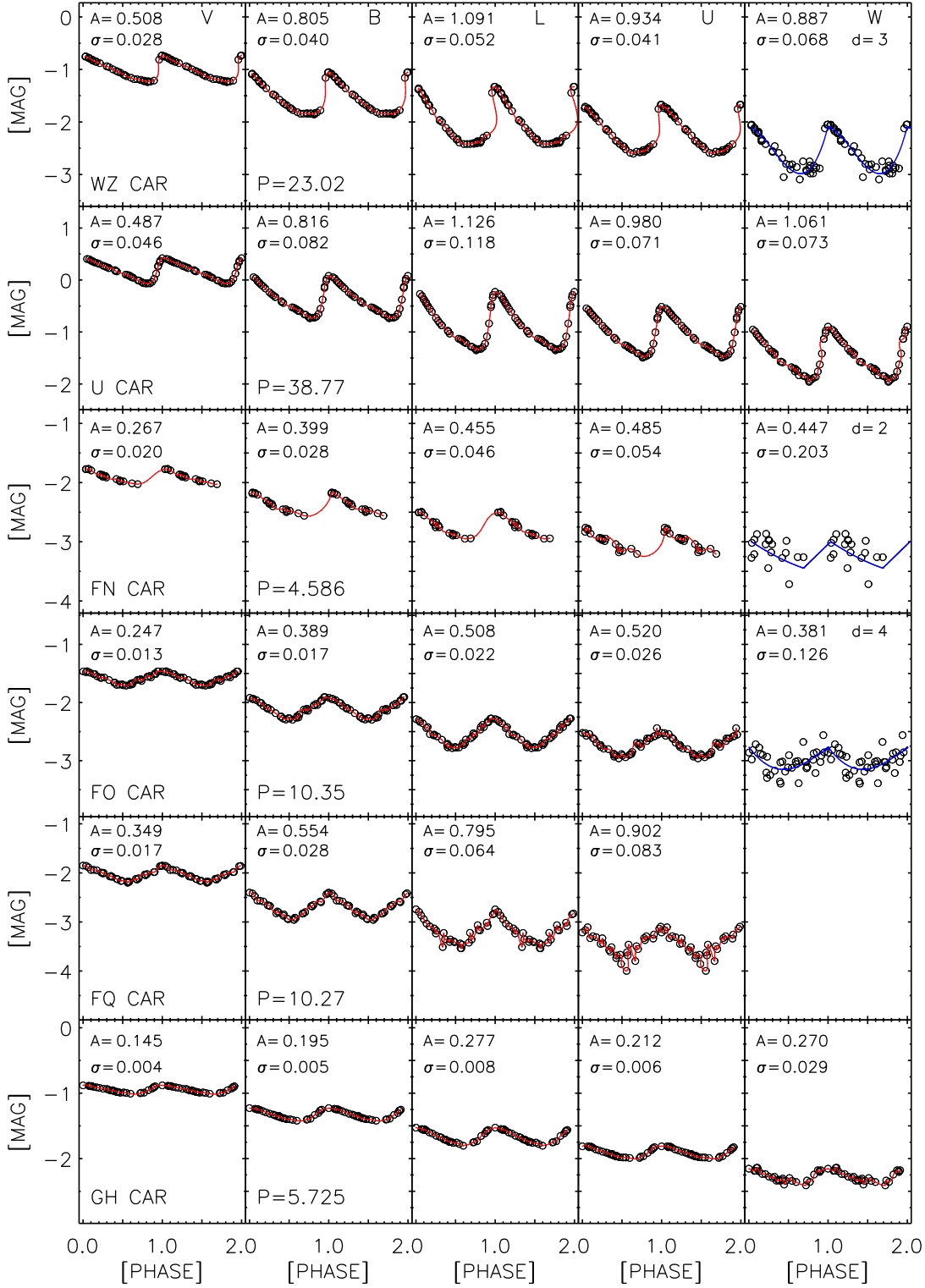


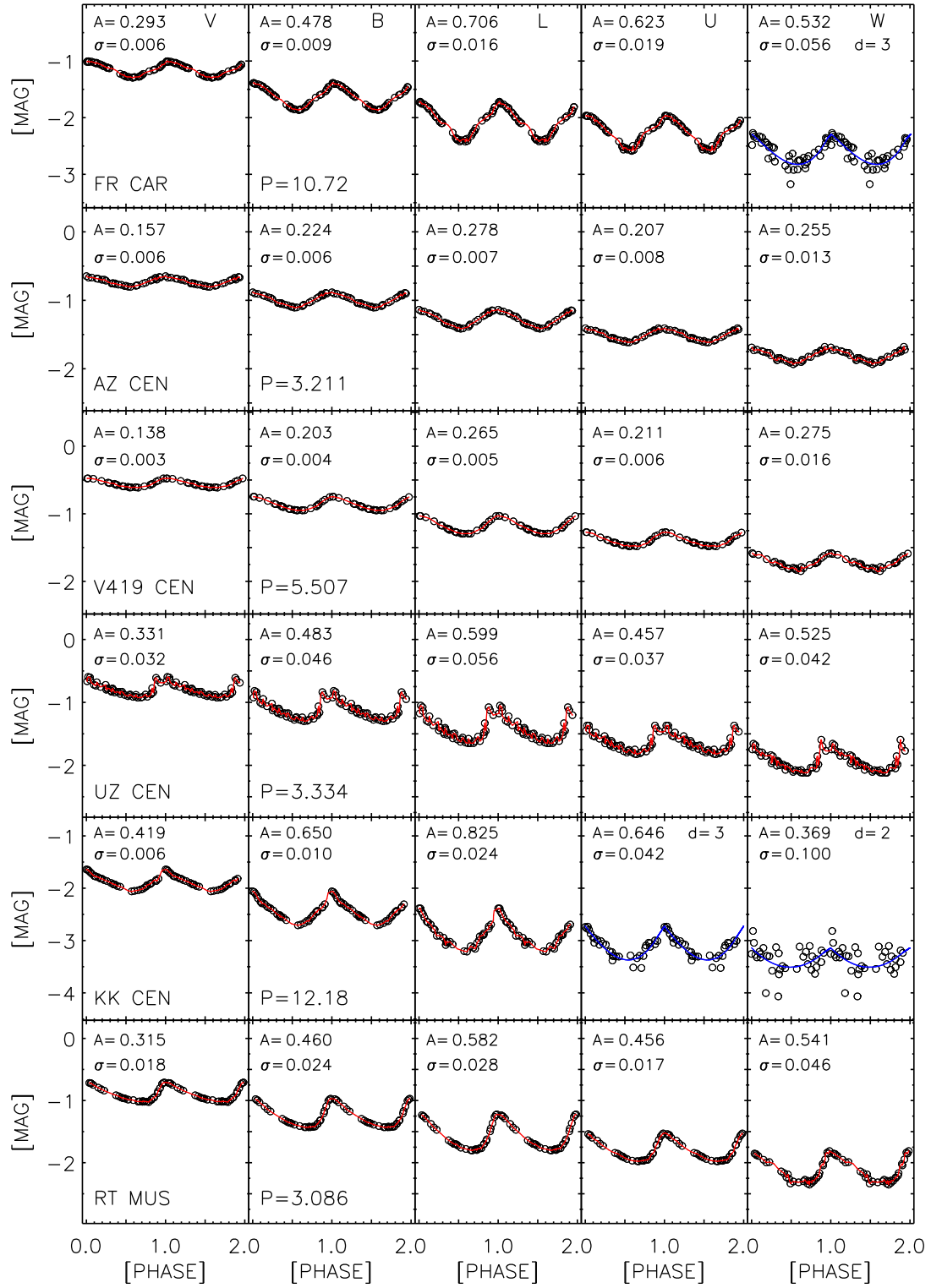


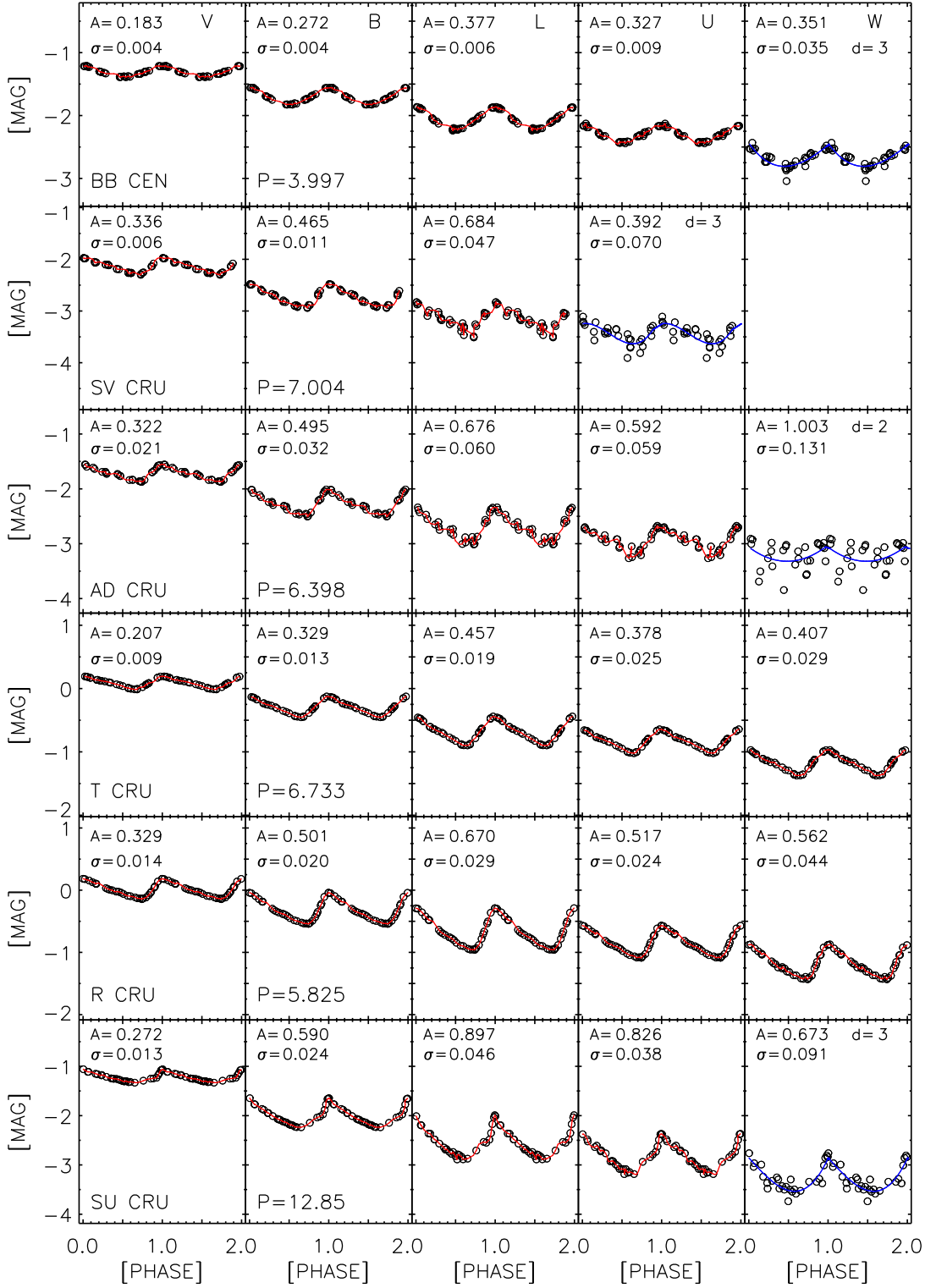


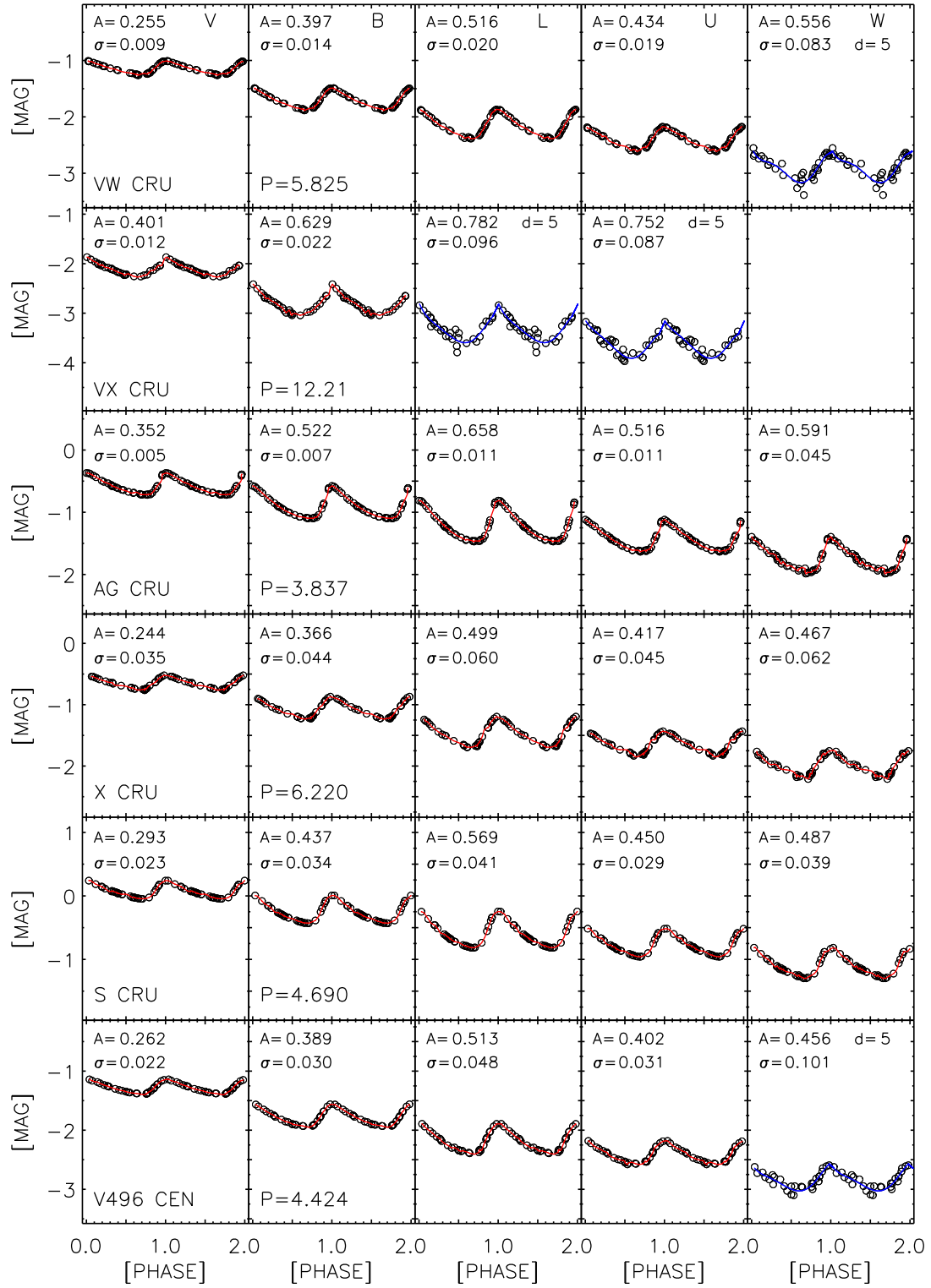


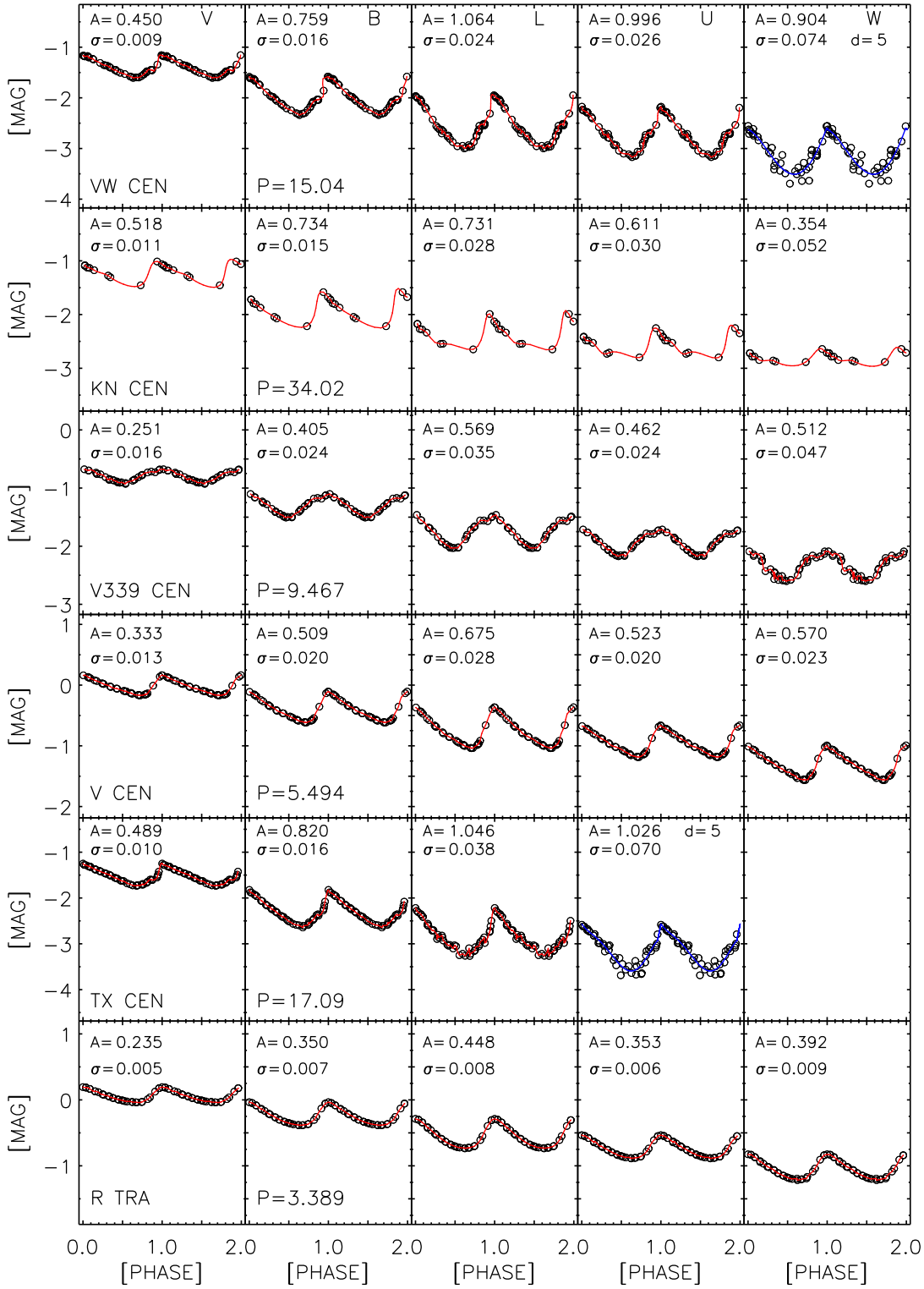


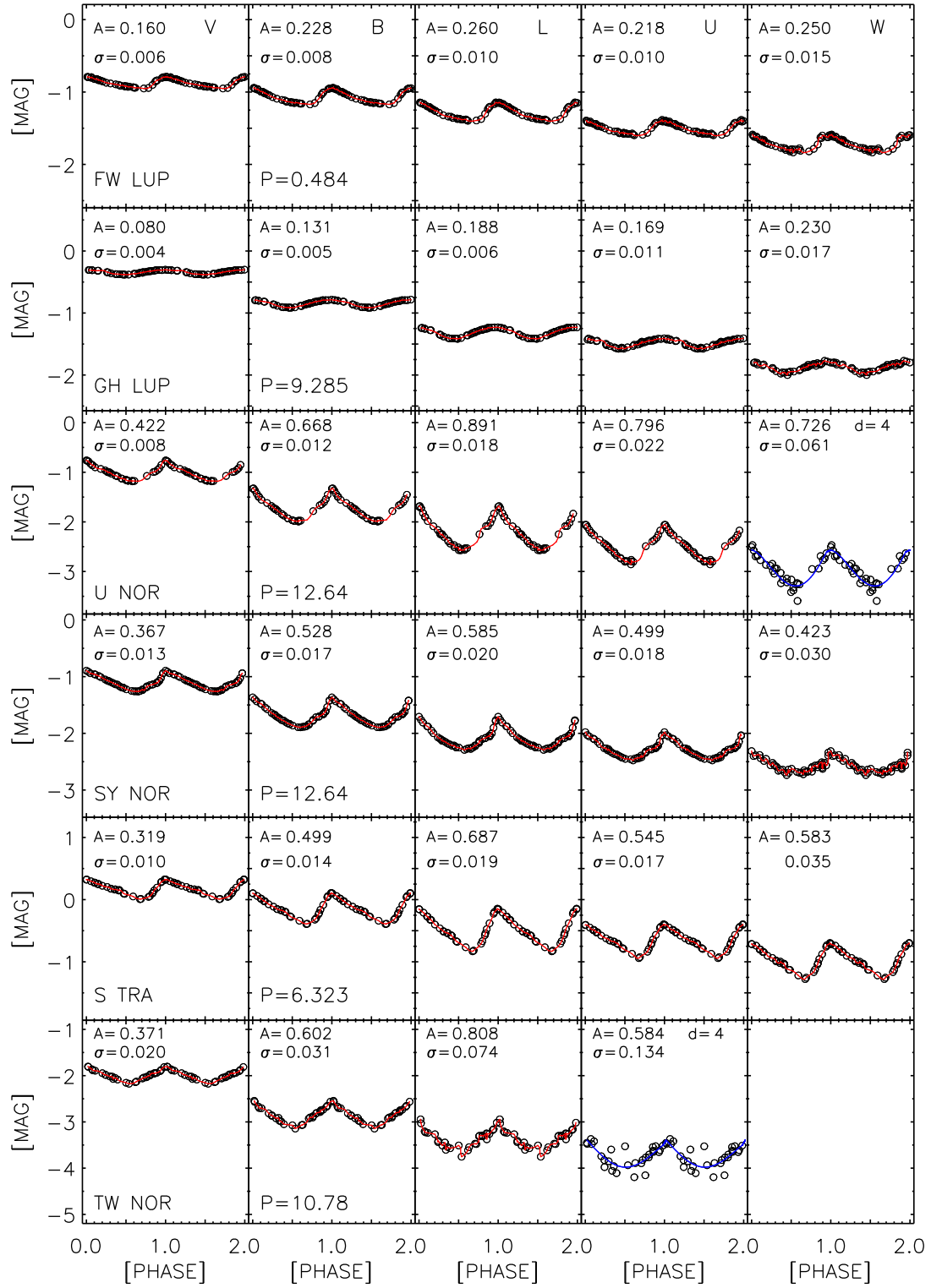


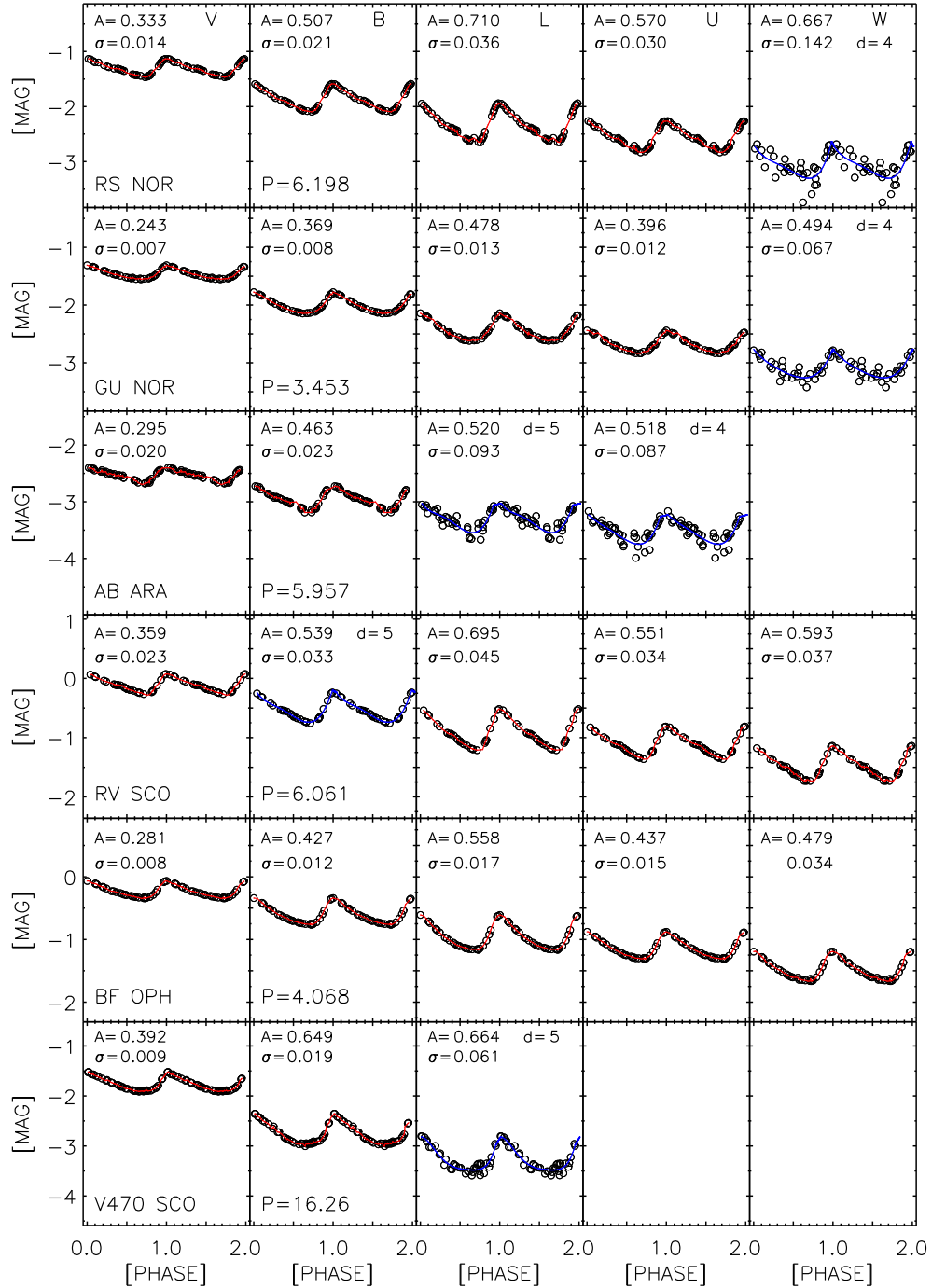


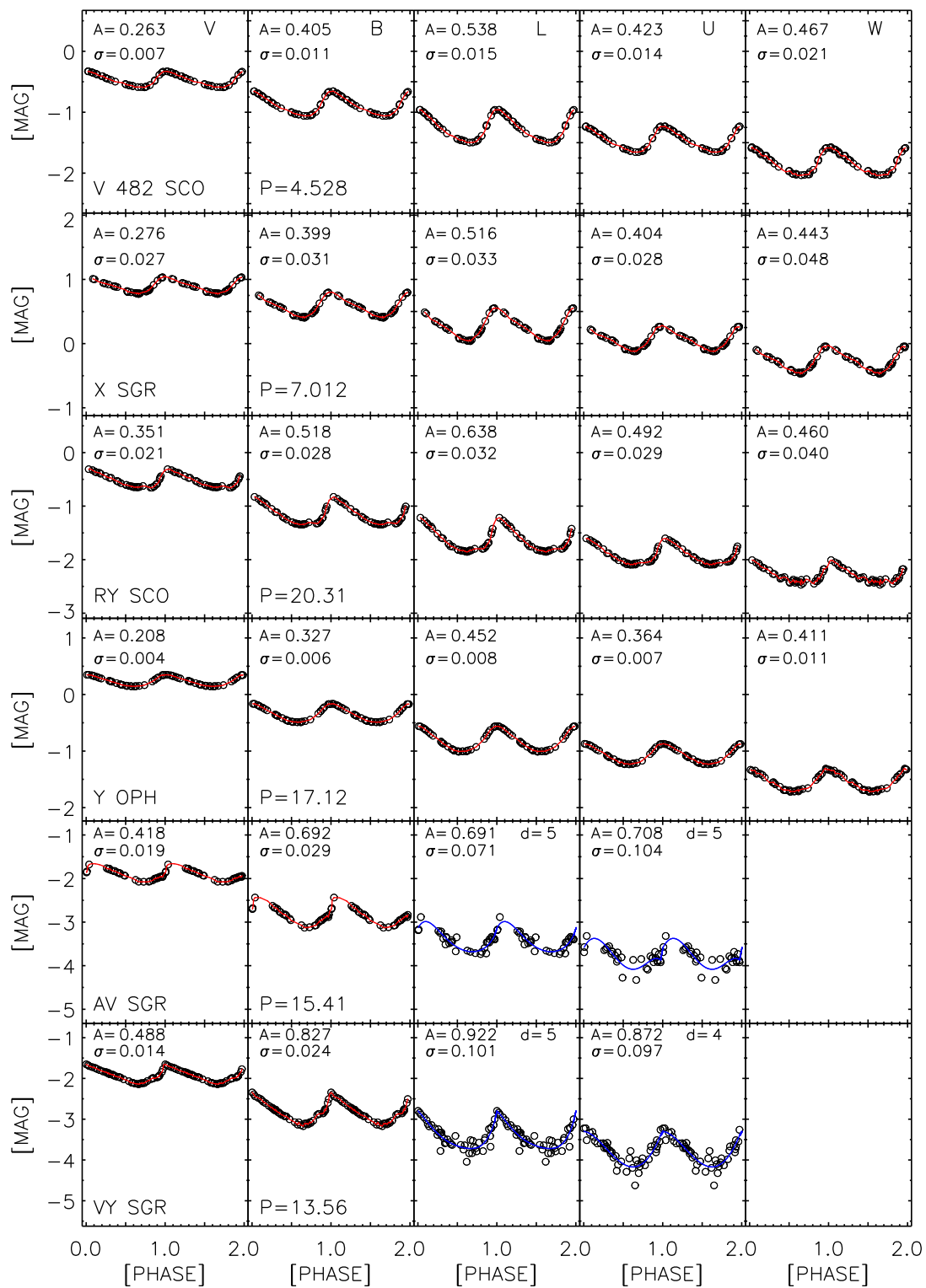


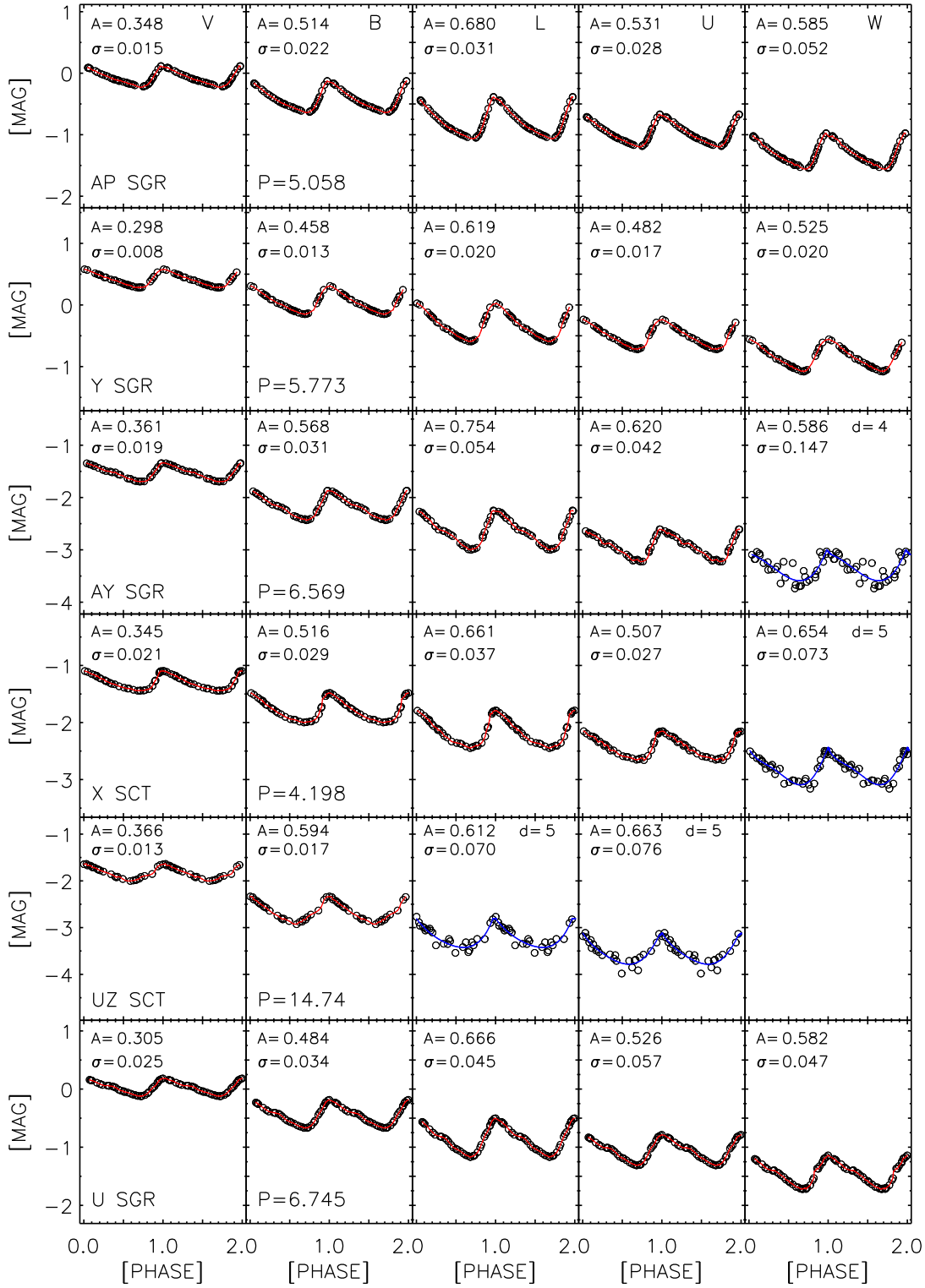


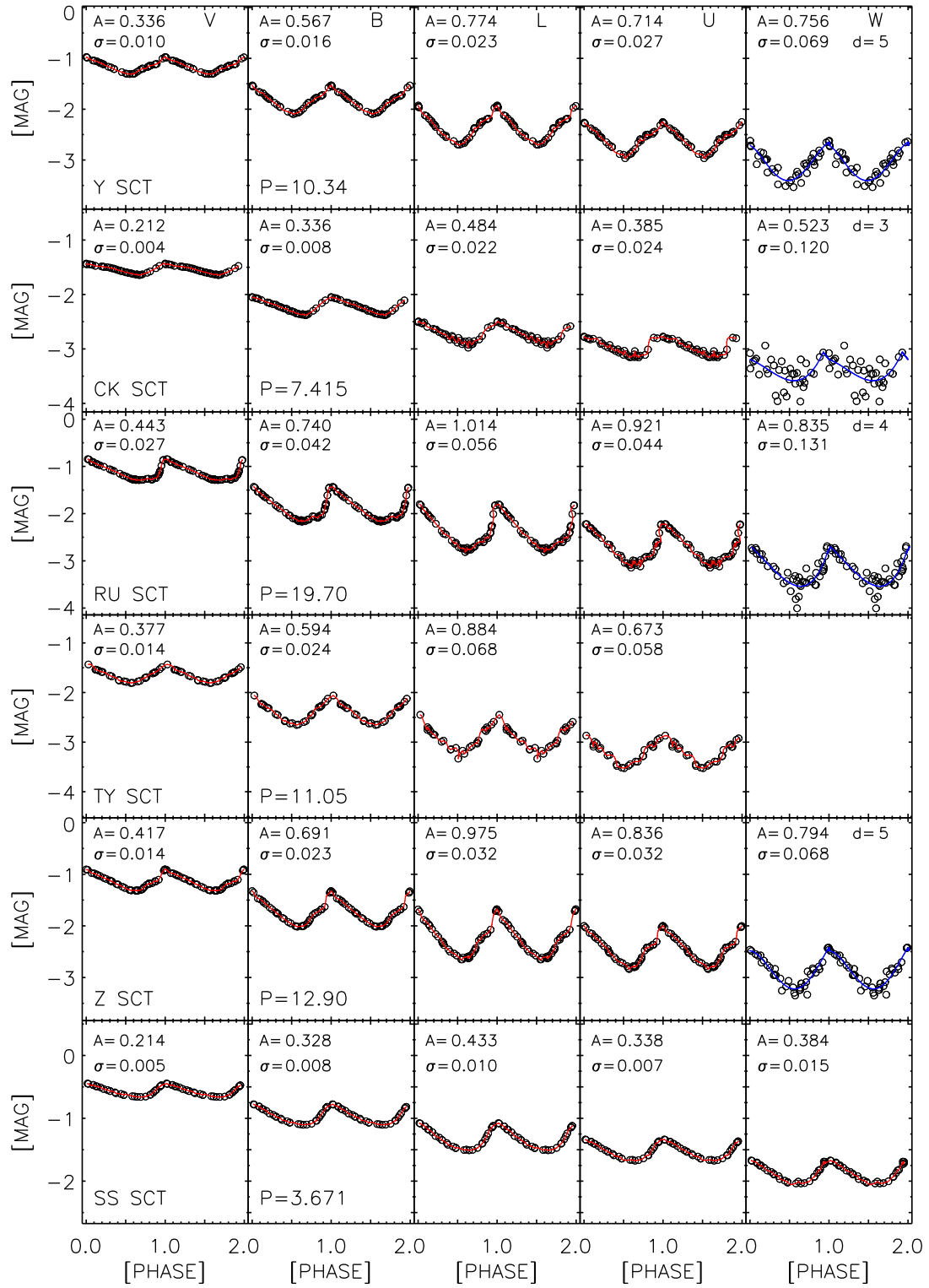


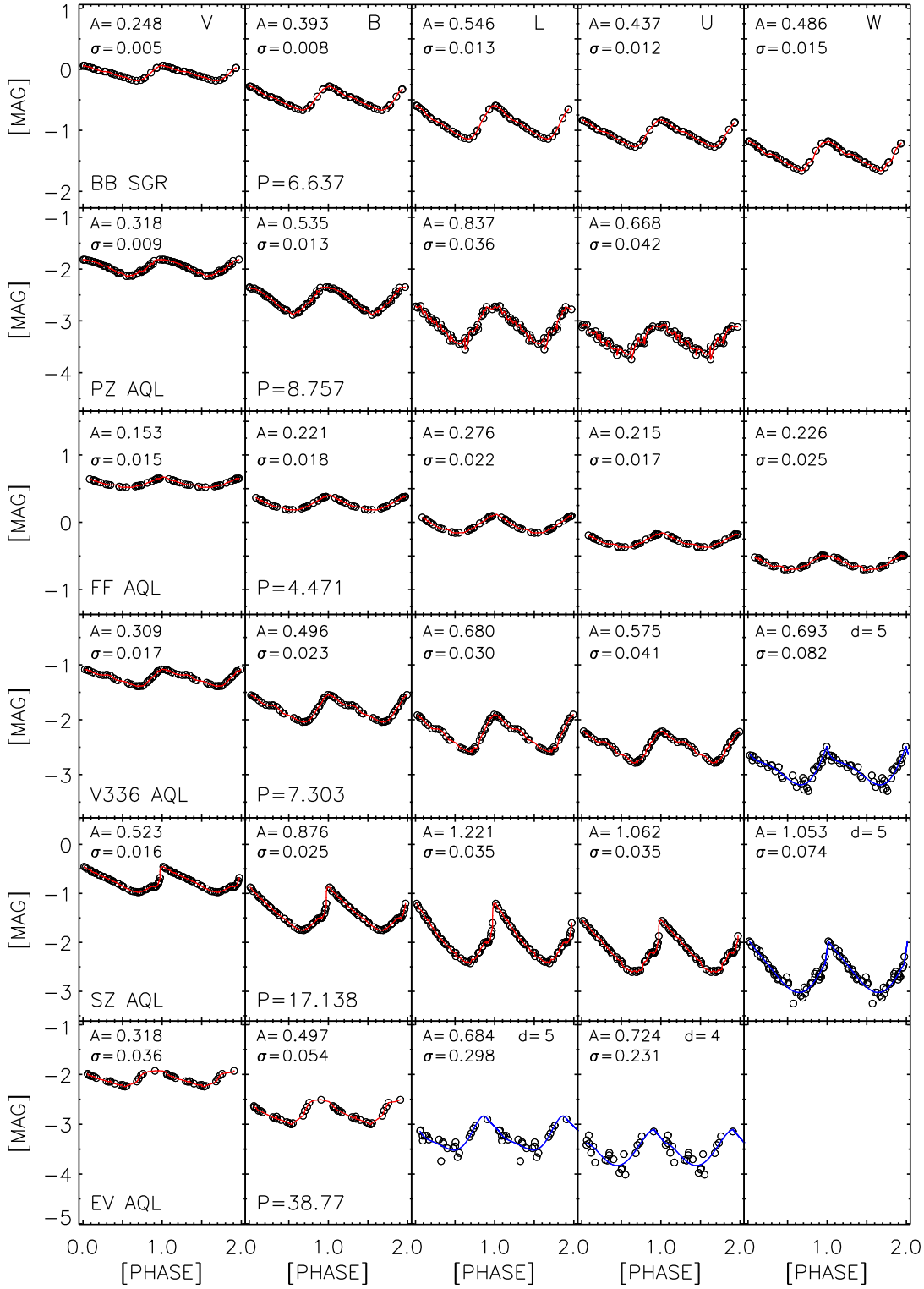


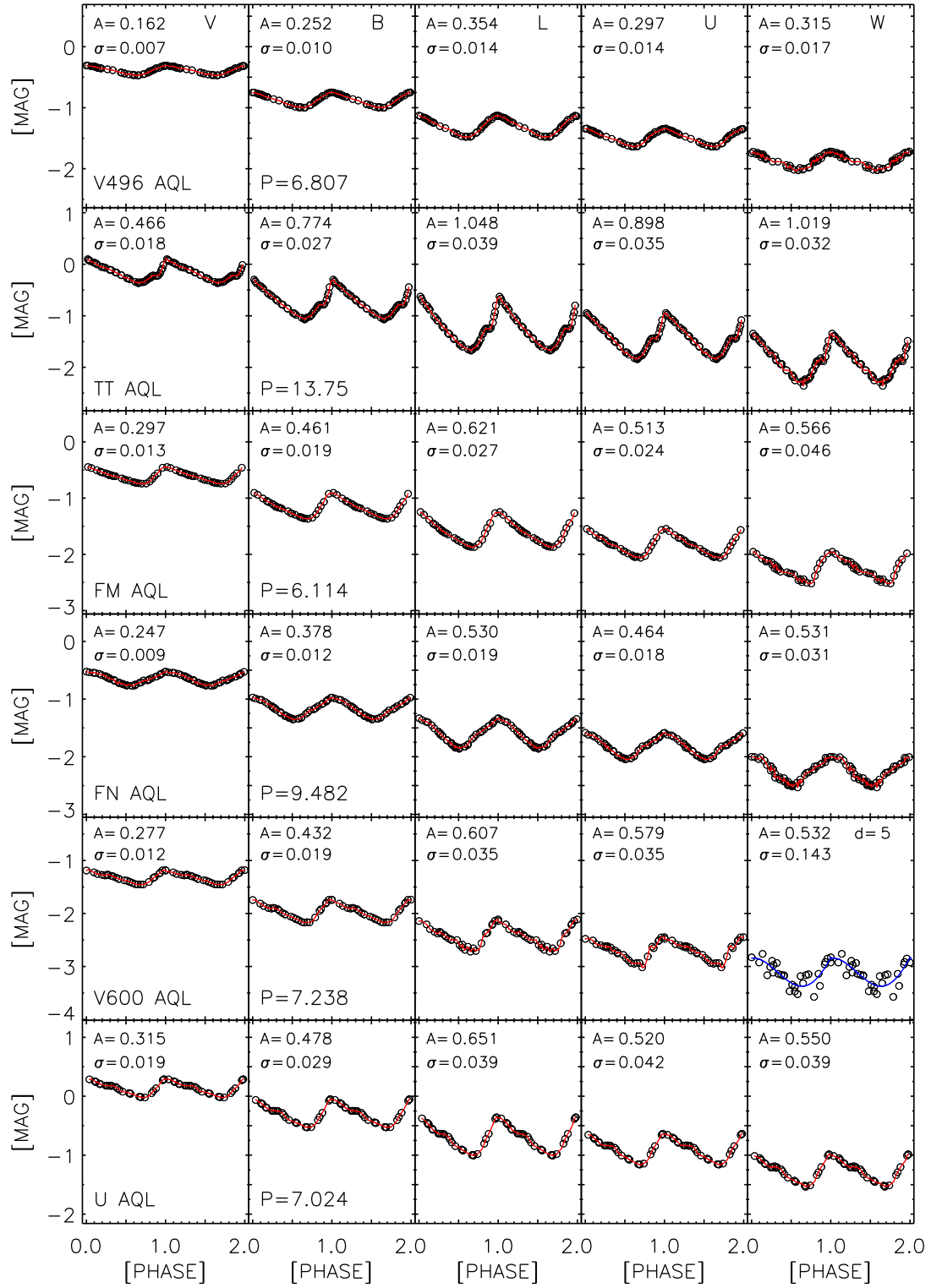


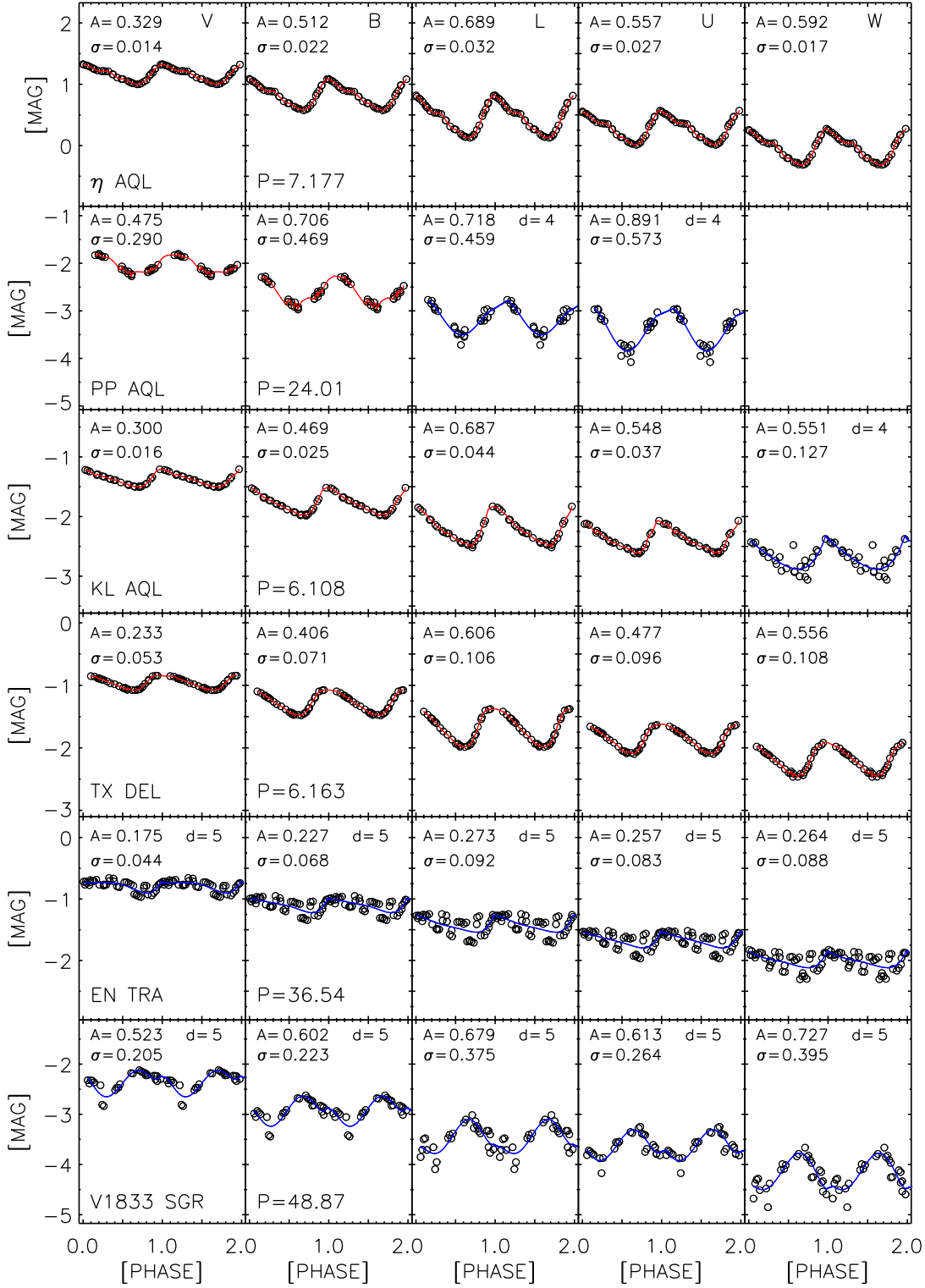












APPENDIX B

Line list

Table B.1: Complete line list with wavelength, ion identification, excitation potential (EP) and log gf values.

λ [Å]	Ion	EP	log gf
4892.87	FeI	4.22	-1.34
4917.23	FeI	4.19	-1.29
4924.77	FeI	2.28	-2.24
4932.08	FeI	4.65	-1.49
4950.10	FeI	3.42	-1.67
4973.11	FeI	3.96	-0.95
4994.13	FeI	0.91	-3.08
5029.62	FeI	3.41	-2.05
5044.21	FeI	2.85	-2.04
5049.82	FeI	2.28	-1.36
5054.64	FeI	3.64	-1.92
5056.84	FeI	4.26	-1.96
5067.15	FeI	4.22	-0.97
5072.67	FeI	4.22	-0.84
5083.34	FeI	0.96	-2.96
5090.77	FeI	4.26	-0.40
5126.19	FeI	4.26	-1.08
5133.69	FeI	4.18	0.14
5171.60	FeI	1.48	-1.79
5198.72	FeI	2.22	-2.14
5215.18	FeI	3.27	-0.87
5216.28	FeI	1.61	-2.15
5217.40	FeI	3.21	-1.07
5242.49	FeI	3.63	-0.97
5243.78	FeI	4.26	-1.15
5257.65	FeI	3.57	-2.79
5281.80	FeI	3.04	-0.83
5288.52	FeI	3.69	-1.51
5307.37	FeI	1.61	-2.99
5324.18	FeI	3.21	-0.10
5326.14	FeI	3.57	-2.07
5339.93	FeI	3.27	-0.65
5364.87	FeI	4.45	0.23
5365.40	FeI	3.57	-1.02
5367.47	FeI	4.42	0.44
5373.71	FeI	4.47	-0.86
5379.57	FeI	3.69	-1.51
5383.37	FeI	4.31	0.65
5389.49	FeI	4.41	-0.57
5391.46	FeI	4.15	-0.78
5393.18	FeI	3.24	-0.72
5398.28	FeI	4.45	-0.67
Continue ...			

λ [Å]	<i>Ion</i>	<i>EP</i>	$\log gf$
5405.78	<i>FeI</i>	0.99	-1.84
5410.91	<i>FeI</i>	4.47	0.40
5415.20	<i>FeI</i>	4.39	0.64
5417.04	<i>FeI</i>	4.41	-1.42
5424.07	<i>FeI</i>	4.32	0.52
5434.53	<i>FeI</i>	1.01	-2.22
5445.04	<i>FeI</i>	4.39	-0.02
5452.09	<i>FeI</i>	3.64	-2.86
5464.28	<i>FeI</i>	4.14	-1.40
5466.40	<i>FeI</i>	4.37	-0.63
5497.52	<i>FeI</i>	1.01	-2.85
5501.46	<i>FeI</i>	0.96	-3.05
5506.78	<i>FeI</i>	0.99	-2.80
5522.45	<i>FeI</i>	4.21	-1.47
5531.98	<i>FeI</i>	4.91	-1.61
5543.15	<i>FeI</i>	3.69	-1.57
5554.89	<i>FeI</i>	4.54	-0.44
5560.22	<i>FeI</i>	4.43	-1.10
5561.24	<i>FeI</i>	4.61	-1.21
5562.71	<i>FeI</i>	4.44	-0.66
5565.71	<i>FeI</i>	4.61	-0.21
5568.62	<i>FeI</i>	3.41	-0.49
5572.84	<i>FeI</i>	3.40	-0.27
5576.09	<i>FeI</i>	3.43	-1.00
5584.76	<i>FeI</i>	3.57	-2.32
5586.77	<i>FeI</i>	3.37	-0.10
5633.97	<i>FeI</i>	4.99	-0.23
5635.85	<i>FeI</i>	4.26	-1.52
5638.27	<i>FeI</i>	4.22	-0.68
5641.46	<i>FeI</i>	4.26	-0.87
5653.89	<i>FeI</i>	4.39	-1.36
5658.82	<i>FeI</i>	3.40	-0.85
5661.36	<i>FeI</i>	4.28	-1.79
5679.02	<i>FeI</i>	4.65	-0.71
5686.53	<i>FeI</i>	4.55	-0.66
5691.51	<i>FeI</i>	4.30	-1.46
5707.05	<i>FeI</i>	3.64	-2.40
5717.85	<i>FeI</i>	4.28	-0.99
5720.89	<i>FeI</i>	4.55	-1.76
5731.77	<i>FeI</i>	4.26	-1.08
5741.86	<i>FeI</i>	4.26	-1.61
5752.01	<i>FeI</i>	4.55	-0.88
5753.12	<i>FeI</i>	4.26	-0.69
5762.43	<i>FeI</i>	3.64	-2.30
5762.99	<i>FeI</i>	4.21	-0.36
5775.07	<i>FeI</i>	4.22	-1.08
Continue ...			

λ [Å]	<i>Ion</i>	<i>EP</i>	$\log gf$
5778.47	<i>FeI</i>	2.59	-3.49
5793.93	<i>FeI</i>	4.22	-1.60
5804.06	<i>FeI</i>	3.88	-2.15
5806.73	<i>FeI</i>	4.61	-0.88
5809.25	<i>FeI</i>	3.88	-1.61
5814.80	<i>FeI</i>	4.28	-1.82
5816.37	<i>FeI</i>	4.55	-0.60
5834.02	<i>FeI</i>	4.91	-0.95
5848.13	<i>FeI</i>	4.61	-1.06
5852.19	<i>FeI</i>	4.55	-1.14
5855.13	<i>FeI</i>	4.61	-1.51
5856.08	<i>FeI</i>	4.29	-1.54
5859.56	<i>FeI</i>	4.55	-0.57
5862.36	<i>FeI</i>	4.55	-0.26
5873.21	<i>FeI</i>	4.26	-1.97
5877.77	<i>FeI</i>	4.18	-2.12
5883.84	<i>FeI</i>	3.96	-1.08
5902.52	<i>FeI</i>	4.59	-1.74
5905.67	<i>FeI</i>	4.65	-0.69
5909.99	<i>FeI</i>	3.21	-2.62
5916.25	<i>FeI</i>	2.45	-2.88
5927.80	<i>FeI</i>	4.65	-1.01
5930.17	<i>FeI</i>	4.65	-0.14
5934.66	<i>FeI</i>	3.93	-1.00
5952.73	<i>FeI</i>	3.98	-1.44
5956.70	<i>FeI</i>	0.86	-4.52
5858.33	<i>FeI</i>	2.18	-4.16
5975.35	<i>FeI</i>	4.83	-0.69
5976.78	<i>FeI</i>	3.94	-1.17
5983.69	<i>FeI</i>	4.55	-0.58
5984.79	<i>FeI</i>	4.73	-0.19
5987.05	<i>FeI</i>	4.80	-0.23
5997.78	<i>FeI</i>	4.61	-1.70
6003.03	<i>FeI</i>	3.88	-0.89
6005.54	<i>FeI</i>	2.59	-3.60
6007.96	<i>FeI</i>	4.65	-0.61
6008.56	<i>FeI</i>	3.88	-0.83
6012.21	<i>FeI</i>	2.22	-4.04
6020.19	<i>FeI</i>	4.61	-0.27
6024.07	<i>FeI</i>	4.55	0.04
6027.06	<i>FeI</i>	4.08	-1.10
6056.01	<i>FeI</i>	4.73	-0.46
6062.89	<i>FeI</i>	2.18	-3.93
6065.48	<i>FeI</i>	2.61	-1.53
6078.50	<i>FeI</i>	4.80	-0.22
6079.02	<i>FeI</i>	4.65	-0.93
Continue ...			

λ [Å]	<i>Ion</i>	<i>EP</i>	$\log gf$
6082.72	<i>FeI</i>	2.22	-3.57
6085.27	<i>FeI</i>	2.76	-2.86
6089.57	<i>FeI</i>	5.02	-0.84
6093.66	<i>FeI</i>	4.61	-1.32
6096.69	<i>FeI</i>	3.98	-1.75
6127.91	<i>FeI</i>	4.14	-1.39
6136.62	<i>FeI</i>	2.45	-1.40
6137.70	<i>FeI</i>	2.59	-1.40
6151.62	<i>FeI</i>	2.18	-3.30
6157.73	<i>FeI</i>	4.08	-1.18
6165.37	<i>FeI</i>	4.14	-1.46
6170.49	<i>FeI</i>	4.80	-0.30
6173.34	<i>FeI</i>	2.22	-2.81
6180.22	<i>FeI</i>	2.73	-2.65
6188.04	<i>FeI</i>	3.94	-1.58
6191.57	<i>FeI</i>	2.43	-1.42
6200.32	<i>FeI</i>	2.61	-2.31
6213.43	<i>FeI</i>	2.22	-2.55
6215.15	<i>FeI</i>	4.19	-1.14
6219.28	<i>FeI</i>	2.20	-2.41
6226.77	<i>FeI</i>	3.88	-2.05
6229.23	<i>FeI</i>	2.85	-2.85
6230.73	<i>FeI</i>	2.56	-1.33
6232.65	<i>FeI</i>	3.65	-1.13
6240.66	<i>FeI</i>	2.22	-3.28
6246.32	<i>FeI</i>	3.60	-0.63
6252.55	<i>FeI</i>	2.40	-1.68
6265.13	<i>FeI</i>	2.18	-2.51
6270.23	<i>FeI</i>	2.86	-2.46
6301.51	<i>FeI</i>	3.65	-0.58
6302.50	<i>FeI</i>	3.69	-0.97
6311.51	<i>FeI</i>	2.83	-3.09
6322.69	<i>FeI</i>	2.59	-2.28
6330.86	<i>FeI</i>	4.73	-1.14
6335.34	<i>FeI</i>	2.20	-2.25
6336.84	<i>FeI</i>	3.69	-0.67
6344.15	<i>FeI</i>	2.43	-2.89
6355.04	<i>FeI</i>	2.85	-2.32
6358.69	<i>FeI</i>	0.86	-4.11
6380.75	<i>FeI</i>	4.19	-1.27
6392.55	<i>FeI</i>	2.28	-3.94
6393.60	<i>FeI</i>	2.43	-1.58
6400.01	<i>FeI</i>	3.60	-0.29
6408.01	<i>FeI</i>	3.69	-1.02
6411.65	<i>FeI</i>	3.65	-0.49
6419.98	<i>FeI</i>	4.73	-0.17
Continue ...			

λ [Å]	<i>Ion</i>	<i>EP</i>	$\log gf$
6421.35	<i>FeI</i>	2.28	-2.12
6430.85	<i>FeI</i>	2.18	-2.06
6469.19	<i>FeI</i>	4.83	-0.77
6475.63	<i>FeI</i>	2.56	-2.94
6481.88	<i>FeI</i>	2.28	-2.91
6494.98	<i>FeI</i>	2.40	-1.43
6496.47	<i>FeI</i>	4.79	-0.57
6498.95	<i>FeI</i>	0.96	-4.62
6518.38	<i>FeI</i>	2.83	-2.54
6533.97	<i>FeI</i>	4.56	-1.11
6546.25	<i>FeI</i>	2.76	-1.54
6569.22	<i>FeI</i>	4.73	-0.42
6574.23	<i>FeI</i>	0.99	-5.02
6575.04	<i>FeI</i>	2.59	-2.71
6592.91	<i>FeI</i>	2.73	-1.62
6593.88	<i>FeI</i>	2.43	-2.29
6597.61	<i>FeI</i>	4.80	-0.85
6608.03	<i>FeI</i>	2.28	-3.94
6609.12	<i>FeI</i>	2.56	-2.61
6627.56	<i>FeI</i>	4.55	-1.46
6646.93	<i>FeI</i>	2.61	-1.99
6648.08	<i>FeI</i>	1.01	-5.42
6677.99	<i>FeI</i>	2.69	-1.37
6703.57	<i>FeI</i>	2.76	-3.01
6705.10	<i>FeI</i>	4.61	-1.39
6710.31	<i>FeI</i>	1.49	-4.78
6713.05	<i>FeI</i>	4.61	-0.96
6713.76	<i>FeI</i>	4.80	-1.37
6715.38	<i>FeI</i>	4.61	-1.64
6725.36	<i>FeI</i>	4.10	-2.30
6726.64	<i>FeI</i>	4.61	-1.01
6733.15	<i>FeI</i>	4.64	-1.58
6737.99	<i>FeI</i>	4.55	-1.75
6739.52	<i>FeI</i>	1.56	-4.79
6750.15	<i>FeI</i>	2.42	-2.58
6752.72	<i>FeI</i>	4.64	-1.19
6783.70	<i>FeI</i>	2.59	-3.98
6804.00	<i>FeI</i>	4.65	-1.50
6806.85	<i>FeI</i>	2.73	-3.09
6810.28	<i>FeI</i>	4.61	-0.94
6820.43	<i>FeI</i>	4.64	-1.10
6828.61	<i>FeI</i>	4.64	-0.80
6837.00	<i>FeI</i>	4.59	-1.69
6839.83	<i>FeI</i>	2.56	-3.31
6841.35	<i>FeI</i>	4.61	-0.77
6843.67	<i>FeI</i>	4.55	-0.78
Continue ...			

λ [Å]	<i>Ion</i>	<i>EP</i>	$\log gf$
6855.15	<i>FeI</i>	4.56	-0.57
6855.74	<i>FeI</i>	4.61	-1.64
6858.16	<i>FeI</i>	4.61	-0.91
6945.20	<i>FeI</i>	2.42	-2.43
6951.25	<i>FeI</i>	4.56	-0.89
6999.90	<i>FeI</i>	4.10	-1.38
7022.98	<i>FeI</i>	4.19	-1.10
7090.38	<i>FeI</i>	4.23	-1.06
7093.09	<i>FeI</i>	4.56	-2.02
7095.43	<i>FeI</i>	4.21	-2.02
7107.46	<i>FeI</i>	4.19	-1.34
7112.18	<i>FeI</i>	2.99	-3.00
7127.56	<i>FeI</i>	4.99	-1.36
7130.92	<i>FeI</i>	4.22	-0.73
7132.99	<i>FeI</i>	4.08	-1.63
7142.51	<i>FeI</i>	4.96	-0.82
7145.32	<i>FeI</i>	4.61	-1.53
7187.32	<i>FeI</i>	4.10	-0.15
7212.43	<i>FeI</i>	4.96	-0.85
7219.69	<i>FeI</i>	4.08	-1.69
7382.02	<i>FeI</i>	4.61	-1.42
7411.15	<i>FeI</i>	4.28	-0.30
7435.59	<i>FeI</i>	5.31	-0.71
7440.95	<i>FeI</i>	4.91	-0.68
7443.02	<i>FeI</i>	4.19	-1.82
7445.75	<i>FeI</i>	4.26	-0.24
7447.39	<i>FeI</i>	4.96	-1.21
7461.52	<i>FeI</i>	2.56	-3.58
7491.65	<i>FeI</i>	4.30	-1.01
7495.06	<i>FeI</i>	4.22	-0.10
7498.53	<i>FeI</i>	4.14	-2.25
7506.01	<i>FeI</i>	5.06	-1.22
7507.26	<i>FeI</i>	4.41	-1.48
7511.02	<i>FeI</i>	4.18	0.10
7531.14	<i>FeI</i>	4.37	-1.31
7547.90	<i>FeI</i>	5.10	-1.35
7559.72	<i>FeI</i>	5.06	-1.08
7568.89	<i>FeI</i>	4.28	-0.88
7583.79	<i>FeI</i>	3.02	-1.89
7586.01	<i>FeI</i>	4.31	-0.87
7661.19	<i>FeI</i>	4.26	-0.95
7719.04	<i>FeI</i>	5.03	-1.31
7748.27	<i>FeI</i>	2.95	-1.75
7751.11	<i>FeI</i>	4.99	-0.75
7807.91	<i>FeI</i>	4.99	-0.54
7832.20	<i>FeI</i>	4.43	0.11
Continue ...			

λ [Å]	<i>Ion</i>	<i>EP</i>	$\log gf$
7855.40	<i>FeI</i>	5.06	-1.02
7869.61	<i>FeI</i>	4.37	-1.88
7912.87	<i>FeI</i>	0.86	-4.85
4893.82	<i>FeII</i>	2.83	-4.45
4923.93	<i>FeII</i>	2.88	-1.35
4993.35	<i>FeII</i>	2.81	-3.56
5100.66	<i>FeII</i>	2.81	-4.16
5132.67	<i>FeII</i>	2.81	-3.95
5197.58	<i>FeII</i>	3.23	-2.23
5234.63	<i>FeII</i>	3.22	-2.22
5256.94	<i>FeII</i>	2.89	-4.25
5325.56	<i>FeII</i>	3.22	-3.18
5362.87	<i>FeII</i>	3.20	-2.62
5414.07	<i>FeII</i>	3.22	-3.54
5425.26	<i>FeII</i>	3.20	-3.27
5534.85	<i>FeII</i>	3.24	-2.75
5627.49	<i>FeII</i>	3.39	-4.01
5932.06	<i>FeII</i>	3.20	-4.81
5991.37	<i>FeII</i>	3.15	-3.50
6084.10	<i>FeII</i>	3.20	-3.80
6113.33	<i>FeII</i>	3.22	-4.12
6147.74	<i>FeII</i>	3.89	-2.72
6149.25	<i>FeII</i>	3.89	-2.72
6238.39	<i>FeII</i>	3.87	-2.52
6247.56	<i>FeII</i>	3.89	-2.33
6369.46	<i>FeII</i>	2.89	-4.14
6383.72	<i>FeII</i>	5.55	-2.07
6416.92	<i>FeII</i>	3.89	-2.65
6432.68	<i>FeII</i>	2.89	-3.69
6442.94	<i>FeII</i>	5.55	-2.46
6446.40	<i>FeII</i>	6.22	-2.07
6456.38	<i>FeII</i>	3.90	-2.18
6516.08	<i>FeII</i>	2.89	-3.45
7310.22	<i>FeII</i>	3.89	-3.36
7449.34	<i>FeII</i>	3.89	-3.09
7479.69	<i>FeII</i>	3.89	-3.68
7515.83	<i>FeII</i>	3.90	-3.55
7533.37	<i>FeII</i>	3.90	-3.99
7711.44	<i>FeII</i>	5.51	-3.21
7711.72	<i>FeII</i>	3.90	-2.50

Bibliography

- [1] Alloin, D. 1988, *Astrophysical and Laboratory Spectroscopy*. Proceedings of the Thirty-Third Scottish Universities' Summer School in Physics, held in St. Andrews, Scotland, September 1988. Editors, R. Brown, J. Lang; Publisher, The Scottish Universities' Summer School in Physics, Edinburgh, Scotland
- [2] Alves, D. 2004, *NewAR*, 48, 659
- [3] Andrievsky, S.M., Kovtyukh, V.V., Korotin, S.A. et al. 2001, *A&A* 367, 605
- [4] Andrievsky, S.M., Kovtyukh, V.V., Luck, R.E. et al 2002a, *A&A* 381, 32
- [5] Andrievsky, S.M., Bersier, D., Kovtyukh, V.V. et al 2002b, *A&A* 384, 140
- [6] Andrievsky, S.M., Kovtyukh, V.V., Luck, R.E. et al 2002c, *A&A* 392, 491
- [7] Andrievsky, S.M., Luck, R.E., Martin, P. & Lepine, J.R.D. 2004, *A&A* 413, 159
- [8] Antonello, E., Fossati, L., Fugazza, D., Mantegazza, L., & Gieren, W. 2006, *A&A*, 445, 901
- [9] Baraffe, I. & Alibert, Y. 2001, *A&A* 371, 592
- [10] Barnes, T. G., Jeffery, E. J., Berger, J. O., et al. 2003, *ApJ*, 592, 539
- [11] Barnes, T. G., Jeffery, E. J., Montemayor & T. J., Skillen, I. 2005, *ApJS*, 156, 227
- [12] Barnes, T. G., Storm, J., Jefferys, W. J., Gieren, W. P., & Fouqu, P. 2005, *ApJ*, 631, 572
- [13] Barnes, T. G.; Evans, D. S.; Parsons, S. B., 1976, *MNRAS*, 174, 503
- [14] Becker, S. A. & Iben, I., Jr. 1979, *ApJ*, 232, 831
- [15] Benedict, G.F., McArthur, B.E., Fredrick, L.W. et al 2002, *AJ* 123, 473
- [16] Benedict, G.F., et al. 2006, *AAS*, 209.10201
- [17] Benedict, G. F., McArthur, B. E., Feast, M. W., et al., 2007, *AJ* 133, 1810.
- [18] Bersier et al., 1994, *A&AS*, 108,25
- [19] Bohm-Vitense, E. 1994, *AJ* 107, 6731
- [20] Bono, G., Caputo, F., Santolamazza, P., Cassisi, S., Piersimoni, A., 1997, *AJ*, 113, 2209
- [21] Bono, G.; Marconi, M., 1998, *MmSAI*, 69, 109

- [22] Bono, G.; Marconi, M., 1998, *ASPC*, 135, 287
- [23] Bono, G., Caputo, F., Castellani, V., & Marconi, M. 1999, *ApJ* 512, 711
- [24] Bono, G., et al. 2000, *ApJ*, 529, 2930
- [25] Bono, G., Caputo, F., Cassisi, S., Marconi, M. et al. 2000, *ApJ*, 543, 955
- [26] Bono, G., Caputo, F., Marconi, M. 2001, *MNRAS* 325, 1353
- [27] Bono, G., Groenewegen, M. A. T., Marconi, M. et al. 2002, *ApJ* 574, 33
- [28] Bono, G., et al. 2005, *ApJ*, 621, 966
- [29] Bono, G., Caputo, F., Fiorentino, G., et al., *ApJ* accepted, arXiv:0805.1592
- [30] Borissova, J., Minniti, D., Rejkuba, M. et al 2004, *A&A* 423, 97
- [31] Caldwell, J.A.R. & Laney, C.D. 1991, in *The Magellanic Clouds*, 148th IAU Symposium, Kluwer Academic Publisher, Dordrecht, p.249
- [32] Cameron, L. M., 1985, *A&A*, 152, 250
- [33] Caputo, F., Marconi, M., Musella, I. & Santolamazza, P. 2000, *A&A* 359, 1059
- [34] Caputo, F., Bono, G., Fiorentino, G., Marconi, M., Musella, I., 2005, *ApJ*, 629, 1021
- [35] Caputo, F. 2008, *Mem Sait*, in press
- [36] Cardelli, J.A., et al. 1989, *ApJ*, 345, 245
- [37] Carpenter, J. M., 2001, *AJ*, 121, 2851
- [38] Carraro, G., Ng, Y.K., Portinari, L., 1998, *MNRAS*, 296, 1045
- [39] Carraro, G., Geisler, D., Villanova, S., Frinchaboy, P. M., Majewski, S. R., 2007, *A&A*, 476, 217
- [40] Carter, 1990, *MNRAS* 242, 1
- [41] Carter, B. S. & Meadows, V. S. 1995, *MNRAS* 276, 734
- [42] Castelli, F., Gratton, R.G. & Kurucz, R.L. 1997, *A&A* 318, 841
- [43] Castelli, F. & Kurucz, R.L. 2003, in *Modelling of Stellar Atmospheres*, 210th IAU Symposium, ed. by N. Piskunov, W.W. Weiss, D.F. Gray (San Francisco: ASP), 841
- [44] Catelan, M. & Corts, C., 2008, *ApJ*, 676, 135
- [45] Cayrel, R 1988, in *The Impact of Very High S/N Spectroscopy on Stellar Physics*, 132th IAU Symposium, Kluwer Academic Publishers, Dordrecht., p.345
- [46] Cescutti, G., Matteucci, F., Francois, P., Chiappini, C., 2007, *A&A*, 462, 943
- [47] Chalonge, D., 1958, *AJ*, 63, 186
- [48] Charbonneau, P. 1995, *ApJSS* 101, 309
- [49] Chiappini, C., Matteucci, F., Romano, D., 2001, *ApJ*, 554, 1044

- [50] Chiosi, C., Wood, P., Bertelli, G. & Bressan, A. 1992, *ApJ* 387, 320
- [51] Chiosi, C., Wood, P.R., Capitanio, N. 1993 *ApJS* 86, 541
- [52] Christy, R.F., 1966, *ApJ* 144, 108
- [53] Ciardullo, R., Feldmeier, J.J., Jacoby, G.H., et al. 2002, *ApJ* 577, 31
- [54] Cignoni, M.; Degl'Innocenti, S.; Prada Moroni, P. G.; Shore, S. N. 2006, *A&A*, 459, 783
- [55] Cioni, M.-R.L., van der Marel, R.P., Loup, C. & Habing, H.J. 2000, *A&A* 359, 601
- [56] Clegg, R. E. S. & Bell, R. A., 1973, *MNRAS*, 163, 13
- [57] Clementini, G., Carretta, E., Gratton, R. et al, 1995, *AJ* 110, 2319
- [58] Collinge, M. J., Sumi, T., Fabrycky, D., 2006, *ApJ*, 651, 197
- [59] Costa, R. D. D., Uchida, M. M. M., Maciel, W. J., 2004, *A&A*, 423, 199
- [60] Cox, J. P., 1980, *SSRv* 27, 389
- [61] Daflon, S., Cunha, K., 2004, *ApJ*, 617, 1115
- [62] Deharveng, L., Pena, M., Caplan, J., Costero, R., 2000, *MNRAS*, 311, 329
- [63] Dekker, H., D'Odorico, S., Kaufer, A et al 2000, *SPIE* 4008, 534
- [64] Diaz, A. I.; Castellanos, M.; Terlevich, E.; Luisa García-Vargas, M., 2000, *MNRAS*, 318, 462.
- [65] D'Odorico, S., Peimbert, M., Sabbadin, F., 1976, *A&A*, 47, 341
- [66] Dolphin, A. E., Saha, A., Skillman, E. D., et al. 2003, *AJ*, 125, 1261
- [67] Eddington, A.S., 1927, *MNRAS* 87, 539
- [68] Eddington, A.S., 1941, *MNRAS* 101, 182
- [69] Eddington, A.S., 1942, *MNRAS* 102, 154
- [70] Emerson, D., 1996, "Interpreting Astronomical Spectra", pp. 472., Wiley-VCH
- [71] Edvardsson, B., Andersen, J., Gustafsson, B., Lambert, D. L., Nissen, P. E., Tomkin, J., 1993, *A&A*, 275, 101
- [72] Eisenhauer, F., Genzel, R., Alexander, T., et al., 2005, *ApJ*, 628, 246
- [73] Evans, N.R., Schaefer, G. H., Bond, H. E., Bono, G., Karovska, M., Nelan, E., Sasselov, D., Mason, B. D., 2008, *AJ*, 136, 1137
- [74] Evans, N.R. 1991, *ApJ* 372, 597
- [75] Feast, M.W. & Catchpole, R.M. 1997, *MNRAS* 286, L1
- [76] Feast, M.W. 1999, *IAUS* 192, 519
- [77] Feast, M.W., Laney, C.D., Kinman, T.D., van Leeuwen, F., Whitelock P.A., arXiv:0803.0466

- [78] Feast, M. & Whitelock, P., 1997, MNRAS, 291, 683
- [79] Fernie, J.D., Evans, N.R., Beattie, B. & Seager S. 1995, IBVS 4148, 1
- [80] Ferrarese, L., Freedman, W.L., Hill, R.J., Saha, A. et al., 1996, ApJ, 464, 568
- [81] Fich, M.; Silkey, M., 1991, ApJ, 366, 107
- [82] Fiorentino, G., Caputo, F., Marconi, M. & Musella, I. 2002, ApJ 576, 402
- [83] Fitch, W. S. 1970 ApJ 161, 669
- [84] Fitzsimmons, A.; Brown, P. J. F.; Dufton, P. L.; Lennon, D. J. 1990, A&A, 232, 437
- [85] Fitzsimmons, A.; Dufton, P. L.; Rolleston, W. R. J., 1992, MNRAS, 259, 489
- [86] Fouqué, P. & Gieren, W.P. 1997, A&A 320, 799
- [87] Fouqué, P., Storm, J., & Gieren, W. P. 2003, in Stellar candles for the extragalactic distance scale, Lect. Notes Phys., 635, 21
- [88] Fouqué, P., Arriagada, P., Storm, J., et al., 2007, A & A 476, 73.
- [89] Freedman, W.L. 1988, ApJ 326, 691
- [90] Freedman, W.L. & Madore, B.F. 1990, ApJ 365, 186
- [91] Freedman, W.L., Madore, B.F., Gibson, B.K., et al 2001, ApJ 553, 47
- [92] Friel, E. D.; Janes, K. A., 1993, A&A, 267, 75
- [93] Friel, E. D., 1995, ARA&A, 33, 381
- [94] Friel, E. D., 1999, Ap&SS, 265, 271
- [95] Friel, E. D., Janes, K. A., Tavarez, M., Scott, J., Katsanis, R., Lotz, J., Hong, L., Miller, N., 2002, AJ, 124, 2693
- [96] Fry, A.M. & Carney, B.W. 1997, AJ 113, 1073 (FC97)
- [97] Fuhr, J. R., Martin, G. A., & Wiese, W. L. 1988, J. Phys. & Chem. Ref. Data, 17, Suppl. 4
- [98] Gehren, T.; Kudritzki, R. P.; Butler, K.; Nissen, P. E., 1985, ESOC, 21, 171
- [99] Geisler, D., Suntzeff, N., Mateo, M., Graham, J., 1992, IAUS, 149, 422
- [100] Gibson, B.K. 2000, MmSAI 71, 693
- [101] Gieren, W. P., Barnes T. G., & Moffett, T. J. 1993, ApJ, 418, 135
- [102] Gieren, W. P., Fouqué, P., & Gómez, M. 1997, ApJ, 488, 74
- [103] Gieren, W. P., Fouqué, P., & Gómez, M. 1998, ApJ, 496, 17
- [104] Gieren, W. P., Storm, J., Barnes, T. G., et al. 2005, ApJ, 627, 224
- [105] Glass, 1973, MNRAS 164, 155

- [106] Gould, A. 1994, ApJ 426, 542
- [107] Gratton, R., Sneden, C. & Carretta, E. 2004, ARA&A 42, 385
- [108] Gray, D.F. 1992, Book-Review: "Observations and Analysis of Stellar Photospheres", Sci 257, 1978
- [109] Gray, D.F. 1994, PASP 106,1248
- [110] Grevesse, N. & Sauval, A.J. 1998, SSRv 85, 161
- [111] Grocholski, A. J., Cole, A. A., Sarajedini, A., Geisler, D., & Smith, V. V. 2006, AJ, 132, 1630
- [112] Groenewegen, M.A.T 2004, MNRAS 353, 903
- [113] Groenewegen, M.A.T., Romaniello, M., Primas, F. & Mottini, M. 2004, A&A 420, 655
- [114] Groenewegen, M. A. T. 2007, A&A, 474, 975
- [115] Groenewegen, M. A. T., Udalski, A., Bono, G., 2008, A&A, 481, 441
- [116] Groenewegen, M. A. T. 2008, A&A, 488, 25
- [117] Gummertsbach, C. A., Kaufer, D. R., Schafer, D. R., Szeifert, T., Wolf, B., 1998, A&A, 338, 881
- [118] Gustafsson, B., Bell, R. A., Eriksson, K., Nordlund, A., 1975, A&A, 42, 407.
- [119] Harris, H. C., 1981, AJ, 86, 707
- [120] Harris, H. C., 1984, ApJ, 282, 655
- [121] Harris, H. C.; Pilachowski, C. A., 1984, ApJ, 282, 655
- [122] Henry, R. B. C., Kwitter, K. B., Balick, B., 2004, AJ, 127, 2284
- [123] Herrstein, J. R., Moran, J. M., Greenhill, L. J., Trotter, A. S., 2005, ApJ, 629, 719
- [124] Hertzsprung, E. 1926, BAN 3, 2031
- [125] Hill, V., Andrievsky, S.M. & Spite, M. 1995, A&A 293, 347
- [126] Hill, V. 1997, A&A 324, 435
- [127] Hoskin M. 1999, The Cambridge Concise History of Astronomy, Edited by Michael Hoskin, pp. 376. ISBN 0521572916. Cambridge, UK: Cambridge University Press, March 1999
- [128] Hou, J. L., Prantzos, N., Boissier, S., 2000, A&A, 362, 921
- [129] Ibata, R. A.; Irwin, M. J.; Lewis, G. F.; Ferguson, A. M. N.; Tanvir, N., 2003, MNRAS, 340, 21
- [130] Iben, I., Jr. & Tuggle, R. S. 1975, ApJ 197, 39
- [131] Isobe, T., Feigelson, E. D., Akritas, M. G. & Babu, G. J. 1990, ApJ, 364, 104
- [132] Janes, K. A., 1979, ApJS, 39, 135
- [133] Jaschek, C. & Jaschek, M. 1995, Books-Review: "The Behavior of Chemical Elements in Stars", Sci, 270, 1236

- [134] Jennens, P. A., Helfer, H. L., 1975, MNRAS, 172, 681
- [135] Jensen, J.B., Tonry, J.L., Barris, B.J. et al. 2003, ApJ 583, 712
- [136] Kaler, J.B. 1989, Book Review: "Stars and their spectra", Ap&SS 162, 176
- [137] Kaufer, A.; Szeifert, Th.; Krenzin, R.; Baschek, B.; Wolf, B., 1994, A&A, 289, 740
- [138] Kaufer, A., D'Odorico, S. & Kaper, L. 2004, UVES User Manual, Issue 1.9, VLT-MAN-ESO-13200-1825
- [139] Kennicutt, R.C., Stetson, P.B., Saha, A., et al 1998, ApJ 498, 181
- [140] Kervella, P., Bersier, D., Mourard, D., et al., 2004, A&A, 428, 587.
- [141] Kilian-Montenbruck, J.; Gehren, T.; Nissen, P. E., 1994, A&A, 291, 757
- [142] King, D. S., Hansen, C. J., Ross, R. R. et al. 1975, ApJ 195, 467
- [143] Kiss, L.L. & Vinko, J. 2000, MNRAS 314, 420
- [144] Kochanek, C.S. 1997, ApJ 491, 13
- [145] Koen, C., Marang, F., Kilkenney, D., Jacobs, C., 2007, MNRAS, 380, 1433
- [146] Korn, A.J., Becker, S.R., Gummersbach, C.A. & Wolf, B. 2000, A&A 353, 655
- [147] Kovtyukh, V.V. & Gorlova, N.I. 2000, A&A 351, 597
- [148] Kovtyukh, V.V., Andrievsky, S.M, Belik, S.I. & Luck, R.E. 2005a, AJ 129, 433
- [149] Kovtyukh, V.V., Wallerstein, G. & Andrievsky, S.M 2005b, PASP 117,1173
- [150] Kraft, R.P. 1961, ApJ 134, 6161
- [151] Kraft, R.P., & Schmidt 1963, ApJ, 137, 249
- [152] Kupka, F., Piskunov, N.E., Ryabchikova, T.A., Stempels H.C. & Weiss W.W. 1999, A&AS 138, 119
- [153] Kurucz, R.L. 1993, CD-ROMS #1, 13, 18
- [154] Laney, C.D. & Stobie, R.S. 1992, A&AS, 93, 93
- [155] Laney, C.D. & Stobie, R.S. 1993, MNRAS, 263, 291
- [156] Laney, C.D. & Stobie, R.S. 1994, MNRAS, 266, 441
- [157] Laney, C.D. & Stobie, R.S. 1995, MNRAS, 274, 337
- [158] Laney, C. D. & Caldwell, J.A.R., 2007, MNRAS, 377, 147
- [159] Leavitt, H.S., Pickering, E.C., 1912, HarCi. 173, 1
- [160] Lemasle, B.; Francois, P.; Bono, G. et al., 2007, A&A, 467, 283.
- [161] Lemasle, B.; Francois, P.; Piersimoni, A., Pedicelli, S., Bono, G. et al., 2008, A&A, 490, 613

- [162] Lub, J. & Pel, J. W. 1977, *A&A* 54, 137
- [163] Luck, R.E. & Lambert, D.L. 1981, *ApJ* 245, 1018
- [164] Luck, R. E., 1982, *ApJ*, 263, 215
- [165] Luck, R.E. & Lambert, D.L. 1985, *ApJ* 298, 872
- [166] Luck, R.E. & Lambert, D.L. 1992, *ApJSS* 79, 303 (LL92)
- [167] Luck, R.E., Moffet, T.J., Barnes, T.G. III & Gieren, W.P. 1998, *AJ* 115, 605 (L98)
- [168] Luck, R.E., Gieren, W.P., Andrievsky, S.M., et al. 2003, *A&A*, 401, 939
- [169] Luck, R.E. & Andrievsky, S.M. 2004, *AJ* 128, 343
- [170] Maciel, W. J.; Koppen, J., 1994, *A&A*, 282, 436
- [171] Maciel, W. J. & Quireza, C., 1999, *A&A*, 345, 629
- [172] Macri, L.M., Stanek, K. Z., Jr., Bersier, D., Greenhill, L. J. & Reid, M. J., 2006, *ApJ*, 652, 1133.
- [173] Madore, B.F. & Freedman, W.L. 1991, *PASP* 103, 933W
- [174] Marconi, M., Musella, I. & Fiorentino, G. 2005, *ApJ* 632, 590
- [175] Marconi, M., et al. 2006, *Mem. Soc. Astr. It.*, 77, 67
- [176] Mérand, A., Kervella, P., Coudé du Foresto, V., et al. 2005, *A&A*, 438, L9
- [177] Moffett, T. J., Barnes, T. G. 1984, *ApJS*, 55, 389
- [178] Nardetto, N., Mourard, D., Mathias, Ph., Fokin, A., & Gillet, D. 2007, *A&A*, 471, 661
- [179] Natale, G., et al. 2007, *ApJ*, in press
- [180] Neese, Carol L.; Yoss, Kenneth M., 1988, *AJ*, 95, 463
- [181] Newberg, H.J.; Y., B.; Rockosi, C.; Grebel, E. K.; Rix, H.W. , 2002, *ApJ*, 569, 245
- [182] Panagia, N., Tosi, M., 1981, *A&A*, 96, 306
- [183] Pardo, I.& Poretti, E. 1997, *A&A* 324, 121
- [184] Pasquali, A.; Perinotto, M., 1993, *A&A*, 280, 581
- [185] Peacock, J.A. 1999, *Cosmological Physics*, pp. 704., Cambridge University Press
- [186] Pel, J. W., van Genderen, A. M., Lub, J., 1981, *A&A*, 99, 1
- [187] Pel, J. W., 1978, *A&A*, 62, 75
- [188] Pel, J.W. & Lub, J., 1978, *IAUS*, 80, 229
- [189] Pel, J.W. & Lub, J., 2007, *THE FUTURE OF PHOTOMETRIC, SPECTROPHOTOMETRIC AND POLARIMETRIC STANDARDIZATION*, ASP Conference Series, Vol. 364
- [190] Pena, M.; Deharveng, L.; Caplan, J.; Costero, R., 2000, *RMxAC*, 9, 184

- [191] Persson, S.E., Murphy, D.C., Krzeminski, W., Roth, M., Rieke, M. J. 1998, AJ 116, 2475
- [192] Persson, S.E., Madore, B.F., Krzeminski, W., et al. 2004, AJ, 128,2239
- [193] Pietrzyński, G., Gieren, W., Soszyński, I. et al. 2006, ApJ, 642, 216
- [194] Phelps, R. L.; Tollefson, J.; Reafsnyder, S.; Frinchaboy, P. et al., 2000, AAS, 197, 4104
- [195] Pompéia, L., Hill, V., Spite, M., et al. 2008, A&A, 480, 379
- [196] Press, W. H., Teukolsky, S. A., Vetterling, W. T. & Flannery, B. P. 1992, in Numerical Recipes in Fortran, 77 (Cambridge U.P.)
- [197] Pritchard, J.D. 2004, FEROS-II User Manual, Issue 1.4, LSO-MAN-ESO-22200-0001
- [198] Reddy, B. E.; Tomkin, J.; Lambert, D. L.; Allende Prieto, C., 2003, MNRAS, 340, 304
- [199] Rodrguez, M., 1999, A&A, 351, 1075
- [200] Rolleston, W.R.J., Dufton, P.L., Fitzsimmons, A. et al. 1993, A&A 277, 10
- [201] Rolleston, W. R. J., Smartt, S. J., Dufton, P. L., Ryans, R. S. I., 2000, A&A, 363, 537
- [202] Rolleston, W.R.J., Trundle, C. & Dufton, P.L. 2002, A&A 396, 53
- [203] Romaniello, M., Primas, F., Mottini, M., Groenewegen, M.A.T., Bono, G. & Francois, P. 2005, A&A 429, L37 (Paper I)
- [204] Romaniello, M., Primas, F., Mottini, M., Pedicelli, S., Lemasle, B., Bono, G., Francois, P., Groenewegen, M.A.T. & Laney, C.D., 2008, A&A 488, 731
- [205] Rudolph, A. L.; Simpson, J. P.; Haas, M. R. et al., 1997, ApJ, 489, 94
- [206] Russell, S.C. & Bessell, M.S. 1989, ApJS 70, 865
- [207] Russell, S.C. & Dopita, M.A. 1992, ApJ 384, 508
- [208] Ryabchikova T.A. Piskunov N.E., Stempels H.C., Kupka F., Weiss W.W. 1999, proc. of the 6th International Colloquium on Atomic Spectra and Oscillator Strengths, Victoria BC, Canada, 1998, Physica Scripta T83, 162
- [209] Saha, A., Thim, F., Tammann, G.A. et al. 2006, ApJS, 165, 108.
- [210] Sakai, S., Ferrarese, L., Kennicutt, R.C. & Saha, A. 2004, ApJ 608, 42
- [211] Sandage, A., ApJ 127, 513
- [212] Sandage, A., Bell, R.A. & Tripicco, M.J. 1999, ApJ 522, 250
- [213] Sandage, A. & Tamman, G.A., arXiv:0803.3836.
- [214] Sasselov, D.D., Beaulieu, J.P., Renault, C., et al 1997, A&A 324, 471
- [215] Schaefer, B. E., 2008, AJ, 135, 112S
- [216] Schwarz, G. 1978, Ann. Stat., 6, 461

- [217] Searle, L., 1971, *ApJ*, 168, 327
- [218] Shapley, H. 1914, *ApJ* 40, 448
- [219] Shaver, P. A.; McGee, R. X.; Newton, L. M.; Danks, A. C.; Pottasch, S. R., 1983, *MNRAS*, 204, 53
- [220] Simpson, Janet P.; Colgan, Sean W. J.; Rubin, Robert H. et al., 1995, *ApJ*, 444, 721
- [221] Simpson, J. P.; Rubin, R. H., 1990, *ApJ*, 354, 165
- [222] Skillman, E. D., Tolstoy, E., Cole, A. A. et al. 2003, *ApJ*, 596, 253
- [223] Smartt, Stephen J.; Rolleston, William Robert J., 1997, *ApJ*, 481, 47
- [224] Sneden, C., 1973, *ApJ*, 184, 839
- [225] Sollima, A., Cacciari, C., Arkharov, A. A. H. et al., 2008, *MNRAS*, 384, 1583
- [226] Soszyński, I.; Gieren, W.; Pietrzyński, G.
- [227] Stanghellini, L., Guerrero, M. A., Cunha, K., Machado, A., Villaver, E., 2006, *ApJ*, 651, 898
- [228] Storm, J., Carney, B.W., Gieren, W.P., Fouqué, P., Latham, D.W. & Fry, A.M. 2004, *A&A* 415, 531
- [229] Szabados, L. 1995, *ASPC* 83, 357
- [230] Szabados, L. 2003, *Inf. Bull. Var. Stars*, No. 5394
- [231] Sziládi, K., Vinkó, J., Poretti, E., Szabados, L., Kun, M., 2007, *A&A*, 473, 579.
- [232] Tammann, G. A., Sandage, A., Reindl, B., 2007, *arXiv0712.2346*.
- [233] Thogersen, E. N.; Friel, E. D.; Fallon, B. V., 1993, *PASP*, 105, 1253
- [234] Trundle, C., Dufton, P. L., Hunter, I., Evans, C. J., Lennon, D. J., Smartt, S. J., Ryans, R. S. I. 2007, *A&A*, 471, 625
- [235] Turner, D. G., Burke, J. F., 2002, *AJ*, 124, 2931
- [236] Twarog, B. A., Ashman, K. M., Antony-Twarog, B. J., 1997, *AJ*, 114, 2556
- [237] van Belle, G. T., Lane, B. F., & Thompson, R. R. 1999, *AJ*, 117, 521
- [238] van der Marel, R. P. & Cioni, M.R.L., 2001, *AJ*, 122, 1807
- [239] Van Leeuwen, F., Feast, M. W., Whitelock, P. A., Laney, C. D., 2007 *MNRAS*, 379, 723
- [240] van Leeuwen, F., 2007, *A&A*, 474, 653
- [241] Vilchez, J. M.; Esteban, C., 1996, *MNRAS*, 280, 720
- [242] Udalski, A., Soszynski, I., Szymanski, M. et al. 1999a, *AcA* 49, 45
- [243] Udalski, A., Soszynski, I., Szymanski, M. et al. 1999b, *AcA* 49, 1
- [244] Udalski, A., Soszynski, I., Szymanski, M., et al., 1999, *AcA*, 49, 437.

- [245] Udalski, A., Wyrzykowski, L., Pietrynski, G., et al 2001, *Acta Astron.* 51, 221
- [246] Yanny, Brian; Newberg, Heidi Jo; Grebel, Eva K.; Kent, Steve et al., 2003, *ApJ*, 588, 824
- [247] Yong, D., Carney, B. W., de Almeida, M. L. T., Pohl, B. L., 2005, *AJ*, 131, 2256
- [248] Yong, D., Carney, B. W., de Almeida, M. L. T., 2006, *AJ*, 130, 597
- [249] Walker, A.R. 2003, in: *Stellar candles for the extragalactic distance scale*, *Lect. Notes Phys.* 635, 265
- [250] Walraven, Th. & Walraven, J. H. 1960, *BAN* 15, 67
- [251] Walraven, J.H., Tinbergen, J., Walraven, Th., 1964, *Bull. Astron. Inst. Neth.*, 14, 81
- [252] Westerlund, B.E. 1997, in: *The Magellanic Clouds*, *Cambridge Astrophysics Series* 29
- [253] Zaritsky, D., Kennicutt, R. C., Jr., Huchra, J. P., 1994, *ApJ*, 420, 87.
- [254] Zhevakin, S. A., 1963, *ARA&A* 1, 367

CURRICULUM VITAE

Silvia Pedicelli

Address:

Via Sangemini, 7
00135, Roma

Office Telephone: +39-(0)6-94286449
Fax: +39-(0)6-9447243
E-mail: spedicelli@gmail.com
Place and Date of Birth: Rome, 09/04/1977
Nationality: Italy
Marital Status: Single

CURRICULUM STUDIORUM

- **College 1991-1996:** Liceo Scientifico Statale "Farnesina" di Roma
- **Graduate 1997-2005:** Università degli Studi di Roma "La Sapienza", Physics Degree (Astrophysics and space physics); mark 107/110; advisor Prof.: G. Bono, Capuzzo Dolcetta; Master thesis title: "Fotometria a grande campo della galassia sferoidale nana Sculptor"
- **Ph.D Student 2005-2008:** Università di Roma "Tor Vergata", Dipartimento di Fisica; advisor Prof.: Roberto Buonanno, Giuseppe Bono, Martino Romaniello
PhD. thesis title: "Classical Cepheids as distance indicators and tracers of the disk abundance gradient"

RESEARCH INTERESTS

Observations, reductions and analyses of Globular Clusters and Variable stars.

COMPUTER SKILLS

Languages: IDL, SuperMongo
Systems: MS-DOS, Windows, Unix, Linux
Astronomical Software: IRAF, MIDAS, DS9, Skycat, P2PP, FPOSS

FELLOWSHIPS

ESO-Studentship June/2006-Jun/2008: Studentship for PhD students;
 Advisor: Dr. Martino Romaniello

PUBLICATIONS

- **2008:** Lemasle, B.; Franois, P.; Piersimoni, A.; Pedicelli, S.; Bono, G.; Laney, C. D.; Primas, F.; Romaniello, M., 2008, *A&A*, 490, 613.
- **2008:** Romaniello, M.; Primas, F.; Mottini, M.; Pedicelli, S.; Lemasle, B.; Bono, G.; Franois, P.; Groenewegen, M. A. T.; Laney, C. D., 2008, *A&A*, 488, 731.
- **2008:** Pedicelli, S.; Lub, J.; Pel, J. W.; Lemasle, B.; Bono, G.; Francois, P.; Laney, D.; Piersimoni, A.; Primas, F.; Romaniello, M.; and 6 co-authors, 2008, *MmSAI*, 79, 539.
- **2008:** Lemasle, B.; Piersimoni, A.; Pedicelli, S.; Bono, G.; Francois, P.; Primas, F.; Romaniello, M., 2008, *MmSAI*, 79, 534.
- **2007:** Bono, G.; Pedicelli, S.; Ferraro, I.; Stetson, P. B.; Corsi, C. E.; Pulone, L.; Calamida, A.; Monelli, M.; Buonanno, R.; Chadid, M.; and 4 coauthors, 2007, *EAS*, 25, 125.
- **2006:** Giuffrida, G.; Pedicelli, S.; Buonanno, R.; Stetson, P. B.; Bono, G.; Pulone, L.; Corsi, C.; Monelli, M.; Dall'ora, M., 2006, *MmSAI*, 77, 125.
- **2004:** Rossi, C.; Polcaro, V. F.; Viotti, R. F.; Filippi, A.; Pedicelli, S.; Omizzolo, A., 2004, *ASPC*, 314, 30.

CONFERENCES AND SCHOOLS

- **2008:** Talk (20 min) in the International School of Astrophysics "F. Lucchin", First cycle 2008 Tarquinia (Italy) June 8-14, 2008. (<http://www.mporzio.astro.it/tasca/>)
- **2007:** International Workshop "Nonlinear stellar hydrodynamics" and "The pulsation of Cepheids: Observation & Theory (Cassini project)". Paris 9-13th July 2007. <http://www.lesia.obspm.fr/astro/ce>
- **2007:** Talk (15 min) in the International Workshop "XXI I Century challenges for stellar evolution", Cefalu' (Sicily, Italy), 29.08-02.09. <http://www.oa-teramo.inaf.it/cefalu07/>

- **2005:** Poster in the International Astrophysics Meeting "Stellar Pulsation and Evolution". Monte Porzio Catone (Italy), 19-24 June. <http://www.mporzio.astro.it/step/>

OBSERVING RUNS

- **2008:** Paranal (Chile): 1 night of observation at the "Very Large Telescope" (VLT) with FLAMES.
- **2007:** Pic Du Midi (France): 5 nights of observations at the "Bernard Lyot Telescope" (BLT).
- **2005:** La Palma (Canarian Islands): 3 nights of observations at the new "Telescopio Nazionale Galileo" (TNG).